Inflow and Outflow Rates Control in SAGD Wells: An Integrated Approach of Data-Driven and Physical-Based Analysis

by

Hossein Izadi

A thesis submitted in partial fulfillment of the requirements for the degree of

Doctor of Philosophy

in

Petroleum Engineering

Department of Civil and Environmental Engineering
University of Alberta

Abstract

The utilization of the Steam-Assisted Gravity Drainage (SAGD) method entails significant natural gas consumption and extensive water handling and treatment. The effective inflow and outflow rates control in producer and injector wells holds paramount importance. It serves multiple objectives, including the maximization of oil production, the enhancement of steam chamber development, and the reduction of the cumulative Steam Oil Ratio (cSOR), thereby minimizing freshwater usage. Flow Control Devices (FCDs) represent one of the technological solutions available to facilitate the control of the SAGD well's inflow and outflow rates.

Despite the broad utilization of different devices by operators to control inflow and outflow rates in SAGD projects, there is a notable absence of comprehensive and quantitative evaluations concerning the impact of flow rates control in real-world SAGD operations. Moreover, there has been limited exploration of flow rates control impact in various operational and subcooling conditions to enhance well performance, which implies increasing oil production while reducing freshwater consumption. Empirical relationships have been used in the FCDs numerical simulations, and the impact of reservoir heterogeneity on FCD's performance has not been widely investigated. As a result, the development of efficient FCD design and evaluation remains a persistent challenge within the industry.

This project combines physics-based modeling (numerical simulations) with data-driven modeling using real SAGD data to comprehensively evaluate the effects of inflow and outflow rates control in SAGD wells. Comparing real data analysis and simulation results will provide valuable insights into the significance of different flow rates control strategies.

In the physics-based modeling approach, core analysis and Particle Size Distribution (PSD) data from several wells in Western Canada are collected. Permeability is estimated using PSDs based on a correlation we have developed using an optimization algorithm. The reservoir model is constructed using core analysis, PSD, and geology data, and the performance of different FCDs in different subcool scenarios is compared by assigning real flow-loop data to simulate FCDs responses. The primary benefit of incorporating flow-loop experiment data into the simulation lies in the creation of a mechanistic model based on physics rather than relying on empirical correlations. The findings revealed that by controlling the inflow rate, the creation of hot-spot

regions could be prevented, and improved steam conformance was achieved through the management of both inflow and outflow rates. Additionally, the effective rates control led to an increase in oil production and a reduction in cSOR. The findings highlight the effectiveness of inflow and outflow rates control at various subcooling levels and their potential application in SAGD projects.

In the data-driven modeling approach, we analyzed the impact of FCDs and lateral length of wells on SAGD well performance using data from major SAGD projects in Western Canada, spanning from 1997 to mid-2022. We utilized a normalization technique to evaluate the production history of wells, considering geological and operational parameters. The findings demonstrated that effective inflow and outflow rates control resulted in both increased oil production and reduced cSOR. Long-Short Term Memory (LSTM) Artificial Neural Networks (ANN) are also used to predict oil production and cSOR for the next 12 months for a new well to be drilled. The findings contribute to the optimization of SAGD operations and serve as a valuable guide for future Canadian SAGD well planning and decision-making strategy.

What sets this process apart is its adaptation from a carefully labeled real database, providing valuable insights for decision-making in future SAGD pad developments aimed at reducing freshwater consumption and increasing oil production. Completion and production engineers can leverage these findings to enhance their understanding of relative production performance, ultimately leading to the development of more effective operational designs.

Acknowledgement

I express my admiration and gratitude to the divine, the creator, and the bestower of illumination and wisdom, to whom I turn for solace and guidance.

I wholeheartedly dedicate this thesis to my beloved mother, father, sisters, and brothers, who have been my unwavering pillars of love, support, and encouragement throughout my entire life. Their endless sacrifices, guidance, and belief in my abilities have been the driving force behind my achievements.

I wish to express my sincere gratitude and appreciation to my supervisor, Prof. Juliana Leung, for providing a friendly and stressless environment, in addition to her scientific support. Also, I would like to thank the supervisory committee, Dr. Rashid Mirzavand and Dr. Vahidoddin Fattahpour for guiding and supporting me from the very start of my studies and helping me overcome all the difficulties on the way. I would like to extend my gratitude to the esteemed jury committee, Prof. Clayton Deutsch, Prof. Ian Gates, and Dr. Andy Li for their invaluable time and insightful feedback on my PhD thesis.

I would like to acknowledge Alberta Innovates for their financial contribution through the prestigious scholarship "Alberta Innovates Graduate Student Scholarship" and support of the research innovation, financial and technical support by Variperm Energy Services as our industry partner, the financial support by Mitacs Accelerate (project# IT15632), the Future Energy Systems under the Canada First Research Excellence Fund, and the academic licenses of AccuMap™ by IHS Markit, CMG STARS by Computer Modeling Group, and MATLAB by MathWorks.

I want to convey my profound gratitude to Dr. Mahdi Mahmoudi, Dr. Mazda Irani, and Dr. Arian Velayati for generously sharing their knowledge and experiences with me. It was a wonderful opportunity to get to know them and gain valuable insights from their expertise.

Table of Contents

Table of Tables

Table of Figures

Chapter 1: Introduction

1.1 Overview and Problem Statement

Horizontal well drilling and utilization represent dynamic and vibrant sectors within the oil and gas industry. Over the past decade, significant advancements in thermal applications have leaned towards harnessing the potential of horizontal wells to enhance oil recovery. Moreover, inflow and outflow rates control strategies by emerging completion technologies like Flow Control Devices (FCDs) have brought revolutionary improvements to thermal recovery methods like Steam-Assisted Gravity Drainage (SAGD). This thesis provides comprehensive insights into the design and analysis of inflow and outflow rates control by FCDs deployed in Canadian horizontal wells in SAGD projects. It delves into ongoing developments and optimization efforts, offering a thorough review and discussion of current activities within this field.

Inflow and outflow rates control by using FCDs have a longstanding history of use in conventional projects [1]. However, ConocoPhillips Canada has demonstrated that FCDs can lead to a significant increase in oil production, showcasing an average uplift of approximately 40% in the Surmont Pad 103 trial in 2008. This discovery has marked a substantial shift in the industry landscape, with the FCD market experiencing rapid growth, particularly in SAGD projects across Canada. ConocoPhillips Canada, for example, has adopted FCDs as the standard completion method for their future wells due to the reduced cost per barrel achieved through horizontal drilling and FCD utilization. This shift has rendered older techniques like vertical cold production wells, such as Cold Heavy Oil Production with Sand (CHOPS), economically less viable [1]. Currently, most operators are striving to establish a standardized approach to developing thermal projects, focusing on modular, smaller-scale projects. This approach becomes increasingly crucial because most new reserves are characterized by discontinuity, and payzone thickness varies across the asset. In such scenarios, the deployment of FCDs plays a pivotal role in mitigating operational challenges in both greenfield and brownfield developments [1].

Achieving success in a SAGD operation entails substantial costs and necessitates a comprehensive grasp of operational and well design parameters to ensure profitability and environmental sustainability [2]. Unfortunately, there has been a scarcity of publicly available studies focused on analyzing SAGD well performance, which implies increasing oil production while reducing freshwater consumption, using existing historical data. These studies are crucial in identifying best

practices for well completion design that optimize facility capacity and minimize freshwater consumption.

Controlling the inflow and outflow rates in SAGD wells in accordance with reservoir heterogeneity has the potential to enhance oil recovery and reduce the cumulative Steam Oil Ratio (cSOR) [2]. FCDs offer a solution to control the inflow and outflow rates to address challenges arising from reservoir heterogeneity SAGD wells, including suboptimal steam chamber growth, conformance issues, and hot-spot zones along the producer wells [3, 4, 5, 6]. Conducting an analysis of inflow and outflow rates control considering operational factors, geological barriers, and reservoir heterogeneity is valuable in maximizing production while minimizing freshwater usage, ultimately leading to more efficient operational designs and improving well performance.

This thesis employs two distinct approaches to investigate the influence of inflow and outflow rates control in SAGD wells. The first approach leverages physics-based modeling (numerical simulation), which serves as a modeling tool to simulate the SAGD process. Various inflow and outflow rates control strategies are implemented in the simulations to analyze their impact on oil production and cSOR. The second approach involves a data-analytics methodology, utilizing real data extracted from major SAGD projects in Western Canada. This comprehensive database encompasses steam injection and oil production data, well data, and geological information. By comparing the oil production and cSOR of wells completed with FCDs to nearby wells without FCDs, the effectiveness of rate control can be assessed based on real-world data. By comparing the findings obtained from the data analysis of real-world information and the results derived from the numerical simulations, a more comprehensive understanding of the effects of rates control is obtained. These comparative insights will contribute to a deeper understanding of the significance of rates control strategies in SAGD operations.

Three problem statements are defined as follows:

1. How different subcool temperatures integrated by different inflow and outflow rates control strategies affects oil recovery and cSOR.
2. The current studies examining the influence of inflow and outflow rates on enhancing well performance are predominantly restricted to reservoir simulations that employ empirical correlations for FCDs modeling or rely on limited real production databases. This reliance on reservoir simulations alone introduces uncertainties. Notably, critical parameters related

to industrial FCDs, such as resistance and corresponding pressure drop along the device, are not publicly accessible. Consequently, the simulation results may not accurately reflect the actual values of produced oil and injected steam when FCDs are utilized.

3. To achieve reliable future forecasting regarding the potential contribution of flow rate control strategies in enhancing well performance, a normalized production rate obtained from a large-scale real database is required. However, this approach has not been widely explored in current investigations.

To tackle these challenges effectively, an analysis using real historical data from significant SAGD projects in Western Canada over the past 25 years, along with flow-loop experiments, can provide reliable characteristics of FCDs. These findings will aid in devising an efficient well completion design for upcoming pad developments, especially when dealing with reservoir heterogeneity.

1.2. Research Objectives

This research outlines five objectives to effectively tackle the mentioned issues:

1. Gather data on key parameters such as production rates, reservoir properties, and operational variables for major SAGD project in Western Canada and Analyze trends and patterns in SAGD project performance over time.
2. Compare well performance metrics for SAGD projects using various flow rate control strategies by assessing the impact of operational variables to identify optimal flow rate control configurations based on production efficiency and reservoir characteristics.
3. Examine the relationship between different flow control devices deployment and oil production rates in extended-reach SAGD wells and propose improvements in FCD design for enhanced their performance.
4. Investigate the correlation between reservoir quality indicators, such as Particle Size Distributions (PSDs), and oil recovery efficiency to integrate reservoir quality data into flow control design algorithms.
5. Replicate SAGD conditions in physical-based models to mimic real-world scenarios to analyze different flow control configurations to identify the most effective one for diverse reservoir qualities.
6. Integrate data-analytics and physics-based modeling insights into a comprehensive decision-making framework.

1.3. Research Hypothesis

1. Flow rate control has the potential to concurrently reduce freshwater usage and increase oil production.
2. PSD measurements provide a dependable means to assess the heterogeneity in porosity and permeability distribution in bitumen deposits.
3. The performance of FCDs is influenced by reservoir heterogeneity, making it imperative to incorporate it into FCDs design considerations.
4. FCDs play a crucial role in enhancing well performance, especially when it comes to future pad developments.

1.4. Research Methodology

The general workflow of the thesis is shown in Fig. 1-1. This project aims to explore the impact of inflow and outflow rates control in SAGD wells using two distinct approaches. The first approach involves employing physics-based modeling using numerical simulations, which proves to be a valuable tool for replicating the SAGD process. To enhance the reliability of the permeability distribution in the reservoir, a correlation has been developed initially, allowing for the estimation of permeability based on easily collected data such as PSDs. Subsequently, various inflow and outflow rates control strategies are incorporated into the SAGD reservoir simulations to analyze their influence on oil production and cSOR. This modeling approach provides a controlled environment, enabling a detailed examination of the effects of rate control on the SAGD process.

The second approach involves utilizing a data-analytics methodology that relies on real data obtained from major SAGD projects in Western Canada. This extensive dataset includes crucial information such as steam injection and oil production data, well data, and geological data. To assess the effectiveness of rate control, the oil production and cSOR of wells completed with FCDs are compared to nearby wells without FCDs. By drawing conclusions from real-world data, the practical implications of rate control can be better understood.

By conducting a thorough analysis and comparison of the findings obtained from the data analysis of real-world information and the results derived from the numerical simulations, a more comprehensive understanding of the effects of rate control in SAGD operations is achieved. The insights gained from this comparative study will contribute significantly to the existing knowledge

and shed light on the significance of rate control strategies in optimizing SAGD operations. Ultimately, this research will aid in improving well performance, which implies increasing oil production while reducing freshwater consumption, for future pad developments and advance the efficiency of SAGD processes.

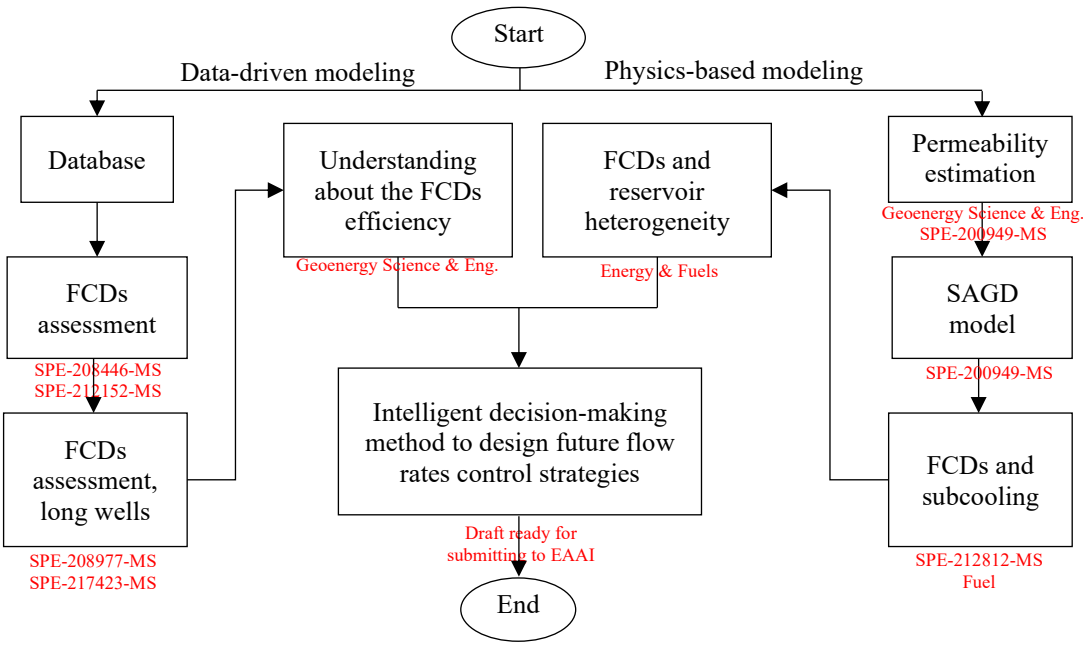

Fig. 1-1. General workflow of the project and the corresponding published or submitted papers.

1.5. Thesis Outline

The remaining parts of this thesis are structured as follows. Chapter 2 delves into the SAGD process and explores the influence of regulating inflow and outflow rates in SAGD operations. It also introduces the essential principles and concepts of FCDs as a means to control these rates. Chapter 3 encompasses physics-based modeling through numerical simulations, analyzing the control of flow rates across various reservoir heterogeneities and subcooling scenarios. This chapter extensively discusses how well-designed FCDs can enhance oil production and reduce cSOR. In Chapter 4, we delve into an examination of the historical experiences of implementing FCDs in SAGD projects in Western Canada. We extract real data from significant SAGD projects and evaluate well performance of those with and without FCDs. Chapter 5 leverages the real data obtained in Chapter 4 to train various LSTM neural networks. These networks are designed to predict the oil production and cSOR for newly drilled wells, comparing them to cases employing various flow rate control strategies and those without such strategies. This chapter aims to provide industry insights into how wells with and without FCDs are expected to perform in terms of oil

production and steam consumption. Chapter 6 wraps up the thesis with conclusions, discussions, an exploration of limitations, and suggestions for future research endeavors.

Chapter 2: SAGD Operation and Flow Rates Control Strategies

2.1. Preface

The term "steam-assisted gravity drainage" was initially coined by Roger Butler and his colleagues at Canada's Imperial Oil in the late 1970s [7]. In 1981, Butler and Stephens proposed the first closed-form solution for predicting oil production rates in the SAGD process. In what is known as the "Butler theory," Butler described the SAGD process as follows: when steam is injected, it creates a steam-saturated zone referred to as a "steam-depletion chamber" or simply a "steam chamber." In this chamber, the temperature matches that of the injected steam: chamber temperature equals steam temperature. The steam moves towards the steam chamber's interface, where it condenses and releases its latent heat, causing bitumen to flash. The latent heat from the steam is transferred through thermal conduction to the surrounding reservoir, mobilizing the bitumen. The resulting steam condensate and mobile bitumen flow towards the production well located below the injector through side-drained pathways.

SAGD stands as a highly effective thermal recovery method mostly employed in the Athabasca and Peace River reservoirs in Western Canada. In the SAGD process, steam is pumped into a horizontal injection well and pushed outward, shedding its latent heat upon encountering the cold bitumen at the periphery of a depletion chamber. Consequently, the viscosity of the bitumen decreases significantly, causing the bitumen to flow under the influence of gravity towards a horizontal production well positioned several meters below and parallel to the injection well (typically around 5 meters, but variations of 3 to 7 meters may occur due to drilling tolerances) [8]. As the oil flows away and is extracted, the steam chamber expands both upwards and sideways, as depicted in Sections B and C of Fig. 2-1.

SAGD process is illustrated in Fig. 2-1-a, where Section A illustrates the circulation stage, Section B portrays the initial phase with an underdeveloped chamber, and Section C displays the mature steam chamber during the injection phase [8]. Although the SAGD operation looks simply, there is many technical characteristics needs to be addressed for a successful SAGD process.

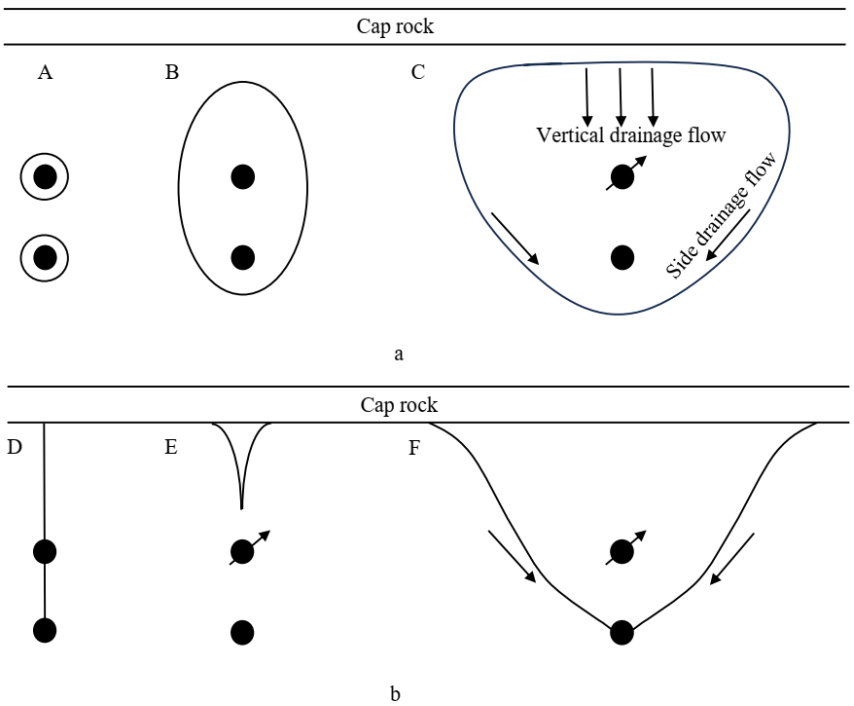

Fig. 2-1. Cross-sectional views of a SAGD process: a. section A presents circulation phase, section B presents early phase, and section C presents steam injection phase. b. S-shaped process of SAGD in Butler model, section D presents circulation phase, section E presents early phase, and section F presents steam injection phase [8].

2.2. Introduction

Horizontal wells find their most prevalent application in thermal operations, particularly in SAGD. While SAGD stands as the favored method for bitumen production from Athabasca deposits in Western Canada, oil producers face persistent challenges in adapting SAGD to various geological conditions [4]. SAGD is a relatively recent addition to the oil industry's repertoire, with economic viability hinging on oil prices being at or above $40 per barrel [19]. The primary hurdle lies in the substantial initial capital investment and the time required to attain economically viable production rates. Despite the steam requirements, the operational expenditure remains relatively low compared to alternative processes. Moreover, SAGD boasts a comparatively high recovery rate, reaching up to 80% [19].

From a sustainability perspective, SAGD represents a less intrusive alternative to open-pit oil sands operations, minimizing landscape disruption. The striking images of colossal tailing ponds have drawn international attention to oil sands practices. While SAGD has a relatively small footprint, it is characterized by high carbon intensity, and challenges related to water treatment and gas consumption to generate steam in SAGD operations are yet to be fully resolved [9].

Over time, various enhancements have been made to SAGD to boost efficiency and reduce the amount of steam needed for the oil recovery. These improvements encompass (not limited to) drilling infills, controlling the inflow and outflow rates by the deployment of FCDs, and solvent injection. The cSOR serves as a pivotal efficiency metric for SAGD operations, signifying the ratio of injected steam in Cold Water Equivalent (CWE) volumes to the volume of produced oil. Lower cSOR values equate to improved economics and reduced environmental impacts. For most SAGD projects, cSOR typically ranges between 2 to 5. cSOR is often favored over instantaneous SOR (iSOR) due to its consistency, whereas iSOR can exhibit fluctuations depending on the measurement timeframe [10].

The recovery factor and cSOR are particularly sensitive to operational parameters and the distribution of reservoir heterogeneities [11, 12]. The effect of reservoir heterogeneity is more significant in SAGD than in conventional recovery techniques since SAGD heavily relies on gravity drainage. Reservoir heterogeneity may increase total heat loss in addition to lowering drainage area. In addition, they may cause unconformity of the steam distribution in the reservoir.

Production challenges in SAGD can be classified into two main categories: sand production-related issues and steam chamber conformance or the lack thereof [3, 4]. Due to the unconsolidated nature of oil sands in Western Canada, SAGD operations can experience sand influx, particularly in locations with higher fluid inflow rates. Melting of bitumen that bonds sand grains at in-situ conditions and thermal-induced stress changes can lead to formation collapse over time, filling the gap between the drilled open-hole and horizontal liner. Steam Breakthrough (SBT) zones can destabilize the sand pack near the well, exacerbating sand production, which, if excessive, can cause erosion, tubing plugging, and premature failure of Electric Submersible Pumps (ESPs) [2, 3, 4]. Conformance, a qualitative term, gauges the extent to which the producer communicates with the injector and actively extracts the emulsion from the reservoir. Several factors can contribute to conformance issues, including clay lenses or breccia layers between injector and producer, excessive steam injection at the well's toe or heel, and the development of early hot-spot zones [1].

Inflow and outflow rates control by using FCDs represent an innovative solution to tackle steam conformance issues in SAGD projects. The deployment of various FCDs configurations in injector and producer wells can significantly influence the inflow and outflow rates, ultimately leading to

improved steam conformance and the prevention of hot-spot zones formation [3, 4]. This section provides a technical overview of the SAGD method and the implementation of FCDs, laying the groundwork for the subsequent section where we will analyze how FCDs impact SAGD well performance in terms of enhancing oil production and reducing cSOR.

2.3. Steam-Assisted Gravity Drainage Operation

Fig. 2-2 which is adapted from an unpublished textbook illustrates the complete SAGD water-steam cycle, while Fig. 2-3 showcases the corresponding enthalpy variations on a pressure-enthalpy diagram [10, 13]. Within this diagram, the boundaries of the central two-phase region delineate the enthalpies of saturated steam, represented by the dew-point line in red, and liquid water, denoted by the bubble-point line in blue. These lines converge at the critical point, characterized by 22.064 MPa pressure and 2086 kJ/kg enthalpy [13]. The process commences with steam generation in the steam drum at pressures close to 10 MPa, akin to those generated by most boilers [13]. Heated water ascends into the steam drum, enhancing steam quality as it traverses the air dryer (Point 1). After exiting the steam separator (Point 2) and the subsequent removal of the liquid water phase at the plant, steam quality is further improved. Subsequently, pressure reduction occurs at the pad entrance to reach the Maximum Operational Pressure (MOP) (Point 3), followed by additional reduction at the injector wellhead (Point 4). It is assumed that the minor pressure drop within the steam chamber, equivalent to the saturation temperature from the injector to the liquid pool level (Point 4 to 5), remains constant.

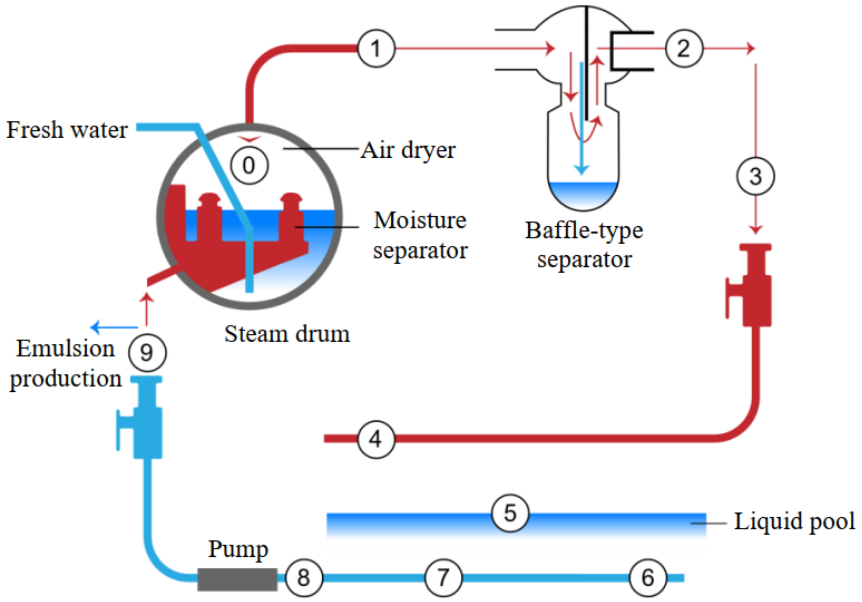

Fig. 2-2. Full steam cycle in a SAGD operation (adapted from an unpublished textbook).

As illustrated in Fig. 2-3, within the subcooled liquid zone located to the left of the bubble point line (encompassing Points 5 to 8), the temperature isothermal lines exhibit nearly vertical orientations. Since pressure measurements along the producer are unavailable, Fig. 2-3 depicts a constant pressure from the producer tubing inlet to the pump (Points 6 to 8) [10]. During the fluid's production to the surface, a reduction in pressure within the fluid stream occurs due to diminished hydrostatic pressure (head) and friction-induced pressure drop. In deep wells featuring extended vertical sections, this substantial pressure drop may result in steam flashing (Point 9).

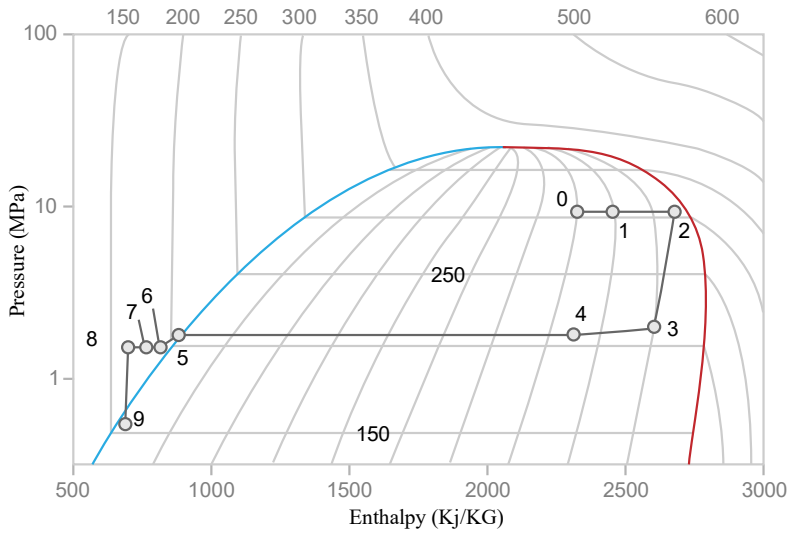

Fig. 2-3. Pressure-Enthalpy diagram for steam [13].

The condensed steam mixes with the heated bitumen and flows downward along the periphery of the steam chamber, forming an emulsion which gradually accumulates in a designated liquid pool (as illustrated in Fig. 2-4) [14]. To extract this emulsion from the pool, the producer relies on the pressure gradient between the well and the liquid pool (Fig. 2-4). Achieving a state where the rate of emulsion supply from the reservoir matches the rate of production leads to a quasi-steady state in the SAGD process, a concept discussed by Yuan and Nugent in 2013, is very critical [15]. Maintaining a consistent liquid level in the pool is vital for the success of SAGD operations, as it serves as a preventive measure against SBT.

To ensure a consistent liquid level and optimize SAGD production while preventing SBT and liner failure, operators often rely on "thermodynamic steam-trap control," commonly referred to as "subcool control". This strategy aims to maintain a liquid level above the producer well, regulated by the temperature differential between the producer well and the saturation temperature at the

local wellbore pressure. Subcool serves as an indicator of the liquid level above the producer, where lower subcool values indicate a smaller liquid level and an increased risk of SBT. Fig. 2-4 illustrates this concept, showing that high subcool levels (possibly due to pump limitations) may lead to injector flooding, while low subcool levels may result in an inadequate steam trap to prevent SBT and creation of hot-spot zones [14].

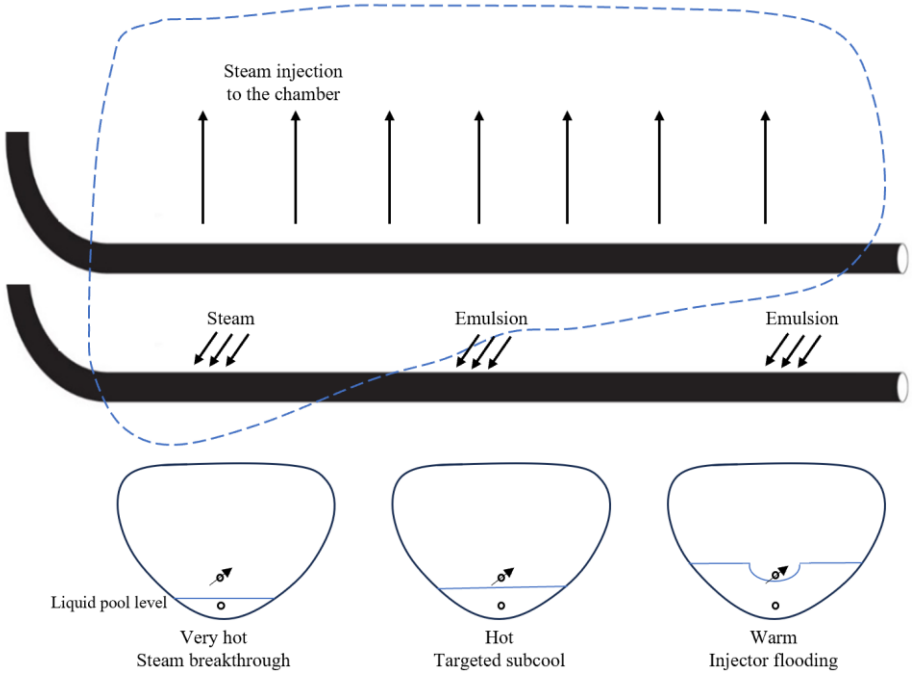

Fig. 2-4. Illustration of subcool temperature effect on SBT in production tubing [14].

The high temperature of hot-spot zones causes the emulsion's viscosity to drop, leading to increased local flow rates that get higher with time [3]. These hot-spot zones may cause the fluid fronts to deviate from their expected behavior of conformity which is connected to the local permeability. These areas become more prone to SBT, resulting in SAGD failure, and damaging the liner. The non-uniform profile due to the hot-spot zones can be made because of the differences in the horizontal and/or vertical permeability distribution [16, 17, 18, 19], variations in porosity [20], water saturation heterogeneity [17], variations in the distance between the wellbore and fluid contacts [16, 17, 21], variations in localized reservoir pressure [16, 22], changes in capillary pressure and relative permeability along the wellbore [23], localized skin damage or fractures [24, 25], changes in mineralogy or wettability [26, 27, 28], changes in thermal properties [29, 1], and changes in fluid density, viscosity, or both [30, 31]. Therefore, it is crucial to assess the importance of reservoir heterogeneity on inflow and outflow rates in SAGD wells. This analysis helps in

understanding bitumen recovery from oil sands, ultimately leading to improved oil production while reducing cSOR [32, 2]. In addition, when subcool temperatures are low, liquid levels near the producer may lead to the transport of sand into the producer well. This transport of sand has the potential to inflict significant damage on pumps and production facilities, sometimes necessitating costly interventions in severe cases. Erosion of slots due to the impact of entrained sand particles is a common occurrence in SAGD operations and may be exacerbated by low subcool conditions, which can result in SBT events. Fig. 2-5 illustrates an instance of tubing erosion attributed to SBT into the production liner [14].

FCDs, as an innovative technology can deal with the mentioned problem to prevent hot-spot zones formation by providing an additional pressure drop on top of the liquid pool. In the next subsection, the details of FCDs are provided.

Fig. 2-5. Example of eroded tubing from MacKay River SAGD project [14].

2.4. Flow Rates Control Strategies

FCD represents a cutting-edge technology integrated into the design of SAGD well completions. They play a crucial role in efficiently controlling inflow and outflow rates in both injector and producer wells, with the primary objectives being the augmentation of oil production and the reduction of cSOR. To address conformance challenges in injector wells, Outflow Control Devices (OCDs) are deployed as FCDs [33]. These OCDs are strategically placed within injector wells and function by limiting the outflow rate of steam, based on predetermined design and manufacturing specifications. Fig. 2-6, derived from a study conducted by Yusuf et al. (2021), illustrates how

different types of OCDs possess varying capabilities to restrict the mass flow rate (ṁ) at perforations along an injector well [34]. In producer wells, Inflow Control Devices (ICDs) are installed to address issues related to hot-spot zones and balance the inflow rate to contribute on conformance. These ICDs introduce an additional pressure drop (ΔP), specifically targeting hot-spot zones, to achieve uniformity and equalization in inflow rates, as depicted in Fig. 2-7 [3]. Furthermore, the integration of FCDs can occur through two distinct approaches: as part of the initial completion phase, known as liner-deployed FCDs (LDFCDs), or retrofitted at a later stage as tubing-deployed FCDs (TDFCDs). The decision to employ LDFCDs or TDFCDs is typically determined when traditional sand control completions have proven inadequate or have failed to meet the desired performance benchmarks.

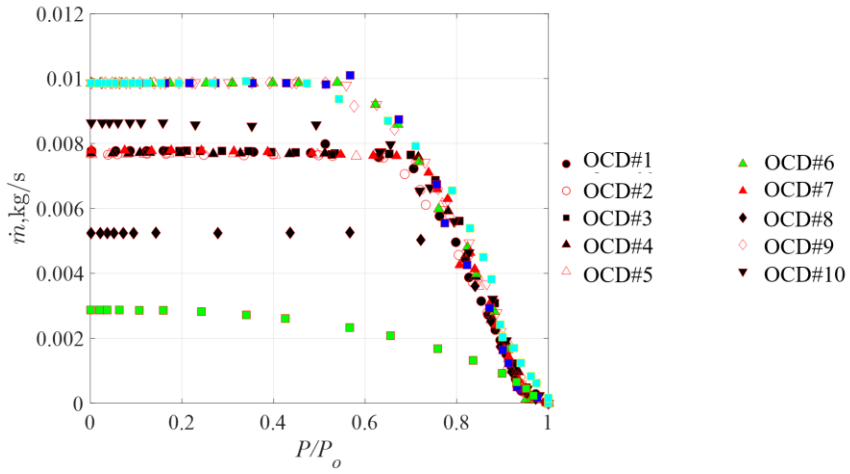

Fig. 2-6. Different OCDs restrict the mass flow rate (ṁ) of steam within the injector wells to enhance conformance along the well [34].

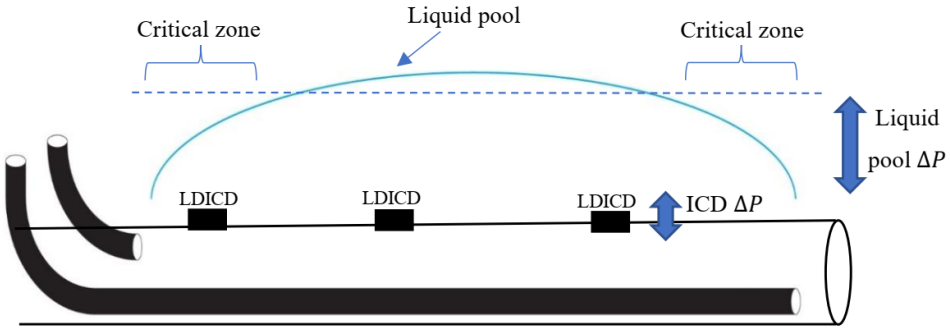

Fig. 2-7. Typical liquid level variation along the producer well in a homogeneous reservoir [3].

On the one hand, more restrictive FCDs with larger ΔP can be implemented in hot-spot zones to prevent the high inflow rate and therefore to deal with the SBT. On the other hand, it is not uncommon to see hot-spot zone's locations being changed over time. Additionally, because hot-

spot zones can be quite productive, severely restricting them will significantly decrease wellbore production [4]. As a result, a well-designed FCD is required, and it may be carried out by considering the reservoir quality, particularly around the wells. The crucial issue that requires attention is how to design the FCDs effectively to regulate ΔP and manage inflow and outflow rates, specifically to address hot-spot zones, mitigate the SBT, increase oil production, and reduce cSOR.

Permeability distribution in the reservoir is a sign of reservoir heterogeneity. Fig. 2-8 shows an application of permeability distribution in FCDs design through a reservoir modeling and simulation. An example of an assumed Inflow Performance Relationship (IPR) of a well with different reservoir quality in different parts: dark brown solid line represents the highest quality and permeability part, while the light orange solid line is the lowest quality and permeability part [35, 36]. To manage the production rate and pressure drawdown in these different parts and to postpone STB, different FCDs should be used. The three dashed lines show the performance of three FCDs with different resistances; the lighter blue represents a lower resistance FCD setting while the darker blue represents the higher resistance setting. Note that these curves are only related to FCDs not the deliverability of the well. This figure just tries to say that a high resistant FCD design could limit oil production, and the resistance should be designed very carefully. The workflow of the design is discussed in detail in the next Chapter. As shown in Fig. 2-8, the difference between the FCDs settings is so small in lower reservoir quality; however, it increases as the reservoir quality increases. The deliverable oil rate for each part of the reservoir and each FCDs setting is the point at which each IPR curve and each FCDs curve intersects if the same fluid composition is assumed in Fig. 2-8. Therefore, oil production is extremely dependent on the completion and the designed FCDs, meanwhile designing FCDs is also extremely dependent on the reservoir quality and permeability.

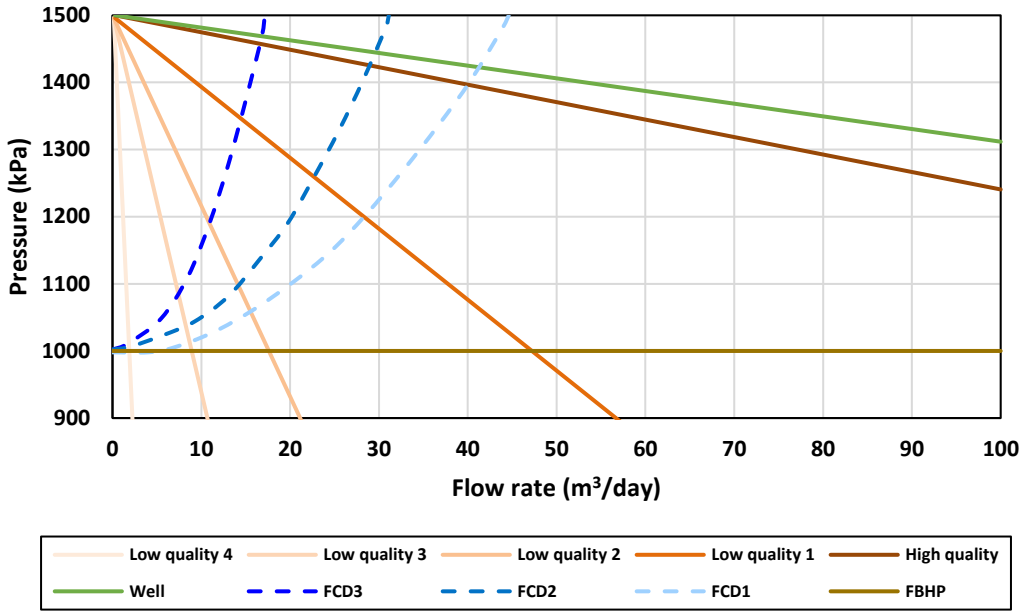

Fig. 2-8. Different deliverable oil rates for different reservoir quality and permeability by different flow rates control strategies.

2.5. Conclusions

SAGD stands as the predominant method for oil production in Western Canada. While the SAGD process may appear straightforward at first glance, it entails a multitude of intricate technical considerations for achieving a successful operation. Among these considerations, a well-designed inflow and outflow rates control strategies emerges as one of the most critical aspects, exerting a significant influence on factors such as the thickness of the liquid pool, subcool temperature, and postponing the SBT. Moreover, adept controlling inflow and outflow rates can significantly impact cSOR, a key indicator of the environmental sustainability of SAGD operations. By reducing the amount of steam required to produce a specific quantity of oil, efficient inflow and outflow rates control contributes to a more environmentally responsible operation. Achieving this level of control in inflow and outflow rates is made possible through the innovative use of FCDs, which represent cutting-edge technology in the realm of SAGD operations. FCDs can be strategically deployed within the tubing or liner, introducing an additional pressure drop mechanism to effectively balance and equalize the flow rates between the injection well and the production well. In the forthcoming sections, we present a comprehensive analysis of the effectiveness of inflow and outflow rates control in increasing SAGD wells performance, in terms of increasing oil production and decreasing cSOR. These analyses have been performed based on numerical simulations that delves into the physics and mechanism of the FCDs to improve SAGD wells

performance, and real data that delves into the historical implementation of FCDs in Western Canada. These analyses aim to shed light on the extent to which the inflow and outflow rates control strategies contribute to enhanced oil production and a reduction in cSOR, thus underlining the pivotal role of FCDs in optimizing SAGD operations.

Chapter 3: Physics-Based Modeling (Numerical Simulation)

This chapter has been derived from the following papers:

Izadi, H., Roostaei, M., Hosseini, S.A., Soroush, M., Mahmoudi, M., Devere-Bennett, N., Leung, J.Y. and Fattahpour, V., **2022**. A hybrid GBPSO algorithm for permeability estimation using particle size distribution and porosity. **Journal of Petroleum Science and Engineering**, 217, p.110944.

Izadi, H., Roostaei, M., Mahmoudi, M., Rosi, G., Stevenson, J., Tuttle, A., Sutton, C., Mirzavand, R., Leung, J.Y. and Fattahpour, V., **2023**, March. Unsupervised PSD Clustering to Assess Reservoir Quality Along the Horizontal Wells: An Efficient Inflow Control Devices Design. **In SPE Canadian Energy Technology Conference and Exhibition**. OnePetro.

Izadi, H., Leung, J.Y., Roostaei, M., Mahmoudi, M., Stevenson, J., Tuttle, A., Sutton, C., Mirzavand, R. and Fattahpour, V., **2024**. A practical workflow to design inflow control devices in SAGD projects to increase production and lower fresh water usage. **Fuel**, 356, p.129454.

Izadi, H., Leung, J.Y., Roostaei, M., Mahmoudi, Stevenson, J., Tuttle, A., Sutton, C., Mirzavand, R., and Fattahpour, V., **Submitted**. Inflow and Outflow Rates Management in SAGD Projects: Operating with Fewer Greenhouse Gas Emissions. **Energy & Fuels**.

3.1. Preface

This chapter discusses the significance of inflow and outflow rates control in SAGD operations and its impact on well performance in various reservoir heterogeneity and subcool scenarios. Several numerical simulations were conducted for homogeneous, simple with shale barriers, and heterogeneous reservoirs, incorporating FCDs based on published flow-loop experiment data. The key advantage of employing flow-loop experiment data in the simulation would be a physics-based mechanistic model rather than using empirical correlations.

In the first phase, core analysis data from three wells and PSD data from four wells at the same location are gathered. A correlation is then established to estimate permeability using PSDs, employing an optimization algorithm known as Genetic Binary Particle Swarm Optimization (GBPSO). The estimated permeability, derived from the PSD data, is utilized to improve the permeability distribution within the reservoir model. This leads to more dependable numerical simulations, enhancing overall reliability. In all simulations in this chapter, we tried to isolate the effects of FCDs by keeping all other parameters fixed. In addition, FCDs are installed in all perforations in the cases with FCDs in this thesis. We have conducted numerous simulations on not implementing FCDs in every perforations and have observed breakthrough at points where ICDs were not installed, or there was reduced conformance in areas where OCDs were not deployed.

In the second phase, several numerical simulations were conducted for homogeneous, simple with shale barriers, and heterogeneous reservoirs. In the homogeneous reservoir, using both ICDs and OCDs improved oil production by 26% and reduced cSOR by 19%. For the simple reservoir with shale barriers, LDOCDs contributed to a 13% increase in steam chamber volume. Optimal results were obtained by combining LDICDs and LDOCDs, leading to a 24% increase in oil production and a 20% reduction in cSOR. In the heterogeneous reservoir, ICDs managed hot-spots and improved steam conformance, resulting in a 26% increase in oil production and a 17% reduction in cSOR when combined with OCDs. Moreover, using ICDs alone decreased cSOR by 20%.

The third phase involves offering more comprehensive insights into designing ICDs considering reservoir heterogeneity. By employing a relatively conservative production approach with subcooling between 10°C and 15°C, the cases with LDICDs demonstrate higher oil production rates, improved steam conformance, and lower cSOR compared to the case without LDICDs.

However, in a relatively challenging production scenario with subcooling between 1°C and 5°C, the case without ICDs cannot be simulated at the desired subcooling temperature and the cases with LDFCDs improved the productivity. LDICD#1 is identified in both scenarios as the best case due to its enhanced steam conformance and provided slightly higher oil production rate. Compared to the case without ICDs, the application of LDICD#1 at higher subcooling temperatures leads to a 17% increase in oil production rates, while reducing cSOR and natural gas usage by 8% and 10% respectively. Similarly, at lower subcooling temperatures, the case with LDICD#1 shows a 21% increase in oil production rates and reductions of 12% and 17% in cSOR and consumed natural gas respectively, compared to the case without ICDs.

The findings are validated by real-world production data in Western Canada, contributing to a better understanding of flow rates control effects on production performance. The research aims to facilitate more efficient well designs with lower greenhouse gas (GHG) emissions to meet climate change targets.

3.2. Introduction

The recovery factor and cSOR are particularly sensitive to operational parameters and the distribution of reservoir heterogeneities [11, 12]. The effect of reservoir heterogeneity is more significant in SAGD than in conventional recovery techniques since SAGD heavily relies on gravity drainage. Reservoir heterogeneity may increase total heat loss in addition to lowering drainage area. In addition, they may cause unconformity of the steam distribution in the reservoir. Therefore, it is crucial to assess the impact of reservoir heterogeneity on inflow and outflow rates in SAGD wells. This analysis helps in understanding bitumen recovery from oil sands, ultimately leading to improved oil production while reducing cSOR [32, 2].

Reservoir characterization is an essential aspect of reservoir modeling, field development planning, and asset management, and one of the most important reservoir parameters relevant to subsurface flow is permeability [37, 38, 39, 40]. PSD, as a physical property of oil-sands in Western Canada, is an important variable in many complex hydrological, geological, and geophysical applications and can be considered to develop correlations for permeability estimation [41]. Permeability can potentially be estimated using PSD and porosity data. In the literature, many investigations have been carried out to develop a relationship between permeability versus PSD and porosity using statistical correlations [42, 43]. Table 1 presents the porosity function and

effective diameter of existing formulations in the literature. Some equations are originally expressed in terms of the void ratio, and they are converted to porosity in Table 1 for consistency. The literature formulation of permeability estimation based on PSD is based on a general porosity function ($F(\phi)$) times to a function of the effective particle diameter (${d_e}^n$).

Table 1. Porosity function and effective diameter of existing correlations of permeability estimation in the literature.

Author(s)	$F(\phi)$	${d_e}^n$	Author(s)	$F(\phi)$	${d_e}^n$
Hazen (1892) [44]	1	${D_{10}}^2$	Slichter (1899) [45]	$\phi^{3.287}$	${D_{10}}^2$
Kruger (1918) [46]	$\left(\frac{\phi}{(1-\phi)^2}\right)$	$\left(\frac{1}{\sum_{i=1}^{m}\Delta f_i(\frac{2}{d_i^g+d_i^d})}\right)^2$	Terzaghi (1925) [47]	$(\frac{\phi-0.13}{\sqrt[3]{1-\phi}})^2$	${D_{10}}^2$
Zamarin (1928) [48]	$(1.275-1.5\phi)^2\left(\frac{\phi^3}{(1-\phi)^2}\right)$	$\left(\frac{1}{\sum_{i=1}^{m}\Delta f_i(\frac{ln\frac{d_i^g}{d_i^d}}{d_i^g-d_i^d})}\right)^2$	Sauerbrey (1932) [49]	$\frac{\phi^3}{(1-\phi)^2}$	d_{17}^2
Zunker (1932) [50]	$\left(\frac{\phi}{1-\phi}\right)$	$\left(\frac{1}{\sum_{i=1}^{m}\Delta f_i(\frac{d_i^g-d_i^d}{d_i^g d_i^d ln\frac{d_i^g}{d_i^d}})}\right)^2$	Kozeny (1953) [51]	$\frac{\phi^3}{(1-\phi)^2}$	$\left(\frac{1}{\sum_{i=1}^{n}\Delta f_i(\frac{d_i^g+d_i^d}{2d_i^g d_i^d})}\right)^2$
Beyer (1964) [52]	1	$\log\frac{500}{C_u}D_{10}^2$	Terzaghi and Peck (1964) [53]	$\left(\frac{\phi-0.13}{(1-\phi)^{\frac{1}{3}}}\right)^2$	${D_{10}}^2$
Amer and Awad (1974) [54]	$\frac{\phi^3}{(1-\phi)^2}$	$D_{10}^{2.32}$	USBR (1978) [55]	1	$D_{20}^{2.3}$
Kenney et al. (1984) [56]	1 in the original form	${D_5}^2$	Shahabi et al. (1984) [57]	$\frac{\phi^3}{(1-\phi)^2}$	$C_u^{0.735}D_{10}^{0.89}$
Chapuis et al (1989) [58]	$10^{1.291\frac{\phi}{1-\phi}-0.6435}$	$D_{10}^{10^{0.5504-0.2937e}}$	Koenders and Williams (1992) [59]	$\frac{\phi^3}{(1-\phi)^2}$	${D_{50}}^2$
Alyamani and Sen (1993) [60]	1	$\left(I_0+0.025(D_{50}-D_{10})\right)^2$	Kasenow (2002) [61]	$\frac{\phi}{(1+\phi)^2}$	$\left(\frac{1}{\sum_{i=1}^{m}(\frac{2\Delta f_i}{d_i^g-d_i^d})}\right)^2$
Mbonimpa et al. (2002) [62]	$\frac{\phi^{3+x}}{(1-\phi)^{2+x}}$	$C_u^{\frac{1}{3}}{D_{10}}^2$	Chapuis et al. (2004)	$\left(\frac{\phi}{(1+\phi)^2}\right)^{0.7825}$	$(D_{10}^2)^{0.7825}$
Carrier (2003) [63]	$\frac{\phi}{(1+\phi)^2}$	$\left(\frac{100}{\sum\frac{f_i}{D_{li}^{0.404}\times D_{si}^{0.595}}}\right)^2\times\left(\frac{1}{S_F}\right)^2$ $S_F=S_sD_{eff}$	Arshad et al. (2020) [42]	$\left(\frac{\phi}{1-\phi}\right)^{6.7}$	$\left(\sqrt{\begin{matrix}0.3D_{10}\\0.2D_{30}+\\0.3D_{50}+\\0.2D_{60}\end{matrix}}\right)^{6.7}$

		$D_{eff} = \frac{100}{\sum \frac{f_i}{D_{li}^{0.5} \times D_{si}^{0.5}}}$			

A common drawback in these formulations is that the role of fines content was not widely investigated. Moreover, the correlations were developed based on limited data points of the PSD curve; it is postulated that the correlation accuracy could be improved by using more relevant features (here D-values) as inputs to obtain better estimations.

Several studies in the literature have applied numerical simulations and illustrated the negative impacts of barriers on oil production and the overall recovery of SAGD projects. They also proposed hydraulic fracturing and a high-pressure cycling method as solutions to increase the reservoir permeability and minimize the barriers' effect [19, 64, 28, 65, 26, 27]. Some researchers have investigated the position and length of the barriers. They observed that shale barriers located distant from the producer and injector wells had a lower impact on production, whereas barriers bigger than 50 meters act as an extended flow barrier, reducing oil production significantly [66, 67, 68,69, 70, 71,72, 73]. However, regarding dealing with the barriers, the contribution of flow control devices (FCDs) in SAGD injector and producer wells to deal with the shale barriers nearby wells to enhance oil production and lower cSOR have not been widely investigated.

Several research studies were conducted on combining dynamic reservoir flow performance and improving the design and location of ICDs. Kyanpour and Chen (2013, 2014) have implemented reservoir simulation and wellbore modelling to determine the size and position of flow control devices (FCDs), considering reservoir heterogeneity [74, 75]. Ghesmat and Zhao (2015) have presented general well-completion strategies using scab liners and FCDs for reservoirs with different structures [76]. Su and Gates (2015) used a numerical simulation and showed that ICDs provide a great uplift in homogeneous SAGD reservoirs [77]. Becerra et al. (2018) implemented dynamic reservoir and wellbore simulation to evaluate the integrated performance of ICDs in Mackay River SAGD wells [78]. Nejadi et al. (2018) developed a reservoir simulation model to optimize the placement of FCDs in SAGD well pair completion [79]. Li et al. (2018) developed a CFD model of steam flow through a systematic investigation of different domain sizes to study the effect of the ΔP across the outflow control devices (OCDs) and the steam distribution [33]. Every study in the literature either reported a specific field implementation of ICDs or attempted to optimize the placement of ICDs. However, to the best of our knowledge, there were very limited

studies on the integration of flow-loop and numerical simulation to investigate the ICDs design. A practical approach that integrates reservoir real data, flow-loop experiments, and reservoir simulation to design ICDs, while relating that design to the representative PSD data corresponding to specific reservoir conditions or using PSD properties as a starting point, is missing.

3.3. Numerical Scheme and Reservoir Models

The commercial software CMG STARS was employed to conduct numerical simulations of the SAGD operation [82]. This section of the thesis discusses the governing equations and reservoir models used in the study. Two distinct reservoir models were constructed for specific purposes. The first one was designed to evaluate various flow rate control strategies and their impact on increasing oil production while reducing cSOR. The second reservoir model aimed to assess the effects of different subcool temperatures and pressure drops provided by ICDs on increasing oil production and decreasing cSOR. Real data, including topography, porosity, permeability, and PSDs data, were utilized in the creation of these reservoir models. PSDs data played a crucial role in estimating permeability for use in the reservoir models and determining the permeability distribution within the reservoir model, in addition to permeability data resulted from ore analysis experiments.

In the first reservoir model, core analysis data and PSDs data which some of them are incorporated along with their corresponding permeability values were used. This allowed for the development of a correlation between PSDs and permeability. Subsequently, this correlation was applied to estimate permeability values for use in the reservoir model using other PSDs data which do not have permeability value in addition to permeability obtained from care analysis data.

In contrast, the second reservoir model lacked the associated permeability values for PSDs data. To validate whether the correlation developed for the first reservoir model to estimate permeability using PSDs could be applied to the second reservoir model, an unsupervised and self-adaptive clustering algorithm was employed. This algorithm compared the representative PSDs from the location where the second reservoir model was situated with those from the location of the first reservoir model. The analysis confirmed the validity of using the developed correlation for permeability estimation in the second reservoir model. Consequently, the established correlation was utilized to determine permeability values based on PSDs in addition to core analysis data within the reservoir model, enhancing the reliability of the reservoir model.

Flow control devices are incorporated into simulations for both injector and producer wells, covering all perforations within the reservoir model.

3.3.1. Numerical Scheme

Presently, two methods are employed to assess wellbore and reservoir interactions for capturing deliverability: numerical software packages such as CMG, Intersect, and tNavigator, and Nodal Analysis tools like NETool and Prosper. Within numerical software packages (which used in this theses), the reservoir undergoes discretization (gridding), and the wellbore is similarly gridded as a separate entity. As illustrated in Fig. 3-1, the reservoir and wellbore are addressed independently, and the solver's objective is to determine the flow rate from the grid to the wellbore while adhering to user-defined constraints at the producer's heel.

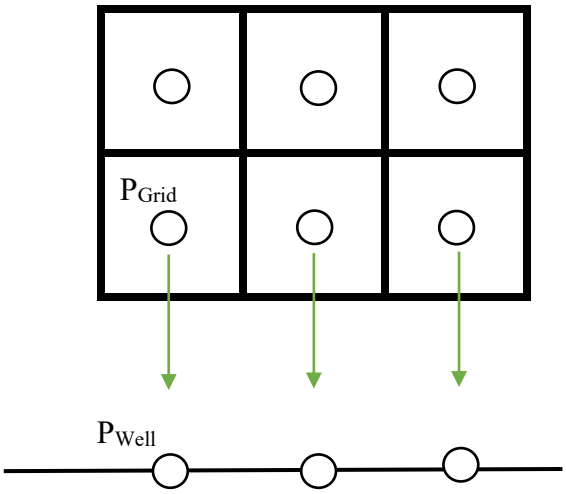

$$q_{Well} = WI \times (P_{Grid} - P_{Well})$$

Fig. 3-1. The reservoir and wellbore coupling in the commercial numerical simulation software [4].

For multiphase flow in the porous media, Darcy's law applies as Eq. 2 [80]:

$$U^* = -\frac{k^*}{\mu^*}\nabla\Phi^* \qquad (2)$$

where for phase $*$, U is velocity of the phase, k is the effective permeability tensor of the phase in the rock, μ is the viscosity of the phase, and $\nabla\Phi$ is the potential gradient includes pressure and gravity as Eq. 3 [81]:

$$\Phi = g(z - z_{datum}) + \int_{P_{datum}}^{P} \frac{dP}{\rho} \qquad (3)$$

where g is gravity, ρ is the density of the fluid, and z is the elevation above the datum location. In combination with the material balance, the governing equation for flow is as Eq. 4 [81]:

$$\nabla.\left[\frac{R_{sw}k_w}{\mu_w B_w}(\nabla P_w - \rho_w g\nabla z) + \frac{R_{so}k_o}{\mu_o B_o}(\nabla P_o - \rho_o g\nabla z) + \frac{k_g}{\mu_g B_g}(\nabla P_g - \rho_g g\nabla z)\right] = \frac{\partial}{\partial t}\left[\phi\left(\frac{R_{sw}S_w}{B_w} + \frac{R_{so}S_o}{B_o} + \frac{S_g}{B_g}\right)\right] + \frac{R_{so}q_o}{B_o} + \frac{q_{fg}}{B_g} \quad (4)$$

where subscripts w, o, and g refer to the water, oil, and gas phases, respectively. Accordingly, R is the solution-gas ratio, k is effective permeability, and B is the formation volume factor. μ, ρ, and S are viscosity, density, and saturation for different phases.

Conductive heat transfer obeys Fourier's law as Eq. 5 [81]:

$$q = -k_{th}\nabla \mathrm{T} \quad (5)$$

where q is the heat transfer flux, k_{th} is the thermal conductivity tensor, and T is the temperature. The total energy balance in x, y, and z directions for isotropic formation thermal conductivity is then as Eq. 6 for systems where phase transition can occur [81].

$$\frac{\partial}{\partial x}\left(-k_{th_x}\frac{\partial T}{\partial x} + \sum_{i=1}^{n_p} u_{i,x}\rho_i h_i\right) + \frac{\partial}{\partial y}\left(-k_{th_y}\frac{\partial T}{\partial y} + \sum_{i=1}^{n_p} u_{i,y}\rho_i h_i\right) + \frac{\partial}{\partial z}\left(-k_{th_z}\frac{\partial T}{\partial z} + \sum_{i=1}^{n_p} u_{i,z}\rho_i\left(h_i + {}^{gz}/_{Jg_c}\right)\right) = \frac{\partial}{\partial T}\left[(1-\varphi)M_r(T - T_{ref}) + \varphi\left(S_w\rho_w U_w + S_o\rho_o U_o + S_g\rho_g U_g\right)\right] + Q \quad (6)$$

where h_i is the enthalpy of each phase, M_r is the volumetric heat capacity of the reservoir's rocks, u is the specific internal energy of each phase, and Q is the energy input per unit volume. Eqs. 2 to 6 are solved using the CMG thermal reservoir simulator STARS™, which employs the finite volume approach to discretize Eqs. 4 and 6 [81, 82]. The discretized set of equations is solved using Newton's technique with an implicit time integrator to step across time. A K-value based compositional solver is utilized for each grid block at each time step for the phase equilibrium calculations [81].

In CMG, for different FCD types, different equations have been developed. These equations replace well index equation in the simulation [82]. In this thesis, actual data collected from a flow-loop configuration is utilized to provide the FCD responses in the simulation. Consequently, CMG STARS interpolates the associated pressure for the flow rate from this real data. This interpolated pressure would then be regarded as the bottomhole flowing pressure within the well index equation.

The block size has been refined from its previous dimensions as ½ Δx, ½ Δy, ½ Δz, and comparisons have been conducted for oil rate and cSOR (Fig. 3-2). Through these observations, it has been determined that the chosen block size is appropriate for the comparisons outlined in this thesis.

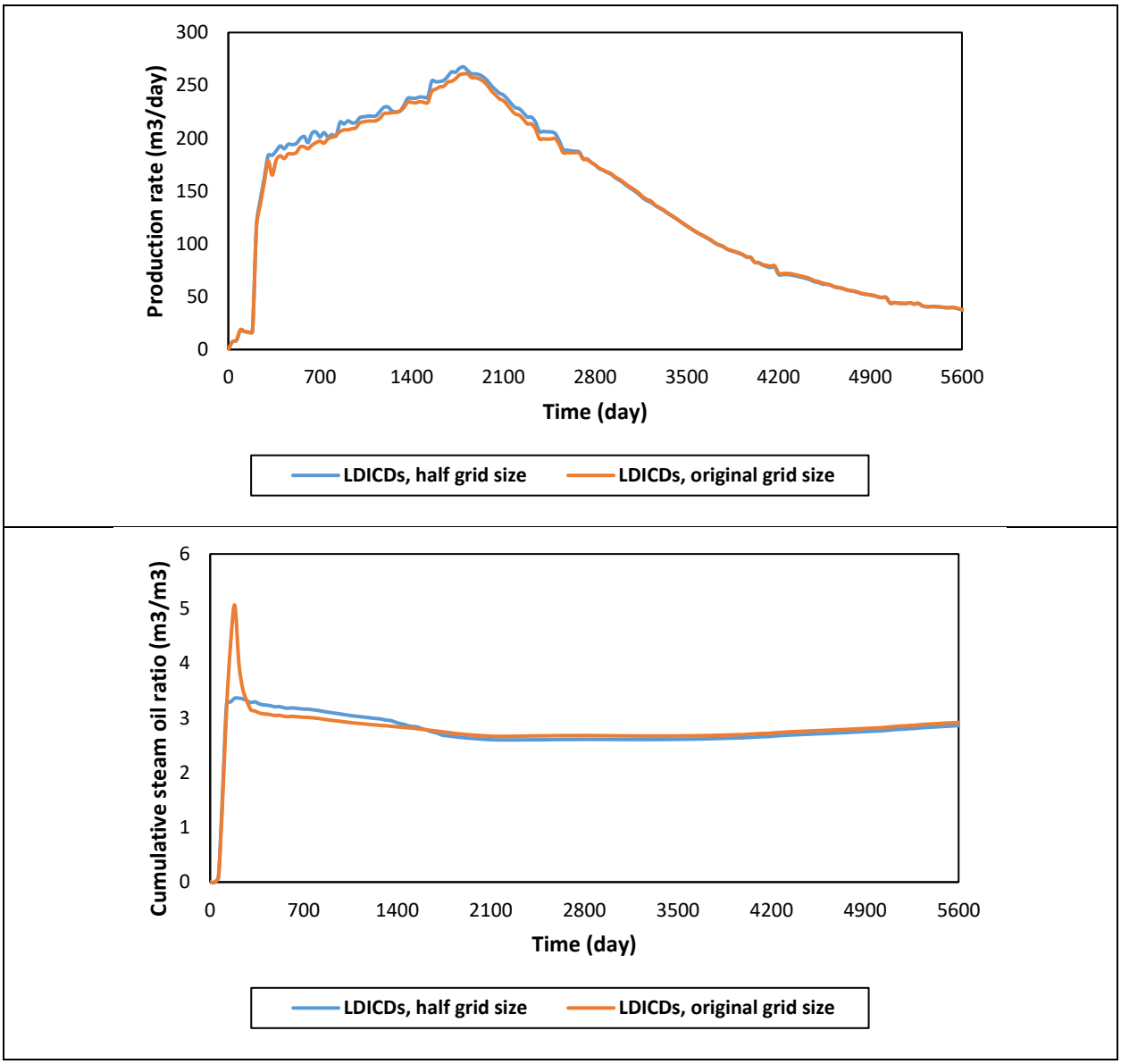

Fig. 3-2. Refining grid resolution to study the impact of grid size on the results.

3.3.2. Reservoir Model# 1

In reservoir model #1, we investigate the effects of varying inflow and outflow rate control in different reservoir heterogeneity scenarios. It's important to note that in this same reservoir model, the subcool temperature remains consistent across all flow rate control strategies.

3.3.2.1 Permeability Estimation

In this thesis, the GBPSO algorithm proposed by Sadri and Suen (2006) [83] is used to optimize the coefficients of our relationships to estimate permeability based on PSD characteristics. GBPSO introduces birth and death operations to make the population very dynamic. Since birth and mortality rates change naturally with time, the model allows oscillations in population size. Compared to the original Particle Swarm Optimization (PSO) model, and Genetic Algorithms (GA), this strategy proposes a more natural simulation of the social behavior of intelligent animals, and it significantly improved the algorithm results [83]. For more details regarding the GBPSO please see (Izadi et al. 2022) [84, 23].

Based on the literature review of predictive models presented in Table 1 and available data, we selected 25 features for model development. These features include passing D5 to D95 in 5% increments, the volume of shale, fines content, sorting coefficient, porosity, and uniformity coefficient. A scatter plot of these features with respect to permeability is created in Fig. 3-3. According to Fig. 3-3, permeability is more sensitive to smaller D-values than larger ones, which is reasonable as permeability is mostly influenced by the lower portion of PSD.

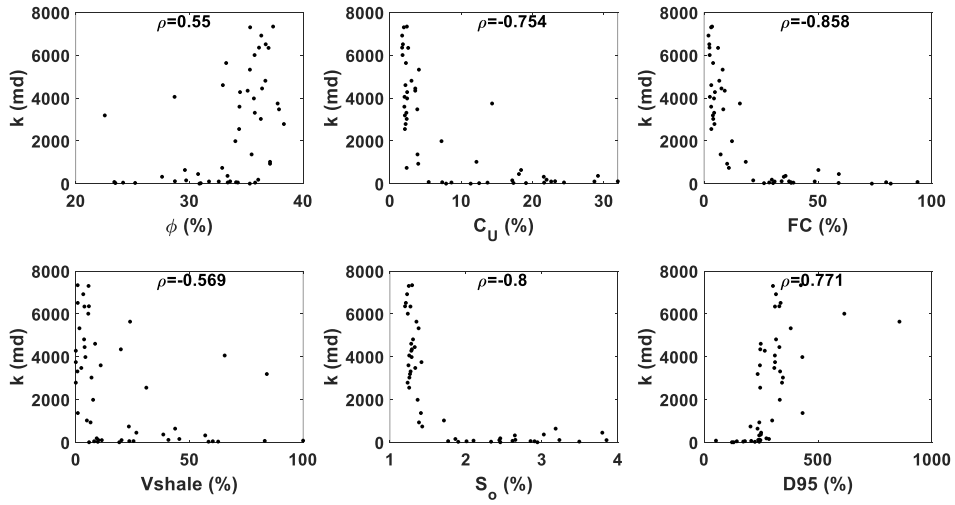

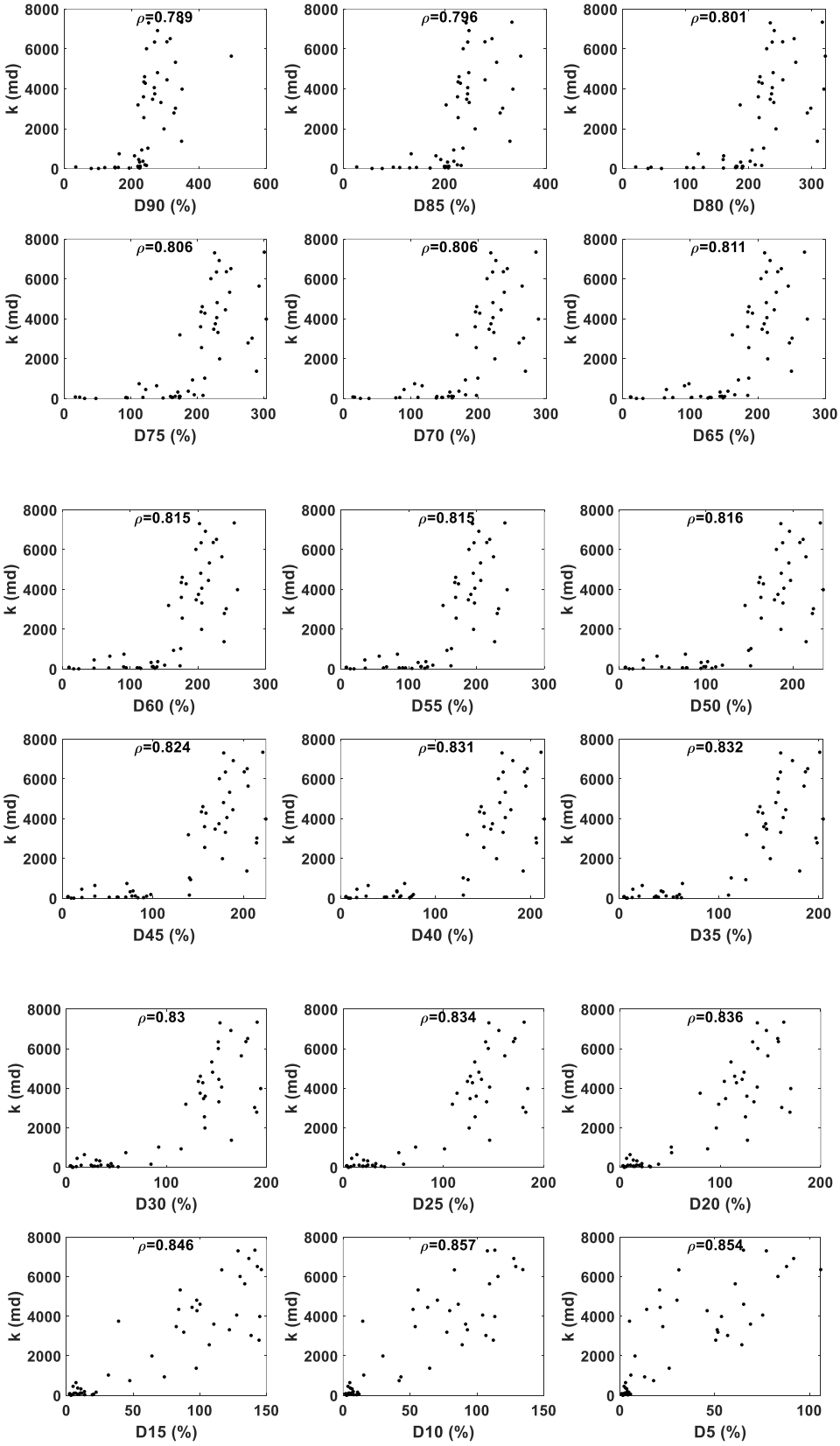
ρ=0.789
k (md)
D90 (%)
ρ=0.796
D85 (%)
ρ=0.801
D80 (%)
ρ=0.806
D75 (%)
ρ=0.806
D70 (%)
ρ=0.811
D65 (%)
ρ=0.815
D60 (%)
ρ=0.815
D55 (%)
ρ=0.816
D50 (%)
ρ=0.824
D45 (%)
ρ=0.831
D40 (%)
ρ=0.832
D35 (%)
ρ=0.83
D30 (%)
ρ=0.834
D25 (%)
ρ=0.836
D20 (%)
ρ=0.846
D15 (%)
ρ=0.857
D10 (%)
ρ=0.854
D5 (%)

Fig. 3-3. Correlation between permeability and selected features. The Spearman's correlation coefficient (ρ) shows how the feature in X axis correlates with permeability.

To identify the multicollinearity between features, the Spearman's correlation coefficient matrix is plotted in Fig. 3-4. A diverse set of features can be selected to avoid multicollinearity based on the matrix. In this work, based on correlations reported in Fig. 3-3, and the Spearman's correlation reported in Fig. 3-4, we have selected D5, D10, and D60 from the PSD characteristics since D5 and D10 have high correlations with permeability, and D10 with D60 have been used extensively in the literature in terms of uniformity coefficient). It also follows the physical justification as the effect of grain size on permeability estimation increases at the lower spectrum of the PSD. Furthermore, due to D60 having a very high correlation with D-values greater than D10, the selected three D-values cover the PSD curve as well as the effect of sorting coefficient and uniformity coefficient. Fines content is highly correlated with D5 and D10 and therefore is removed from the feature set. However, the amount of fines would have a significant impact on permeability. This is because of the effect of fines migration on permeability, so it was decided to investigate the estimation capability of the developed correlation at different fines content intervals.

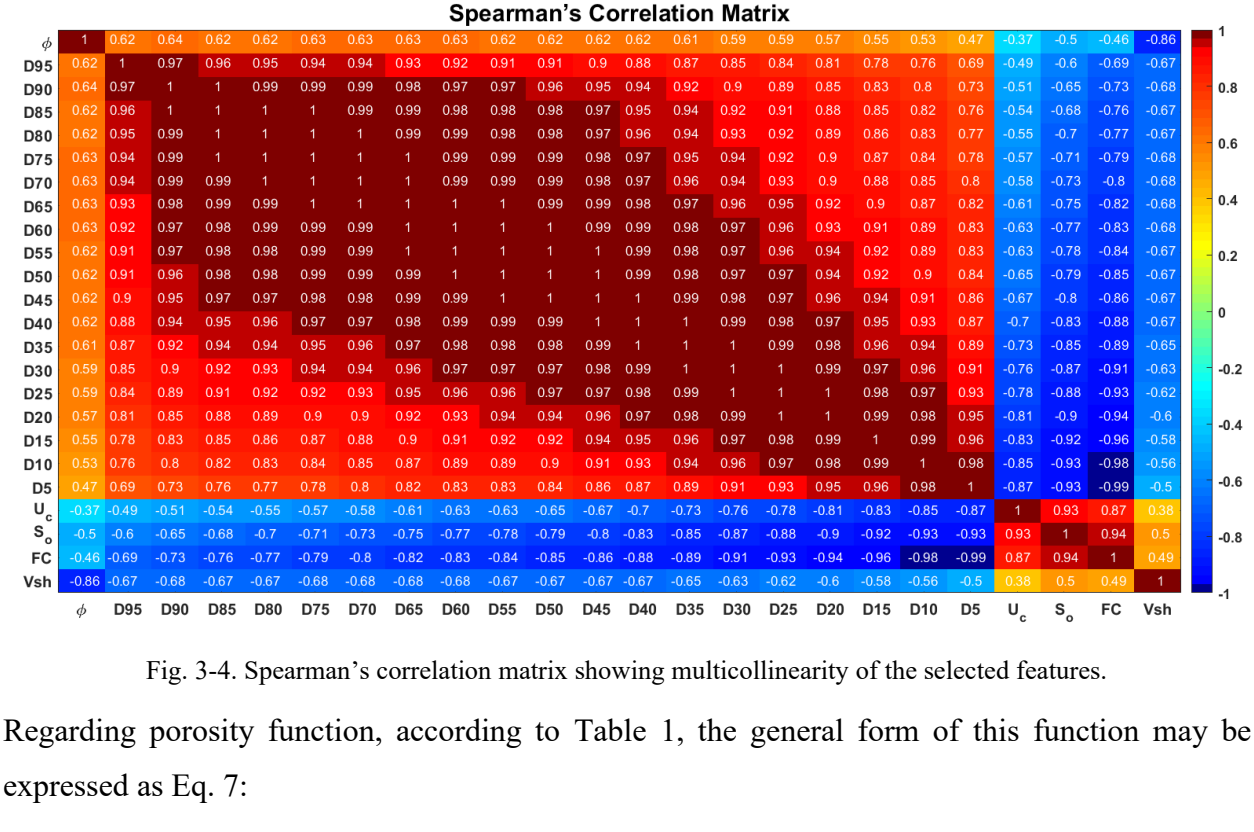

Fig. 3-4. Spearman's correlation matrix showing multicollinearity of the selected features.

Regarding porosity function, according to Table 1, the general form of this function may be expressed as Eq. 7:

$$F(\phi) = \frac{a\phi^b}{(c-\phi)^e} \quad (7)$$

The correlations for permeability estimation are formulated in two modes as Eq. 8 (Mode# 1) and Eq. 9 (Mode# 2):

$$k = (aD_5^2 + bD_{10}^2 + cD_{60}^2) \times \frac{d\phi^e}{(f-\phi)^g} \quad (8)$$

$$k = aD_5^2 + bD_{10}^2 + cD_{60}^2 \quad (9)$$

where a to g are the coefficients that need to be optimized by the GBPSO as the optimization problem. These equations are simple enough to be generalized for other wells for permeability estimation. Besides, their dimension is the same as permeability, and from a reservoir engineering point of view, the parameters are completely relevant for permeability investigation.

To examine the effect of the fines content, we have divided the database into various subsets: less than 10%, less than 20%, and less than 30% fines content.

Fig. 3-5 compares the performance of available empirical equations reported in Table 1. 23 correlations have been reviewed in Table 1 as a part of the literature review, and 15 of which were suitable to be compared to our study in terms of the lithology and other criteria of our correlations. Fig. 3-5 shows the performance of permeability estimation of the 15 correlations. As Fig. 3-5 displays, most estimations are indeed underestimation of the actual value of permeability.

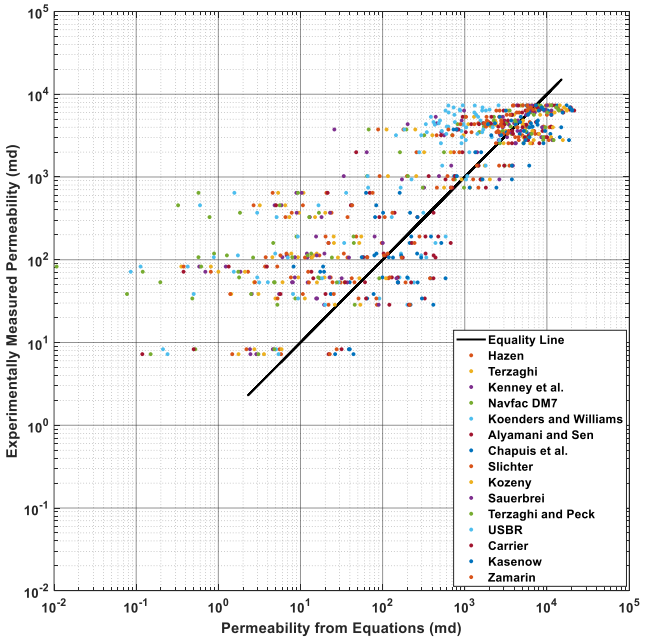

Fig. 3-5. Comparison of performance of available predictors reported in the literature for all wells databases. The estimation ranges by the literature estimations are between 10^{-1} and 10^{+5}.

The effect of fines content on the accuracy of estimations was also investigated for both proposed models. The optimized coefficients are reported in Table 2 and Table 3 for cases with less than 10%, 20%, and 30% fines content. Moreover, the calculated absolute relative errors are displayed in Fig. 3-6, which shows that as the amount of fines content increases, the accuracy of the estimation deteriorates. The correlation coefficients for mode# 1 and #2 are 0.83 and 0.84, respectively, and the Mean Square Error (MSE) and Mean Absolute Error (MAE) for the two modes in Darcy dimension are also provided in Fig. 3-7 and Fig. 3-8, respectively.

Table 2. Optimized coefficients to be used in Eq. 8 based on all wells data in mode#1.

coefficient	all PSDs	less than 10% fines content	less than 20% fines content	less than 30% fines content
a	0.271582	0.146834	0.485899	0.223808
b	0.221815	0.009566	0.035759	0.280664
c	0.004552	0.089893	0.033242	0.000748
d	3.360196	0.038825	0.017366	0.16658
e	1.176038	-1.03258	-0.37786	0.489202
f	7.309735	1.055386	0.338379	0.849123
g	6.70949	-0.41132	-0.15909	0.149418

Table 3. Optimized coefficients to be used in Eq. 9 based on all wells data in mode#2.

coefficient	all PSDs	less than 10% fines content	less than 20% fines content	less than 30% fines content
a	0.115784	0.853052	0.360496	0.08846
b	0.274831	-0.44843	0.112212	0.304658
c	0.002469	0.137788	0.029721	0.000757

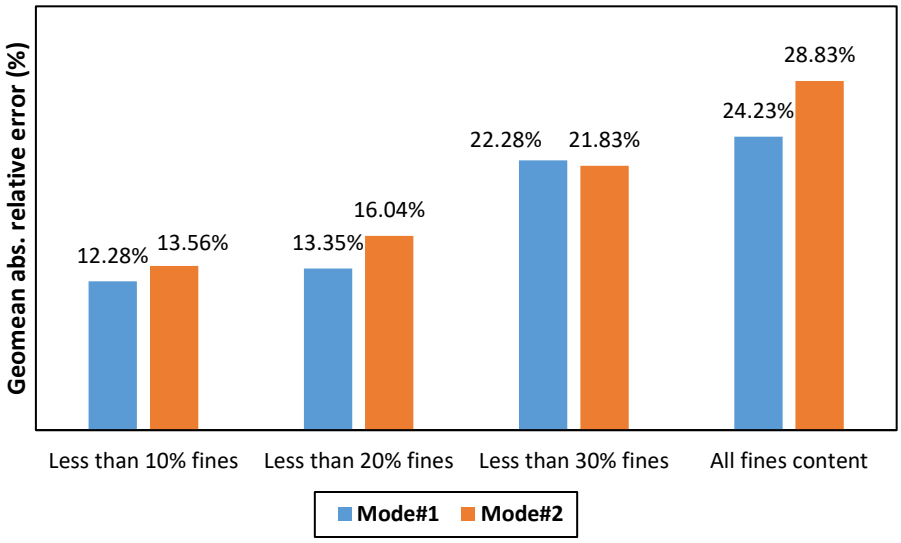

Fig. 3-6. Geomean absolute relative error for all wells data. The Effect of fines content on permeability estimation is presented.

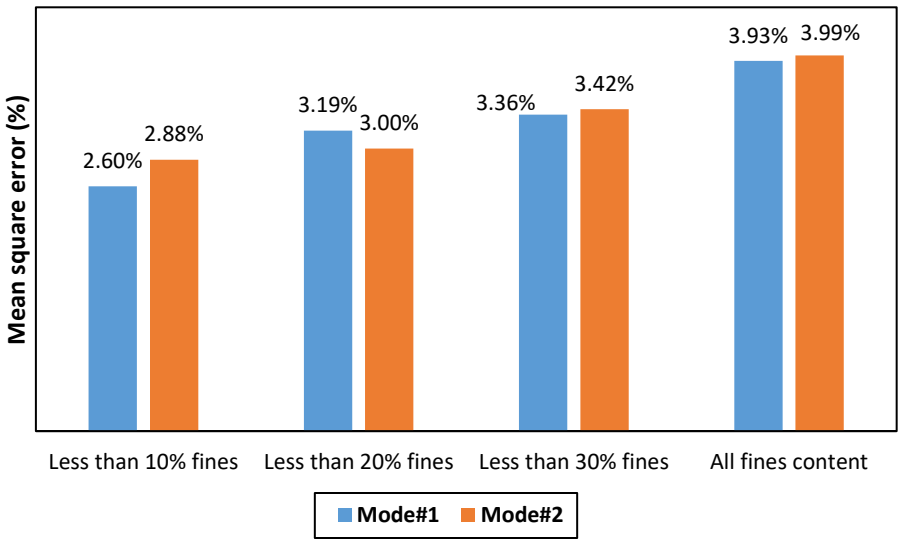

Fig. 3-7. Mean Square Error (MSE) for all wells data.

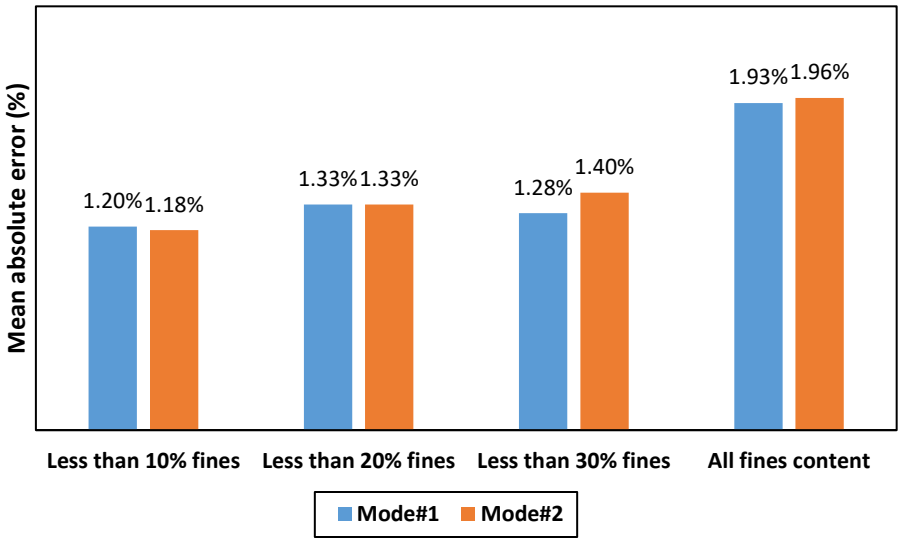

Fig. 3-8. Mean Absolute Error (MAE) of permeability prediction based on all wells data.

To have an assessment of the estimation capability of the proposed models in each well, the D-values and porosity data from each well were used separately to obtain the equations specific to the wells. For brevity, the optimized coefficients for each well are not reported. Fig. 3-9 displays the mean absolute relative error of the equations when employed for wells #1-4. The estimation error decreases compared to the case in which all data points were involved in the model development.

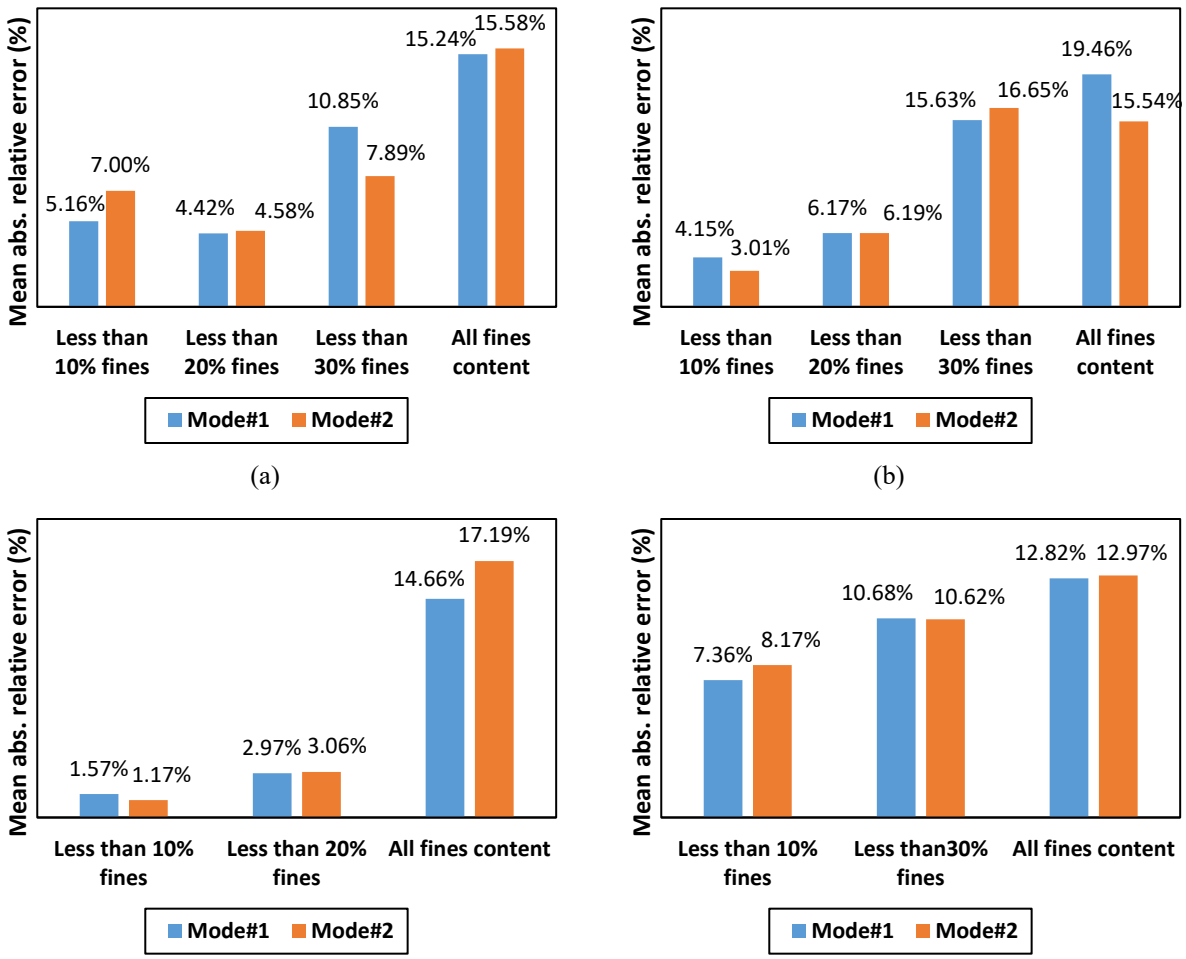

Fig. 3-9. Effect of fines content on permeability estimation for (a) well#1; (b) well#2; (c) well#3; and (d) well#4. It should be noted that in wells# 3 and 4 no fines content between 20% and 30% and 10% and 20% exists, respectively.

To assess the model's predictability for the new data, assess the extent of any overfitting or underfitting, and make sure that our method is generalizable [85, 86], a 5-fold cross-validation was employed. We partitioned the data into five subsets, held out one subset, and trained the model on the remaining datasets. The procedure was repeated for all five subsets. The score of each cross-validation was measured based on the geometric mean of absolute relative errors. Since the obtained score of validation data is remarkably close together (Table 4), we can rely on our method for permeability estimation using other unseen data. Furthermore, as shown in Table 4, the proposed method does not miss any high permeability location in the estimation. This makes the proposed method very reliable for completion engineers to design an appropriate completion method.

Table 4. Five-fold cross-validation in mode#2 for all samples. Since the obtained score of validation data is remarkably close together, we can rely on our method for permeability estimation using other unseen data.

The first cross-validation			The second cross-validation			The third cross-validation			The fourth cross-validation			The fifth cross-validation		
Real value (mD)	Estimate value (mD)	Relative error (%)	Real value (mD)	Estimate value (mD)	Relative error (%)	Real value (mD)	Estimate value (mD)	Relative error (%)	Real value (mD)	Estimate value (mD)	Relative error (%)	Real value (mD)	Estimate value (mD)	Relative error (%)
1990.94	1610.31	19.12	3750.24	2778.82	25.90	327.47	74.61	77.22	4060.83	5836.15	43.72	4452.35	1130.45	74.61
118.75	51.12	56.95	1371.99	1024.08	25.36	2790.91	4083.21	46.30	3316.57	3819.97	15.18	454.86	359.54	20.96
935.07	496.47	46.91	5331.53	1575.48	70.45	28.57	77.57	171.50	3601.27	5056.02	40.40	112.82	51.20	54.62
38.53	9.12	76.33	106.30	173.51	63.24	3986.72	4353.51	9.20	6923.59	6107.49	11.79	3478.06	2887.06	16.99
2556.97	3489.70	36.48	743.33	544.61	26.73	3193.99	2387.75	25.24	61.15	49.83	18.50	7.23	7.77	7.44
7344.30	4289.46	41.59	107.23	146.12	36.27	6347.68	5400.44	14.92	8.29	3.57	56.94	6516.99	6120.56	6.08
190.77	68.07	64.32	59.71	89.54	49.95	4608.33	4270.27	7.34	5641.12	5106.73	9.47	71.60	51.31	28.34
6012.61	5867.69	2.41	6360.24	6394.20	0.53	369.59	80.29	78.28	53.44	18.56	65.26	34.04	65.31	91.88
1024.93	925.30	9.72	643.40	94.55	85.30	82.72	90.93	9.92	4813.30	3718.52	22.74	53.21	44.26	16.82
159.43	96.18	39.68	4281.95	2422.19	43.43	7309.25	4784.65	34.54	3029.15	4504.63	48.71	4348.42	736.53	83.06
Geomean		28.50	**Geomean**		27.85	**Geomean**		28.98	**Geomean**		27.28	**Geomean**		27.40

As shown in Fig. 3-5, all 15 methods in the literature estimate the permeability in the range of 10^{-1} to 10^{+5}; however, based on Fig. 3-10, the proposed method estimates permeability in the range of 10^{+1} to 10^{+4}, showing a significant improvement in the estimation accuracy. The run time using a generic computer setting – Intel® Core™ i5-2410M CPU @ 2.30 GHz and 4 GB of RAM and OS Windows 7 – is 85.56 seconds; therefore, the proposed algorithm is quite efficient.

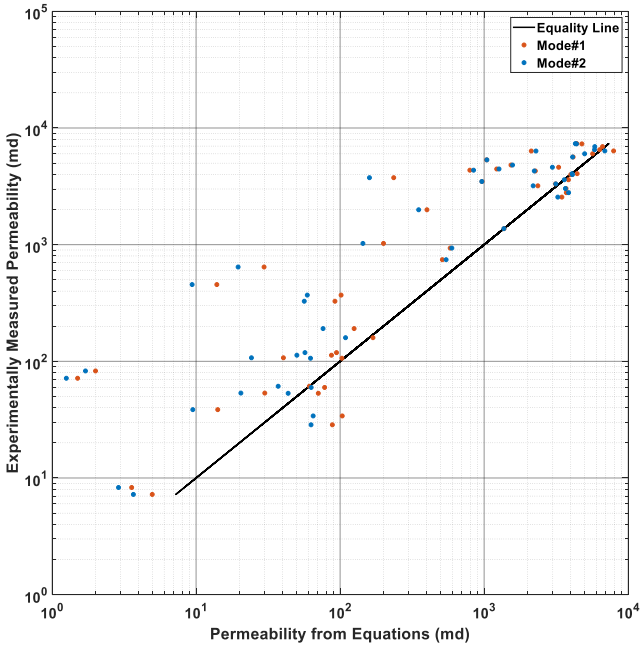

Fig. 3-10. Estimation cross plot for two modes, based on PSD and porosity data (Mode#1), and (2) PSD data only (Mode#2).

Abram and Cain (2014) [87], as the main reference in this field classified the middle McMurray reservoir sand into four sand classes based on the PSDs of the collected samples using an unsupervised hierarchical classification method [88]. Each of the clusters contained at least 13% of the samples. Fig. 3-11 displays the four clusters obtained by Abram and Cain (2014) [87].

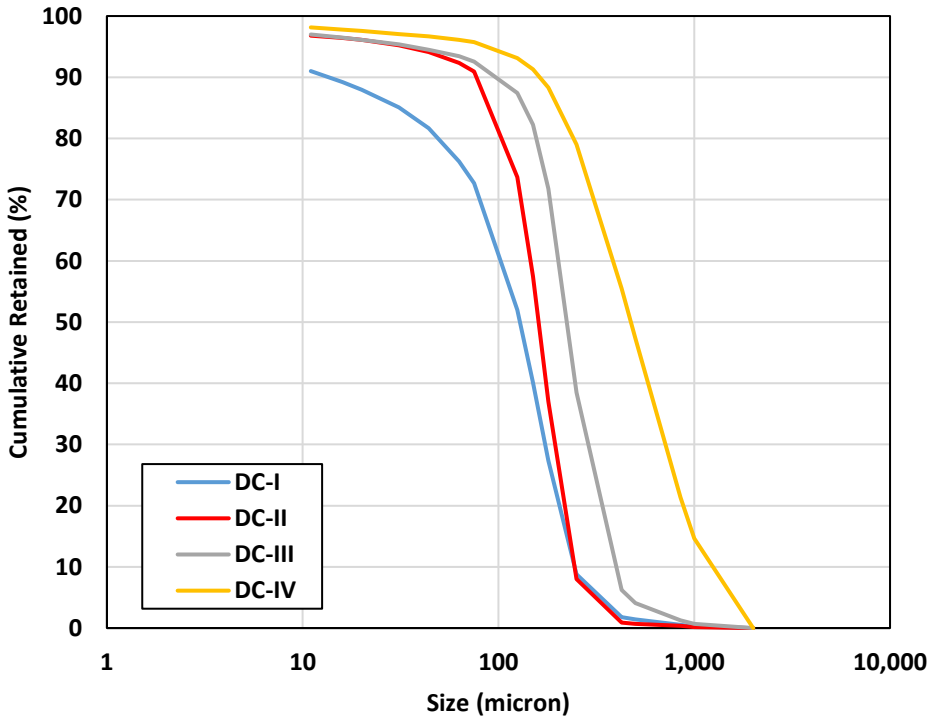

Fig. 3-11. Four distinct clusters of Athabasca oil-sand obtained by Abram and Cain (2014) [87].

However, they did not publish the measured value of the permeability of the cores, and only a range of permeability of each cluster was provided. The characteristics of the center of each cluster are provided in Table 5.

Table 5. Characteristics of cluster centers obtained by Abram and Cain (2014) [87].

Characteristic	DC- I	DC-II	DC-III	DC-IV
No. of Samples	202	556	558	204
Uniformity Coefficient	8.3	2.3	2.3	3.1
Sorting Coefficient	13.1	3.0	3.5	5.9
Fines Content (%)	18.7	5.9	5.4	3.3
D10 (μm)	235	240	380	1080
D20 (μm)	208.28	220.98	350.52	889
D30 (μm)	175.26	198.12	297.18	739.14
D40 (μm)	149.86	175.26	248.92	601.98
D50 (μm)	140	165	230	500

D60 (μm)	106.68	144.78	205.74	391.16
D70 (μm)	81.28	127	185.42	317.5
D80 (μm)	50.8	109.22	160.02	243.84
D90 (μm)	20	80	110	185
Permeability Range (Da)	1.5-4	3-6	4-8.5	5-10

To assess the accuracy of the developed models, several PSD/permeability measurement data of Athabasca oil-sand deposits in Alberta (location of our database) was required to be compared with Abram and Cain (2014) [87] permeability ranges in Table 5. It is important to note that the application of the developed model to one geographic area is justified, as the entire oil-bearing formation has been subjected to the same compaction history. To do this comparison, 102 other samples, in addition to our original 50 samples, were collected from the same geologic setting and their PSD was measured. These samples were clustered into four distinct classes displayed in Fig. 3-12. The details of our clustering algorithm are explained in Izadi et al. (2020) [88].

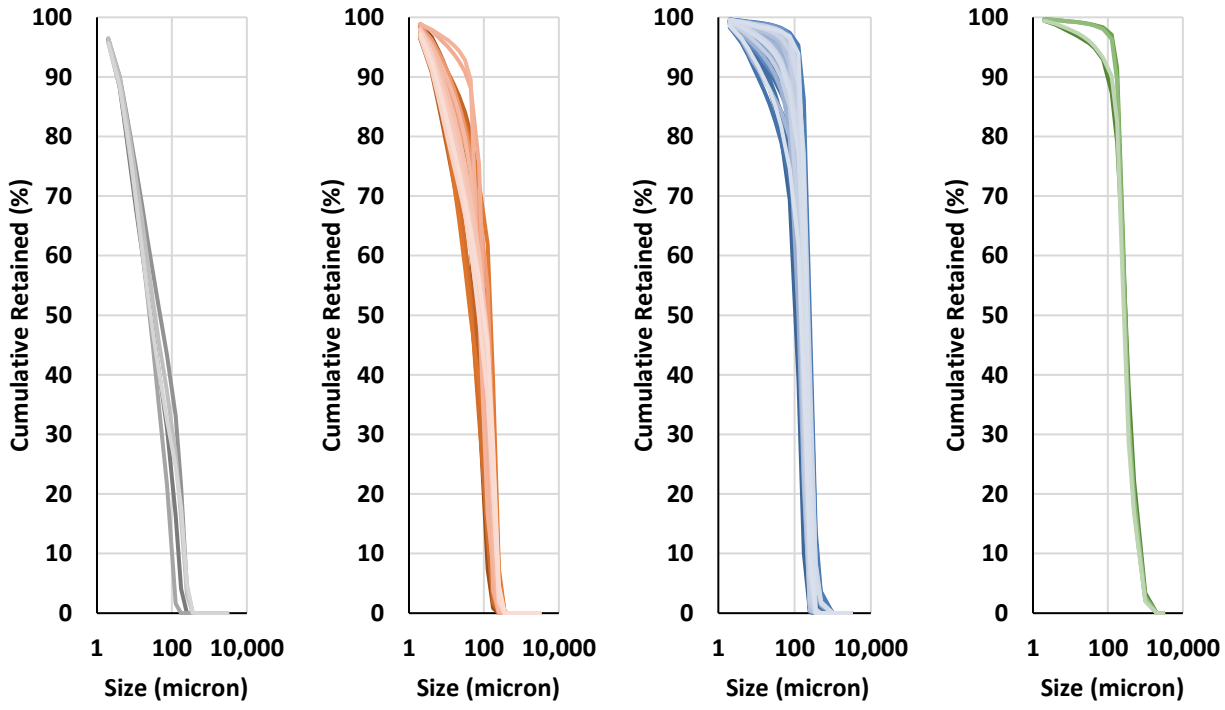

Class 1 Class 2 Class 3 Class 4

Fig. 3-12. Four distinct clusters of the collected samples in this study. The details of our clustering algorithm are explained in (Izadi et al., 2020) [88].

We simply named our clusters Class 1 to 4. Table 6 presents the characteristics of the clusters' centers. The predicted permeabilities for the studied clusters are Class 1: 9 mD, Class 2: 44 mD, Class 3: 4,367 mD, and Class 4: 17,196 mD, considering the fines content.

Table 6. Characteristics of cluster centers of collected samples.

Characteristic	Class 1	Class 2	Class 3	Class 4
No. of Samples	7	27	61	7
Uniformity Coefficient	22.62	17.51	3.35	1.92
Fines Content (%)	41.87	28.09	6.10	3.21
D10 (μm)	170.18	223.52	276.86	782.32
D20 (μm)	147.32	190.5	236.22	492.76
D30 (μm)	127	160.02	218.44	383.54
D40 (μm)	106.68	137.16	198.12	327.66
D50 (μm)	86.36	106.68	180.34	289.56
D60 (μm)	58.42	73.66	160.02	254
D70 (μm)	27.94	43.18	139.7	226.06
D80 (μm)	12.7	22.86	111.76	200.66
D90 (μm)	5.08	7.62	58.42	170.18
Estimated Permeability (mD) [All PSDs]	9	44	1,134	10,392
Estimated Permeability (mD) [Less than 10% fines content]	NA	NA	4,367	17,196
Estimated Permeability (mD) [Less than 20% fines content]	NA	NA	1,780	13,019
Estimated Permeability (mD) [Less than 30% fines content]	NA	NA	1,156	10,582

Comparing channel base sands (Class 4) to disseminated fines in lower quality sands or minor brecciated intervals (Class 3) to poor reservoir (Class 2) to non-reservoir (Class 1), there are significant differences in permeability among these classes (Table 7). These differences would affect the steam chamber growth in SAGD wells (Table 7).

Table 7. The comparison between the permeability of the different classes considering all PSDs.

	Class 1	Class 2	Class 3	Class 4
Class 1	1	5	126	1155
Class 2	5	1	26	237
Class 3	126	26	1	10
Class 4	1155	237	10	1

A comparison of our clusters with the ones obtained by Abram and Cain (2014) [87] is presented in Fig. 3-13. Based on Fig. 3-13, Class 3 has a similar PSD curve to DC-II [87], and the predicted permeability for both cases is close, considering the formula is developed for fines content below 10%. Additionally, Class 4 is between DC-III, and DC-IV clusters of Abram and Cain (2014) [87] and the permeability order is also comparable. Based on the presented results in Table 6 and Table 7, and Fig. 3-13, our estimations are in a reliable and reasonable range in Athabasca oil-sands, which serves to validate our developed models.

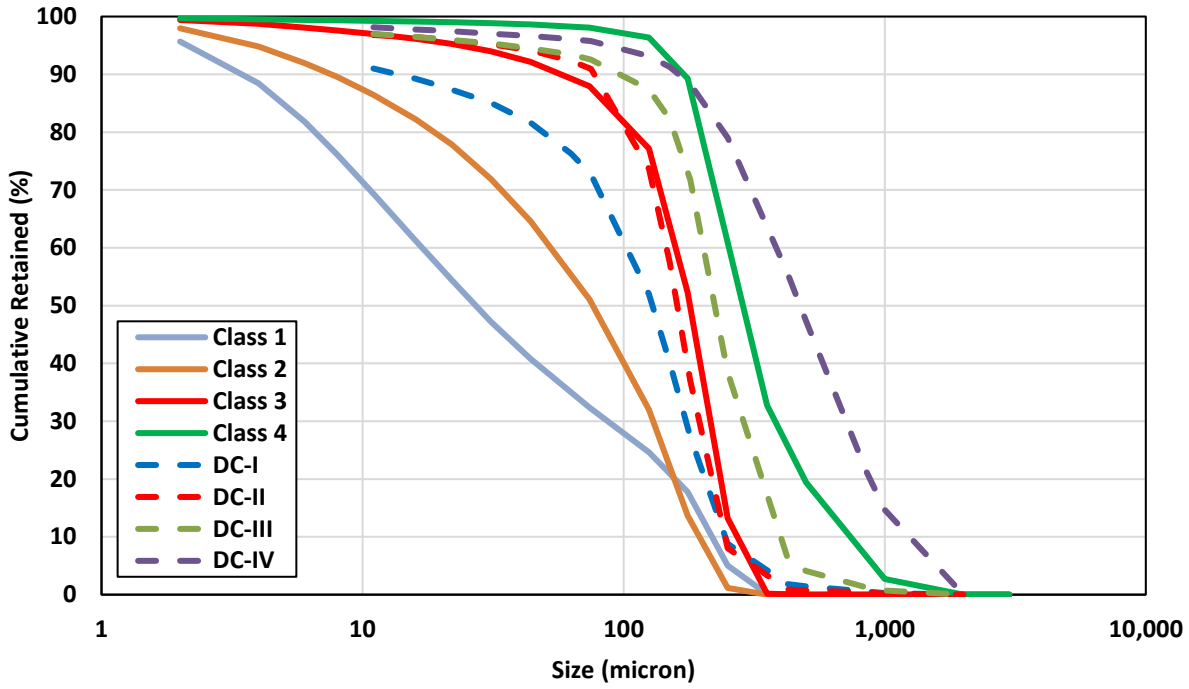

Fig. 3-13. Comparison of cluster centers of collected samples in this study and cluster centers obtained by Abram and Cain (2014) [87].

3.3.3. Reservoir Model# 2

Reservoir model #2 is employed to examine how varying subcool temperatures affects oil production increase and cSOR reduction. Furthermore, different pressure drops in relation to flow rates for various LDICDs are analyzed to determine the optimal LDICD for this reservoir. In contrast, reservoir model #1 maintains constant reservoir heterogeneity across all flow rate control strategies.

3.3.3.1. Clustering

Limited studies have been performed to provide a method to cluster PSDs in SAGD projects. There have been few examples of systematic clustering of the oil sand PSDs in Western Canada. For example, Carrigy (1966) developed a classification based on the similarity of PSDs and particle size by categorizing the PSD curves into three main categories: (1) coarse, (2) fine, and (3) very fine sands and silts [89]. Abram and Cain (2014) have developed another classification for the PSDs of the Devon Pike 1 project [87]. They used a dynamically growing self-organizing hierarchical clustering algorithm previously developed by Luo et al. (2004) [90]. Later, Fattahpour et al. (2017) performed another classification based on the provided data by Carrigy (1966) and two sets of PSDs provided by Mahmoudi et al. (2015) [91] from two wells in the McMurray

Formation [92]. Fattahpour et al. (2017) only used the similarity between D_{10}, D_{50}, and D_{70} for their classification. They finally provided four major and two minor classes. They also compared their results and the classes provided by Carrigy (1966). Abram and Cain (2014) and Fattahpour et al. (2017) argued that having a limited number of PSD classes for sand control design is preferred. Therefore, a major advantage of this clustering approach is that a limited number of groups are identified during the process, maximizing the uniqueness among clusters. The need for a new PSD classification arises because the PSD categories suggested by Abram and Cain (2014) are exclusive to the Pike 1 project. Additionally, it is believed that relying on Carrigy's (1966) proposal of just three PSD groups is inadequate in encompassing the diverse range of size distributions observed in the McMurray oil sands. In addition, Fattahpour et al. (2017) manually manipulated the number of clusters under human expert supervision. In this section, we developed an unsupervised and self-adaptive clustering algorithm for clustering a wide range of PSD, eliminating the need to determine the number of clusters beforehand.

The PSD database contains 40 PSDs collected from four vertical wells in the McMurray Formation of the Athabasca oil sands. As shown in Fig. 3-14, a mechanical sieve size analysis following ASTM D422-63(2007)e2 standard has been conducted with the same procedure and the cumulative retained percentage of the particles versus the mesh size is measured and plotted [93].

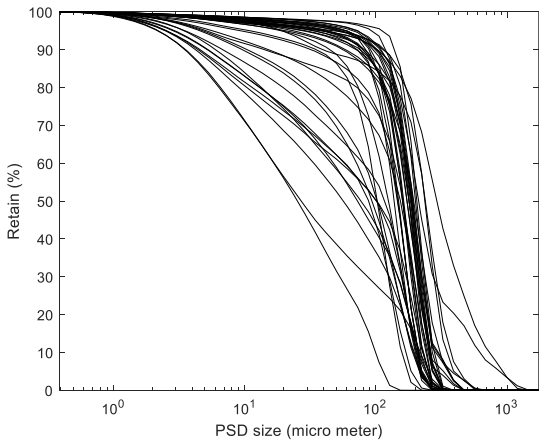

Fig. 3-14. The PSD curves of the database.

Depending on the measurement procedure, PSD values may be measured using various mesh sizes and the quantity of sample that passes or is retained. Therefore, we defined 18 standard mesh sizes (Table 8), and all input data is linearly interpolated to these standard sizes. Our objective was to minimize the need for interpolation in the data, which is why these sizes were specifically chosen

to require the least amount of interpolation. Afterwards, PSD data are assigned to the clustering algorithm to determine the representative PSDs and the corresponding PSD characteristics.

Table 8. Our 18 standard sieve sizes used in this study.

Mesh number	Mesh size (mm)	Mesh number	Mesh size (mm)	Mesh number	Mesh size (mm)	Mesh number	Mesh size (mm)
1	2	6	16	11	125	16	1000
2	4	7	22	12	176	17	2000
3	6	8	31	13	250	18	3000
4	8	9	44	14	354		
5	11	10	74	15	500		

The workflow of the proposed clustering algorithm is shown in Fig. 3-15. The input data for the clustering algorithm consists of the PSD values and their corresponding sieve sizes. Additionally, it is necessary to assign a minimum similarity threshold to the algorithm. In the pre-processing and feature extraction step, interpolation is performed to establish a consistent sieve size scale, and the values are normalized to ensure equal weighting for each sieve size in the clustering algorithm. The proposed clustering algorithm is an online and incremental-dynamic learning algorithm, and the logic to develop the proposed clustering algorithm is adopted from the Adaptive Resonance Theory (ART) [83]. This algorithm is more efficient than the k-means algorithm because it visits agents once. Without any preliminary training, the proposed clustering algorithm allows not only the category templates to adapt to current circumstances but also the online creation of categories during classification sessions. This twofold flexibility could overcome the stability/plasticity dilemma and lead to real-time and incremental-dynamic learning and pattern recognition [94].

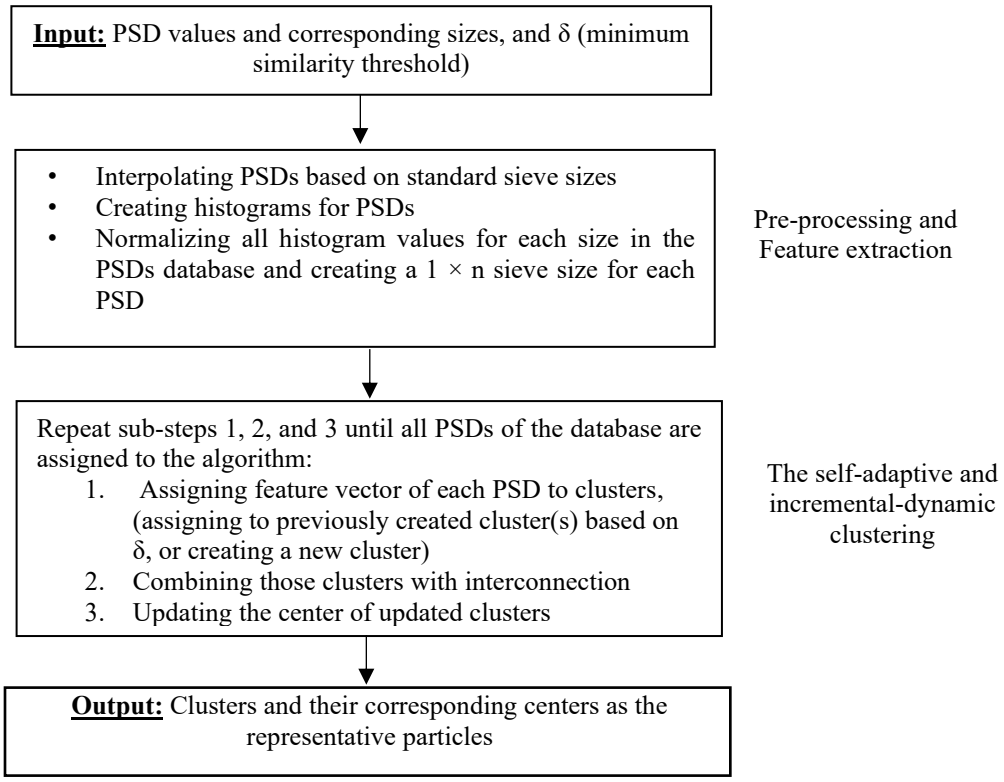

Fig. 3-15. Proposed workflow. PSD values are assigned to the algorithm with the minimum similarity (δ). The output is clusters and their corresponding centers as the representative particles.

The similarity threshold for comparing incoming data with previously created clusters is measured as Eq. 10:

$$Sim = 1 - \frac{Euclidean\_distance}{\sqrt{n}} \quad , \quad 0 \le Sim \le 1 \qquad (10)$$

where $Euclidean\_distance = \sqrt{\sum_{i=1}^{n}(x_i - y_j)^2}$, n is the number of mesh sizes, X_i=[x_1, x_2, ..., x_n] are assigned PSDs and Y_j=[y_1, y_2, ..., y_p] are center of previously created clusters. The steps of the proposed clustering algorithm are presented as follows (Sadri et al., 2006).

1. Adjust the minimum similarity threshold (δ).
2. Cluster centers list= ø.
3. Read the next input PSD.
4. Find all similar clusters' centers to the inputted PSD with a similarity greater than δ.

   If found: assign the PSD to the (those) cluster(s), update the center of the (those) cluster(s), and combine those clusters which have at least one common PSD.

   If not found: create a new cluster and set the inputted PSD as a new cluster center.

5. Repeat steps 3-4 for all the input PSDs.

Based on step#4 (combination of clusters), the algorithm tries to minimize the number of clusters. This approach is based on a common PSD with greater similarity than δ with more than one cluster center, and this PSD merges all clusters with a similarity greater than δ. The criteria for adding the inputted well-pad to the previously created cluster(s) or creating a new cluster is presented in Eq. 11:

$$\forall x_i \,\&\, M_{j,} \quad i = 1{:}N \,\&\, j = 1{:}P \begin{cases} Sim\left(x_i, x_{jc}\right) \geq \delta \rightarrow x_i \in M_j \\ Sim\left(x_i, x_{jc}\right) < \delta \rightarrow create\ M_{j+1} \,\&\, x_i = x_{(j+1)c} \end{cases} \tag{11}$$

where j is the number of created clusters, i is the number of PSDs, M_j is the j[th] cluster, x_i is i^{th} PSD, and x_{jc} is the center of the j[th] cluster. The optimum value of δ (minimum similarity threshold) is set as 0.88 by trial and error; however, the user can change the δ and observe the results of the corresponding clustering and representative PSDs. By selecting larger values for δ, the number of clusters would be increased while the number of PSDs in each cluster would be decreased. In addition, the similarity of the PSD curves in each cluster would be higher. We have also chosen those clusters in which at least 90% of all PSDs in the database are covered. The idea is borrowed from the study conducted by Abram and Cain (2014) [87], each cluster encompasses at least 13% of the dataset, and multiple iterations were conducted to identify these clusters. Classes that represented less than 10% of the total dataset were disregarded. The researchers argued that, while investigating a large number of histogram clusters across a reservoir could be advantageous for scientific purposes, it is more practical and reasonable to categorize the PSD into fewer classes for well completion purposes.

The clustering results for five clusters covering 93% of the database (Fig. 3-14) are also shown in Fig. 3-16. As indicated in Fig. 3-16, particles within Clusters #4 and #5 are larger compared to those in Cluster #1. Additionally, there are variations in the D values. To highlight these differences more prominently, we have depicted the centers of the clusters in Fig. 3-17. The disparities between the centers of the clusters become more evident through this illustration.

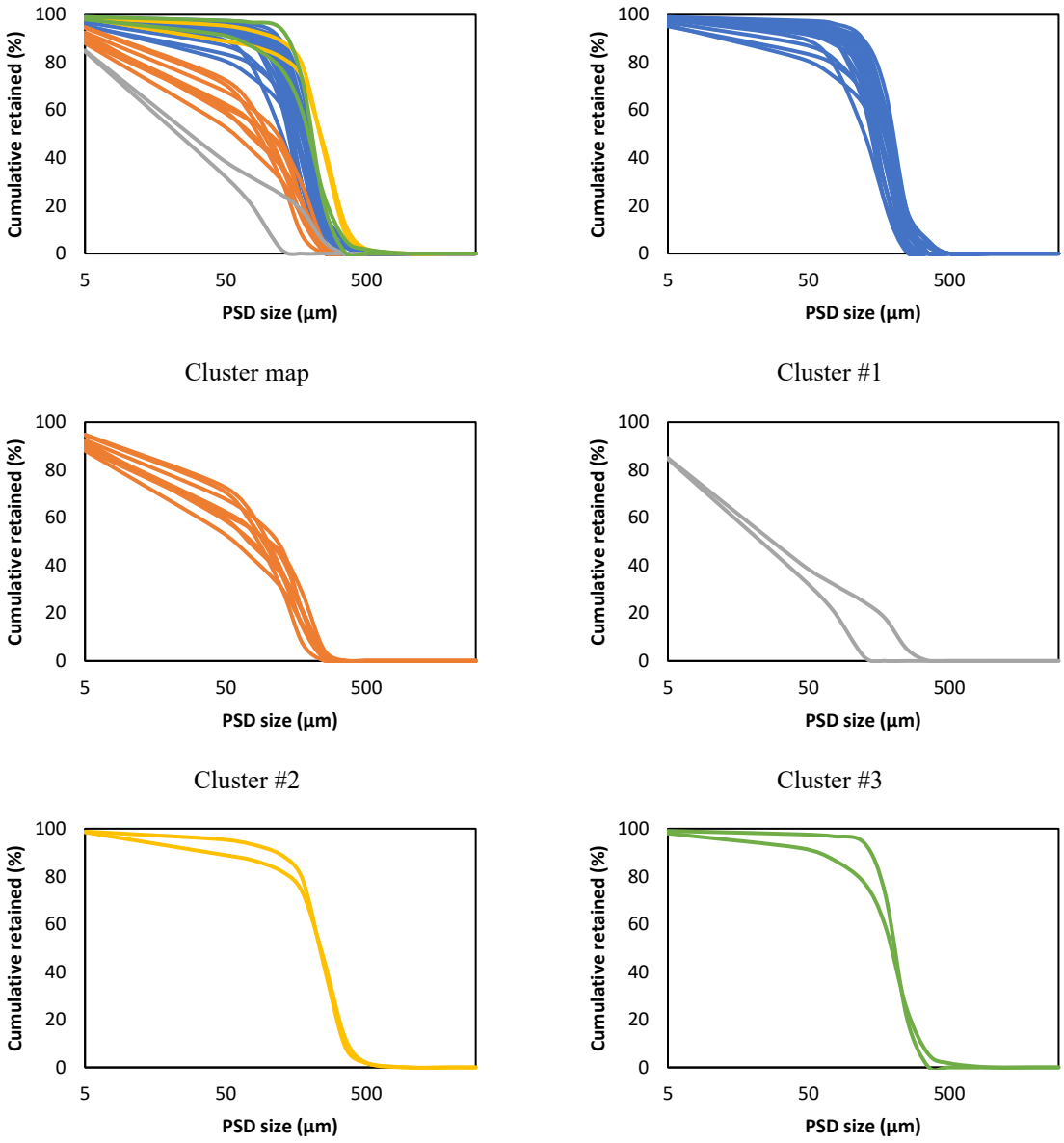

Cluster map

Cluster #1

Cluster #2

Cluster #3

Cluster#4

Cluster#5

Fig. 3-16. Results for the proposed method for clustering.

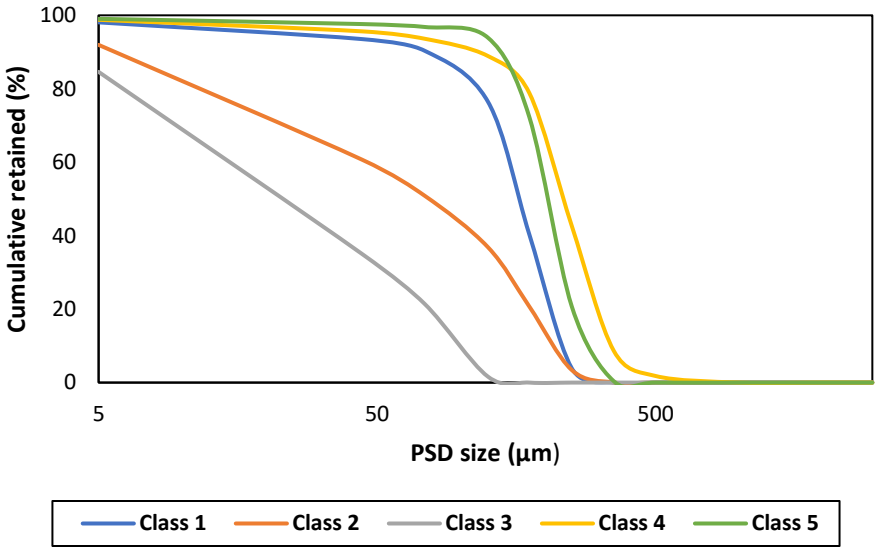

Fig. 3-17. Center of the clusters. These representative PSDs are used to assign porosity and permeability distributions in numerical simulation models.

Table 9. The number of clusters, coverage percentage, retained D_{95}, D_{90}, and D_{40}, average fines content, and estimated permeability using Eq. 9 and Table 3.

	Coverage (%)	Retained D_{95} (mm)	Retained D_{90} (mm)	Retained D_{40} (mm)	Average fine contents (%)	Estimated permeability (mD)	Estimated permeability for the relatively close cluster reported by Izadi et al. (2022-a) (mD)
Cluster #1	55	31.47	75.35	176.69	6.55	5,177	4,367
Cluster #2	23	3.11	7.45	113.62	35.05	1,510	44
Cluster #3	5	1.62	3.25	40.14	62.05	189	9
Cluster #4	5	53.60	93.59	232.72	7.47	8,401	10,392
Cluster #5	5	72.96	85.97	215.20	5.26	7,782	10,392

Fig. 3-17 displays the centers of the clusters, encompassing both the centers of the clusters used to develop Eq. 9, and the centers of the clusters utilized for estimating permeability based on the PSDs of the well in this section. In addition, the number of clusters, coverage percentage, retained D values, average fines content, and estimated permeability using Eq. 9 are presented in Table 9. The number of clusters, coverage percentage, retained D_{95}, D_{90}, and D_{40}, average fines content, and estimated permeability using Eq. 9 and Table 3.. The curves associated with the prominent clusters identified as Class 1, Class 2, and Class 3 in this section closely resemble Class III, Class II, and Class I from section 3.3.2.1 Permeability Estimation, respectively. Additionally, Classes 4 and 5 fall within the spectrum between classes III and VI. Referring to the data presented in Table 9 and the permeability values of the clusters from Table 6, it is observed that, apart from Class II, the permeability values for these clusters are relatively close together. The lower permeability value for Class II can be attributed to the significant fines content, as reported in Table 6.

Consequently, given that the curves for the Classes representing the majority of the database align well with the curves shown in Fig. 3-18, and the estimated permeability are relatively close together by considering the fines content, it is plausible to consider employing the relationship and coefficients presented in Table 3 for permeability estimation.

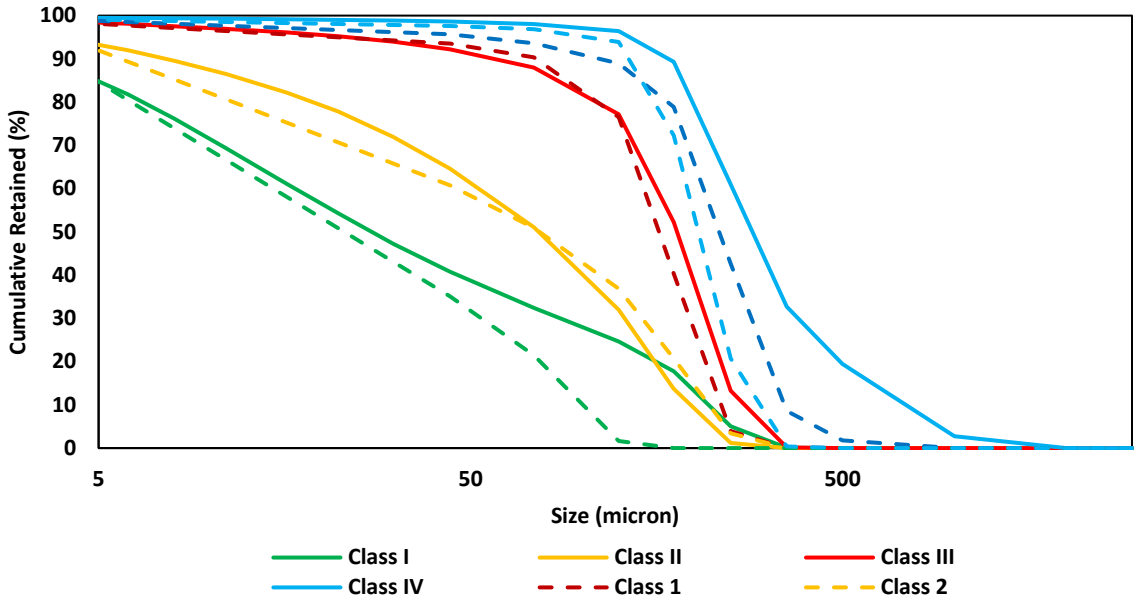

Fig. 3-18. Class I to Class IV are the center of the clusters of the database used to develop Eq. 9 between the PSD and permeability. Class 1 to Class 5 are the center of the clusters of the well in this section.

3.3.3.2. Reservoir Model

A SAGD reservoir model adapted from Athabasca oil sands in Western Canada is created for the field where the core and PSD data were extracted. The reservoir properties of the model can be found in Table 10 [121, 96], and sequential gaussian simulation [97] is performed to construct a realization of porosity and permeability distribution based on core analysis data obtained from Accumap database and PSD data of five neighboring wells using the correlation proposed by [102].

Table 10. The reservoir model properties in this study. The properties are adapted from the Athabasca oil sands in Western Canada [121, 96].

Parameter	Value	Unit	Parameter	Value	Unit
Reservoir Grid	100×31×65		Thermal conductivity phase mixing oil phase	1.25E+04	J/(m×day×C)
Reservoir size	1300×62×65	meters	Thermal conductivity phase mixing water phase	5.35E+04	J/(m×day×C)
Water saturation	0.19		Volumetric heat capacity	2.35E+06	J/(m3×C)
Oil saturation	0.81		T-dependent coefficient	0	J/(m3×C×C)
Initial Temperature	12	˚C	Thermal conductivity phase mixing mode	Complex	
Formation compressibility	2.90E-06	1/kPa	Thermal conductivity phase mixing reservoir rock	6.60E+05	J/(m×day×C)

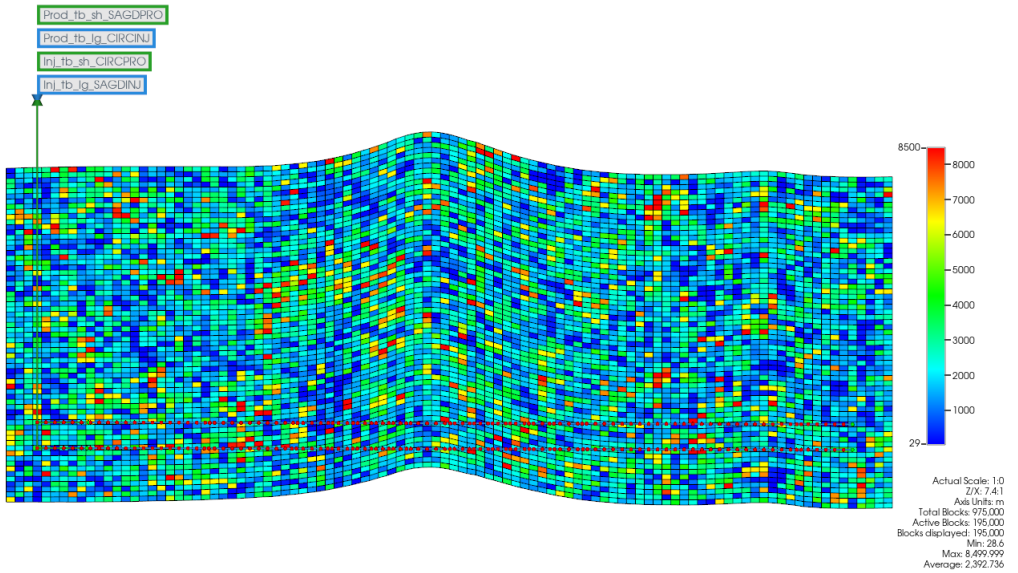

Fig. 3-19. IK view of the permeability distribution in the reservoir model. The porosity and permeability values are populated by the sequential Gaussian simulation based on conditioning data extracted from core and PSD measurements obtained from nearby wells.

To generate a proper table for ICDs simulation, published results of another LDICD experimental study involving a developed testing flow loop are used [34]. Three ICDs used in this study are shown in Fig. 3-20. In the experimental setup of flow capacity and configuration by Yusuf et al. (2021), special consideration was made to ensure the flow regimes closely resemble those during SAGD operating conditions. It is important to note that the pressure measurement locations and types were chosen to record the steady-state circumstances reflecting the change according to the nozzle/orifice shape [95]. The key advantage of employing a table-based ICD input simulation would be a physics-based mechanistic model rather than using empirical correlations. Based on

the passing flow rate inside the ICDs and the given table, the simulator applies the given ΔP in the table.

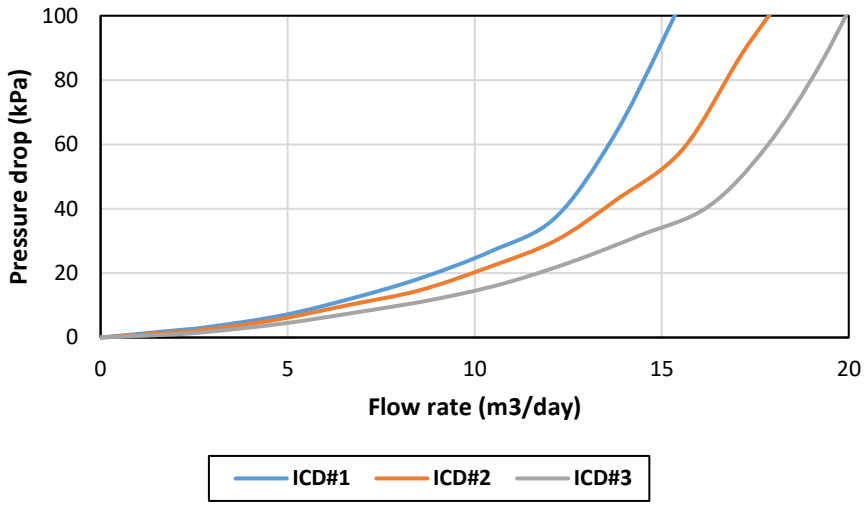

Fig. 3-20. Pressure versus mass flow rate for three ICDs used in this study [34].

3.3.2.2. Reservoir Model

Based on open-source databases, such as Accumap and AER reports [121], a reservoir model derived from a typical SAGD project in Athabasca oilsands is developed and simulated. The top of the reservoir formation is extracted from the reported depth by operators in Accumap and the topography of the models has been generated. Table 11 shows the reservoir characteristics of the model, while porosity and permeability for different cases of reservoir heterogeneity would be different [96 , 121]. The homogeneous, simple with shale barriers, and heterogeneous reservoir models are shown in Fig. 3-21. The homogeneous and simple with shale barriers reservoir models are defined by porosity and permeability of 32.83% and 4925 mD in I and J directions with 4121 mD in the K direction, respectively (Fig. 3-21-a and b). Shale barriers are strategically positioned in various locations, including between the wells, on top and bottom of the injector and the producer wells, and in some blocks where the wells are drilled. For the heterogeneous model, sequential Gaussian simulation [97] is performed to construct a realization of porosity and permeability distribution obtained from core analysis and PSDs data of five neighboring wells using the correlations 8 and 9 [84] (Fig. 3-21-c). To assess various control strategies for inflow and outflow rates, we conducted a single realization of the reservoir through SGS simulation. Essentially, we established a constant reservoir condition and examined different strategies within the same reservoir. Our focus was on investigating the influence of FCDs in regions with

exceptionally low permeability. To achieve this, we modified the reservoir model to position these low-permeability areas in close proximity to wells, creating a heterogeneous model for analysis. Due to the low interfacial tension between oil and water at elevated temperatures, capillary pressure is neglected. For boundary conditions, the top and bottom surfaces of the model are impermeable to flow, but heat transfer is permitted according to Vinsome and Westerveld's (1980) [98] heat loss model. At the side walls of the model, symmetry conditions exist. Subcool for the simulation is set between 10°C to 15°C.

Table 11. The reservoir model properties in this study. The properties are adapted from the Athabasca oil sands, Western Canada.

Parameter	Value	Unit	Parameter	Value	Unit
Reservoir size	1040×62×50	meters	Thermal conductivity – phase mixing oil phase	1.25E+04	J/(m×day×°C)
Water saturation	0.19		Thermal conductivity – phase mixing water phase	5.35E+04	J/(m×day×°C)
Oil saturation	0.81		Volumetric heat capacity	2.35E+06	J/(m^3×°C)
Initial Temperature	12	°C	T-dependent coefficient	0	J/(m^3×C×°C)
Formation compressibility	2.90E-06	1/kPa	Thermal conductivity phase mixing mode	Complex	
Steam temperature	230	°C	Thermal conductivity phase mixing reservoir rock	6.60E+05	J/(m×day×°C)

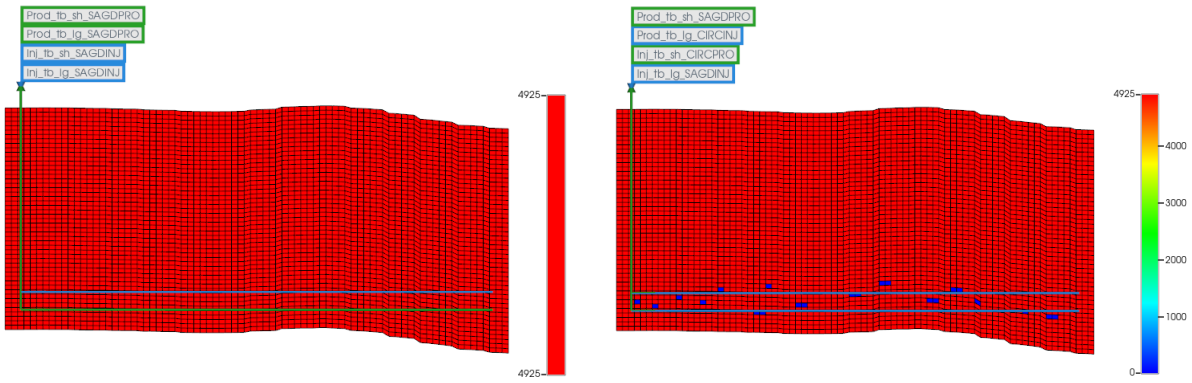

a b

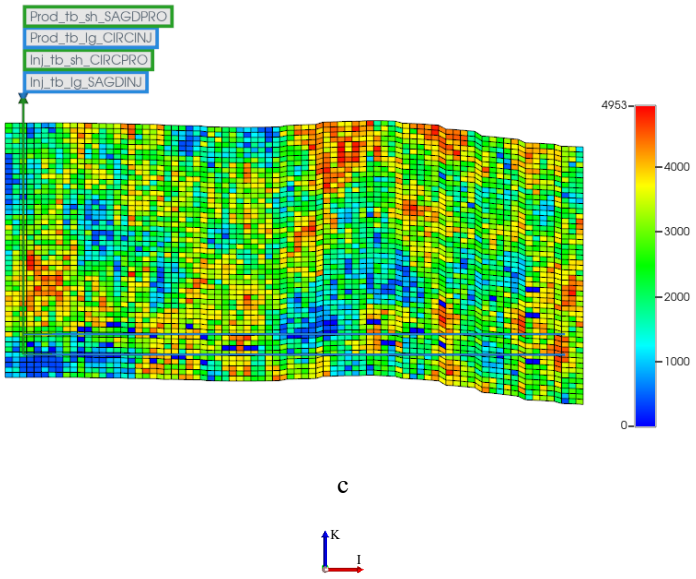

Fig. 3-21. IK view of the permeability in the horizontal direction: (a) homogeneous, (b) simple with shale barriers (blue blocks), and (c) heterogeneous reservoirs.

The geometry of the shale barriers shown in Fig. 3-21-b is summarized in Table 12. As presented in Table 12, different scenarios are introduced, and the impact of OCDs and ICDs is investigated for each case. Based on our investigations and learnings from Fatemi (2012) [67], we decided to distribute the shale barriers in the reservoir model with the mentioned width and length in Table 12. We tried to include the most relevant possible cases for the shale barriers nearby wells. A homogeneous reservoir is also considered as a base case to compare the effects of the FCDs in these locations.

Table 12. The geometry of the shale barriers.

Case#	Size (length × width)	Vertical distance from wells (injector / producer)	location
1	13×14	Two meters from injector	On bottom
2	13×14	One meter from injector	On bottom
3	13×14	One meter from injector	On top
4	13×14	Two meters from injector	On top
5	26×2	Zero	The same block with the well
6	26×2	Two meters from injector	On top
7	26×2	Two meters from injector	On bottom
8	26×2	One meter from injector	On top
9	26×2	One meter from injector	On bottom
10	13×14	One meter from producer	On top
11	13×14	Two meters from producer	On top

12	26×2	Zero	The same block with the well
13	26×2	One meter from producer	On top
14	26×2	Two meters from producer	On top

A published flow-loop data has been used to model ICDs in our SAGD simulation, allowing for generating an appropriate table for the ICDs [34]. Pressure drop versus flow rate tabular data of the ICD used in this reservoir model is shown in Fig. 3-22 [34]. The key advantage of employing a table-based ICD input simulation would be a physics-based mechanistic model rather than using empirical correlations. In the experimental setup of flow capacity and configuration by Yusuf et al. (2021) [34], special consideration was made to ensure the flow regimes closely resemble those during SAGD operating conditions. To simulate OCDs, an orifice nozzle with 4 mm diameter and discharge coefficient of 75% has been used.

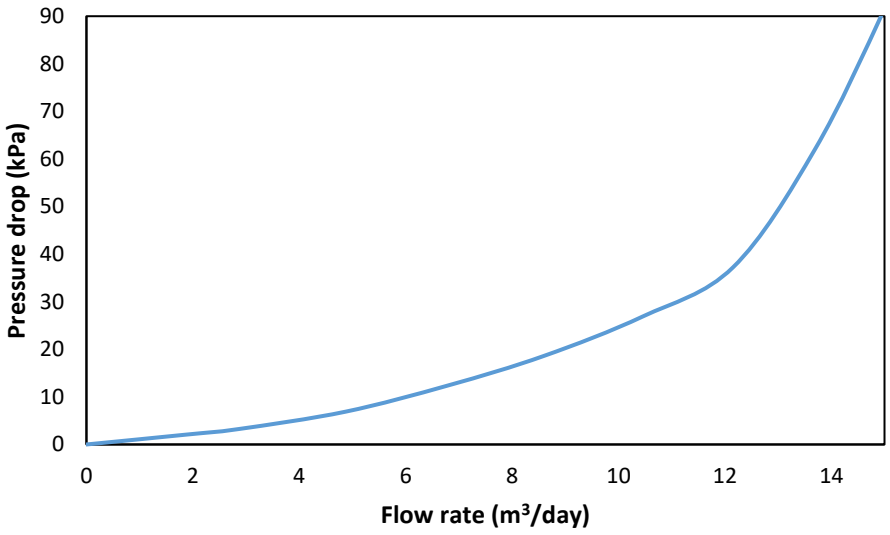

Fig. 3-22. Pressure drop versus flow rate for the ICDs used in reservoir model# 1 [34].

To establish liquid pool control in our simulation, the Steamtrap2 constraint has been used. The liquid pool control creates resistance around the production well to prevent steam escape from the steam chamber to the production well. Steamtrap2 has a smooth transition from the circulation period to the SAGD period; therefore, steam production during this transition period is expected. The simulator would reduce the steam production CWE by a coefficient factor. After this transition period, if the steam production continuously increases or exceeds 0.1 m^3/day CWE, the occurrence of SBT is flagged in our simulations.

3.4. Different Reservoir Heterogeneity Scenarios: Impact of Flow Rates Control

This section delves into the effects of utilizing FCDs to manage inflow and outflow rates on the performance of SAGD wells. The focus is on the impact of FCDs to enhance oil production and reducing the cSOR. To assess the impact of different flow control strategies, a retrospective analysis is conducted using historical data from Canadian SAGD operations. Additionally, numerical simulations are performed for various reservoir types, including homogeneous, simple with shale barriers, and heterogeneous reservoirs [9, 99, [100] 121]. These simulations incorporate FCDs based on findings from published flow-loop experiments. The primary benefit of incorporating flow-loop experiment data into the simulation lies in creating a mechanistic model grounded in physics, as opposed to relying on empirical correlations. By comparing the outcomes of both real-world data and numerical simulations, this study draws conclusions regarding the influence of different flow rate control strategies on SAGD performance.

Drawing from authentic historical data extracted from a database encompassing seven prominent SAGD projects in Western Canada, it is observed that the optimal approach to enhance oil production and reduce cSOR involves the joint utilization of LDICDs and LDOCDs.

Given the limited availability of public information concerning the technical intricacies of flow rate control and its implications on SAGD well performance, a series of simulations across diverse reservoir scenarios were conducted to investigate the mechanisms underlying the impact of FCDs in SAGD well performance. The numerical simulation findings revealed that the combined deployment of LDICDs and LDOCDs effectively managed hot-spot zones, where the inflow rate exceeded that of other sections along the producer well, leading to improved steam distribution. These results showed a potential increase in oil production of up to 26% and a reduction in cSOR of up to 17%.

This section endeavors to enhance our comprehension of how the control of flow rates through FCDs influences the performance of SAGD wells. The primary objective is to pave the way for more efficient well designs that contribute to reduced GHG emissions, aligning with climate change mitigation goals.

3.4.1. Historical Data Analytics

Fig. 3-23 illustrates the cumulative oil production data for wells employing various FCDs strategies. As depicted in Fig. 3-23, the wells that were completed with a combination of LDICDs and LDOCDs yielded the highest cumulative oil production. Fig. 3-24 provides an average representation of the cumulative oil production data presented in Fig. 3-23. Fig. 3-24 further emphasizes that wells equipped with joint LDICDs and LDOCDs consistently achieved superior oil production compared to wells employing other FCD implementations.

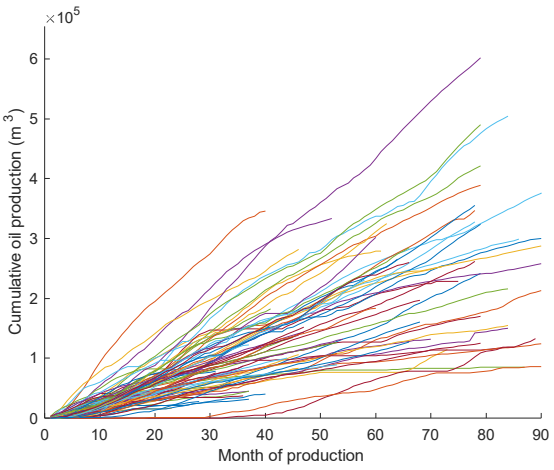

LDICD

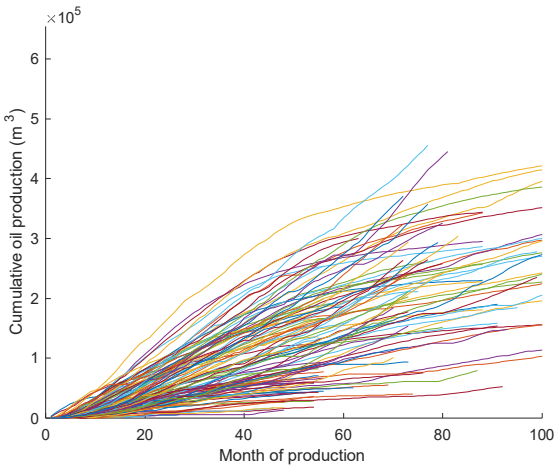

TDICD

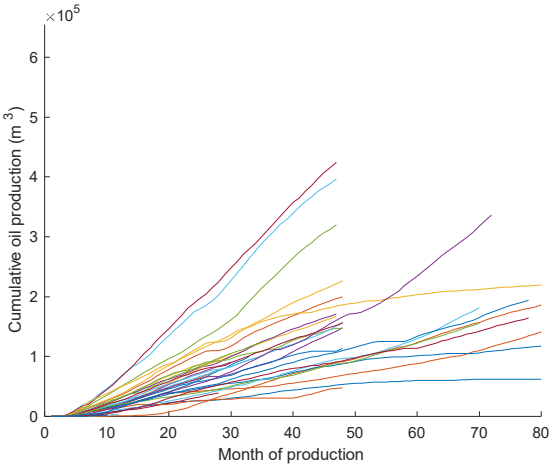

TDOCD

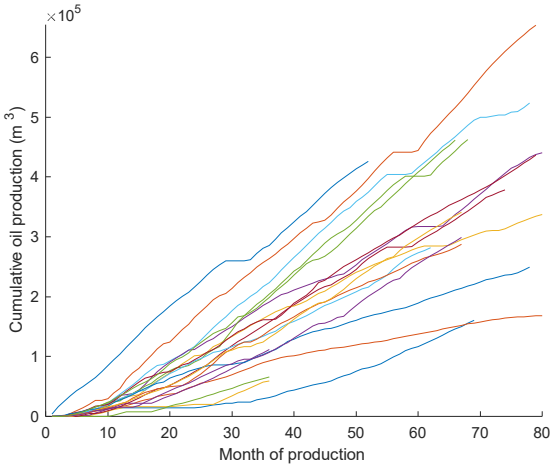

LDICD-LDOCD

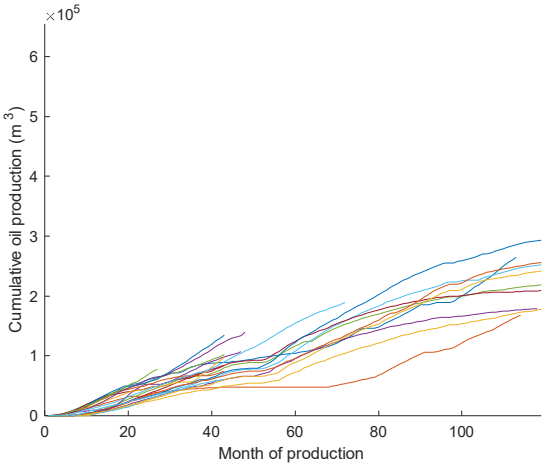

TDICD-TDOCD

Fig. 3-23. Cumulative oil production data for wells employing various FCDs strategies in our database.

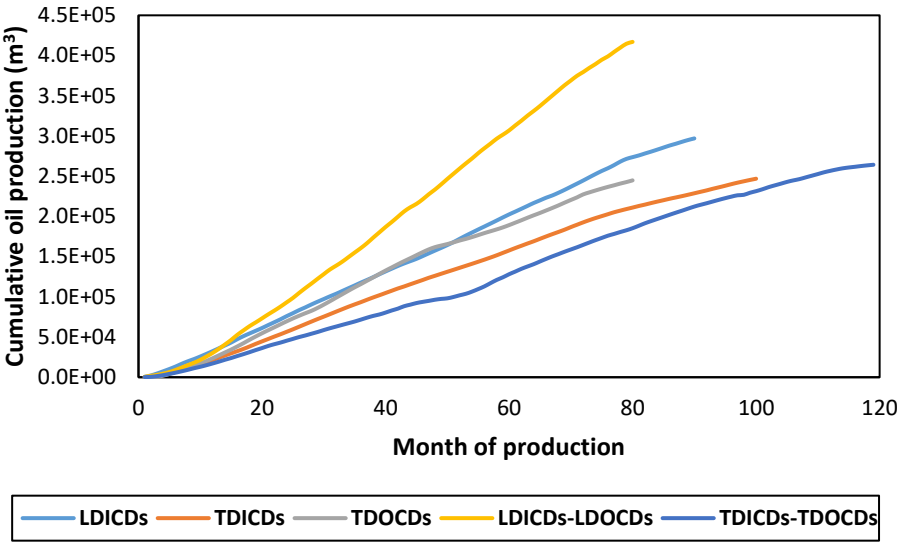

Fig. 3-24. Average representation of the cumulative oil production data presented in Fig. 3-23.

Fig. 3-25 presents cumulative injected steam data for wells utilizing different FCD strategies. As observed in Fig. 3-25, it is apparent that nearly all the wells within each FCD strategy group consumed a similar quantity of steam. However, as depicted in Fig. 3-26, which presents an average depiction of cSOR data derived from the values presented in Fig. 3-23 and Fig. 3-25, wells equipped with TDOCDs and the combined LDICDs and LDOCDs consistently exhibit lower cSOR in comparison to wells implementing other FCD approaches.

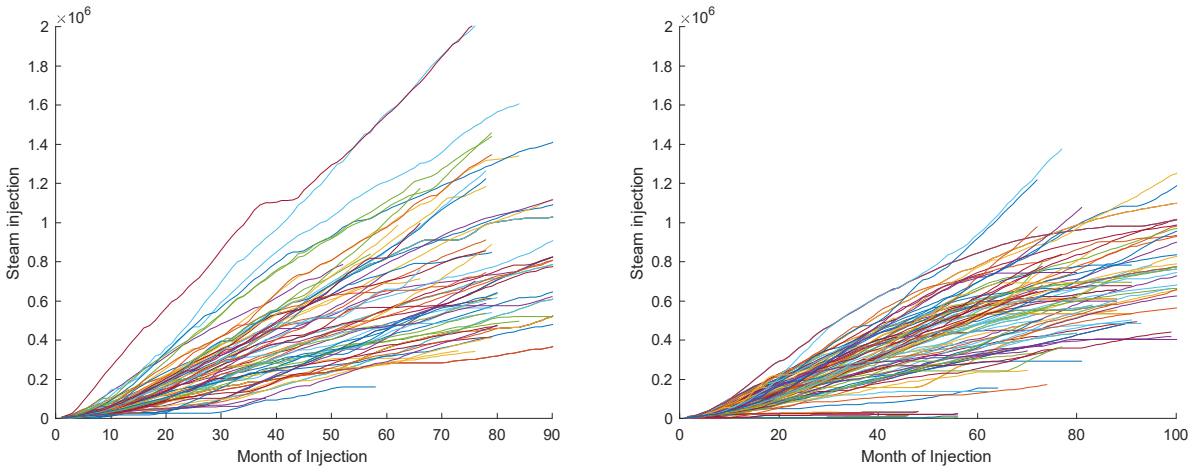

LDICD TDICD

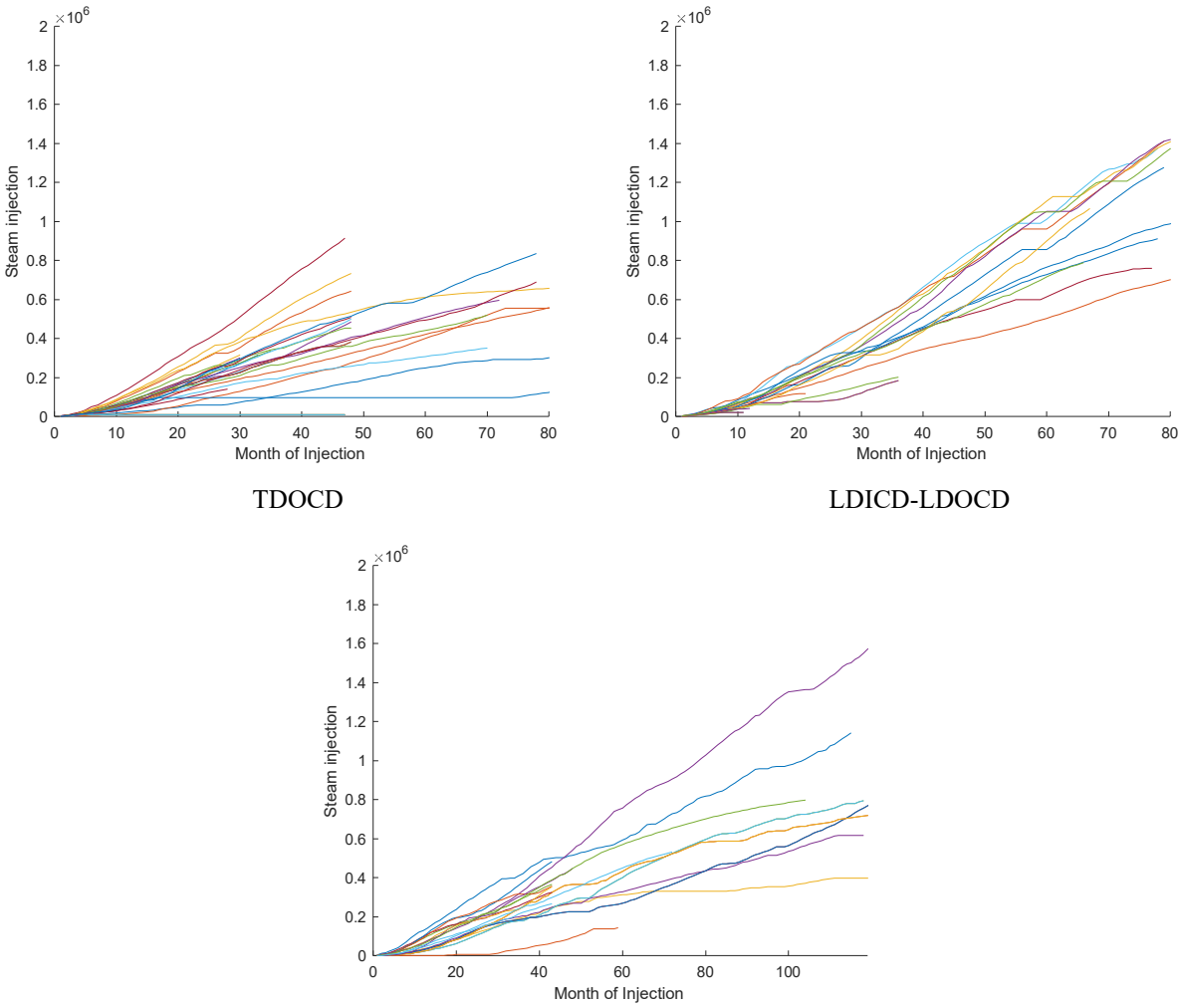

Fig. 3-25. Cumulative injected steam data for wells employing various FCDs strategies in our database.

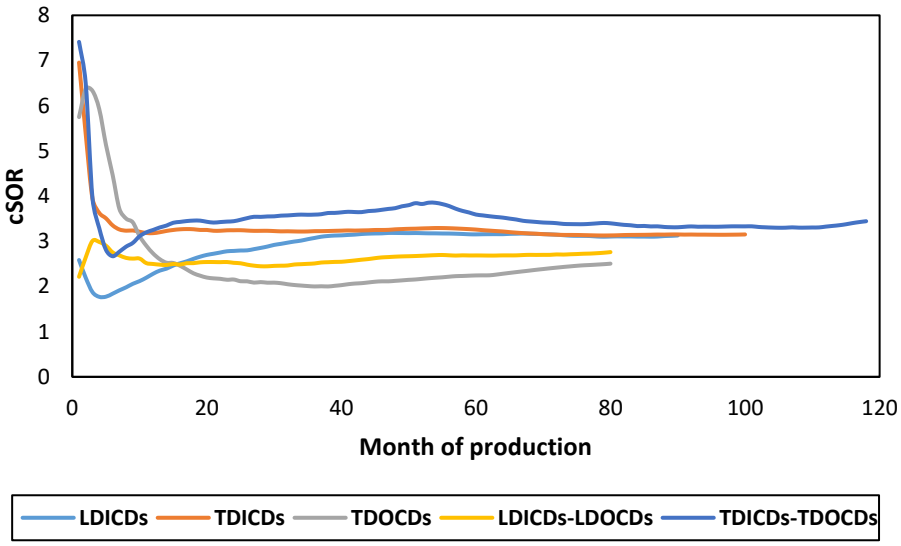

Fig. 3-26. Average representation of the cSOR data based on values presented in Fig. 3-23 and Fig. 3-25.

As indicated in Fig. 3-24 and Fig. 3-26, wells retrofitted by TDFCDs produced lower oil and consumed higher steam. Ongoing discussions within the industry have revolved around the economic best practices of TDFCDs versus LDFCDs deployments. TDFCDs are often considered as remedial tools to wells that faced problems [3, 101]. In addition, wells equipped with TDFCDs are occasionally more susceptible to failures compared to LDFCDs, primarily due to operational factors like erosion by sand grains [115]. Other than that, due to some operational limitations, the increase of injection pressure and rate for wells with TDFCD to enhance oil production in lower subcool temperatures proves to be quite challenging [101, 3, 8]. However, in certain situations, opting for TDFCDs might be a more cost-effective choice by postponing their deployment until challenges arise. On the other hand, this approach is often more intricate and comes with higher costs compared to the deployment of LDFCDs [99]. It is important to highlight that there are notable distinctions between these approaches, and some of the prevalent challenges associated with TDFCDs are cited by [99].

The best practice based on the data-driven analysis in this paper, the literature, and the industry applications can be stated as that using flow rate control strategies by LDFCDs from the initial stages of production could result in higher oil yield and reduced freshwater consumption compared to retrofitting wells with TDFCDs when issues arise.

3.4.2. Numerical Simulation of Different Flow Rates Control Strategies: Homogeneous Reservoir

The oil production and cSOR for the homogeneous reservoir with different well completions strategies are compared with the case without FCDs in Fig. 3-27 and Fig. 3-28, respectively.

Based on Fig. 3-27-a, the oil production rates for the cases with LDICDs-LDOCDs, LDICDs, and LDICDs-TDOCDs are higher than the other FCDs deployments and the case without FCDs. Compared to the case without FCDs, LDICDs-LDOCDs, LDICDs, and LDICDs-TDOCDs cases provided the highest average oil production rate improvement of 26%, 21%, and 18%, respectively (Fig. 3-27-b).

Based on Fig. 3-28-a, cSOR for the cases with LDICDs-LDOCDs, LDICDs-TDOCDs, and LDICDs is lower than the other FCDs deployments and the case without FCDs. Compared to the case without FCDs, LDICDs-LDOCDs, LDICDs-TDOCDs, and LDICDs cases lowered cSOR by 19%, 17%, and 13%, respectively (Fig. 3-28-b).

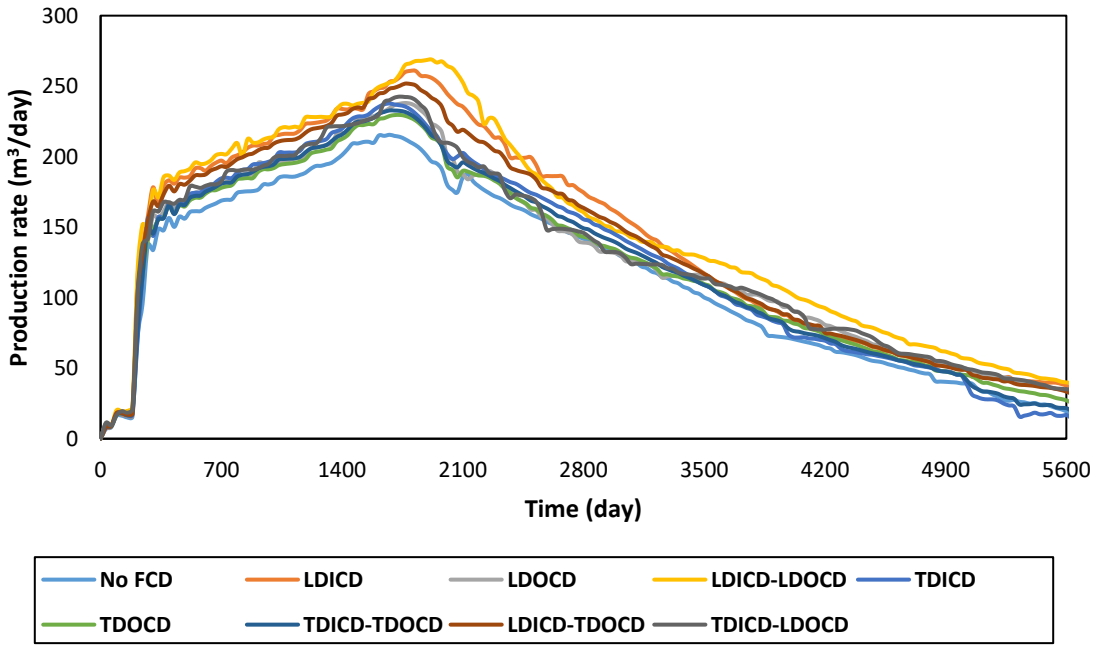

a

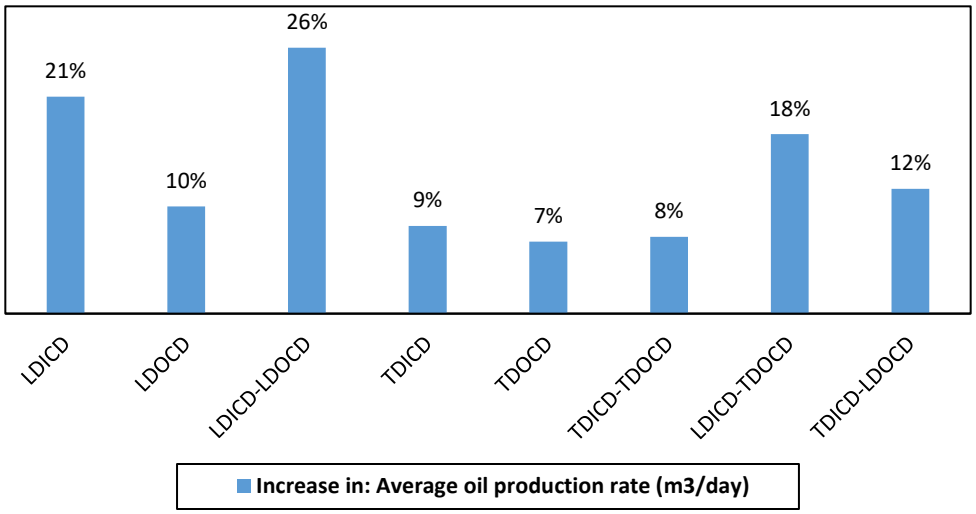

b

Fig. 3-27. Oil production rate for the homogeneous reservoir: (a) oil production rate and (b) increase in oil production rate by comparing the average oil production rate for FCDs deployment cases with the case without FCDs.

Based on results from Fig. 3-27 and Fig. 3-28, the top-three cases of FCDs deployments are LDICDs-LDOCDs, LDICDs-TDOCDs, and LDICDs which will be used in the following detailed comparison against the case without FCDs.

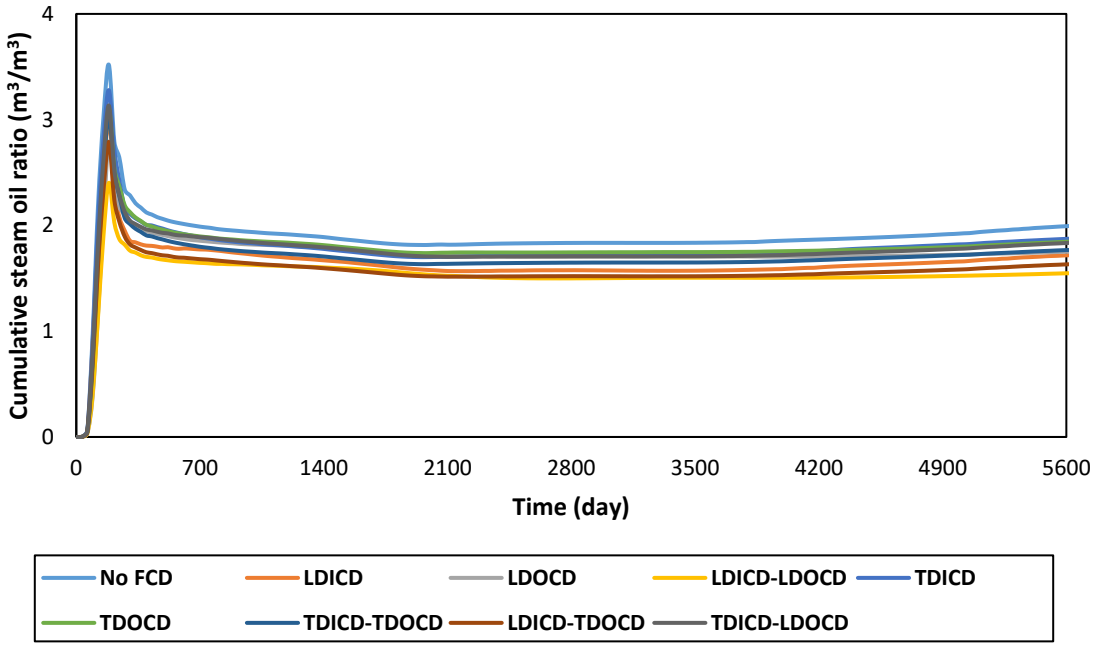

a

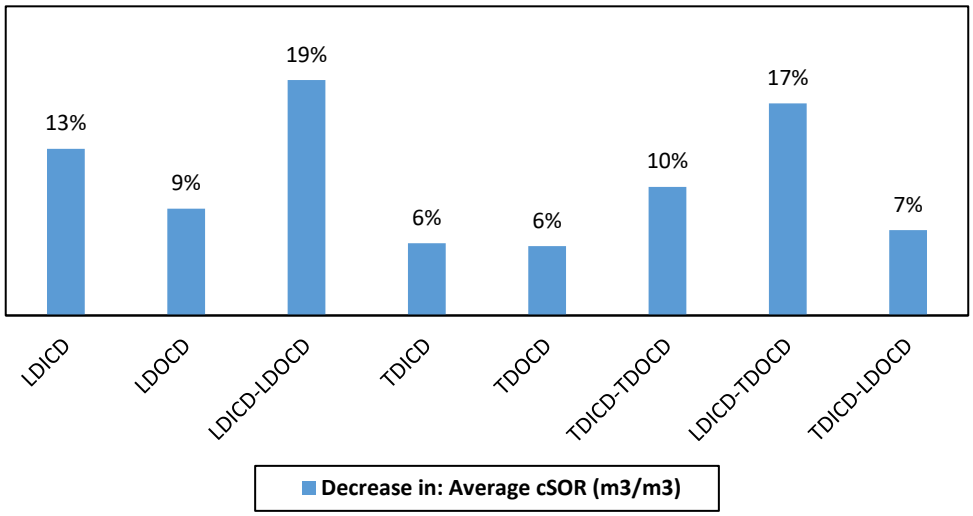

b

Fig. 3-28. cSOR for oil production rate for the homogeneous reservoir: (a) cSOR for different cases and (b) decrease in cSOR by comparing the average cSOR for FCDs deployment cases with the case without FCDs.

Fig. 3-29 shows the steam chamber distribution after 1,279 days for the case without FCDs and the top-three cases of FCDs deployment. Based on Fig. 3-29, steam chamber conformance is improved by using either LD or TD OCDs. When comparing cases with LDICDs-LDOCDs and LDICDs-TDOCDs, the former (Fig. 3-29-c) exhibits better steam chamber conformity. The graphs illustrating the average temperature from the upper to the lower sections of the reservoir are depicted in Fig. 3-30. According to the information presented in Fig. 3-30, the steam chamber exhibits improved growth in the scenario involving LDOCD-LDICDs.

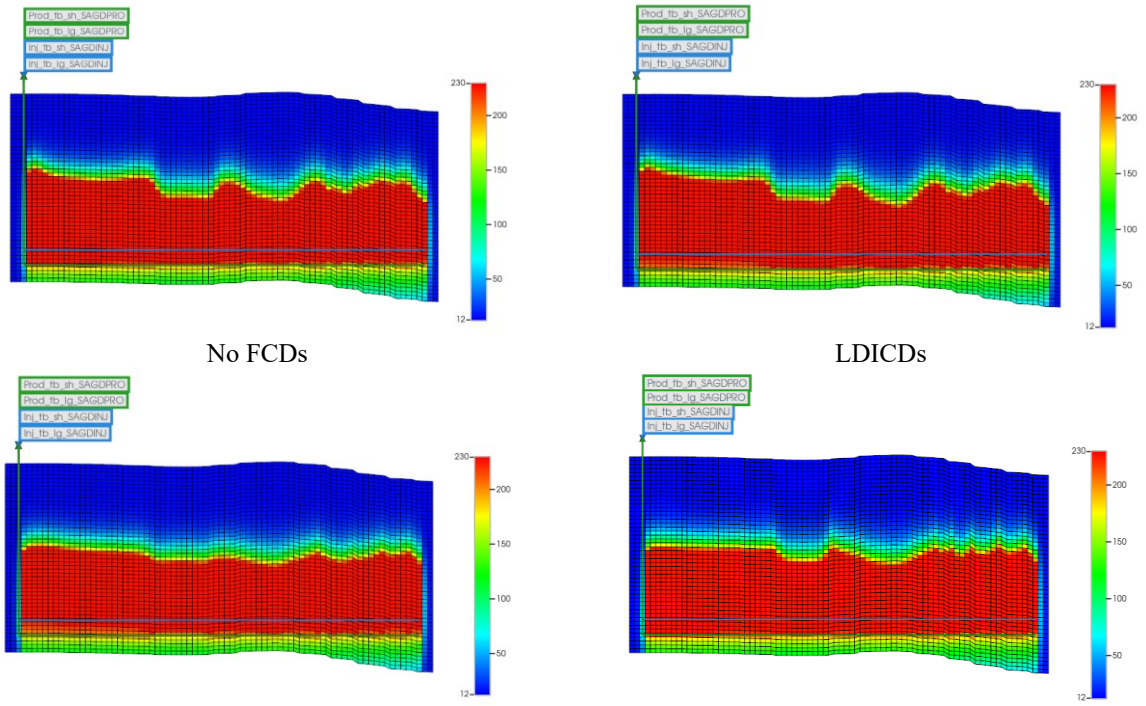

No FCDs LDICDs

LDICD-LDOCDs LDICDs-TDOCDs

Fig. 3-29. The steam conformance for the homogeneous reservoir: (a) the case without FCDs, (b) LDICDs, (c) LDICD-LDOCDs, and (d) LDICDs-TDOCDs.

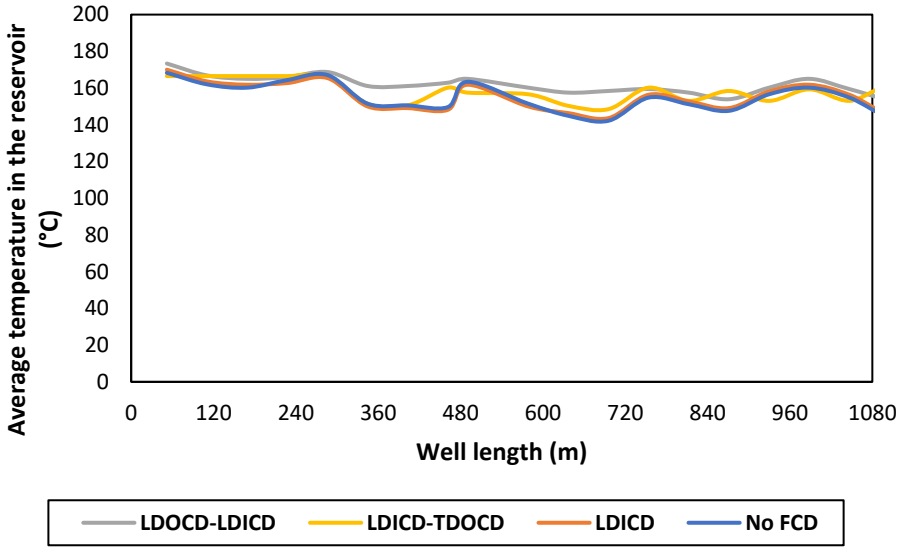

a

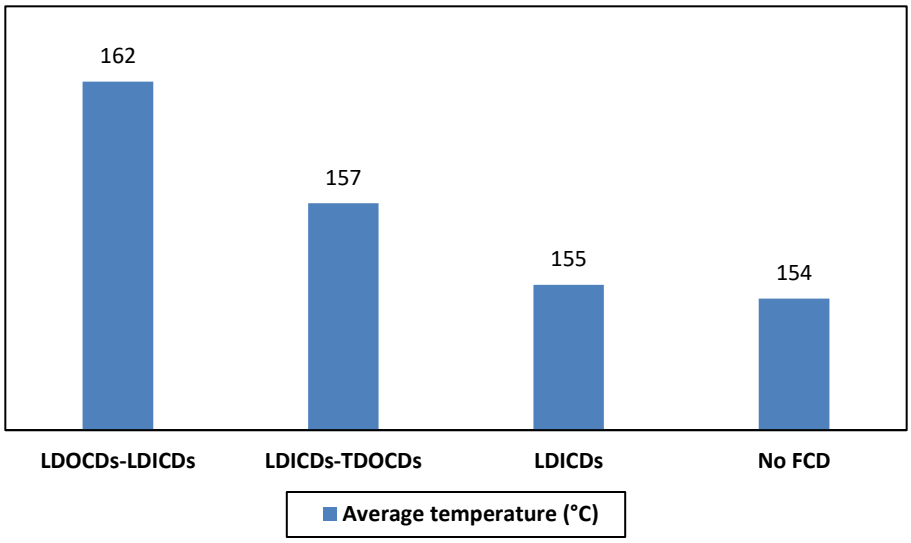

b

Fig. 3-30. The average temperature in the reservoirs shown in Fig. 3-29. (a) shows the fluctuation of the temperature representing the steam chamber in the reservoir, and (b) shows the average of curves shown in part (a).

The steam injection rate and reservoir temperature for the case without FCDs and the top-three cases of FCDs deployments along the injector and producer wells for the 1,279th day of the simulation are presented in Fig. 3-31. Based on Fig. 3-31-a, OCDs significantly contributed to equalizing the injection rate along the injector well. Standard deviation for the curves shown in Fig. 3-31-a is 0.76, 0.58, 1.76, and 1.97 for cases with LDICDs-LDOCDs, LDICDs-TDOCDs, LDICDs, and without FCDs, respectively. Therefore, the injection rate for the cases with OCDs is more uniform than the case without FCDs.

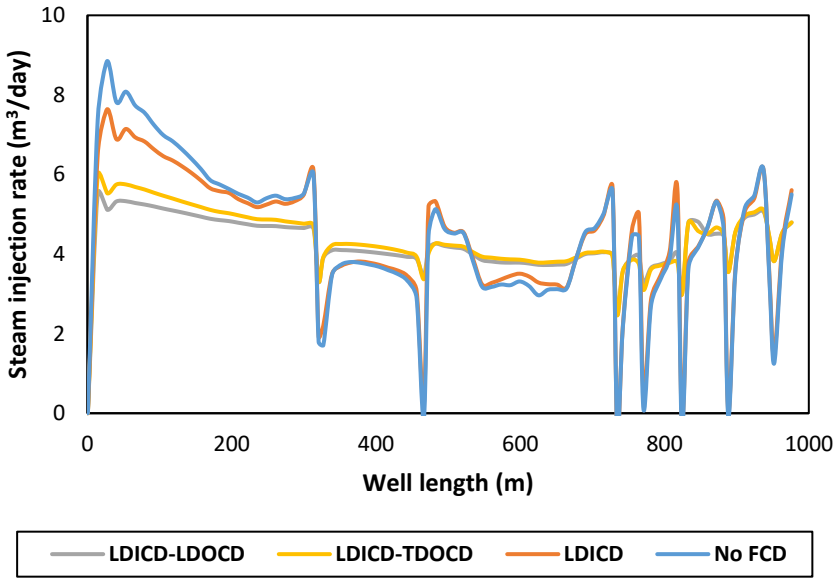

a

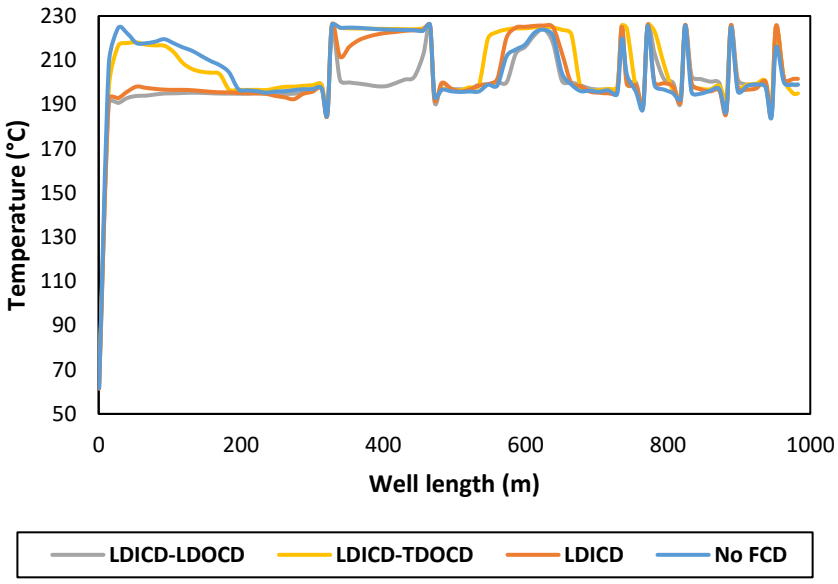

b

Fig. 3-31. Temperature and injection rate profiles along the producer and injector wells for the homogeneous reservoir: (a) the contribution of OCDs to equalize the injection rate along the injector well for the 1,279th day of the simulation, and (b) the contribution of FCDs to manage hot-spot zones.

FCDs also contributed to managing hot-spot zones, as shown in Fig. 3-31-b. Compared to the case without FCDs, the cases with LDICDs-LDOCDs and LDICDs successfully eliminate hot-spot zones in the heel. The case with LDICDs-TDOCDs was unable to reduce the temperature compared to other FCDs deployment scenarios; nonetheless, a little contribution to temperature reduction was made in the heel.

Fig. 3-32illustrates the underlying physics behind how LDICDs play a crucial role in temperature management and the prevention of steam breakthrough. The plot specifically pertains to block numbers {25, 16, 45}, representing a block where the producer well is drilled at its base. According to the information derived from Fig. 3-32, LDICD installed in this specific location activated based on the conditions outlined in Fig. 3-22. Three examples of activated times are exhibited in Fig. 3-32. LDICD lowers fluid inflow, leading to a decrease in temperature. However, when the pressure drop provided by the LDICD decreases due to a reduction in inflow rate, the inflow rate subsequently increases afterward, causing a temperature rise. The LDICD is then reactivated to limit the inflow rate, resulting in a temperature decrease. This cyclic process demonstrates how LDICDs contribute to controlling the inflow rate, effectively managing the temperature and delaying steam breakthrough. As depicted in Fig. 3-32, the Cold-Water Equivalent (CWE), indicative of steam production in CMG STARS, shows a continual increase in the case with no FCDs. In contrast, for the case with LDICDs, the CWE curve remains almost near zero throughout the entire SAGD life. Furthermore, the temperature at this specific location is more closely aligned with the steam temperature in the case with no FCDs compared to the case with LDICDs.

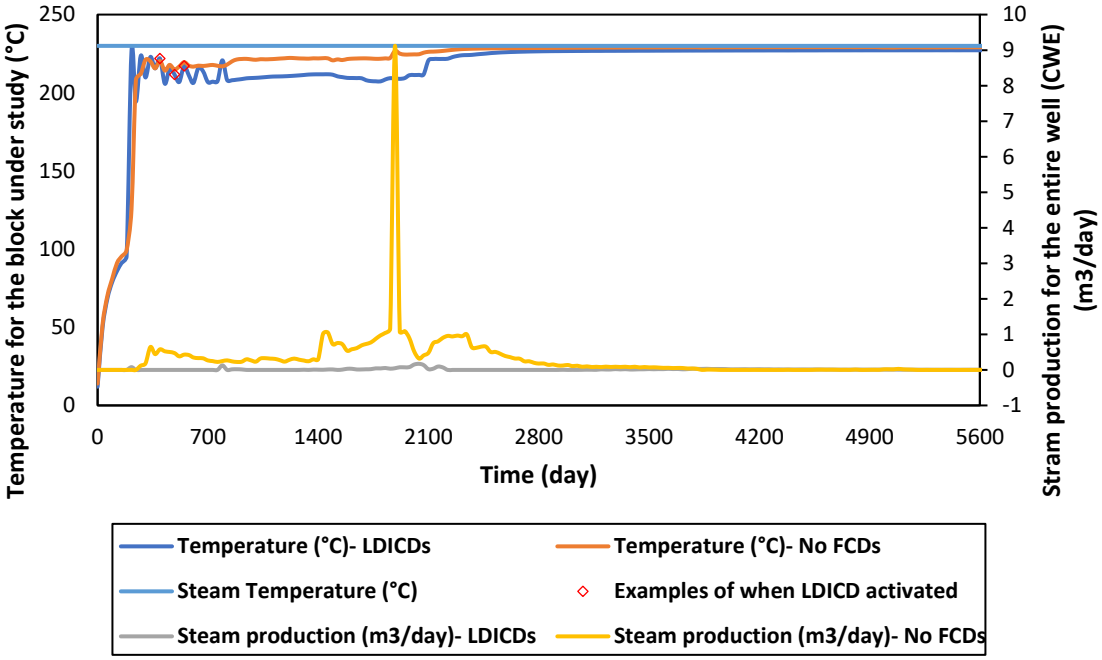

Fig. 3-32. Homogeneous reservoir: the underlying physics of how the LDICD helps to mitigate steam breakthrough and manage the temperature nearby the producer well.

3.4.3. Numerical Simulation of Different Flow Rates Control Strategies: Simple Reservoir with Shale Barriers

Comparisons between the simple reservoir with shale barriers and the case without FCDs are presented for oil production and cSOR for various well completions strategies in Fig. 3-33 and Fig. 3-34, respectively.

Based on Fig. 3-33-a, when compared to the case without FCDs, the oil production rates for the LDICDs-LDOCDs, LDICDs, and LDICDs-TDOCDs cases are all greater, like what already observed in the homogenous reservoir case. There was a 24% increase in average oil production rate in the LDICDs-LDOCDs case, a 19% increase in the LDICDs case, and a 15% increase in the LDICDs-TDOCDs case compared to the case without FCDs (Fig. 3-33-b).

Based on Fig. 3-34-a, as compared to the other FCDs deployments and the case without FCDs, cSOR is lower for the cases involving LDICDs-LDOCDs, LDICDs-TDOCDs, and LDICDs. When comparing cases with and without FCDs, cSOR was reduced by 20% in the LDICDs-LDOCDs case, 18% in the LDICDs-TDOCDs case, and 16% in the LDICDs case (Fig. 3-34-b).

Based on results from Fig. 3-33 and Fig. 3-34, LDICDs-LDOCDs, LDICDs-TDOCDs, and LDICDs will be employed in the following comparison to compare with the scenario without FCDs.

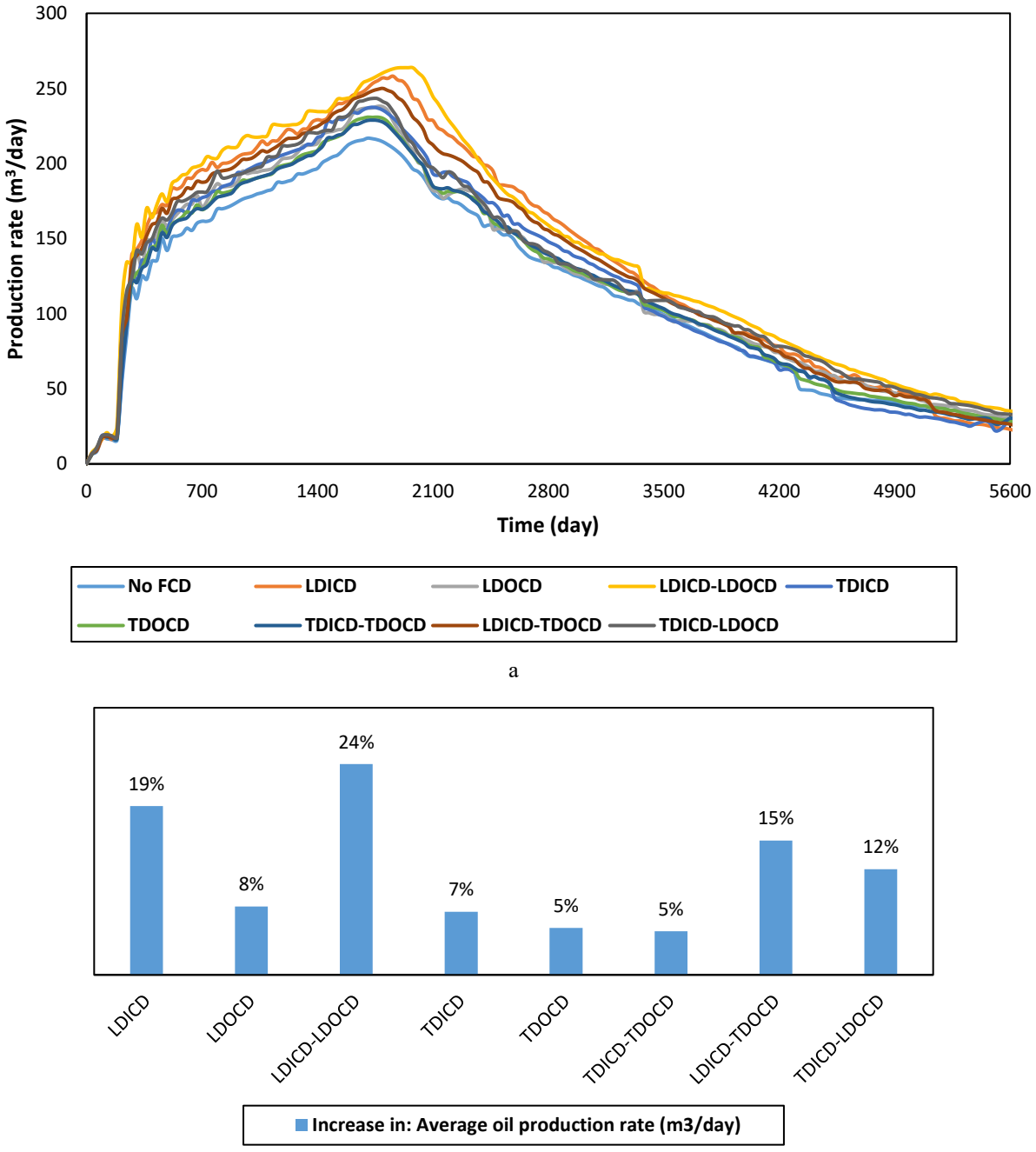

Fig. 3-33. Oil production rate for the simple reservoir with shale barriers: (a) the average oil production rate in cases with FCDs deployment against cases without FCDs, and (b) the increase in oil production rate due to the deployment of FCDs.

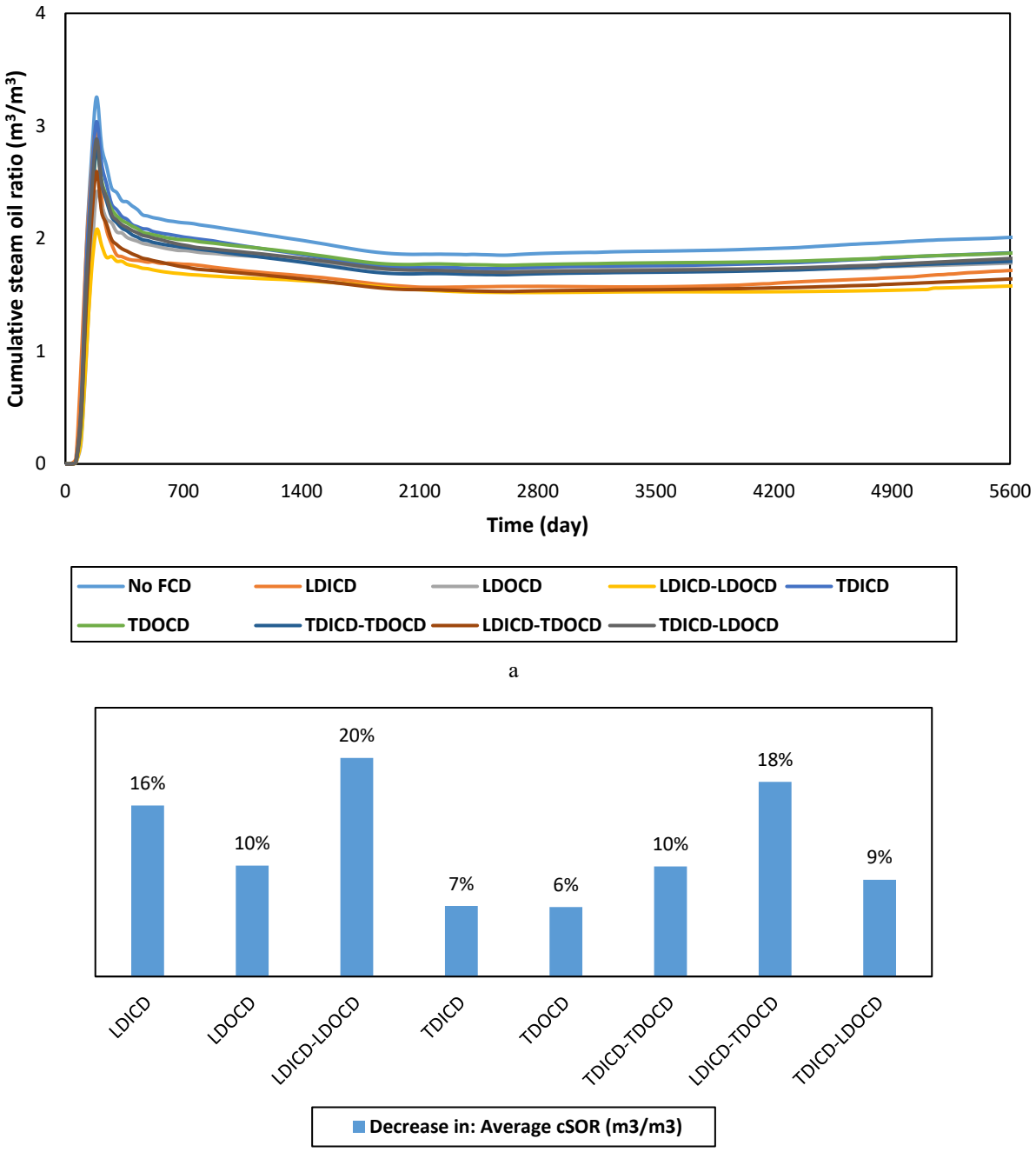

Fig. 3-34. cSOR for the simple reservoir with shale barriers: (a) cSOR for different scenarios, and (b) decrease in average cSOR when comparing scenarios with FCDs by the case without FCD.

After 1,279 days, the distribution of steam chambers is shown in Fig. 3-35 for the no FCDs scenario and the top three FCDs deployment cases. The use of either LD or TD OCDs, as shown in Fig. 3-35, results in greater steam chamber conformity. For LDICDs-LDOCDs, steam chamber conformity is more consistent than in the LDICDs-TDOCDs case. Fig. 3-36 displays graphs

depicting the average temperature distribution from the upper to the lower sections of the reservoir. As per the details provided in Fig. 3-36, the steam chamber demonstrates enhanced growth in the case involving LDOCD-LDICDs.

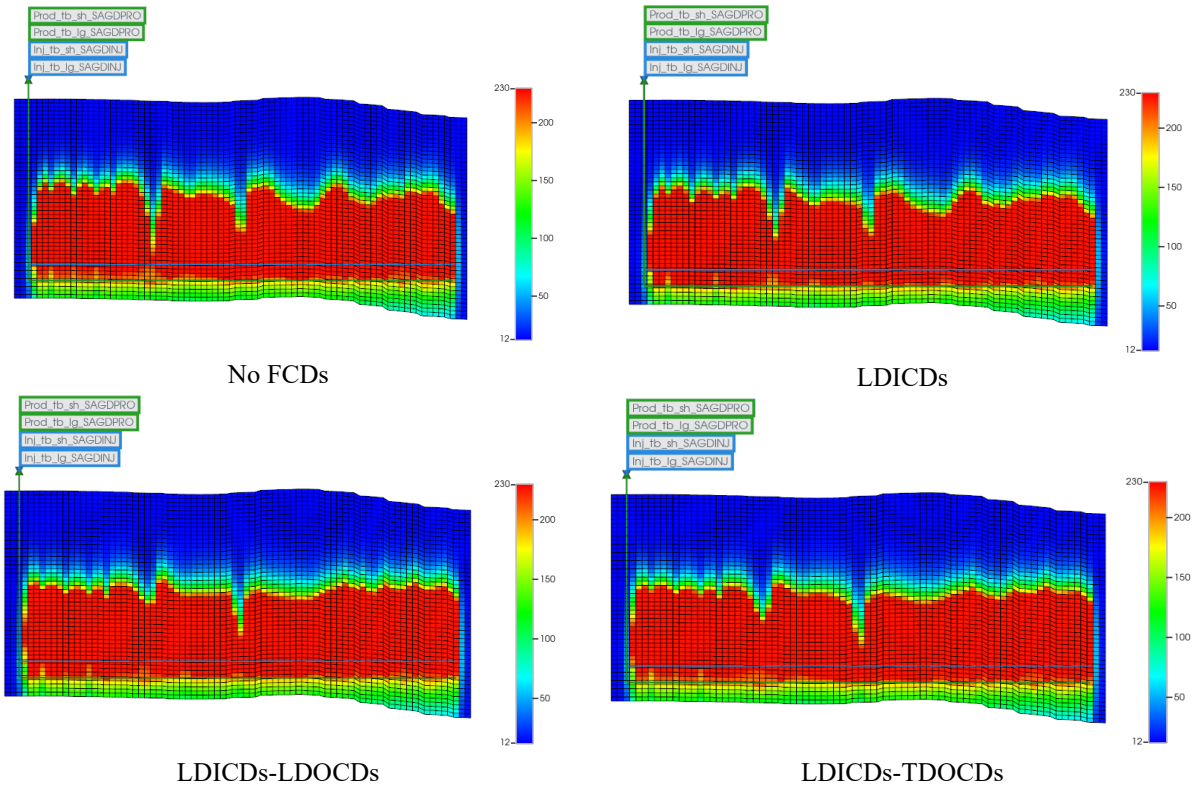

Fig. 3-35. The steam conformance for the simple reservoir with shale barriers: (a) the case without FCDs, (b) LDICDs, (c) LDICDs-LDOCDs, and (d) LDICDs-TDOCDs.

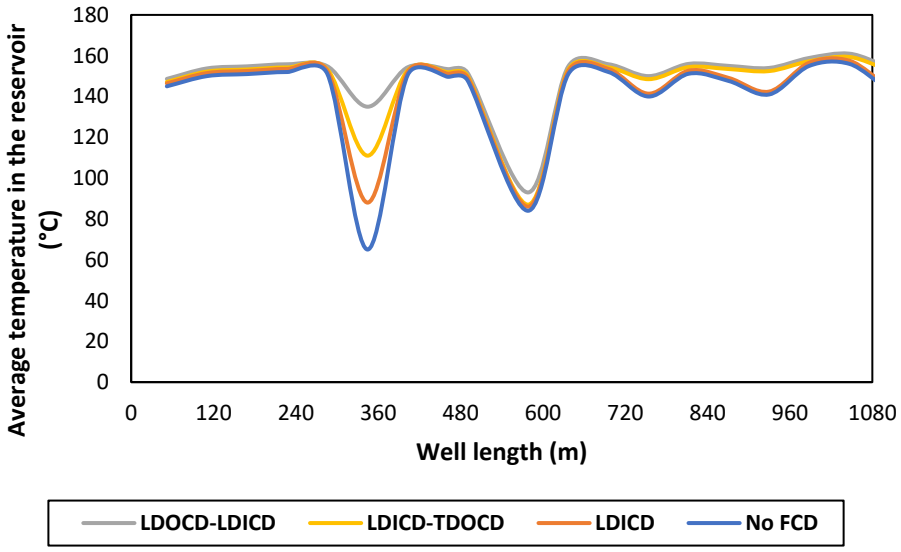

a

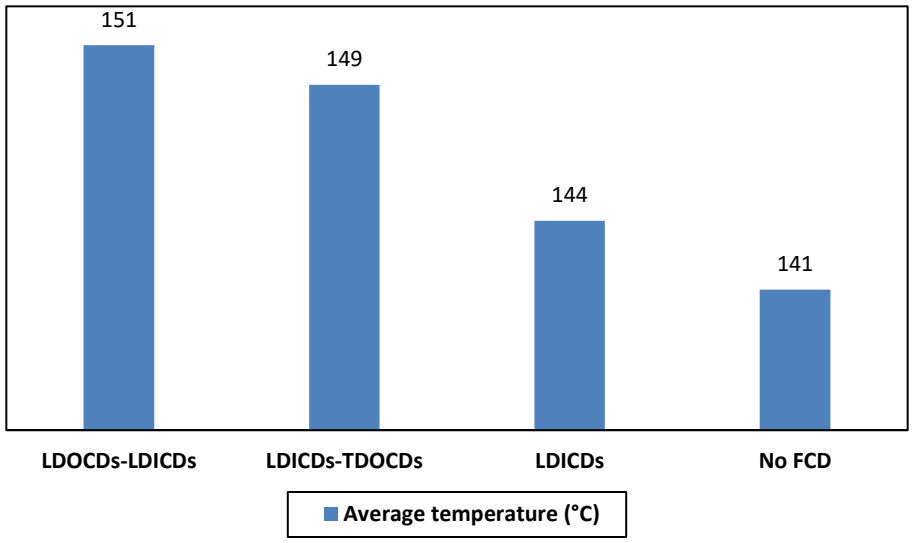

b

Fig. 3-36. The average temperature in the reservoirs shown in Fig. 3-35. (a) shows the fluctuation of the temperature representing the steam chamber in the reservoir, and (b) shows the average of curves shown in part (a).

Fig. 3-37 displays the steam injection rate and reservoir temperature along the injector and producer wells on day 1,279 of the simulation for the no FCDs case, the top three FCDs deployment scenarios. Fig. 3-37-a shows that OCDs helped considerably in balancing the injection rate over the injector well.

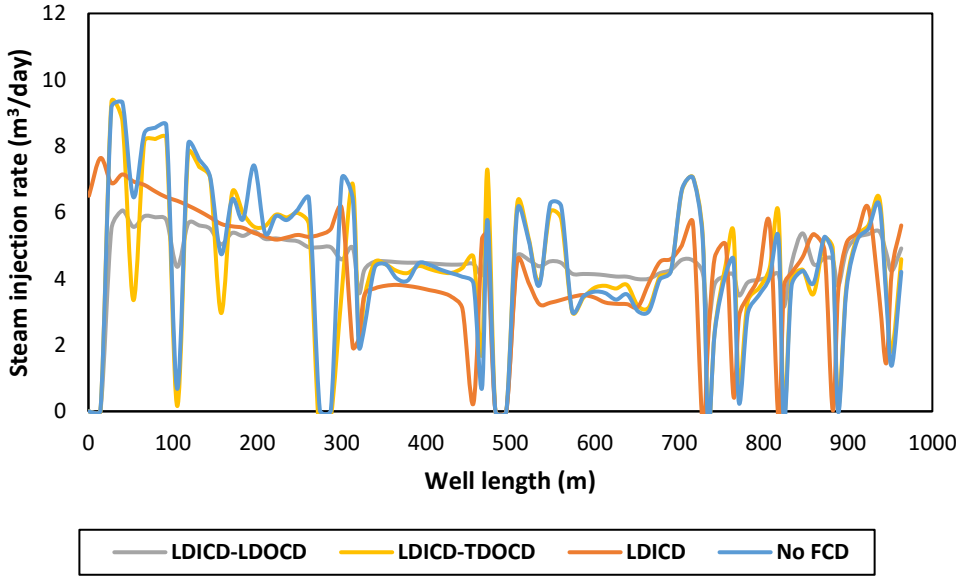

a

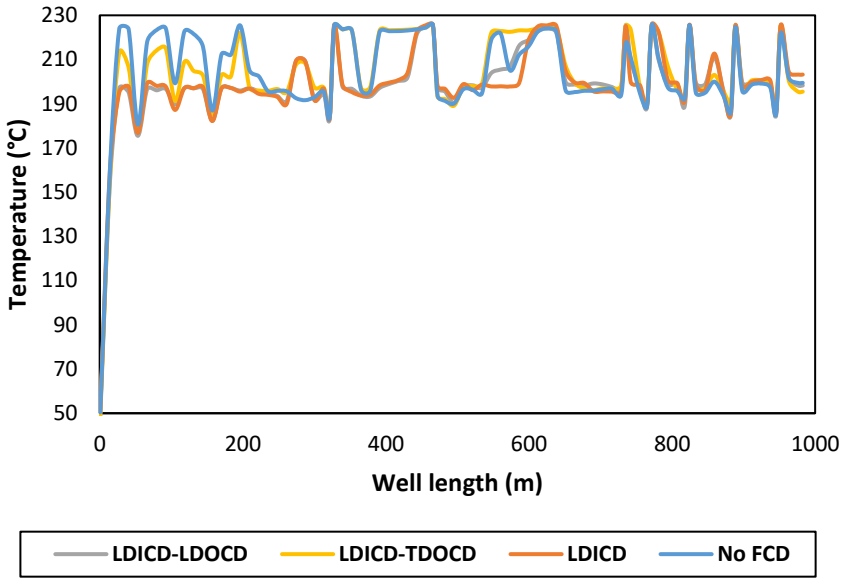

b

Fig. 3-37. Temperature and injection rate profiles along the producer and injector wells for the simple reservoir with shale barriers: (a) the contribution of OCDs to balance the injection rate along the injector well for the 1,279th day of the simulation, and (b) the contribution of FCDs to manage hot-spot zones.

As can be seen in Fig. 3-37-b, FCDs also helped with the management of hot-spot areas. In situations with LDICDs-LDOCDs and LDICDs, the hot-spot zone in the heel is well managed, in contrast to the case without FCDs. Compared to other FCDs deployment scenarios, the LDICDs-TDOCDs case could not significantly bring down the temperature, but it did slightly help in the heel.

To figure out how specific OCDs deployments would respond to different shale barrier configurations, a comparison of the steam chamber volume for LDICDs and LDICDs-LDOCDs cases after 1,279 days is presented in Table 13. Based on Table 13, installing LDOCDs in injector wells significantly improved steam chamber volume near and around the shale barriers by an average of 13%.

Table 13. Steam chamber volume nearby injector well after 1,279 days for the LDICD and LDICDs-LDOCDs cases for different shale barrier locations reported in Table 12.

Case#	Size (length × width)	Distance from the wells	location	Steam chamber growth, no OCDs (m3)	Steam chamber growth, with OCDs (m3)	Improvement resulted from OCDs (%)
1	13×14	Two meters	On bottom	463	540	117%
2	13×14	One meter	On bottom	1470	1563	106%
3	13×14	One meter	On top	1802	1981	110%

4	13×14	Two meters	On top	1246	1346	108%
5	26×2	Zero	The same block with the well	1249	1254	100%
6	26×2	Two meters	On top	4254	4740	111%
7	26×2	Two meters	On bottom	2581	3189	124%
8	26×2	One meter	On top	4539	4992	110%
9	26×2	One meter	On bottom	3991	4699	118%
10	13×14	One meter	On top	1523	1538	101%
11	13×14	Two meters	On top	1515	1827	121%
12	26×2	Zero	The same block with the well	881	1303	148%
13	26×2	One meter	On top	3288	3418	104%
14	26×2	Two meters	On top	3176	3518	111%

The intrinsic principles governing the impact of LDICDs in this scenario are detailed here. As indicated in Fig. 3-38, the block analyzed in Fig. 3-32 is situated atop a shale barrier in the simple reservoir case, denoted by a purplish rectangle in Fig. 3-38. As previously discussed, shale barriers constrain injection and production. According to Fig. 3-35 and Table 13, the steam chamber's growth is limited compared to the homogeneous case (Fig. 3-29), presenting challenges for steam injection in blocks where shale barriers exist. Contrary to Fig. 3-32, as demonstrated in Fig. 3-39, the LDICD-equipped case exhibits a higher temperature, indicating enhanced production, as higher temperatures generally correlate with increased production. However, it is important to note that the temperature remains below the steam temperature, and the LDICD effectively delays steam breakthrough based on the CWE shown in Fig. 3-39. This is attributed to the activation of LDICDs in other perforations, as illustrated in Fig. 3-32, where the liquid pool thickness in those locations is sufficient to impede steam breakthrough (refer to Fig. 2-4). This thickness of the liquid pool serves to push back the steam into nearby zones [99] in the simple reservoir with shale barriers case, contributing to a higher temperature in the LDICD-equipped case compared to the case without LDICDs.

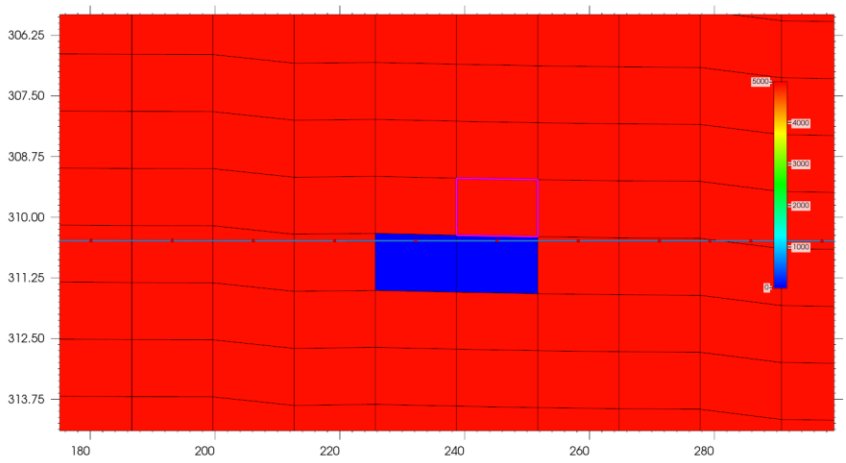

Fig. 3-38. The location of block number {25, 16, 45} which the producer well is drilled on its bottom. The property which is shown is permeability in I direction.

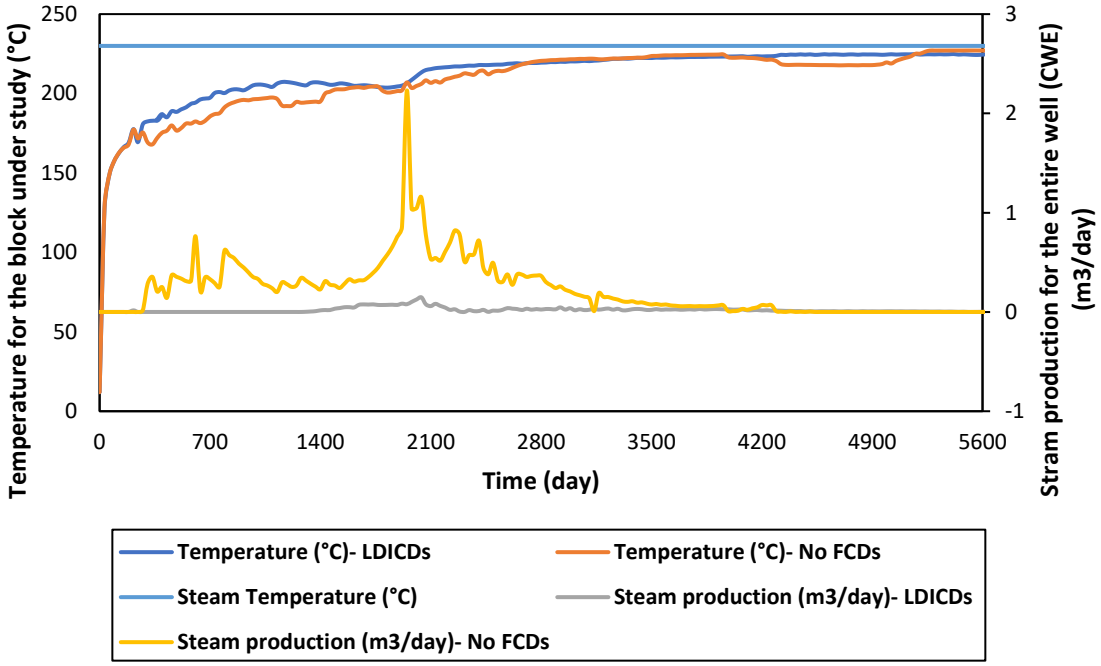

Fig. 3-39. LDICD helps to mitigate steam breakthrough and distribute the temperature within the entire reservoir. Despite Fig. 3-32, the case with LDICD shows higher temperature, however, the steam breakthrough postponed successfully.

3.4.4. Numerical Simulation of Different Flow Rates Control Strategies: Heterogeneous Reservoir

The oil production and cSOR for the simple reservoir with shale barriers for different well completions strategies are compared with the case without FCDs and presented in Fig. 3-40 and Fig. 3-41, respectively.

As shown in Fig. 3-40-a, the oil production rate for the cases involving LDICDs-LDOCDs, LDICDs, and LDICDs-TDOCDs is greater than the oil production rate for the cases with the other FCDs deployments and the case without FCDs. Compared to the case without FCDs, the average oil production rate increased by 26% in the LDICDs-LDOCDs case, 21% in the LDICDs case, and 18% in the LDICDs-TDOCDs case (Fig. 3-40-b).

Fig. 3-41-a shows that compared to the other FCDs deployments and the case without FCDs, cSOR is lower in the LDICDs-LDOCDs, LDICDs-TDOCDs, and LDICDs cases. Cases with LDICDs, LDICDs-LDOCDs, and LDICDs-TDOCDs all resulted in lower cSOR than the base case without FCDs by 20%, 17%, and 12%, respectively (Fig. 3-41-b).

Fig. 3-40 and Fig. 3-41 show that LDICDs-LDOCDs, LDICDs-TDOCDs, and LDICDs are the top three deployments of FCDs; thus, these cases will be considered to compare with the case without FCDs.

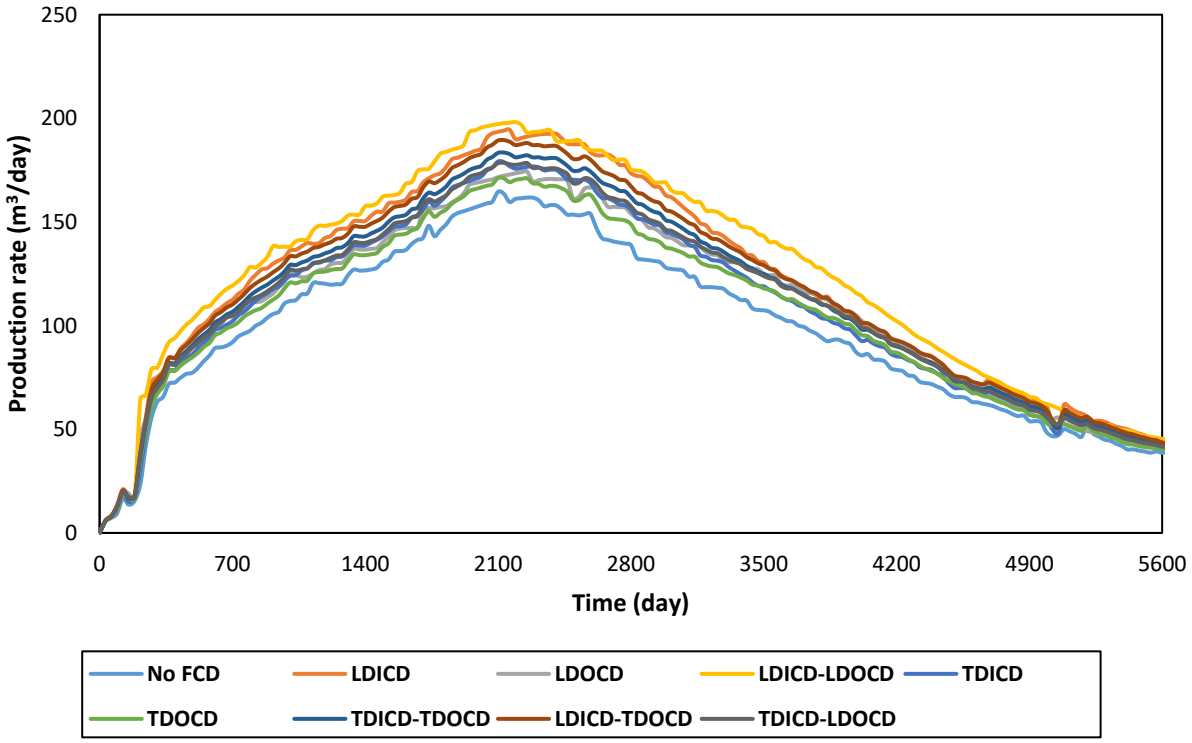

a

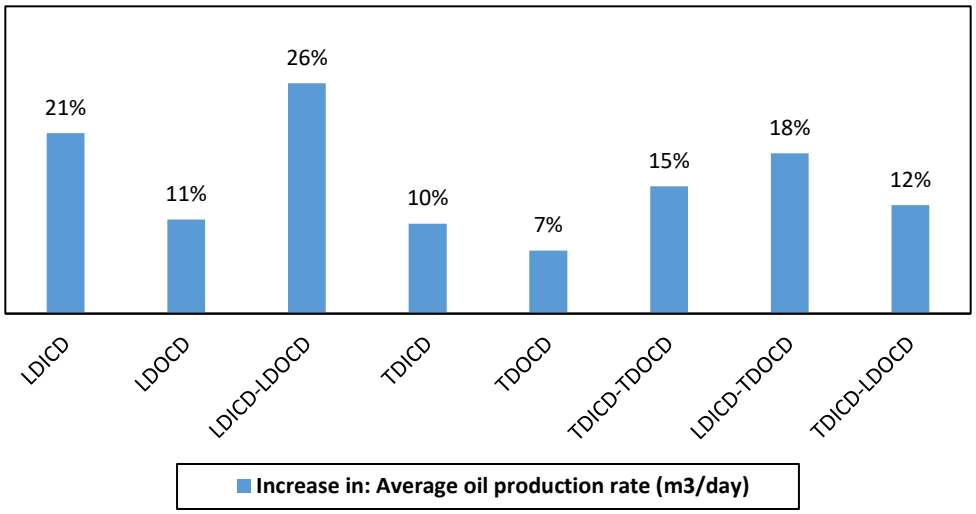

b

Fig. 3-40. Oil production rate for the heterogeneous reservoir: (a) oil production rate and (b) increase in oil production rate by comparing the average oil production rate for FCDs deployment cases with the case without FCDs.

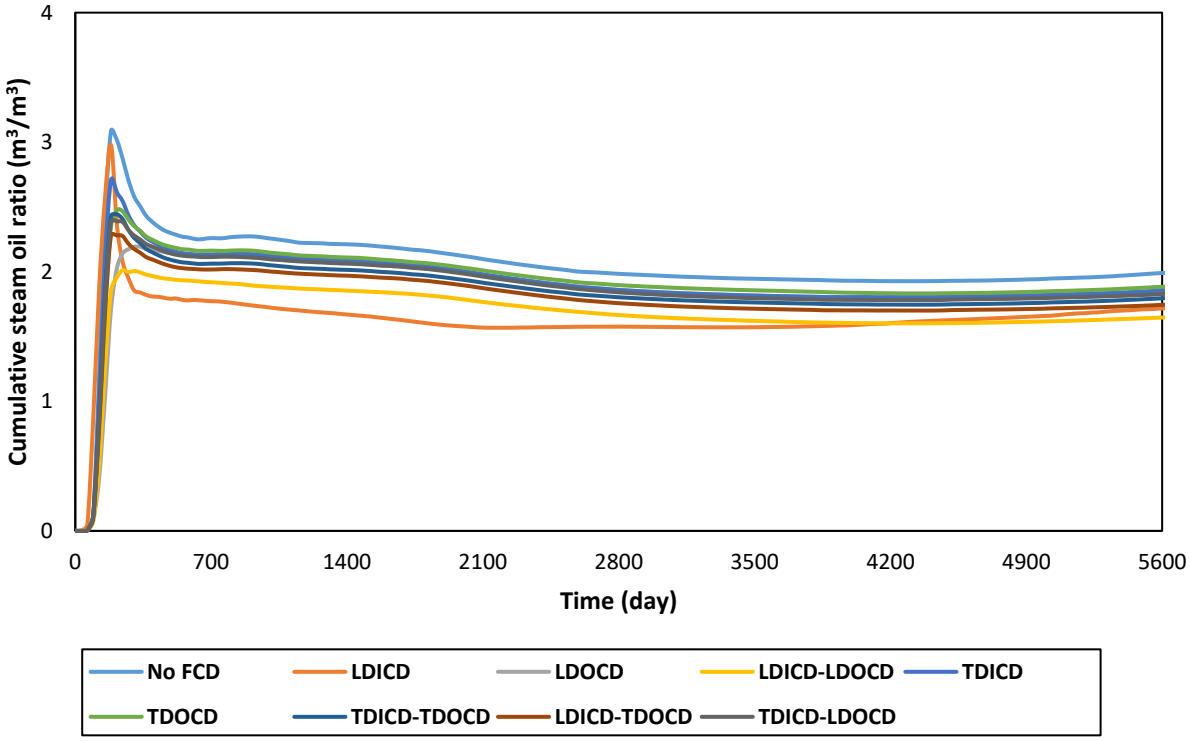

a

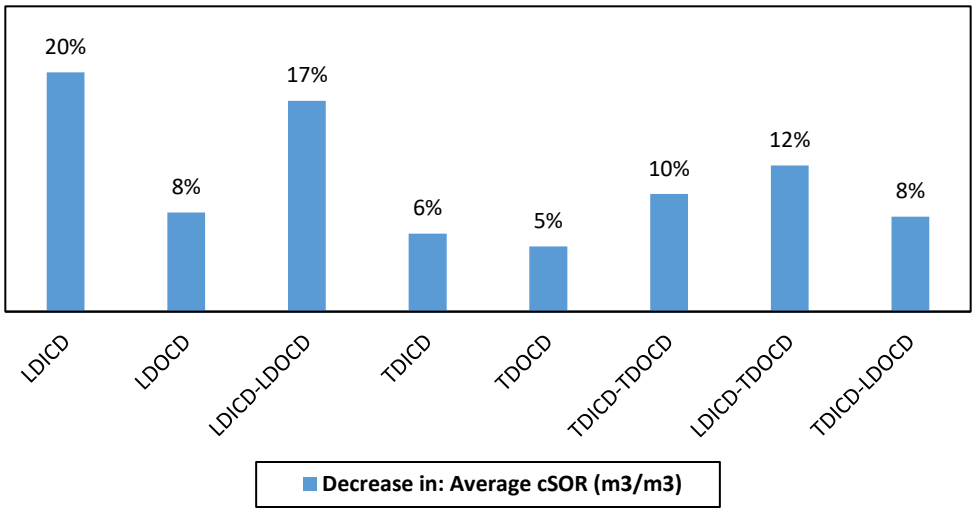

b

Fig. 3-41. cSOR for the heterogeneous reservoir: (a) cSOR for different cases and (b) decrease in cSOR by comparing the average cSOR for FCDs deployment cases with the case without FCDs.

After 1,279 days, the distribution of steam chambers is shown in Fig. 3-42 for the no FCDs case and the top three FCDs deployment cases. Fig. 3-42 shows that LD and TD OCDs improved steam chamber conformity. When comparing the performance of LDICDs-LDOCDs to that of LDICDs-TDOCDs, steam chamber conformance is more consistent for the former. The curves representing the average temperature from the top to the bottom of the reservoir are shown in Fig. 3-43. Based on Fig. 3-43, steam chamber is grown better in the case with LDOCD-LDICDs.

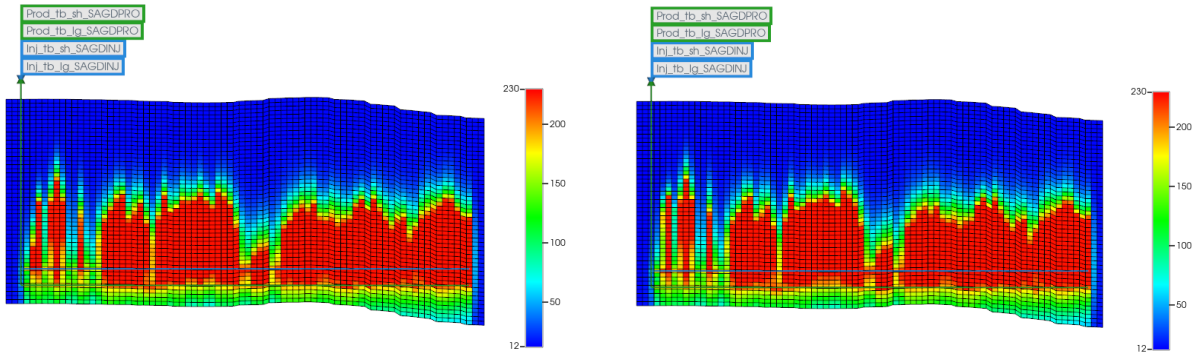

a b

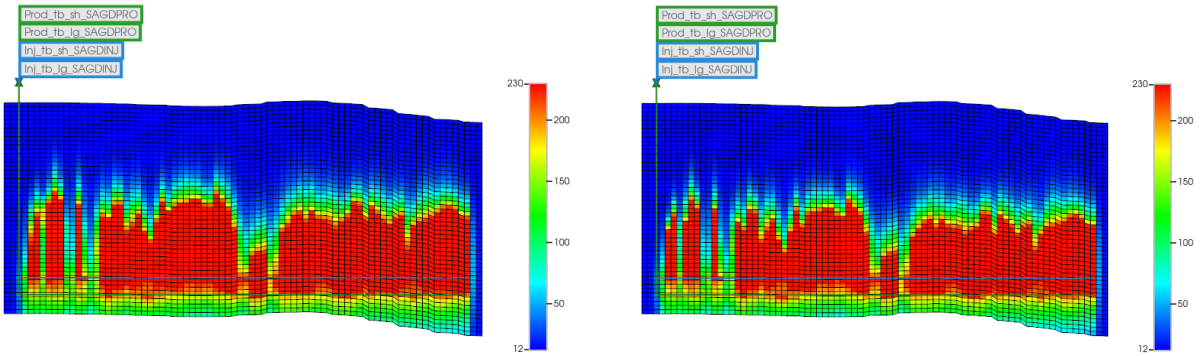

c d

Fig. 3-42. The steam conformance for the heterogeneous reservoir. (a) the case without FCDs, (b) LDICDs, (c) LDICDs-LDOCDs, and (d) LDICDs-TDOCDs.

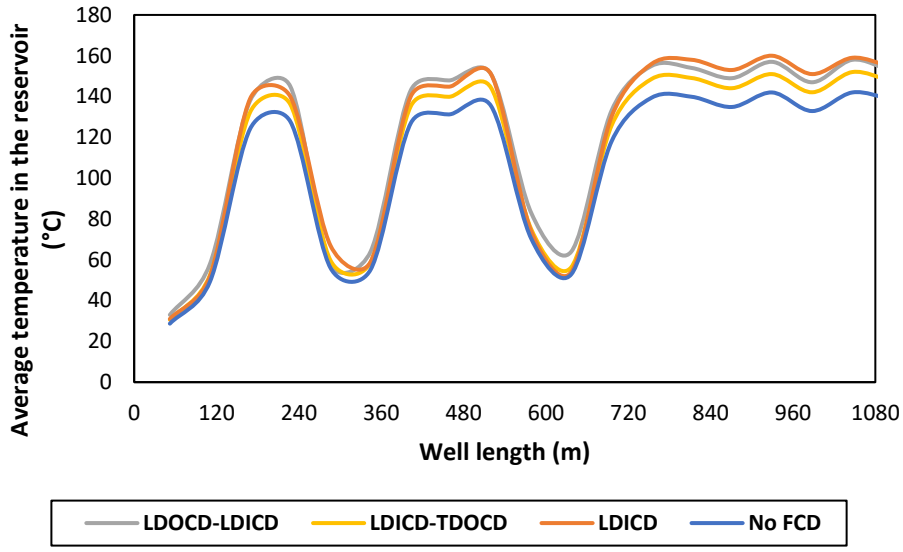

a

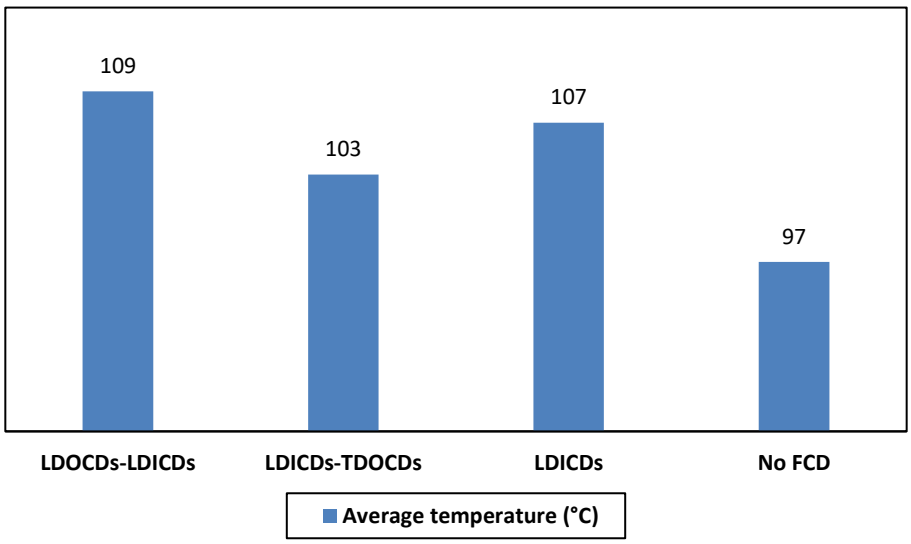

b

Fig. 3-43. The average temperature in the reservoirs shown in Fig. 3-42. The steam conformance for the heterogeneous reservoir. (a) the case without FCDs, (b) LDICDs, (c) LDICDs-LDOCDs, and (d) LDICDs-TDOCDs.. (a) shows the fluctuation of the temperature representing the steam chamber in the reservoir, and (b) shows the average of curves shown in part (a).

The steam injection rate and reservoir temperature for the case without FCDs and the top-three cases of FCDs deployments along the injector and producer wells for the 1,279th day of the simulation are presented in Fig. 3-44. Based on Fig. 3-44-a, OCDs significantly contributed to equalizing the injection rate along the injector well.

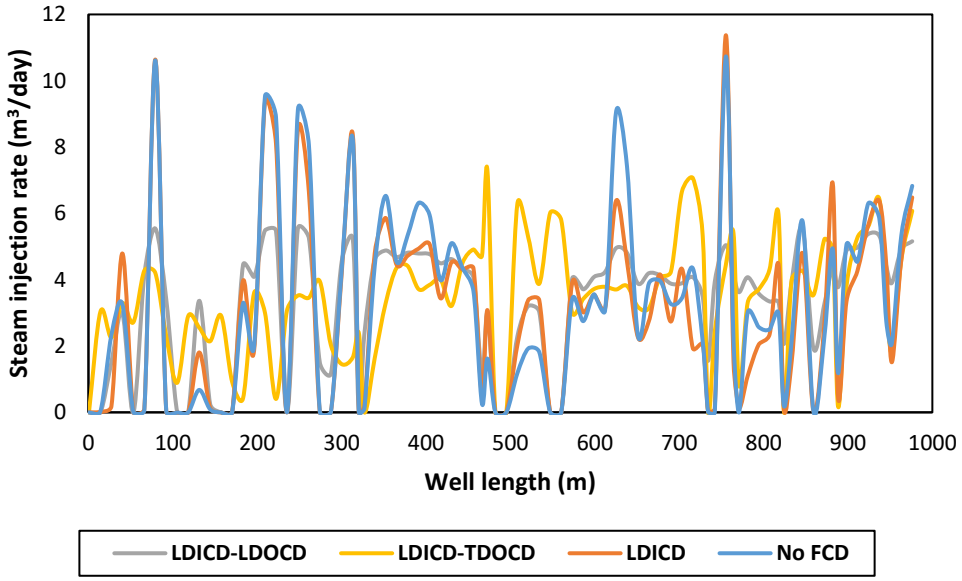

a

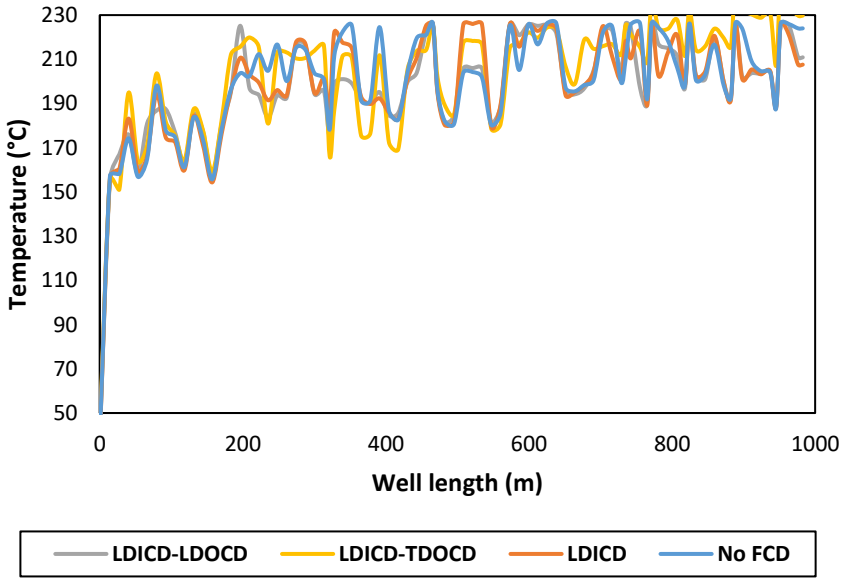

b

Fig. 3-44. Temperature and injection rate profiles along the producer and injector wells for the simple reservoir with shale barriers: (a) the contribution of OCDs to equalize the injection rate along the injector well for the 1,279th day of the simulation, and (b) the contribution of FCDs to manage hot-spot zones.

FCDs also contributed to reducing the severity of hot-spot zones, as shown in Fig. 3-44-b. Compared to the case without FCDs, the cases with LDICDs-LDOCDs and LDICDs successfully manage the hot-spot zone in the heel. The case with LDICDs-TDOCDs was unable to reduce the temperature compared to other FCDs deployment scenarios; nonetheless, a little contribution to temperature reduction was made in the heel.

This part presents the principles of the physics of the effectiveness of LDICDs in a heterogeneous reservoir. The specific block under the study in the heterogeneous reservoir is highlighted in Fig. 3-45 by a purplish rectangle. The reservoir permeability in this scenario is lower than in the two previous cases, owing to the distributed permeability within the reservoir model. As established by Izadi et al. (2023-a), lower permeability correlates with diminished reservoir quality and, consequently, lower oil recovery. Fig. 3-46 illustrates the temperature and CWE of the produced steam. According to the analysis by Izadi et al. (2023-b), simulations flag the occurrence of steam breakthrough if steam production continually increases or exceeds 0.1 m3/day CWE (Fig. 3-46). Similar to the simple reservoir with shale barriers, in this case, the temperature for the LDICD-equipped scenario surpasses that of the case without LDICDs. This temperature disparity underscores the role of LDICDs in directing steam toward nearby grids, thereby heating them and concurrently postponing steam breakthrough.

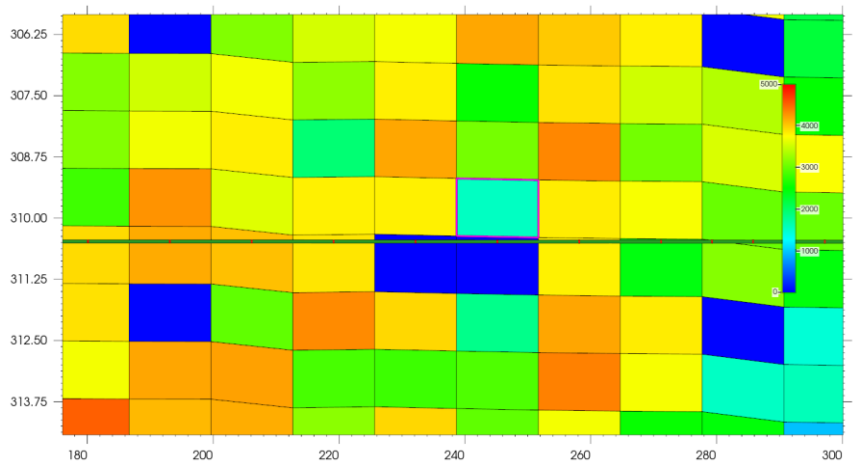

Fig. 3-45. The location of block number {25, 16, 45} in the heterogenous reservoir which the producer well is drilled on its bottom. The property which is shown is permeability in I direction.

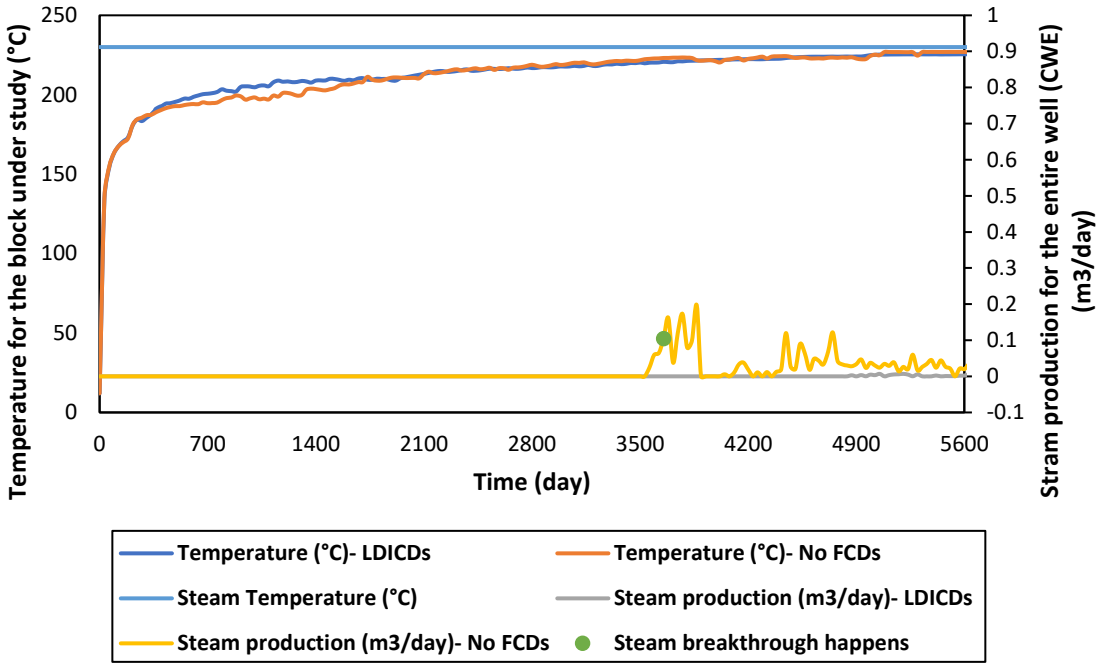

Fig. 3-46. LDICD helps to mitigate steam breakthrough and distribute the temperature within the entire reservoir.

Throughout the simulations in this paper, a subcool temperature ranging from 10°C to 15°C has been consistently employed, characterized as a relatively conservative subcool temperature [84]. A comparative analysis of Fig. 3-27-a, Fig. 3-33-a, and Fig. 3-40-a reveals that the oil production rate in the case of the heterogeneous reservoir is notably lower than in the other two cases. This discrepancy is logically attributed to the lower permeability inherent in the heterogeneous reservoir. As extensively discussed by [101], one potential solution to increase the production rate involves reducing the subcool temperature, although this approach involves operating with a more precarious and challenging subcool temperature, leading to a thinner liquid pool. For scenarios without LDICDs, [101] demonstrated that steam breakthrough would occur quite promptly, in some instances preceding six months from the commencement of SAGD operation. Consequently, LDICDs prove to be more beneficial under lower subcool temperatures, as wells lacking LDICDs struggle to remain operational.

3.4.5. Discussions

In this section, a comparison between the simulation results presented with real data obtained from SAGD operations in Western Canada is provided. Izadi et al. (2022) published an average value for FCD's contribution to oil production and cSOR for uplifted cases compared to the wells without

FCDs in Western Canada [99]. Izadi et al. (2022) defined the uplifted cases as wells completed with FCDs resulting in enhanced normalized oil production or cSOR in comparison to neighboring wells in the same pad without FCDs [99]. The reported average values do not include wells fitted with FCDs that did not improve oil production or cSOR.

The simulation results in this section are presented for the heterogeneous reservoir with described ICDs and OCDs characteristics and a subcool temperature range between 10°C and 15°C. The comparison is shown in Fig. 3-40-b and Fig. 3-41-b for oil production and cSOR, respectively. Izadi et al. (2022) did not report the subcool temperature of the operations they studied, nor other operational parameters since they are not publicly available. Therefore, it is only possible to utilize the comparison between the simulation result and the results reported by Izadi et al. (2022) to determine if FCDs have the same effect and provide the same trend on improving oil production and cSOR in real-world operations as they did in the present study [99].

Simulation results shown in Fig. 3-47 represent the average value for all different FCDs deployments in the different reservoir heterogeneity reported in Fig. 3-27-b, Fig. 3-28-b, Fig. 3-33-b, Fig. 3-34-b, Fig. 3-40-b, Fig. 3-41-b. Field data results have been published by Izadi et al. (2022) and are shown in Fig. 3-47 for the cases with all types of FCDs including liner and tubing-deployed ICDs or OCDs, LDFCDs including LDICDs and LDOCDs, TDFCDs including TDICDs and TDOCDs, ICDs including LDICDs and TDICDs, and OCDs including LDOCDs and TDOCDs. As shown in Fig. 3-47-a, LDFCDs provided the greater improvement in oil production in the simulation results in this study and LDFCDs deployment is the second-ranked strategy that improved oil production in the field data. The ranking trend of different deployment strategies, according to increasing oil production, is identical in both the simulation cases and real SAGD operations. Fig. 3-47-b shows the contribution of FCDs on reducing cSOR in the simulation results in this section and the real cSOR data published by Izadi et al. (2022). The ranking of different deployment strategies, according to decreasing cSOR, is identical in both the simulation cases and real SAGD operations.

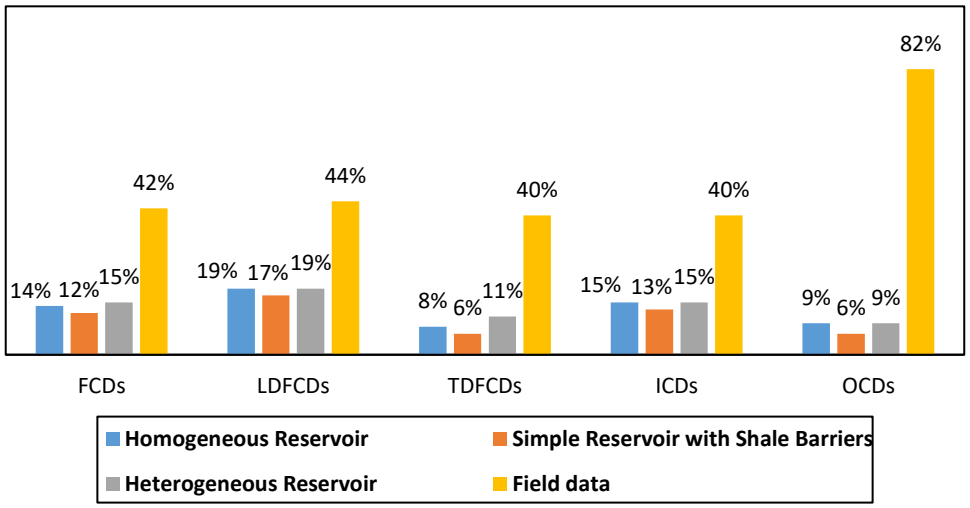

a

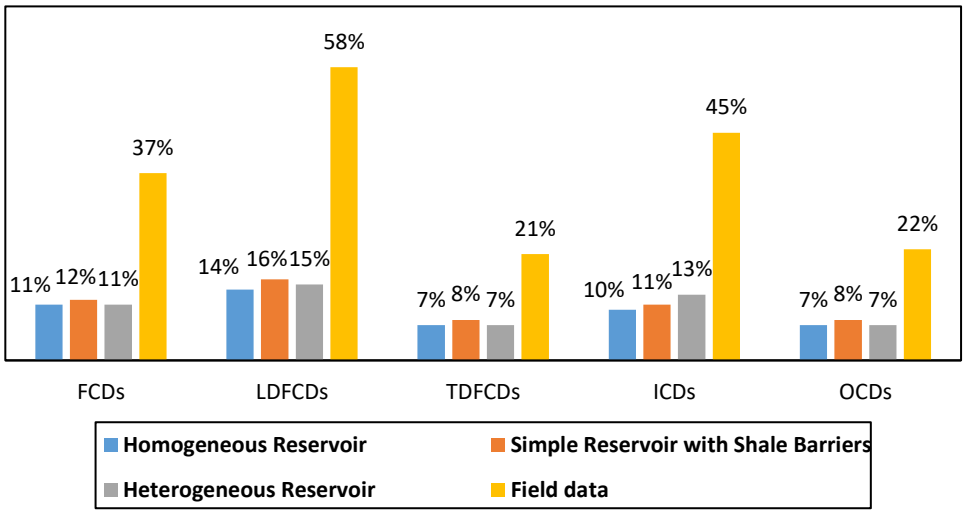

b

Fig. 3-47. Comparison between the simulation data for different reservoir heterogeneity scnarios presented in Fig. 3-27-b, Fig. 3-28-b, Fig. 3-33-b, Fig. 3-34-b, Fig. 3-40-b, Fig. 3-41-b and field data published by Izadi et al. (2022): (a) increase in oil roduction and (b) decrease in cSOR.

The degree of subcool control might explain the trends and variability displayed in Fig. 3-44. Subcool affects the flow control device's performance and can impact the overall efficiency of the SAGD process, as illustrated by Izadi et al. (2023) [102]. Well-designed flow control devices can enhance oil production and reduce cSOR when operating at lower subcool temperatures, as opposed to higher subcool temperatures, as shown in Izadi et al. (2023) [102]. However, it is important to note that excessively low subcool temperatures can also lead to operational challenges. For instance, if the subcool temperature is too low, the flow control devices may fail

to prevent the steam from being produced or become plugged with sands carried along with the steam (Izadi et al., 2023) [102]. Therefore, operational conditions are important controlling factors in oil production and cSOR, and they should be carefully considered when comparing FCD strategies. These are the primary reasons for the observed differences in Fig. 3-47.

In the data-driven analysis by Izadi et al. (2023) [102], LDICDs performed better in terms of increasing oil production and lowering cSOR compared to TDICDs. One reason could be because of the risk of failure associated by TDICDs completion due to sand production if the well completed by TDICDs is run by the same subcool and production rate as a well completed by LDICDs [36]. In this section, the subcool and well operational parameters kept the same for both cases with LDICDs and TDICDs, and still the case with LDICDs performed better than the case with TDICDs. We concluded that this is because LDICDs are in direct contact with the sand face, therefore they can provide the pressure drop more efficiently resulting more equalized fluid rate entering to the well (Fig. 3-48). As shown in Fig. 3-48, in Section #1 and #3, the case with LDICDs provided more equalized production rate than the case TDICDs while the reservoir permeability is relatively higher than other parts of the reservoir. This helps to warm up other parts of the reservoir, as can be seen in Section #2 in which a higher and more balanced production rate is provided by the case with LDICDs.

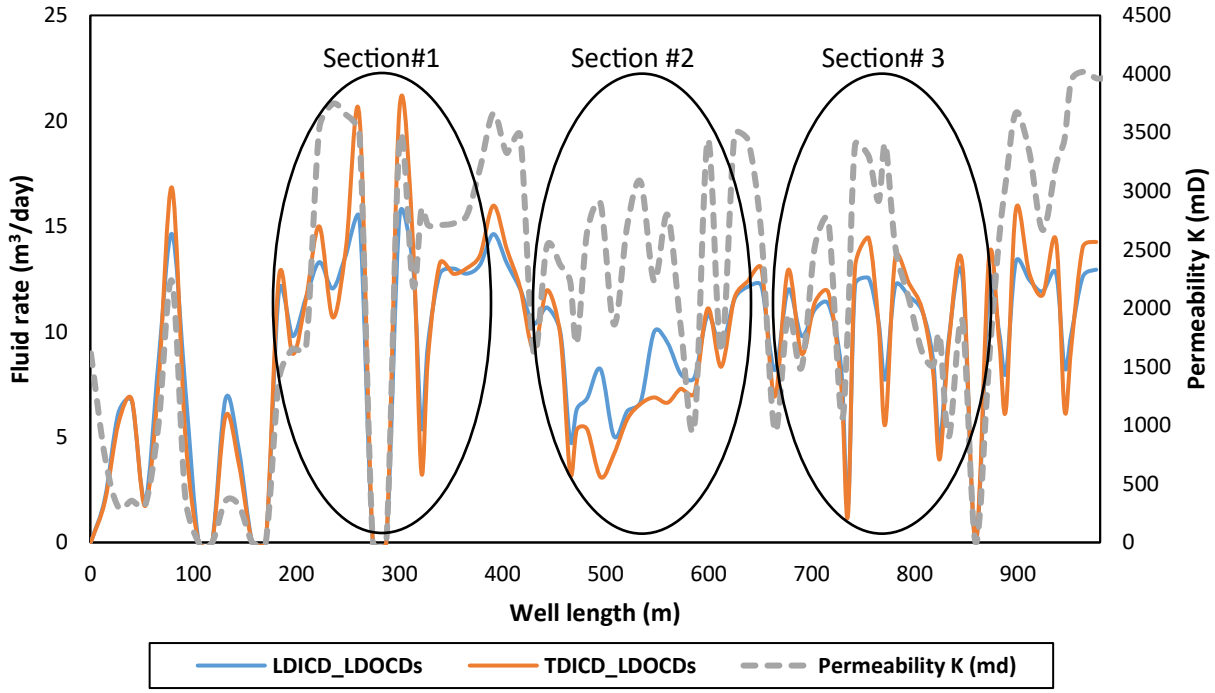

Fig. 3-48. Comparing LDICDs and TDICDs in terms of equalizing the production rate along the producer well.

3.5. Different Subcool Temperature Scenarios: Impact of Inflow Rate Control

In this section, a new reservoir model is constructed using real data to investigate how various flow rate control strategies affect the well performance. To enhance the permeability distribution within the reservoir model, data from neighboring wells, specifically the PSD (Porosity and Permeability Scatter) data, are gathered. These PSD data are utilized along with the developed correlation to estimate permeability. To ensure the suitability of the correlation for this particular well, an initial step involves employing a clustering algorithm. This algorithm helps classify the PSD database and identifies representative PSDs that will be compared with the ones the correlation was based upon. Once this comparison is done, permeability can be estimated using the developed correlation, and subsequently, the reservoir model is created.

The PSD database is clustered using an unsupervised and self-adaptive algorithm to determine the representative PSDs and the corresponding PSD characteristics such as D-values and fines contents. The clustering algorithm generated five groups with a weighted average permeability of 4,013 mD. Afterward, the permeability for each PSD is estimated using a correlation developed in section 3.3.2.1 Permeability Estimation. The reservoir model for the database's location is created using real data, such as porosity, permeability, and topography; three tabular data from the flow-loop experiments are assigned in the simulation model, and the liner-deployed (LD) ICDs' performances are compared in two subcool scenarios. The results show that the cases with LDICDs offer a greater oil production rate, better steam conformance, and lower cSOR than the case without LDICDs. These findings suggest that appropriately designed ICDs can enhance oil production while reducing cSOR. This, in turn, translates to reduced water consumption and lower greenhouse gas emissions, thus contributing to climate change mitigation efforts. Increasing oil production, cost efficiency, and minimizing negative environmental impact ultimately led to a more sustainable oil production approach.

This section presents a comparison between the reservoir simulation case without ICDs and the three cases with ICDs under two production scenarios. The first scenario involves a relatively conservative production with a subcool ranging from 10°C to 15°C, while the second scenario represents a relatively challenging production with subcooling between 1°C to 5°C. Additionally,

to determine the required amount of natural gas for cases with and without ICDs, Eq. 12 suggested by Nimana et al. (2015) is employed [32].

$$Natural\ gas\ required\ \left(\frac{m^3}{m^3}\ of\ bitumen\right) = \frac{iSOR * (H_s - H_w)}{Q_s * \eta_b * LHV} \quad (12)$$

where $iSOR$ is the instantaneous steam oil ratio, H_s is the enthalpy of steam, H_w is the enthalpy of boiler feed water, Q_s is the steam quality, η_b is the steam boiler efficiency, and LHV is the lower heating value of natural gas. Based on Eq. 12, the required natural gas for the cases without FCDs and with ICDs#1depends on iSOR.

3.5.1. Relatively Conservative Production: Subcool Between 10°C to 15°C

Initially, a relatively conservative production is simulated. A subcool of 10°C to 15°C provides a good liquid pool thickness on the producer well, so it helps to prevent steam from being produced. As depicted in Fig. 3-49, the subcool temperature fluctuates between 10°C and 15°C for different cases. For all the cases, the simulator successfully holds the subcool temperature between the desired range.

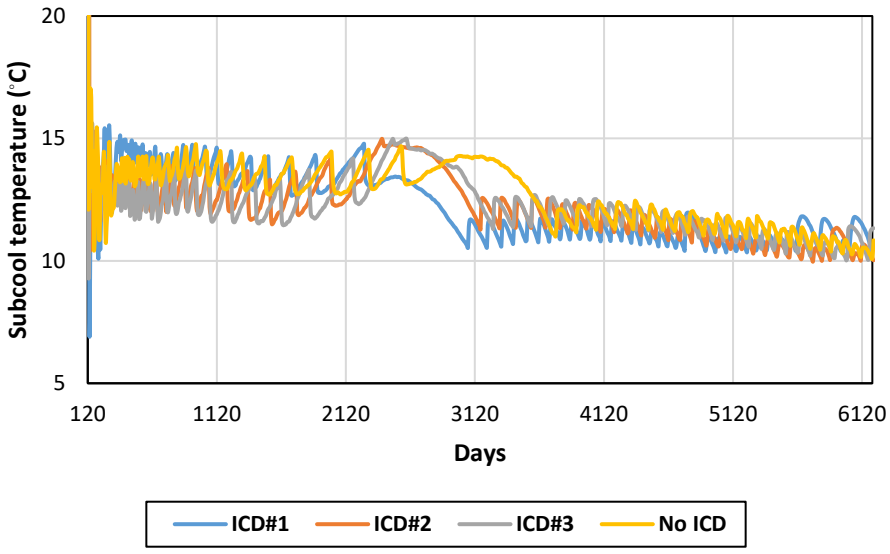

Fig. 3-49. Subcool temperature for the cases with a subcool between 10°C and 15°C. The simulator keeps the subcool temperature between 10°C and 15°C.

Fig. 3-50 shows the CWE of the produced steam. Since the CWE of the produced steam is very low, none of the cases reached the SBT in the simulation period. In other words, the liquid pool provided enough pressure drop to prevent the steam from being produced.

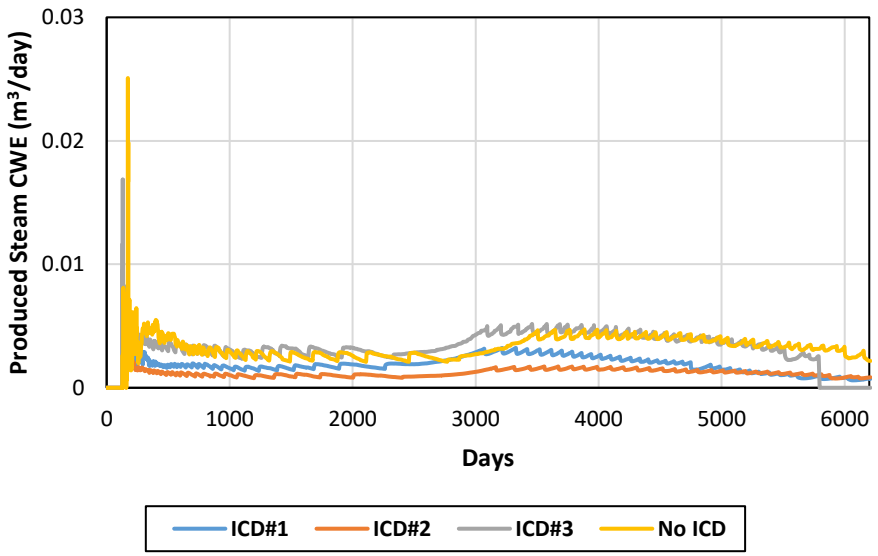

Fig. 3-50. Subcool between 10°C and 15°C: produced steam CWE for all cases is very low, so none of them reached out to SBT.

The oil production rate profiles for the cases are shown in Fig. 3-51. The cases with ICDs provided a higher oil production rate than those without ICDs. The case with ICD#1 provided a slightly higher oil production rate for almost 2,700 days.

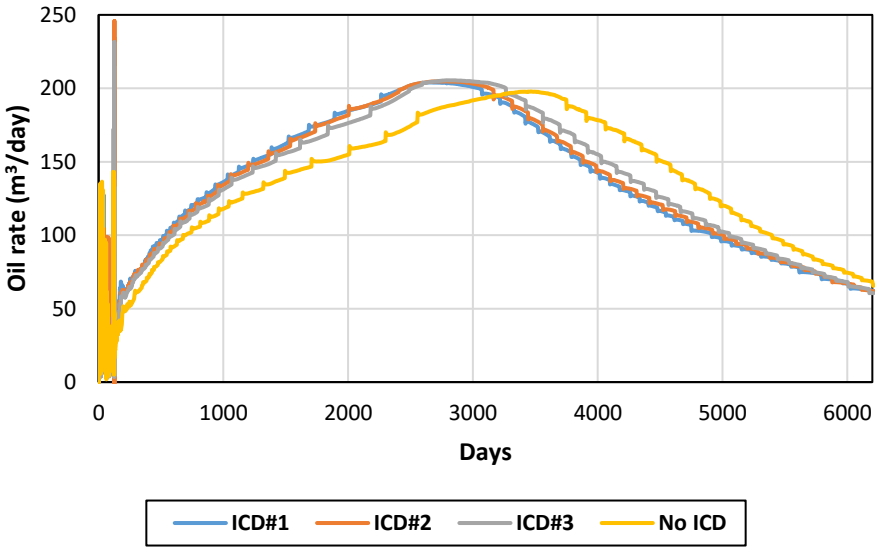

Fig. 3-51. Subcool between 10°C and 15°C: the cases with ICDs provided higher oil production rates.

As shown in Fig. 3-51, if ICDs are properly designed, they can enhance the oil production rate. Before 2,700 days, the cases with ICDs produce more oil, and after 2,700 days, the steam chamber

has grown enough to deplete the reservoir for the case without ICDs. So, the rate for cases without ICDs is larger than the cases with ICDs.

Based on Fig. 3-52, the production rate for the first 2,700 days and after 120 days of circulation, by dividing the slope of the fitted line on the production rate, the case with ICD#1 has a producing oil rate that is 17% higher than the case without ICDs. It means that by using ICDs, the oil in the reservoir would be produced sooner by 17%.

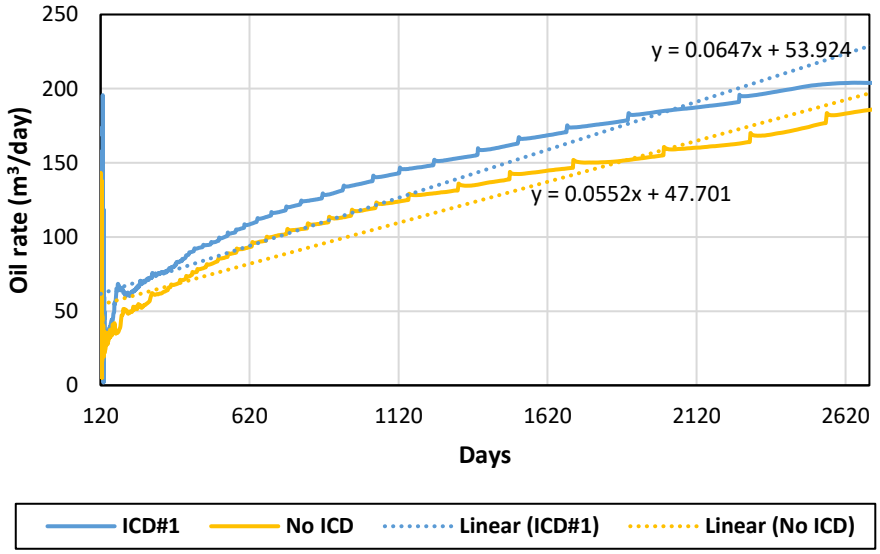

Fig. 3-52. Subcool between 10°C and 15°C: slope of the fitted line to the oil rate production.

The reservoir temperature for the four cases after 2,220 days is shown in Fig. 3-53. The results illustrate how ICDs have contributed to better steam conformance, resulting in a warmer reservoir and a higher oil production rate.

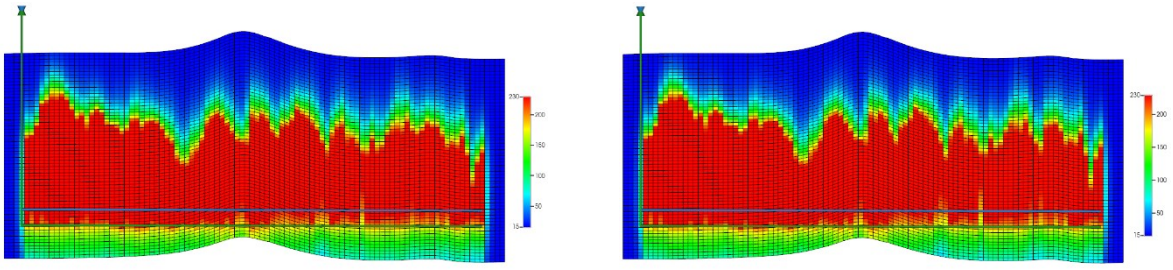

a b

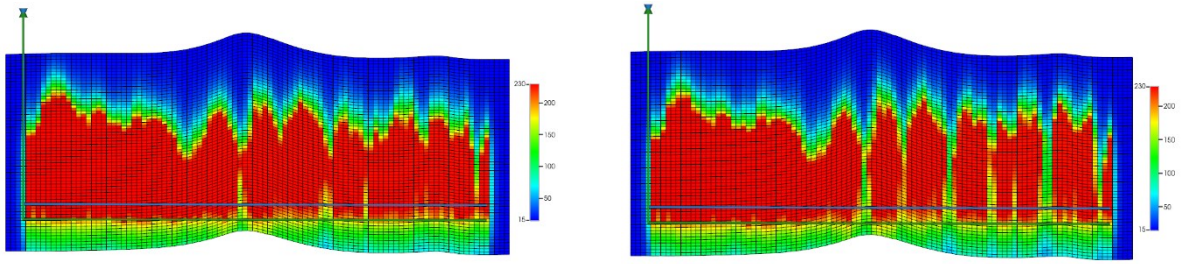

c d

Fig. 3-53. Subcool between 10°C and 15°C: reservoir temperature along the producer well after 2,220 days of simulation. a: the well with ICD#1, b: the well with ICD#2, c: the well with ICD#3, and d: the well without ICD.

The cumulative steam oil production for the four cases is shown in Fig. 3-54. As shown in Fig. 3-54, the cumulative oil production curves for the cases with ICDs are very close, while for the case without ICDs is lower and the case without ICDs produced the same oil as the case with ICDs after 5260 days.

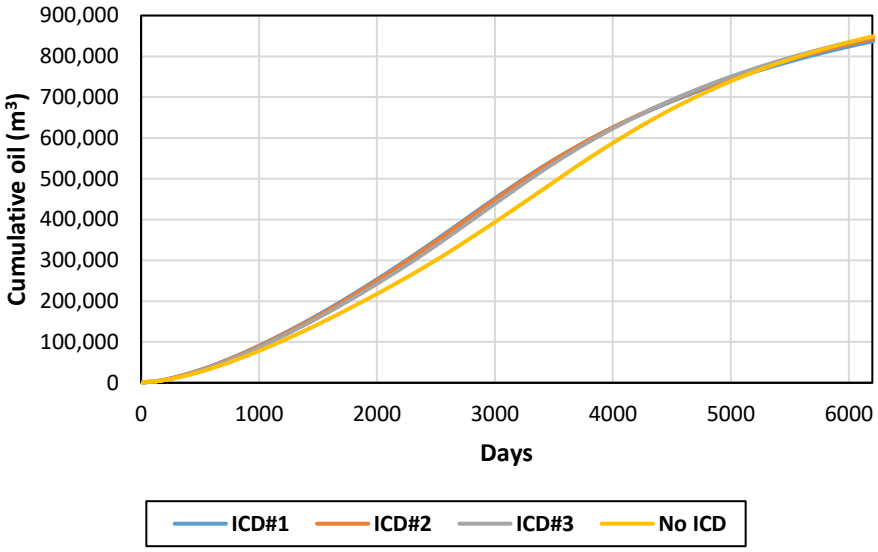

Fig. 3-54. Subcool between 10°C and 15°C: the cases with ICDs provided higher cumulative oil production than the case without ICDs.

The cSOR for the four cases are compared in Fig. 3-55. The cases with ICDs generally show a lower cSOR than those without ICDs. The only exception is for the case of ICD#1, in which the cSOR is slightly higher during the first 850 days of production; however, the final cSOR, at the end of the production phase, is similar to that without ICDs. The overall average cSOR for ICD#1 is 8% lower than for the case without ICDs.

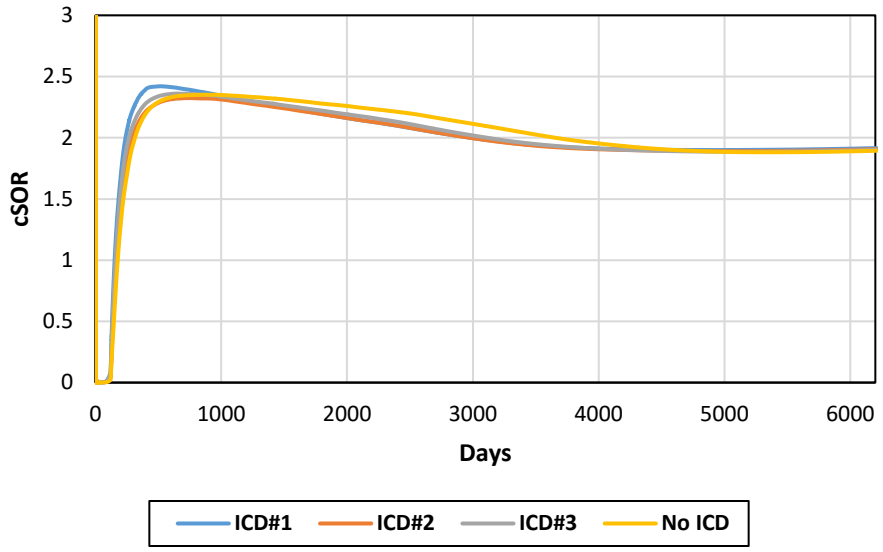

Fig. 3-55. Subcool between 10°C and 15°C: the cases with ICDs provided a little lower cSOR than those without ICDs in a specific time range.

Fig. 3-56 illustrates the iSOR curves for the two cases, showing how the required natural gas is lower for the case with ICD#1 compared to the case without ICDs, leading to lower GHG emissions. Fig. 3-57 presents the ratio of the iSOR curves shown in Fig. 3-56, standing for how much the required natural gas is lowered for the case with ICD#1 compared to the case without ICD. Based on Fig. 3-57, gas usage to generate steam in the initial stage of SAGD production is much lower with ICDs#1. After about 3,700 days, the gas usage for both cases is almost identical, eventually it reduces for the case with ICDs after 4,800 days. On average for the whole SAGD production, the case with ICD#1 consumed 10% less natural gas than without ICDs.

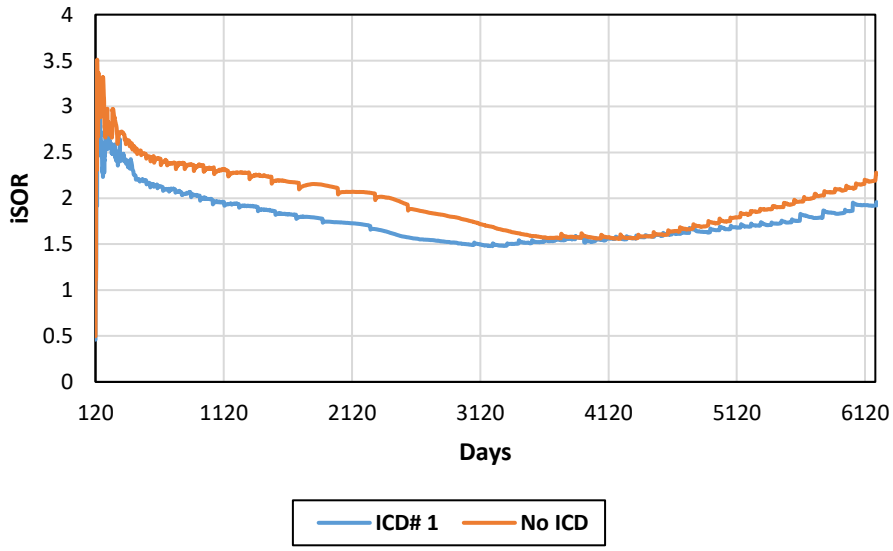

Fig. 3-56. iSOR for the cases with ICD#1 and without ICD illustrating how the required natural gas for the simulated SAGD project is lowered using ICD#1.

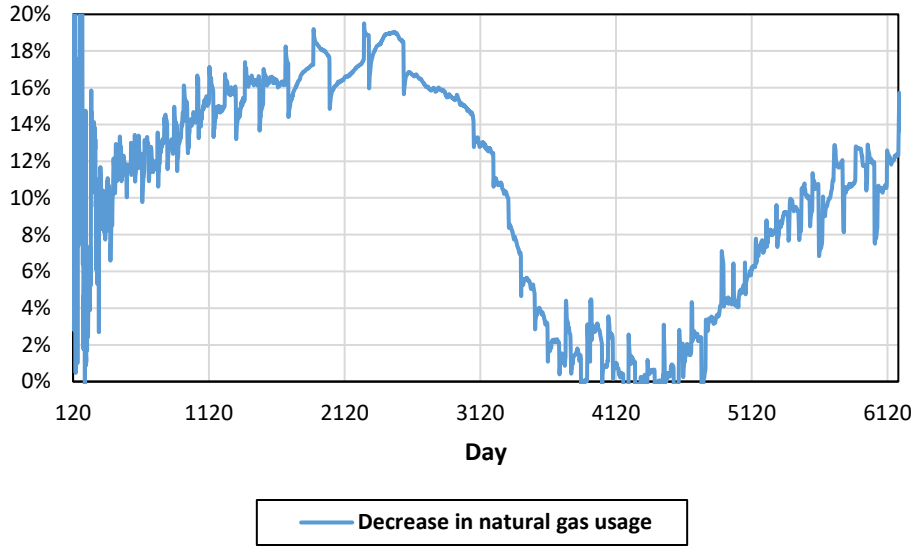

Fig. 3-57. The ratio of the iSOR curves shown in Fig. 3-56, standing for how much the required natural gas is lowered in the simulated SAGD project for the case with ICD#1 compared to the case without ICD.

3.5.2. Relatively Challenging Production: Subcool Between 1°C to 5°C

For the next set of simulations, the subcool level is reduced. ΔP for the case without ICDs is only provided by the liquid pool, which is thinner than the case with a subcool between 10ºC to 15ºC. Therefore, it is expected that steam being produced sooner.

The simulator has failed to simulate the SAGD operation in the desired subcool. In the simulation model, the primary constraint is the well bottomhole pressure (BHP), while the secondary constraint is the pre-defined subcool level. When the BHP drops, violating the primary constraint, the simulator will adjust (lower) the subcool in an effort to increase the oil production and the BHP. As shown in Fig. 3-58, after 686 days, the minimum well BHP (blue curve) constraint is violated. The simulator attempts to maintain the BHP constant at its minimum level, decreasing the fluid rate (orange curve). To avoid a continuous decreasing trend in the fluid production rate, after a slight subcool decrease (grey curve), the simulator increased the subcool temperature constraint to provide more pressure to keep the well BHP constant.

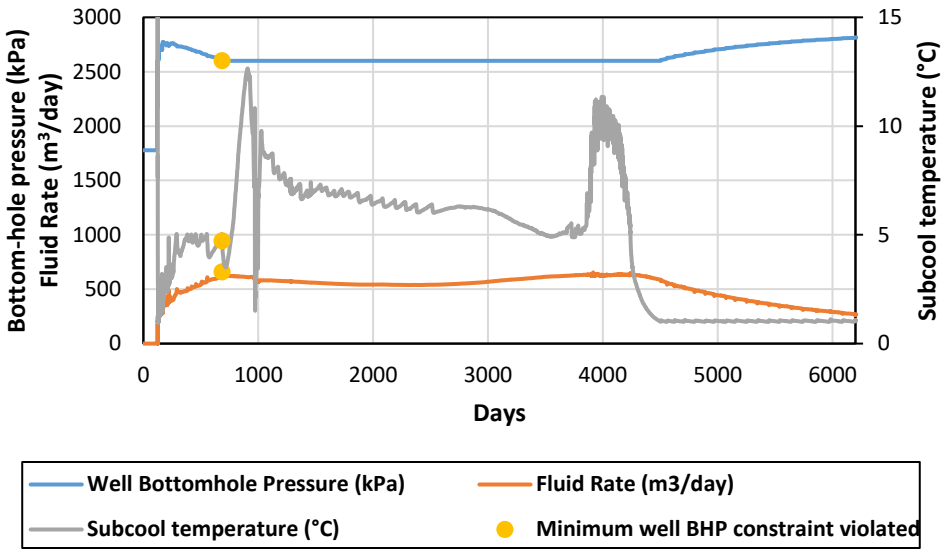

Fig. 3-58. The minimum well BHP constraint is violated, and the simulator increased the subcool temperature to keep the well BHP constant and avoid too much reduction on production fluid rate.

Fig. 3-59 shows the subcool temperature for the four cases. For the three cases with ICDs, the cases with ICD#1 and ICD#2 could be simulated by the desired subcool temperature. The case with ICD#3 is simulated in the desired subcool temperature; however, after 3,760 days, it started to violate the subcool temperature constraints.

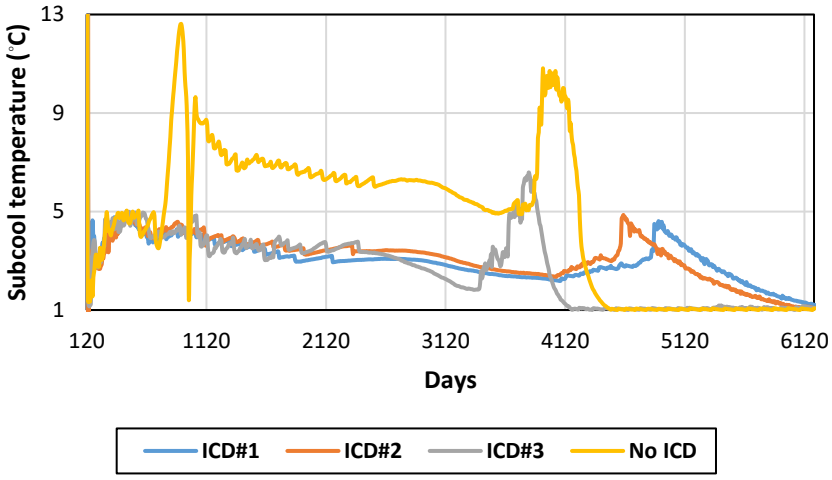

Fig. 3-59. Subcool between 1°C and 5°C: the simulator could not operate the case without ICDs within the desired subcool temperature.

In Fig. 3-60, the steam production for all cases is provided. Still, the case without ICDs keeps producing steam, and SBT is the point at which steam is continuously produced. Similar SBT behavior is observed for the case with ICD#3. The produced steam CWE for cases with ICD#1 and ICD#2 is very low; however, for ICD#3 and no ICD cases, steam production starts to increase

after 2,660 and 1,170 days, respectively. According to Fig. 3-60, cases with ICD#1 and ICD#2 offer the highest resistance (pressure drop); therefore, steam is choked more successfully by the ICDs compared with the case with ICD#3 and the case without ICD.

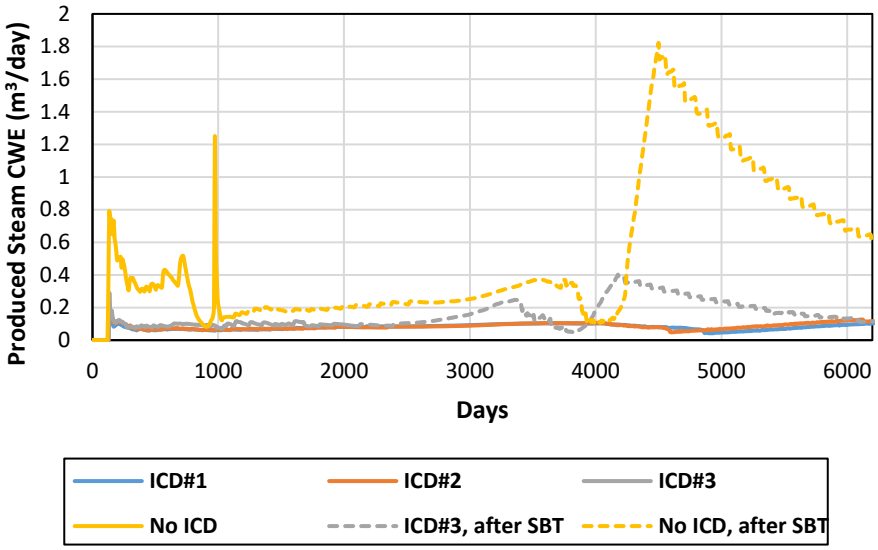

Fig. 3-60. Subcool between 1°C and 5°C: the produced steam CWE for cases with ICD#1 and ICD#2 is very low, while steam production increases quickly for ICD#3 and no ICD cases.

The oil production profiles are shown in Fig. 3-61. Compared to Fig. 3-51, which shows the oil rate for the case with a subcool between 10°C and 15°C, the oil rate in Fig. 3-61 is higher. This increase is expected because a decrease in the subcool would produce more liquid, resulting in a lower liquid pool thickness and a higher probability of SBT. The need for inflow control is more important in this case, and an appropriate ICD design would prevent the SBT.

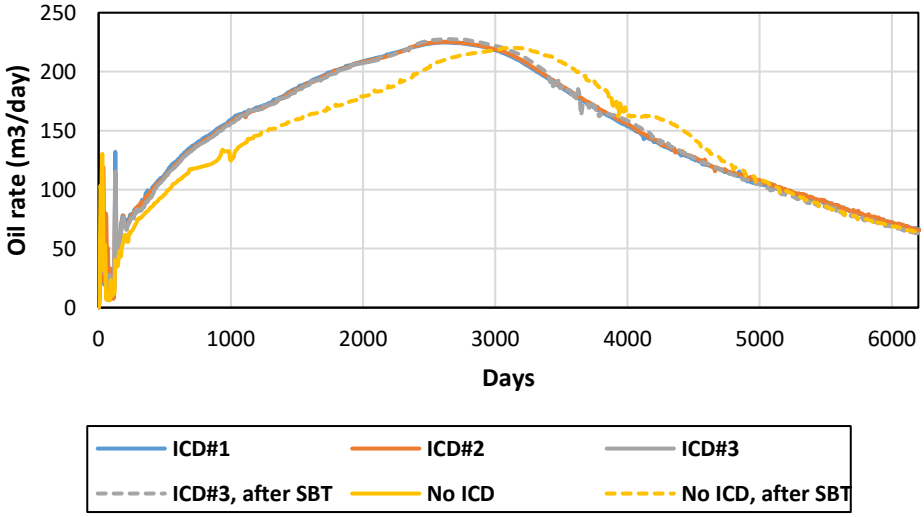

Fig. 3-61. Subcool between 1°C and 5°C: cases with ICDs provide higher oil production rates.

Based on Fig. 3-62, the production rate for the first 1,170 days and after 120 days of circulation, by dividing the slope of the fitted line on the production rate, the case with ICD#1 has a producing oil rate that is 21% higher than the case without ICDs. It means that by using ICDs, the oil in the reservoir would be produced sooner by 21%.

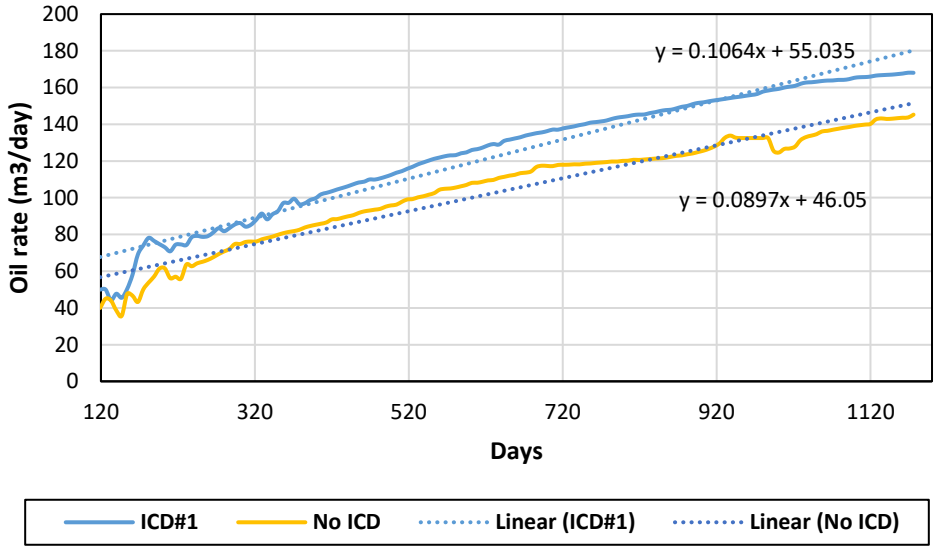

Fig. 3-62. Subcool between 1°C and 5°C: the slope of the fitted line to the oil rate production.

The reservoir temperature after 2,220 days is shown in Fig. 3-63. Compared to Fig. 3-53, the reservoir is heated up more extensively for all cases, demonstrating the reason for the higher oil rate with a subcool between 1°C and 5°C.

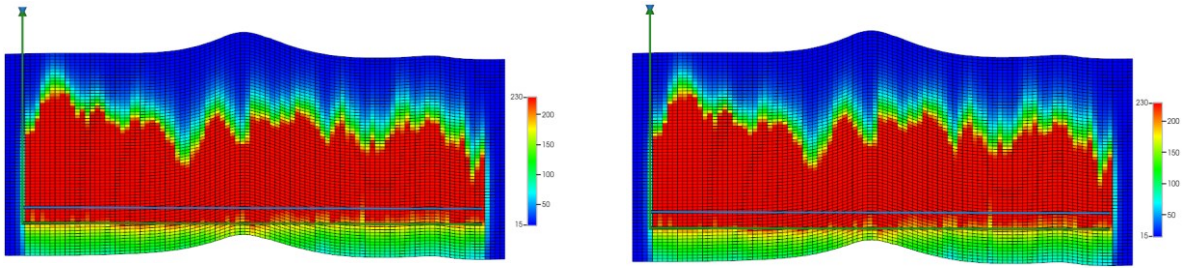

a b

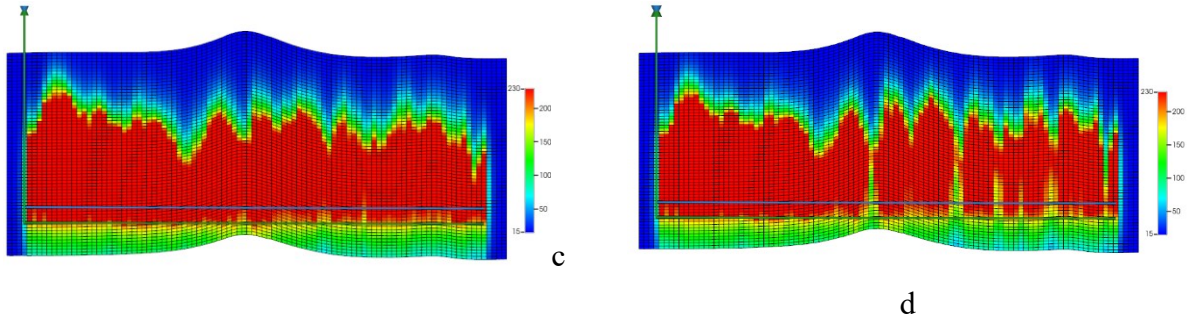

Fig. 3-63. Subcool between 1°C and 5°C: reservoir temperature after 2,220 days. a: the well with ICD#1, b: the well with ICD#2, c: the well with ICD#3, and d: the well without ICD.

The cumulative oil production for the case with a subcool between 1°C and 5°C is shown in Fig. 3-64. The cases with ICD#3 and no ICD experience SBT and produce less oil than the cases with ICD#1 and ICD#2. Another point that needs to be considered is the role of ICDs at various subcool levels: it is clear from comparing Fig. 3-63 and Fig. 3-54 that lower subcool results in higher oil production; a well-designed ICD can facilitate the operation at lower subcool levels by choking back the steam and preventing SBT.

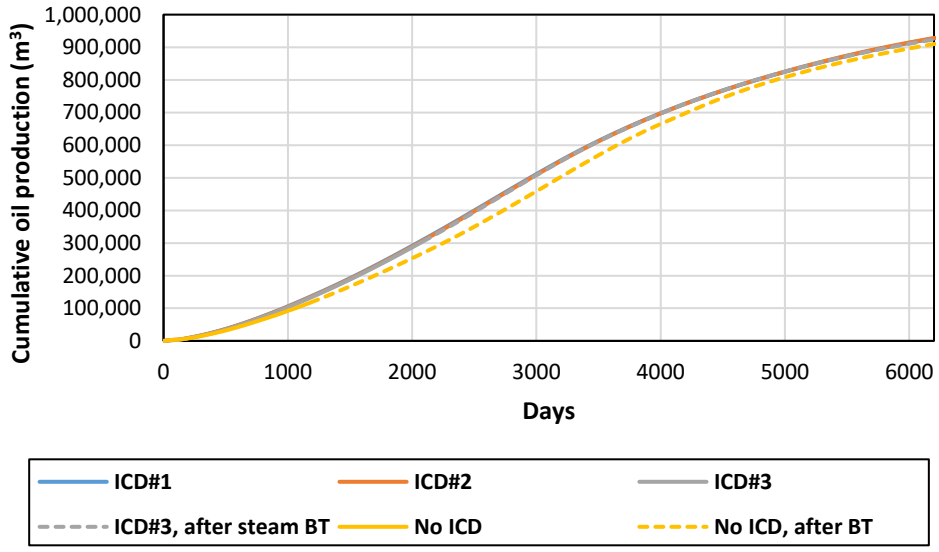

Fig. 3-64. Subcool between 1°C and 5°C: the cases with ICD#1 and ICD#2 produce more oil than those in Fig. 3-54 with higher subcool.

The cSOR curve for the cases is provided in Fig. 3-65. The cSOR for the cases with ICD#1 and ICD#2 is slightly lower than the other cases. Compared to Fig. 3-55, almost the same trend is detected between the four cases, and the cases with ICDs provided a lower cSOR than those without ICDs. The average cSOR for ICD#1 is 12% lower than the case without ICDs.

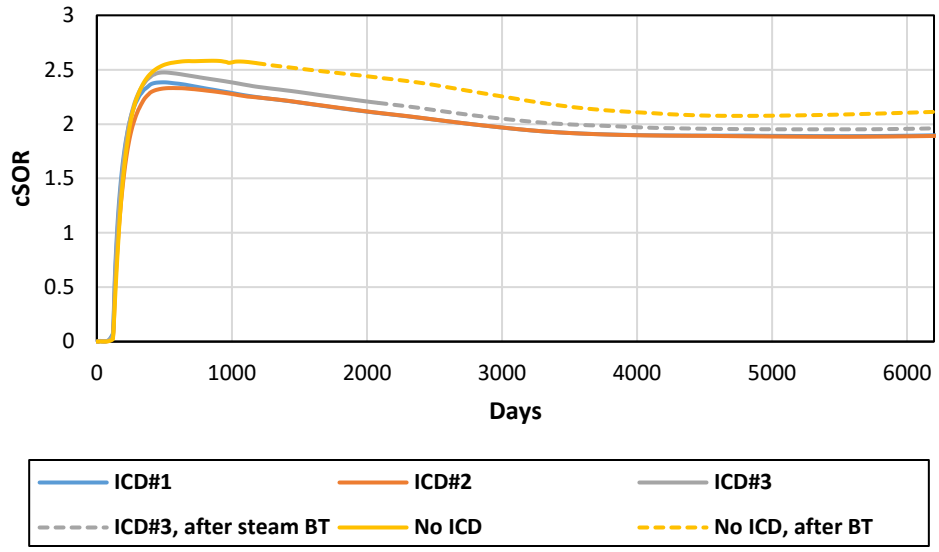

Fig. 3-65. Subcool between 1°C and 5°C: the cases with ICDs provided a lower cSOR compared to the case without ICD.

Based on the production, steam conformance, and cSOR, we concluded that ICD#1 works better for this specific reservoir. The proper well pressure drop provided by ICD#1 helps manage hot-spot zones, keeps the reservoir warm, lowers cSOR, increases the oil production rate, and postpones SBT.

Fig. 27 illustrates the iSOR curves for the two cases, showing how the required natural gas is lower for the case with ICD#1 compared to the case without ICDs, leading to lower GHG emission. Fig. 28 presents the ratio of the iSOR curves shown in Fig. 27, presenting the required natural gas for the simulated SAGD project is lowered using ICD#1 compared to the case without ICDs. Based on Fig. 26, the gas usage to generate steam is lower for the case with ICDs#. On average for the whole SAGD production, the case with ICD#1 consumed 17% less natural gas compared to the case without ICDs.

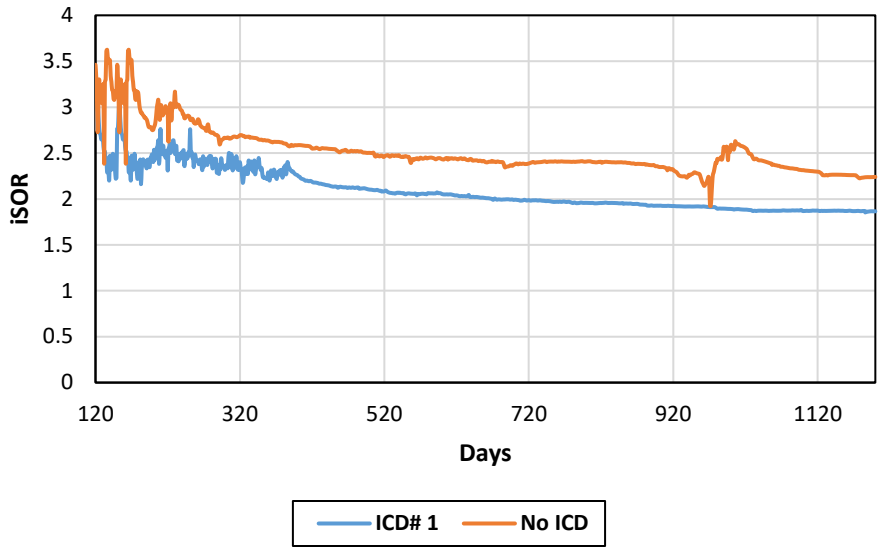

Fig. 3-66. iSOR for the cases with ICD#1 and without ICD presenting the required natural gas for the simulated SAGD project is lowered using ICD#1 compared to the case without ICDs.

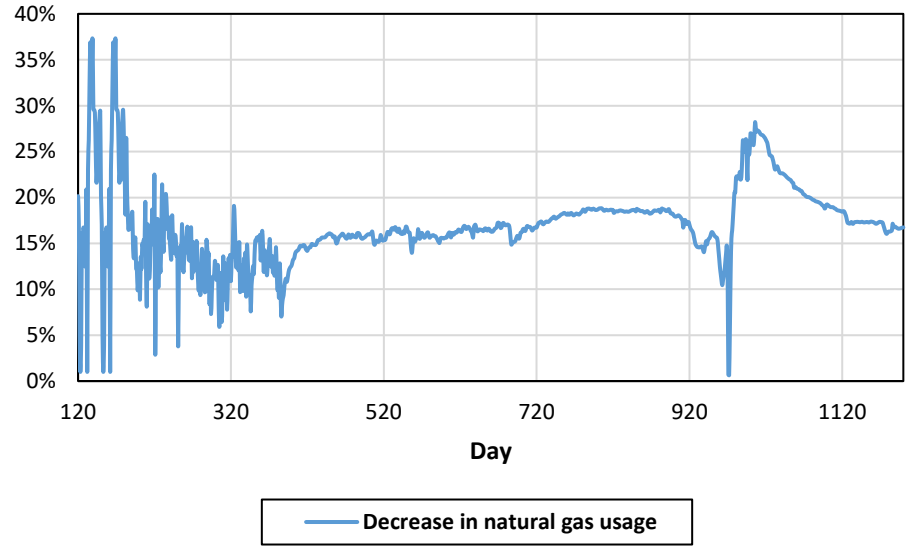

Fig. 3-67. The ratio of the iSOR curves shown in Fig. 3-65, refers to the extent of reduction in the required amount of natural gas in the simulated SAGD model for the case involving ICD#1 compared to the case without ICD.

3.5.3. Discussions

The reservoir temperature for the cases with ICD#1 and no ICDs with a subcool between 1°C to 5°C for 2,220 days of production is shown in Fig. 3-68. ICDs by providing an additional ΔP in high-quality regions and preventing hot-spot zones in the first 400 meters of the producer well.

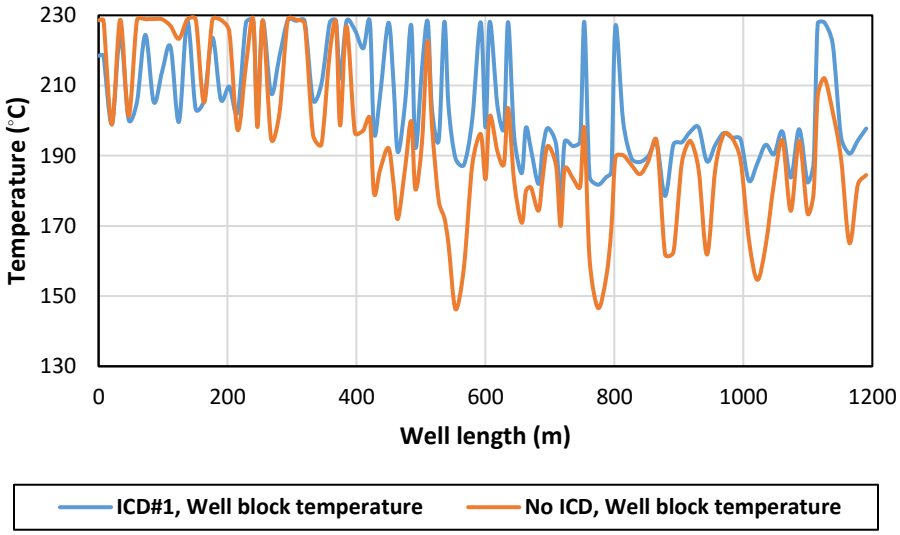

Fig. 3-68. Subcool between 1°C and 5°C: ICDs prevented hot-spot zones and improved steam conformance in 2,220 days of production.

As depicted in Fig. 3-69, ICDs provide an additional ΔP on top of the pressure drop by the liquid pool. This additional ΔP for ICD#1 is shown in Fig. 3-69 for the case with a subcool between 1ºC to 5ºC after 2,200 days of production. The corresponding fluid rate is also shown for the same date. Fig. 3-69 illustrates the ICD performance of adjusting the fluid rate in terms of ΔP. To confirm that the simulated ΔP shown in Fig. 3-68 roughly matches the values from Fig. 3-20 at various rate levels, a scatter plot of the simulated ΔP and the expected ΔP (i.e., flow-loop measurements or simulation inputs) for ICD#1 is shown in Fig. 3-69.

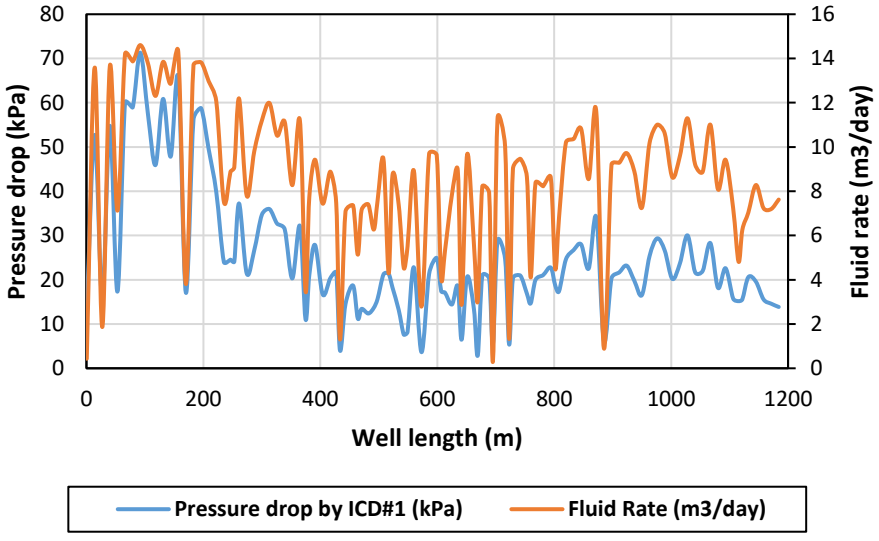

a

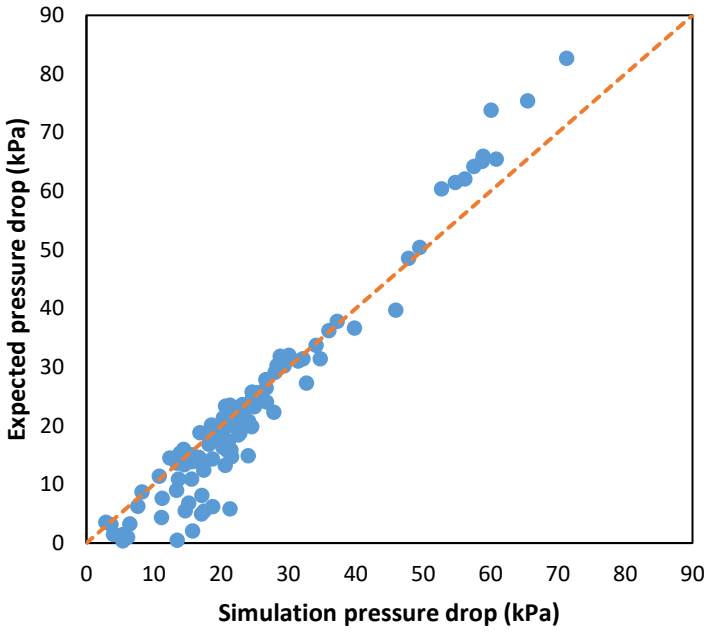

b

Fig. 3-69. a) Subcool between 1°C and 5°C: the ΔP resulted from ICDs and the corresponding fluid rate after 2,200 days of production. B) Simulated ΔP versus expected (experimentally measured) ΔP for ICD#1.

Based on Fig. 3-69, good agreement is observed between the expected and the simulated pressure drop and ΔP by ICD#1 most likely matches with what Yusuf et al. (2021) obtained in their flow-loop experiment, serving as a validation that the simulator successfully applied the ICDs tabular information into the reservoir model [34]. The difference between the simulated and expected pressure drop can be attributed to calculating the ICD pressure drop as the difference in well block pressures between the case without ICDs (lower pressure) and the case with ICDs (higher pressure). Although all the constraints and conditions are the same in both cases, some changes, as depicted in Fig. 3-58 may arise during the simulation.

3.6. Conclusions and Future Works

In Western Canada, SAGD is the major in-situ thermal process for oil production. Innovative technology like FCDs enables operators to enhance oil production rates while supporting a sustainable environment by lowering water usage. A series of SAGD simulations were conducted in this section to model the impact of different FCDs strategies on wells performance in a homogeneous reservoir, a simple reservoir with shale barriers nearby wells, and a heterogeneous reservoir.

Wells completed using both LDICDs and LDOCDs to achieve the best results in the homogenous reservoir by improving the average oil production by 26% and decreasing the average cSOR by 19%. Based on simulation findings for the simple reservoir case with shale barriers nearby the wells, LDOCDs boosted steam chamber growth by 13%. Furthermore, wells completed by both LDICDs and LDOCDs represent the best practices for well completion, increasing average oil production by 24% and lowering average cSOR by 20%.

In the heterogeneous reservoir, LDICDs contributed to managing hot-spots and much better steam conformance along the producer well. The best practice, as in the situations of homogenous and simple reservoirs, was the joint implementation of LDICDs and LDOCDs, which increased average oil production by 26% and lowered average cSOR by 17%. In this scenario, the case with LDICDs decreased the average cSOR by 20%.

A well-designed LDICD could significantly contribute to a higher oil production rate and lower cSOR, with much better steam conformance. On the one hand, ICD design is extremely sensitive to reservoir quality. On the other hand, PSDs reflect the reservoir's hydraulic properties; consequently, considering PSD data in ICD designs could help manage potential issues associated with the hot-spot zones.

Core and PSD data have been collected from the McMurray Formation, Athabasca oil sands using open-source resources such as the AccuMap^{TM} database and Alberta Energy Regulator (AER) reports. A SAGD reservoir model is created based on real data for the same location as core and PSD data extracted from the vertical wells.

Based on this study, the following conclusions are made

1. For a relatively conservative production scenario with subcooling between 10ºC to 15ºC
    a. **SBT did not happen:** Based on the simulation results, the liquid pool pressure drop is enough to prevent the steam from being produced.
    b. **Oil production increased by ICDs**: The oil production rate for the case with ICD#1 is 17% larger than the case without ICDs.
    c. **cSOR decreased by ICDs**: The cSOR for the case with ICD#1 is 8% lower than the case without ICDs.
    d. **Natural gas usage decreased by ICDs:** The natural gas consumed for the case with ICD#1 is 10% lower than the case without ICDs.

e. **Steam conformance enhanced by ICDs**: The steam conformance and distribution along the producer well is much better in the case of ICD#1 than in the case without ICDs.

2. With a relatively challenging production scenario with subcooling between 1ºC to 5ºC
    a. **SBT happened for the case without ICDs**: in a challenging production, the case without ICDs started to produce steam and reached out to the steam BT.
    b. **Oil production increased by ICDs**: The oil production rate for the case with ICD#1 is 21% larger than the case without ICDs.
    c. **cSOR decreased by ICDs**: The cSOR for the case with ICD#1 is 12% lower than the case without ICDs.
    d. **Natural gas usage decreased by ICDs**: The natural gas consumed for the case with ICD#1 is 17% lower than the case without ICDs.
    e. **Steam conformance was enhanced by ICDs**: The steam conformance and distribution along the producer well is much better in the case of ICD#1 than in the case without ICDs.

The inventions in this study are grouped into two categories, and the findings support the current industry trend of incorporating LDICDs and LDOCDs into new wells and pad developments. The second gives information on using FCDs to improve oil production and cSOR. This order of results may be limited by the populated heterogeneity in the reservoir models, and more investigations should be performed in each reservoir case study.

The outcomes would enhance understanding of the impacts of FCDs on production performance, contributing to more efficient well operation designs with lower greenhouse gas emissions to be a part of the climate change Net-Zero Emission by 2050 goals.

Chapter 4: Data-Driven Modeling

This chapter has been derived from the following papers:

Izadi, H., Roostaei, M., Mahmoudi, M., Hosseini, S.A., Soroush, M., Rosi, G., Stevenson, J., Tuttle, A., Sutton, C., Leung, J. and Fattahpour, V., **2021**, November. Data-Driven Well Pad Development Performance Review: Focus on the Role of Liner Design on Well Performance. **In SPE Symposium Compilation** (p. D011S002R004). SPE.

Izadi, H., Roostaei, M., Mahmoudi, M., Hosseini, S.A., Soroush, M., Rosi, G., Stevenson, J., Tuttle, A., Sutton, C., Leung, J. and Fattahpour, V., **2022**, March. The Impact of Increase in Lateral Length on Production Performance of Horizontal Thermal Wells. **In SPE Canadian Energy Technology Conference**. OnePetro.

Izadi, H., Roostaei, M., Mahmoudi, M., Rosi, G., Stevenson, J., Tuttle, A., Sutton, C., Mirzavand, R., Leung, J.Y. and Fattahpour, V., **2022**, November. Data-Driven Decision-Making Strategy for Thermal Well Completion. **In SPE Thermal Well Integrity and Production Symposium**. OnePetro.

Izadi, H., Roostaei, M., Mahmoudi, M., Stevenson, J., Tuttle, A., Bustamante, G., Rhein, S., Sutton, C., Mirzavand, R., Leung, J.V. and Fattahpour, V., **2023**, November. Flow Control Device and Liner Floatation: Key Technology Driver in Extreme Extended Reach Shallow Steam Assisted Gravity Drainage Wells. **In SPE Thermal Integrity and Design Symposium**. OnePetro.

Izadi, H., Leung, J.Y., Roostaei, M., Mahmoudi, M., Stevenson, J., Tuttle, A., Sutton, C., Mirzavand, R. and Fattahpour, V., **2023**. Data-driven analysis of using flow control devices and extended reach wells on SAGD well performance**. Geoenergy Science and Engineering**, 231, p.212336.

4.1. Preface

The ongoing SAGD industry inclination towards decreasing freshwater usage and increasing oil production has prompted the adoption of practices like inflow and outflow rates control and drilling extensive lateral wells. In this Chapter, an examination was conducted on the comparative effectiveness of different flow rates control strategies, using data gathered from major Steam SAGD projects in Western Canada spanning from 1997 to mid-2022. The goal is to investigate the impact of flow rates control and increasing the well lateral length on SAGD well performance.

This chapter employs a normalization technique to assess the production history of wells, considering geological and operational parameters. According to industry convention, wells with lateral lengths exceeding 850 meters are categorized as "long," while those below 850 meters are designated as "short." Subsequently, the normalized oil production and cSOR for all wells are examined. By comparing short and long wells equipped with or retrofitted with FCDs, this analysis provides valuable insights into the impact of completion design on the relative performance of SAGD wells.

The results suggest that implementing flow rate control strategies in SAGD well-pad developments can lead to higher oil production and reduced freshwater consumption, enabling operators to lower emissions. These findings offer valuable insights for exploring potential shifts in the development of heavy oil deposits as technology progresses, while also considering project economics

4.2. Introduction

In addition to FCDs, another promising technique in SAGD projects known as Extended Reach Drilling (ERD) involves drilling high-angle wellbores with extensive horizontal displacements [103]. ERD is theoretically believed to offer more economical production and leave a smaller environmental footprint. Long wells drilled with ERD experience increased oil production and affect a larger portion of the reservoir with steam [104]. However, the assessment of the combined impact of applying flow rates control strategies using FCDs and increased lateral well length on improving the well performance using real historical production data, remains a relatively underexplored area of research.

Nowadays, the prevailing industrial trend in Western Canada revolves around drilling ERD wells. ERD wells are characterized by their unwrapped reach ratio, which represents the along-hole

departure divided by the True Vertical Depth (TVD) at total depth [103]. To assess the distribution of ERD wells, a dog-nose plot has been constructed for a total of 12,492 wells located in 16 major SAGD and Cyclic Steam Stimulation (CSS) projects, spanning from 1973 to the middle of 2022. The criteria provided by K&M Technology Group have been used for this analysis (see Fig. 4-1). Additionally, Fig. 4-2 provides the frequency distribution of these wells. Based on Fig. 4-1, drilled wells are mostly categorized in the extreme reach zone, and Fig. 4-2 shows that 40% of the wells (5,008 wells) in the 16 projects have been drilled between 2011 and mid-2022.

According to estimates provided by the AER and the Canadian Energy Research Institute (CERI), the breakeven price for SAGD operations falls in the range of 50 to 55 USD/bbl [105]. Moreover, for in-situ operators, more than 70% of the sustaining capital cost can be attributed to the drilling and completion of wells, as well as the construction of well pads and gathering pipelines [105]. However, once production commences, several challenges need to be addressed, including pressure drop along the wellbore and ensuring steam chamber conformance [106]. The pressure drop can be determined using Eq. 13, which applies to steady-state fully developed incompressible flow in a horizontal pipe [107, 108].

$$\Delta P = F\left(\frac{L}{D}\right)\left(\frac{v^2}{2G}\right) \tag{13}$$

where L and D (m) are the length and the diameter of the pipe, respectively, v (m/s) is fluid velocity and G (m/s2) is the acceleration of gravity, F (dimensionless) is the friction factor which is a function of the Reynolds number and relative pipe roughness.

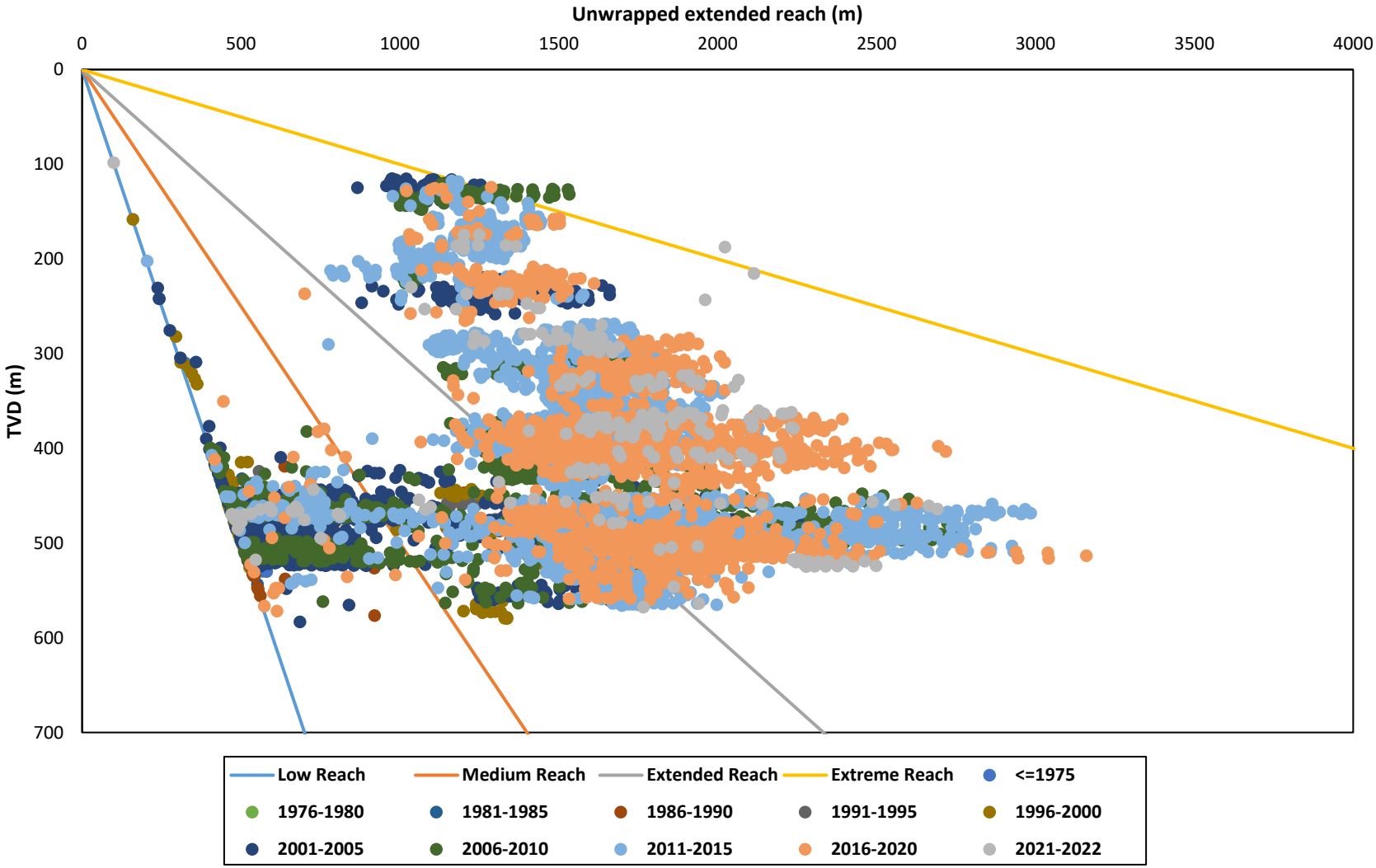

Fig. 4-1. Dog-nose plot for 12,492 wells in 16 major SAGD and cyclical projects from 1973 to 2022, Western Canada. The plot is based on the unwrapped reach ratio of the wells, and the reach lines are based on the criteria provided by K&M Technology Group[1].

[1] https://kmtechnology.com/dog-nose-plot/

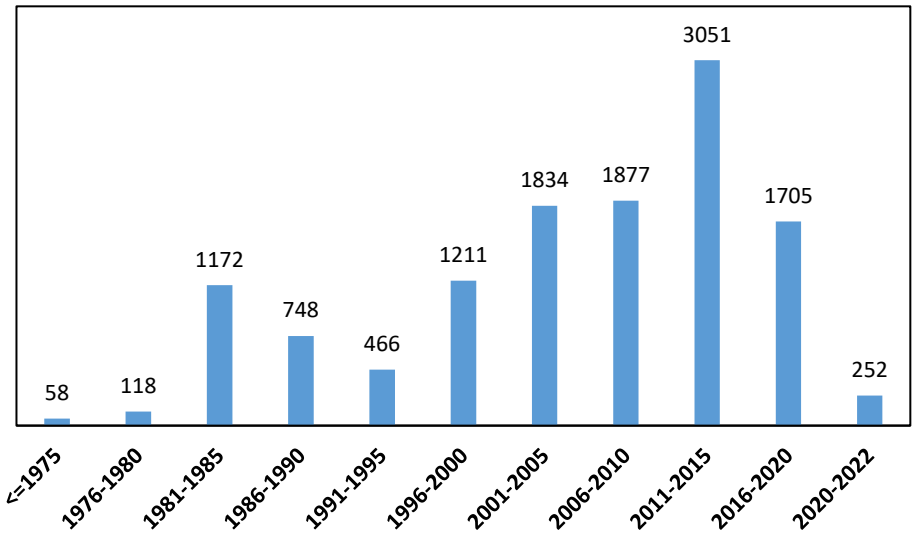

Fig. 4-2. The frequency of the drilled wells in 16 major SAGD and cyclical projects from 1973 to 2022, Western Canada.

According to Eq. 13, the pressure drop along the well is proportional to well length; as the well length increases, the pressure drop increases. Accordingly, it is crucial to comprehend how these diverse factors, such as enhanced reservoir contact, increased wellbore pressure drop, and improved steam chamber conformance, collectively influence oil production and freshwater usage. Additionally, the role of FCDs, which can regulate flow rates to balance production and injection rates along the wells, becomes significant in mitigating the impact of pressure drop.

Numerous studies have been conducted to investigate the impact of FCDs on SAGD projects. Stone et al. (2014) developed a SAGD reservoir simulation, demonstrating that FCDs in injector and producer wells improved steam conformance and oil production [109]. Noroozi et al. (2015) explored the effect of FCDs in the Surmont project, revealing that these devices increased oil production [110]. Banerjee and Hascakir (2018) analyzed LDFCDs' contribution to oil recovery and cSOR through flow-loop testing and numerical simulation, revealing improved oil recovery and lower cSOR [111]. Lastiwka et al. (2019) reviewed laboratory and field testing of FCDs, confirming enhanced oil production and steam conformance [112]. Gorham et al. (2019) implemented liner-deployed FCDs in injector wells at Kern River, indicating several significant advantages, including longer horizontal steam injectors without significant well cost increases [113]. However, Gorham et al.'s study had some limitations, as it ignored the effects of varying steam injection strategies and the successful activation of FCDs in injector wells. Zhu and

Uzcategui (2021) investigated FCDs in an industrial application and numerical simulation, finding high-pressure recovery and reduced cSOR with injector well FCDs and good steam-choking capability with producer well FCDs [114]. Gohari et al. (2021) developed a ranking system based on gamma-ray log responses for injector and producer wells in the Surmont project, evaluating the performance of different well completion strategies [115]. Martinez et al. (2022) focused on FCDs in producer wells of horizontal wells, concluding that this strategy enhances sweeping efficiency, oil recovery, and addresses the production of undesired fluids [116]. Zhu (2022) introduced a dual nozzle application of FCDs in producer wells during CSS to improve oil recovery, steam quality, and conformance [117]. Liang et al. (2022) studied various FCDs used in producer wells in Western Canada, showing enhanced steam chamber conformance, improved ramp-up stage, increased oil production, and lower SOR with more aggressive subcooling [118]. While these studies have made significant progress in enhancing operating practices by controlling the inflow and outflow rates, a comprehensive study of SAGD well performance based on a large field data database remains unexplored. Moreover, to our knowledge, integrating available annual report information with production data and normalizing it to compare different flow rate control strategies, e.g. using LD or TD FCDs in injector and producer wells, with a substantial dataset is an approach not widely considered in previous investigations.

Apart from the studies that focused on examining the influence of FCDs in SAGD wells, there have been additional investigations specifically targeting the impact of increasing the lateral length of SAGD wells. Verney (2015) examined 1,111 well pairs in 13 SAGD projects within the McMurray formation in Alberta, Canada. Their findings indicated that longer wells did not significantly increase oil production, and they did not mention whether the wells were completed or retrofitted with FCDs [106]. Dosunmu and Osisanya (2015) explored the optimum lateral well length for SAGD projects using a productivity equation based on an elliptical drainage area. They concluded that increasing the wells' lateral length did not result in higher oil production due to pressure loss along the wellbore [119]. Another study by Virk (2020) determined the optimum well length from a techno-economic perspective to achieve maximum reservoir contact [120]. Although the aforementioned studies have made significant investigations in understanding the challenges and benefits of SAGD long wells, to the best of our knowledge, no comprehensive study based on real well performance data and FCDs has been conducted yet. Additionally, the

extraction of a database from published annual AER reports for comparing different flow rates control in Western Canada has not been fully addressed in the existing literature.

In this chapter, we compiled an extensive database by extracting geology, well, and production data from open-source databases such as the AccuMapTM database and AER reports. A specific well completion database was also created for seven major SAGD projects, containing information about the type of FCDs deployed in different wells, sourced from AER reports. To account for variations in reservoir quality among different wells, the oil production data was normalized following the procedure proposed by Gohari et al., (2021) [115]. Furthermore, we categorized wells with lateral lengths exceeding 850 meters as "long" and those with lengths below 850 meters as "short" to analyze the impact of lateral length on oil production and cSOR. Subsequently, we separately compared the normalized oil production and cSOR for all wells and long wells, aiming to investigate the influence of FCDs on these two parameters.

4.3. Database

To compare the productivity and cSOR of long wells with short wells, we extracted a total of 5,246 wells from 13 major SAGD projects in Western Canada, spanning from 1997 to mid-2022. For the investigation of FCDs' contribution to production and cSOR, we extracted another database covering the period from 2002 to mid-2022, which consisted of 1,492 wells from seven SAGD projects in Western Canada. However, it is worth noting that the FCD data were not publicly available for the remaining six examined SAGD projects. The well data includes information about FCD placement, such as whether they were deployed as liners or retrofitted through tubing. We also extracted production data, comprising oil production and steam injection rates, along with data on reservoir thickness and net-to-gross ratio, which were collected and detailed in Table 14.

Table 14. Historical database for all projects.

Data category	Existing data
Well data	FCD placement (liner-deployed, tubing-deployed, ICD, and OCD)
	Well length (m)
	Well spacing (m)
Production data (m^3/month)	Oil production and steam injection
Geological data	Reservoir thickness (m)
	Net-to-gross ratio

In all, 258 wells were completed by various forms of FCDs in injector or producer wells, including 95 wells completed by LDICDs, 23 by LDOCDs, 127 by TDICDs, 54 by TDOCDs, 181 by only

ICDs and 37 by only OCDs (Fig. 4-3). The two last terminologies do not consider the deployment method of the devices.

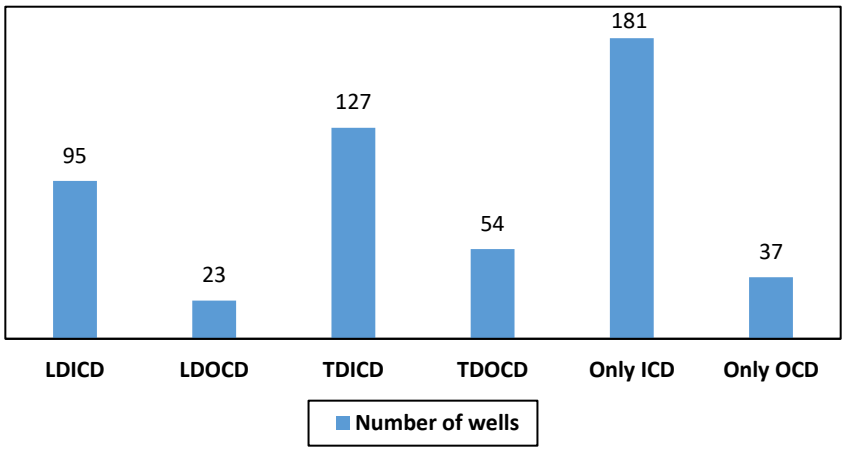

Fig. 4-3. Number of wells with different types of FCDs in the database.

The histogram chart of lateral well length for wells drilled in all projects is shown in Fig. 4-4. The frequency of drilled wells corresponding to the lateral length lower than 850 meters represents the highest frequency of the drilled wells in the chart; therefore, 850 meters is considered as the threshold for longer wells in this section. Besides, based on our personal conversations with experts in the industry drilled wells longer than 850 meters can be considered as "long wells".

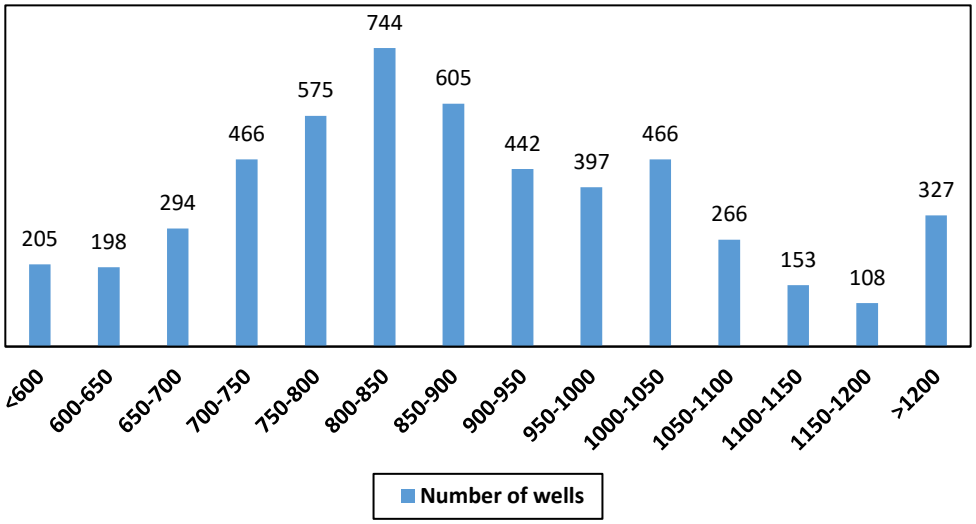

Fig. 4-4. The frequency of lateral well length of all wells drilled in 13 SAGD projects under the study.

4.4. Methodology

In order to evaluate the FCD performance accurately, it is crucial to conduct a dependable comparison using unbiased production data. This entails normalizing the oil production from various wells across different well pads, considering geological, well, and operational factors [99, 115]. The normalization of oil production used in this research is determined through the application of Eq. 14:

$$Normalized\ oil\ \left(\frac{1}{m^3}\right) = \frac{Produced\ oil\left(\frac{\mathrm{m}^3}{\mathrm{month}}\right) \times Reservoir\ quality\left(\frac{\mathrm{m}}{\mathrm{m}}\right)}{Injected\ steam\ (CWE)\left(\frac{\mathrm{m}^3}{\mathrm{month}}\right) \times Reservoir\ thickness(\mathrm{m}) \times Well\ length(\mathrm{m}) \times Well\ spacing(\mathrm{m})} \quad (14)$$

The $Well\ length$ in Eq. 14 is calculated based on the distance from the intermediate casing point (ICP) to the toe of each production well. $Well\ spacing$ in Eq. 14 is the average distance between each well and its neighboring wells in a pad. The $Injected\ steam$ in Eq. 14 is linearly interpolated for infill wells. These three pieces of information for all well-pads have been extracted from the AccuMap™ database.

$Reservoir\ quality(\frac{\mathrm{m}}{\mathrm{m}})$ is the portion of the well length in which gamma ray (GR) responses are lower than a threshold reported by AER reports for each project [121]. To calculate the $Reservoir\ quality$, GR logs should be digitized. An image processing code is developed to digitize the GR well logs. The user should assign the number of grid scales for each log. There are three general cases in which the logs are available in the database. The first case is shown in Fig. 4-5-a to Fig. 4-5-c, where a sharp contrast is observed between the log and the grid scales in color (Fig. 4-5-a) or grey-level (Fig. 4-5-b) images. In this case, extracting the numerical values from the log is carried out by applying a black-and-white filter [122] from the original image, as shown in Fig. 4-5-c.

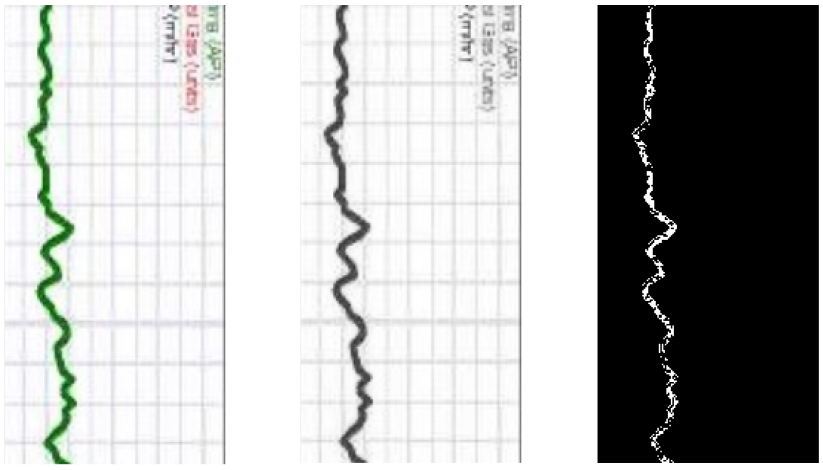

a b c

Fig. 4-5. The first case of log images in our database. There is a sharp contrast between the log and the scaling grids, either in a) color or b) grey-level images. The values of the GR log are in the range of 0 to 150 API.

The second case is shown in Fig. 4-6-a in which there are crossovers between different types of logs. In this case, the contrast still exists between the log and the background grid, either in greyscale or color images (Fig. 4-6-a). Digitization can also be performed by color filtering; however, designing the color filters by hand is very time-consuming when there are many logs. To make the code more intelligent and more suitable for big-data analysis like what we have in this study, the number of colors should be determined automatically. Therefore, a histogram of grey-level intensity is provided, and the number of peaks is specified (Fig. 4-6-b). In the 8-bits unsigned integer grey-level images in our database, the intensity varies between zero, which stands for pure black, and 255, which introduces pure white [122]. Based on Fig. 4-6-b, there are three peaks from zero to 150 grey-level intensities, standing for three well logs with red, black, and green colors (Fig. 4-6-a). Note that in a full-length well log, the largest peak value corresponds to the white background having a grey-level intensity larger than around 230 in Fig. 4-6-b. The grid scales mostly have bright grey-level intensities, as shown between 150 and 210 grey-level intensities in Fig. 4-6-b. To digitize the GR logs as black and green colors in Fig. 4-6-a, the pixel values for the first peak between zero and 10 are extracted and plotted in Fig. 4-6-c. A two-dimensional median filter [122] is also applied for denoising (Fig. 4-6-d). In the next step, the other two peaks are investigated, and the corresponding GR log image is shown in Fig. 4-6-e. Note that the two-dimensional median filter has been applied to the image shown in Fig. 4-6-e. After extracting the pixel positions in the image, the GR well logs would be digitized based on the number of grid scales and the minimum and maximum values of the log measurements already specified by the

user. The grey-level intensities larger than 150 are background information as shown as white color in Fig. 4-6-f.

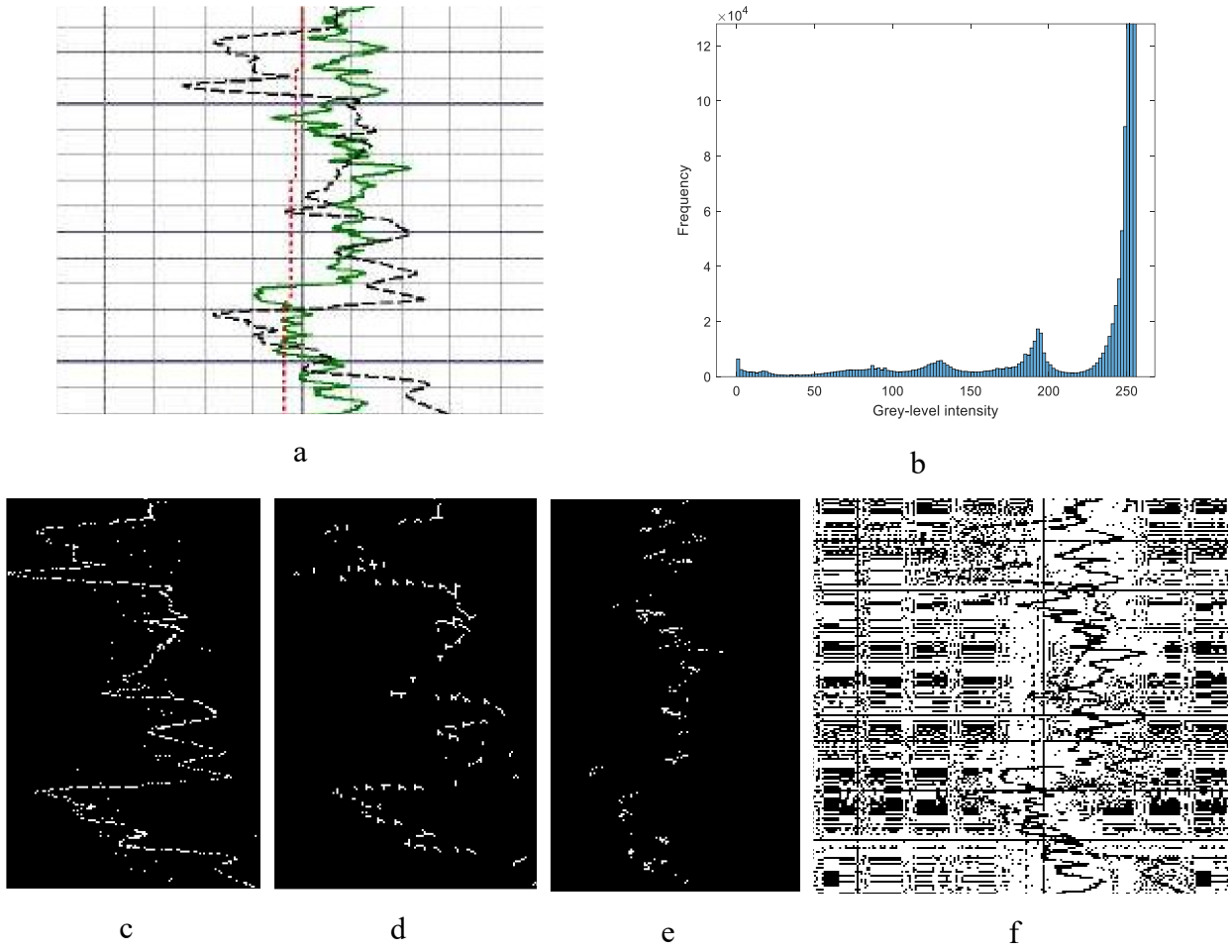

Fig. 4-6. The second case of log images in our database. a) GR well logs in black and green colors with values in the range of 0 to 150 API, b) grey-level intensity distribution, c) digitized black well log with some noises, d) median filter applied on the image in part c, e) digitized filtered green well log, and f) non-required background information.

The third case of log images in our database is shown in Fig. 4-7. There is no distinguishable difference between the log and the grid scales, either in their color or greyscale images. Applying median filters is not a permanent solution for these images (Izadi et al., 2018; Izadi et al., 2015). In this case, the image is converted to a black-and-white image and a pre-determined vertical lag space and radius of investigation is specified. The code inspects the image to find a black pixel value that is not horizontally connected to other black pixels based on the radius of investigation. Therefore, the extracted pixels from grid scales would not be involved in the log digitization. The result of digitization is shown in Fig. 4-7, in which the vertical lag space is defined as 10 pixels, and the radius of investigation is 20 pixels. As shown in Fig. 4-7, three pixels with their colors

turned from black to white and marked by blue circles are points at which the GR values are extracted and digitized.

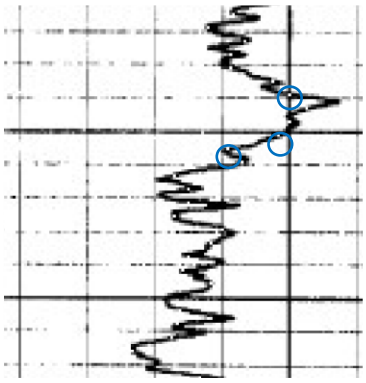

Fig. 4-7. The third case of log images in our database. There were no distinguishable differences between the log and scaling grids. The scales of the GR log are in the ranges of 0 to 150 API.

To provide the $Reservoir\ thickness(\mathrm{m})$ for Eq. 14, contour maps for the projects are digitized based on the color bar legend of the maps using another image processing code that its graphical user interface (GUI) is shown in Fig. 4-8. The direction of the pad, the maximum and minimum thickness values based on the legend of the map provided by AER reports, and the number of well pairs in the pad should be determined by the user. The pixel positions of the starting and ending points of the well in the contour map that located at the top of the pad for horizontal pads, the right side of the pad for vertical pads, and either the top or right side of the pad for slant pads should be assigned by the user as well. By selecting the proper options shown in Fig. 4-8 and providing the information needed, the reservoir thicknesses for the wells in the database are calculated.

By normalizing the oil production for all wells based on Eq. 14, the productivity and cSOR for nearby wells in the same pad can be compared to find the optimal lateral well length and well completion design. To make the comparison, the same number of months of production have been used from the first production date.

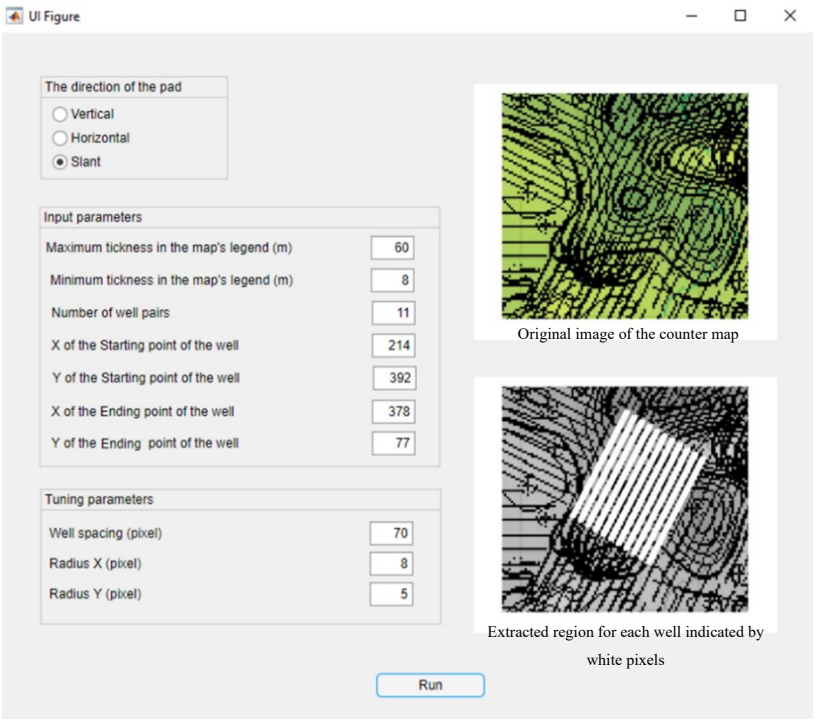

Fig. 4-8. The developed code for digitizing reservoir thickness based on contour maps.

4.5. Results

The overall contribution of the FCDs in all projects based on real data of normalized oil production and cSOR are reviewed here. All wells, including short and long wells, are studied in the first subsection. In the second subsection, the long and short wells are compared. Finally, in the third subsection, FCD's contribution to oil production and cSOR in long wells is investigated. In each case, we added the normalized oil production of wells with FCD and obtained the average of this parameter. Then we calculated the same parameter for nearby wells without FCDs.

4.5.1. Normalization Assessment

To evaluate the cross correlation of the parameters utilized in the normalization equation described as Eq. 14, we computed Pearson linear correlation coefficients of the parameters [123]. The results are illustrated in Fig. 4-9, and it is evident that steam injection and reservoir quality exhibit a strong correlation with oil production, with a correlation coefficient of 0.96 and 0.63, respectively. On the other hand, reservoir thickness, well length, and well spacing parameters which indicate the drainage box of the reservoir demonstrate a notable level of independence of oil production. The drainage box parameters of the reservoir; however, are very important to evaluate and compare the oil production of different wells [99]. With the exception of oil production, the correlation

coefficients among all other parameters are considerably low. This indicates their independence and suggests that the selected parameters effectively mitigate their impact on oil production, thereby facilitating a more reliable comparison.

In order to evaluate the effectiveness of our chosen normalization approach in providing a meaningful definition of normalized production, we plotted the cumulative oil production for 16 randomly selected wells before and after normalization in Fig. 4-10. The graph illustrates that the cumulative oil production after normalization closely aligns with the trend observed before normalization, suggesting that our normalization method captures the underlying patterns effectively.

Fig. 4-11 illustrates the Pearson linear correlation coefficients for the parameters following the normalization process. As depicted in Fig. 4-11, normalization has effectively diminished the influence of other parameters on oil production. Compared to Fig. 4-9, the absolute correlation coefficients between the normalized oil production and other parameters have decreased following the normalization process. Consequently, utilizing the proposed normalized oil production for comparing the performance of wells with and without FCDs may offer greater reliability than non-normalized oil production.

It is important to note that the suggested normalization in Eq. 14 does not involve enthalpy and heat transfer concepts. This relationship only tries to reduce the impact of the mentioned practical and geological features on the produced oil, and thermodynamic features have not been involved.

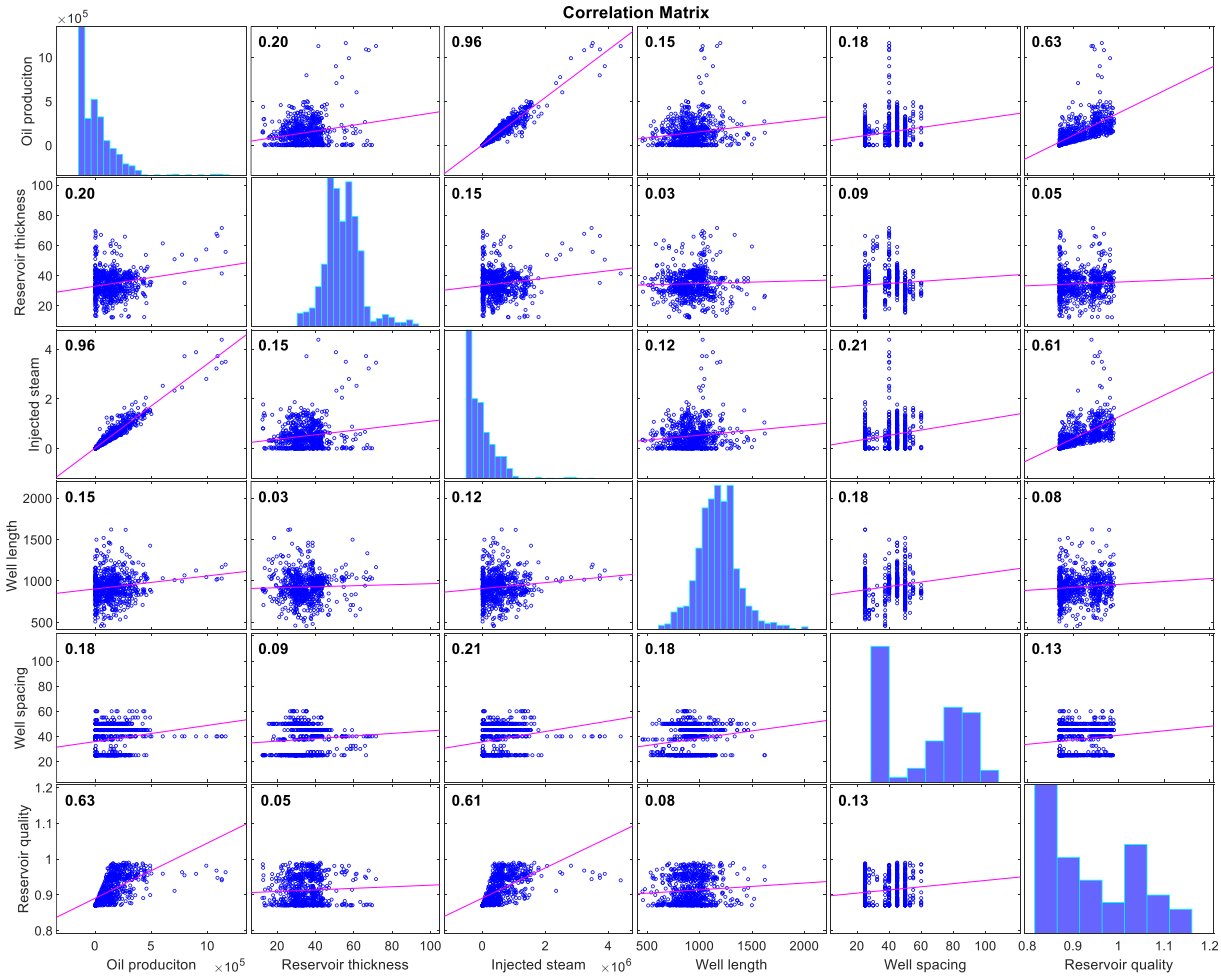

Fig. 4-9. Correlation matrix of the parameters used in Eq. 14. Most parameters utilized for normalizing oil production demonstrate a notable level of independence.

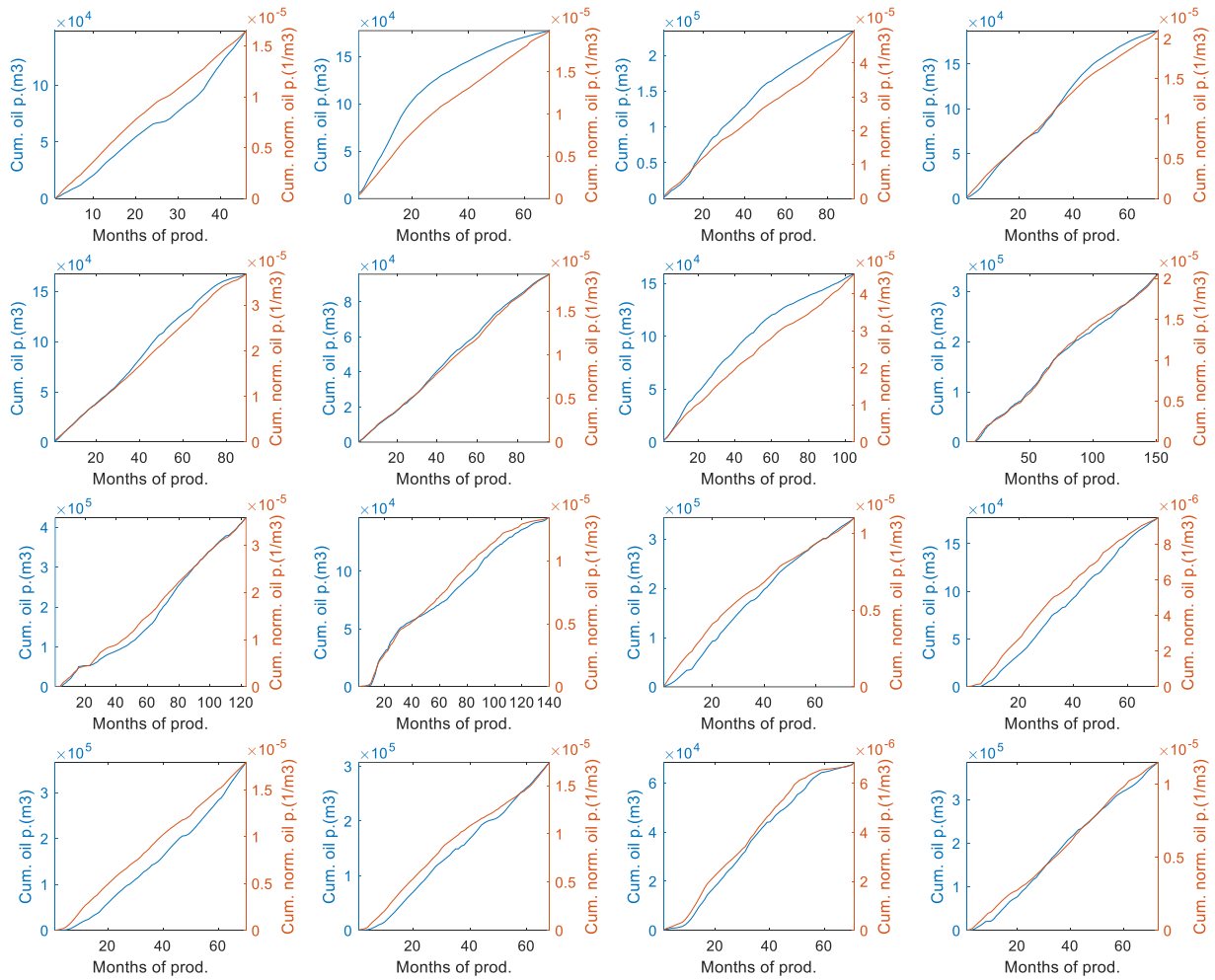

Fig. 4-10. The cumulative oil production for 16 randomly selected wells before and after normalization. The graph illustrates that the cumulative oil production after normalization closely aligns with the trend observed before normalization.

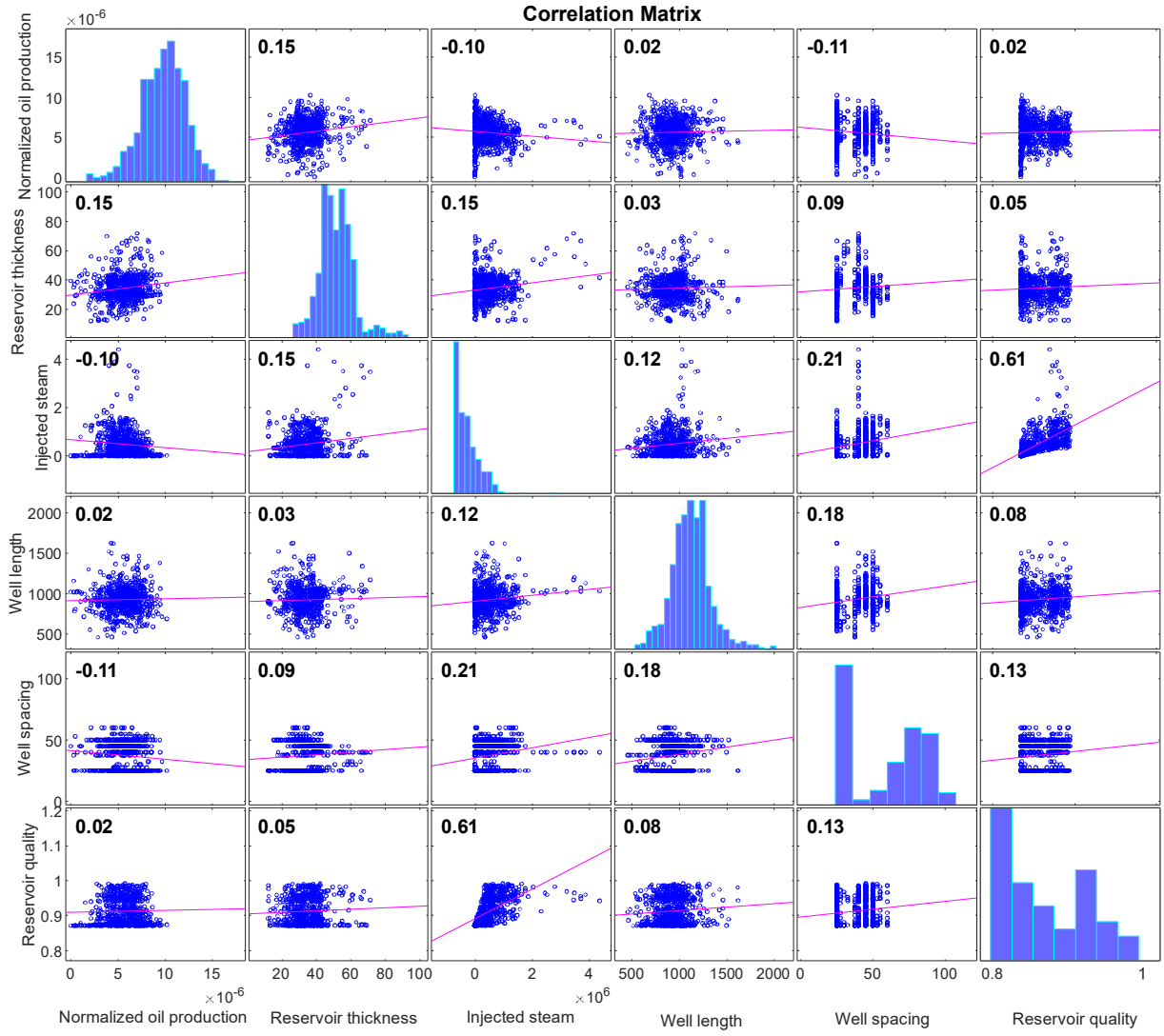

Fig. 4-11. Correlation matrix of the parameters used in Eq. 14 with the normalized oil production. Compared to Fig. 4-9, the absolute correlation coefficients between the normalized oil production with other parameters have decreased following the normalization process.

4.5.2. FCDs Contribution of Oil Production and cSOR: All Wells

Oil production and cSOR for all wells, i.e long and short wells, with FCDs are compared to all wells without FCDs. The comparison of normalized oil production and cSOR for wells with FCDs and nearby wells without FCDs is shown in Fig. 4-12. The contribution of FCDs for uplifted cases is shown in Fig. 4-13. Uplifted cases refer to wells with FCDs that improved normalized oil production or cSOR compared to nearby wells without FCDs in the same pad. Based on Fig. 4-12 and Fig. 4-13:

- In general, FCD deployment raised normalized oil production by 17% while increasing cSOR by 5%. In uplifted cases, which is 56% of the wells completed by FCDs, FCD deployment increased normalized oil production by 52% while reducing cSOR by 18%.
- LDFCDs boosted normalized oil production by 30% while cSOR remained unchanged. In uplifted cases, which is 63% of the wells completed by LDFCDs, LDFCD deployment increased normalized oil production by 59% while decreasing cSOR by 20%.
- Since TDFCDs are commonly installed in problematic wells, two assessments are made for TDFCDs:
    - ✓ Compared to normal wells in the same well pad, TDFCD-retrofitted wells boosted normalized oil production by 10% while cSOR increased by 8%, while in uplifted cases, which is 51% of the wells completed by TDFCDs, it increased normalized oil production by 47% while decreasing cSOR by 16%.
    - ✓ When comparing performance before and after the TDFCDs deployment date, all wells retrofitted with TDFCDs enhanced normalized oil production by 231% while lowering cSOR by 27%.
- ICDs enhanced normalized oil production by 13%, while cSOR increased by 7%. In uplifted cases, which is 54% of the wells completed by ICDs, it increased normalized oil production by 48% while lowering cSOR by 18%.
- OCDs improved normalized oil production by 22% while increasing cSOR by 4%. In uplifted cases, which is 50% of the wells completed by OCDs, it increased normalized oil production by 37% while lowering cSOR by 17%.

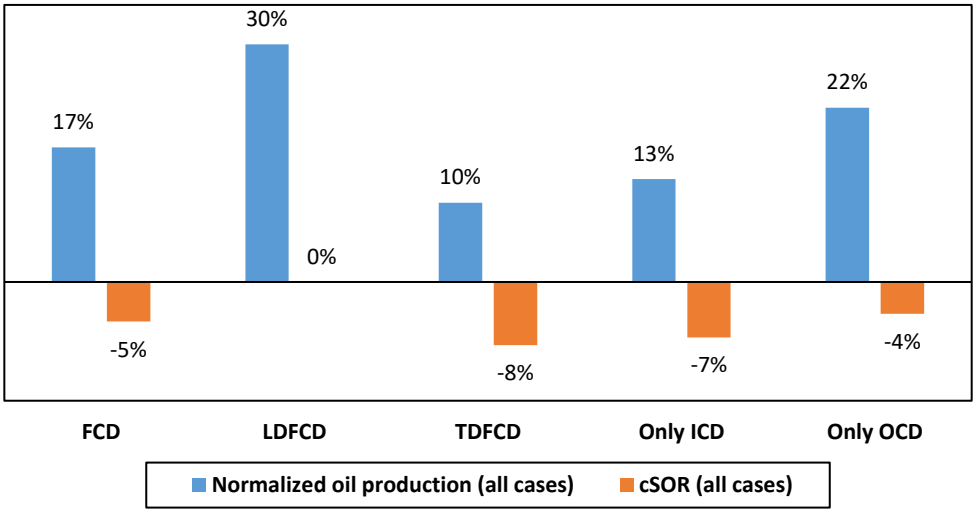

Fig. 4-12. Increase in normalized oil production and decrease in cSOR in all cases using FCD.

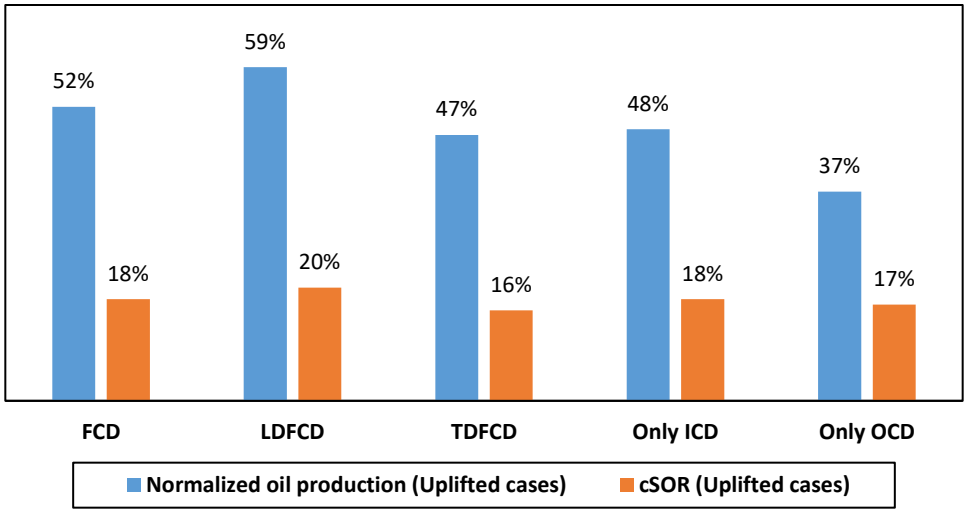

Fig. 4-13. Increase in normalized oil production and decrease in cSOR in uplifted cases using FCD. Uplifted cases correspond to wells with FCDs that improved normalized oil or cSOR compared to wells without FCDs.

4.5.3. Oil Production and cSOR: Long Wells Compared to Short Wells

Fig. 4-14 compares the normalized oil production versus production date for the long and short wells considered in this study. In each year the normalized oil production of the wells in each category are averaged and reported in Fig. 4-14. As shown in Fig. 4-14, the normalized oil production produced by the long wells is lower than short wells, and it can be argued that the pressure drop along the well from the toe to the heel is proportional to the lateral length (Eq. 13).

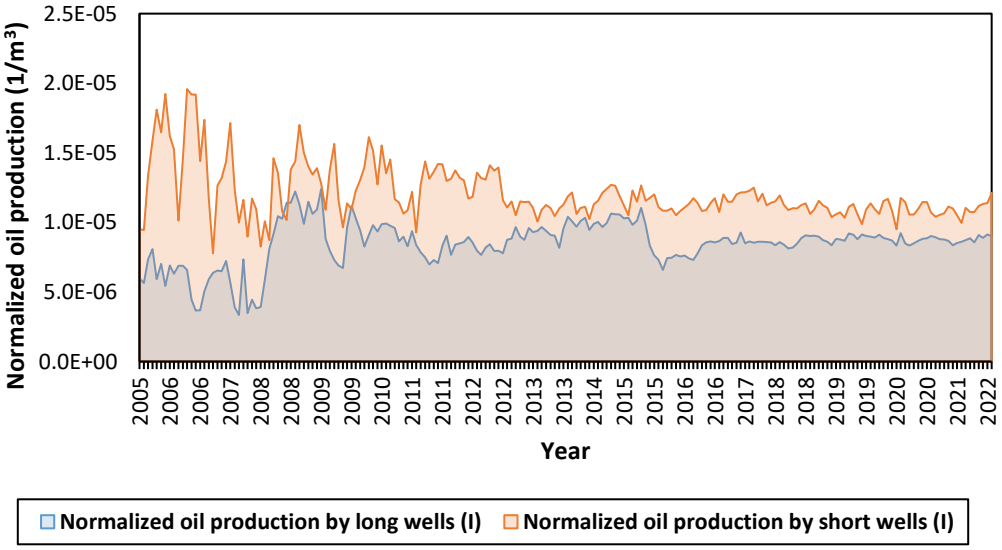

Fig. 4-14. Comparing the normalized oil production for long and short wells (I): the effect of lateral length is involved.

Fig. 4-15 shows the ratio of the average lateral well length of long wells to short wells. According to the data extracted from AccuMap, as of 26 years between 1996 and 2022, 2,764 long wells were drilled in the study area. The lateral length of long wells drilled till 2010 was 27% longer than short wells, reaching 41% after 2010. On average, the lengths of long wells exceed those of the short wells by 12% to 54%, with an average of 38%. We called the plot in Fig. 4-14 as normalized oil production by long or short wells (I) to make a difference with Fig. 4-16. In Fig. 4-16, the $Well\ length$ factor in Eq. 14 is removed in the normalization process to see the effect of well length on the production. The production in Fig. 4-16 is called normalized oil production by long or short wells (II). As shown in Fig. 4-16, the normalized oil production produced by the long wells is now more than short wells. It indicates that for a given oil recovery volume, fewer long wells must be drilled than short wells. Accordingly, the CapEx and drilling footprints would be decreased.

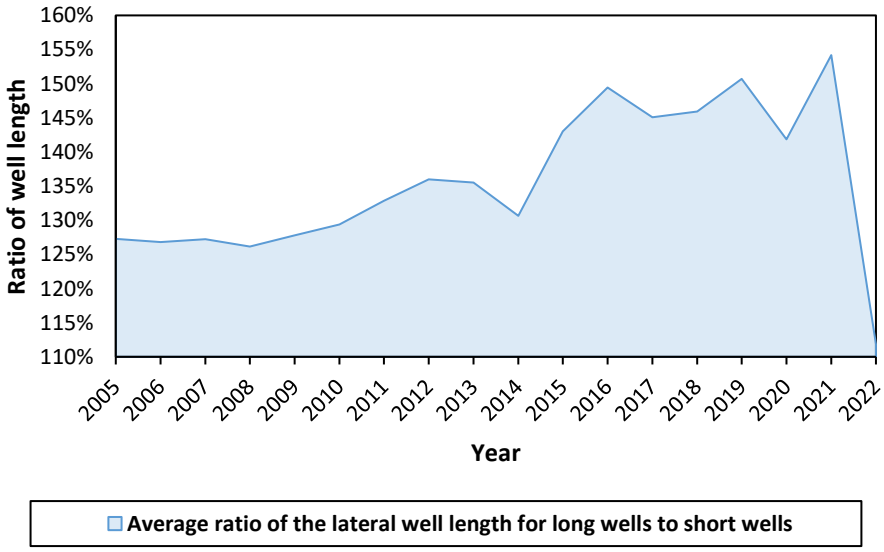

Fig. 4-15. Comparing the well length of long wells to short wells.

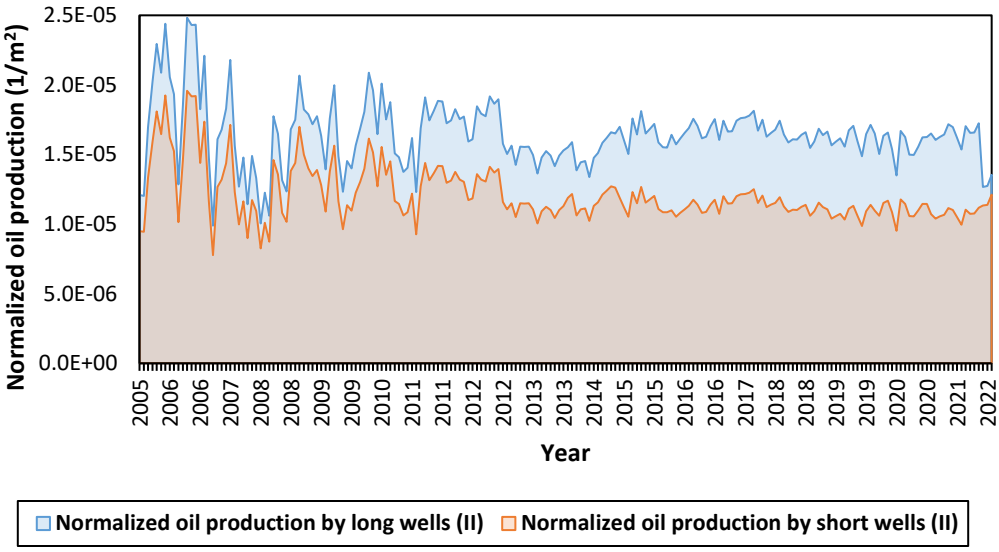

Fig. 4-16. Comparing the normalized oil production for long and short wells (II): the effect of lateral length shown in Fig. 4-15 is excluded.

Fig. 4-17 and Fig. 4-18 present the ratio of normalized oil production and cSOR by long wells to short wells for the 13 projects in the same production period. Based on Fig. 4-17 and Fig. 4-18, and the number of long and short wells in all projects, on average, the oil production by long wells is 18% more than short wells, while cSOR for short wells is 4% lower than cSOR for long wells. In Project# 9 depicted in Fig. 4-17, and Projects# 4 and 11 shown in Fig. 4-18, a notable distinction exists in comparison to the remaining projects. Due to the limited number of wells equipped with FCDs in each project, these wells have the potential to operate with high efficiency, resulting in those significant deviations. Further elucidation on the operational status of these wells is essential to provide a more comprehensive understanding.

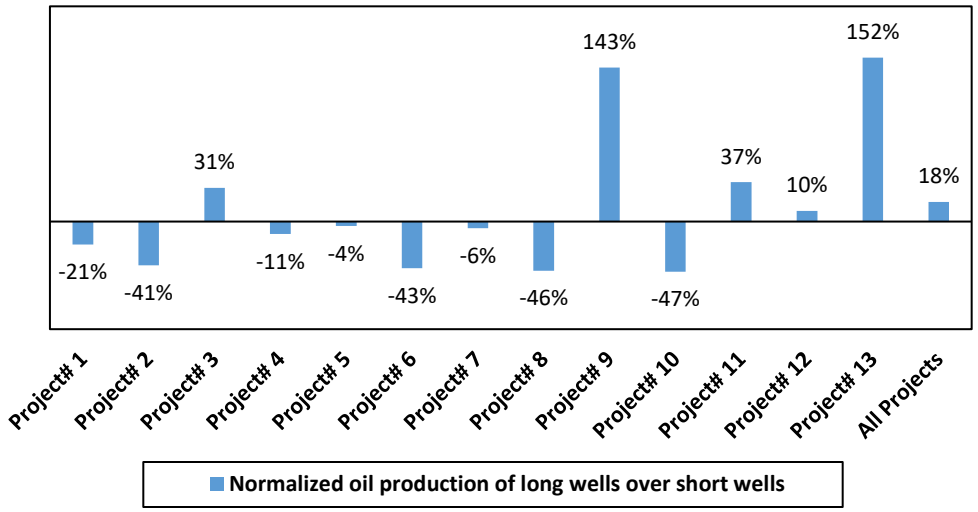

Fig. 4-17. The ratio of normalized oil production for long wells to short wells for all projects.

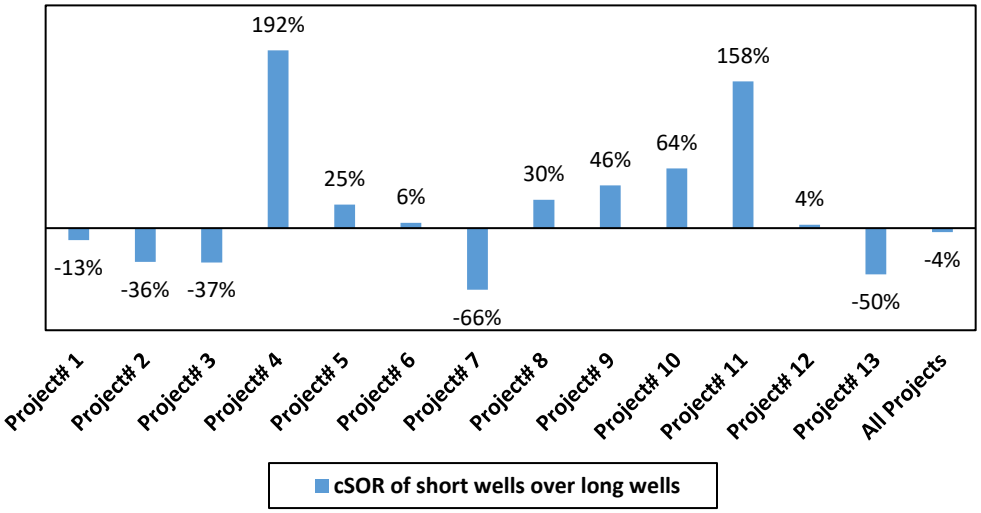

Fig. 4-18. The ratio of cSOR for short wells to long wells for all projects.

4.5.4. FCDs Contribution on Oil Production and cSOR: Long Wells

Oil production and cSOR for long wells with FCDs are compared to long wells without FCDs and short wells without FCDs. The details of the evaluation of the contribution of FCDs, LDFCDs, and TDFCDs in long wells compared to long wells without FCDs in the same pad for seven projects are presented in Fig. 4-19 and Fig. 4-20. Based on Fig. 4-19 and Fig. 4-20:

- In general, FCD deployment raised normalized oil production by 9% while cSOR increased by 5%. Uplifted cases, which is 55% of the wells completed by FCDs, increased normalized oil production by 36% while decreasing cSOR by 17%.

- LDFCDs boosted normalized oil production by 22% while decreasing cSOR by 1%. Uplifted cases, which is 66% of the wells completed by LDFCDs, increased normalized oil production by 42% while decreasing cSOR by 20%.
- Due to TDFCDs are commonly installed in problematic wells, there are two assessments for TDFCDs:
  - ✓ Compared to normal wells in the same well pad, TDFCD-retrofitted wells produced 1% more normalized oil production while cSOR increased by 10%, and uplifted cases, which is 46% of the wells completed by TDFCDs, increased normalized oil production by 30% while decreasing cSOR by 14%.
  - ✓ When comparing performance before and after the TDFCDs deployment date, all wells retrofitted with TDFCDs enhanced normalized oil production by 244% while lowering cSOR by 25%.
- ICDs enhanced normalized oil production by 10%, while cSOR increased by 7%. Uplifted cases, which is 55% of the wells completed by ICDs, increased normalized oil production by 40% while reducing cSOR by 17%.
- OCDs improved normalized oil production by 4% while reducing cSOR by 2%. Uplifted cases, which is 38% of the wells completed by OCDs, increased normalized oil production by 25% while reducing cSOR by 12%.

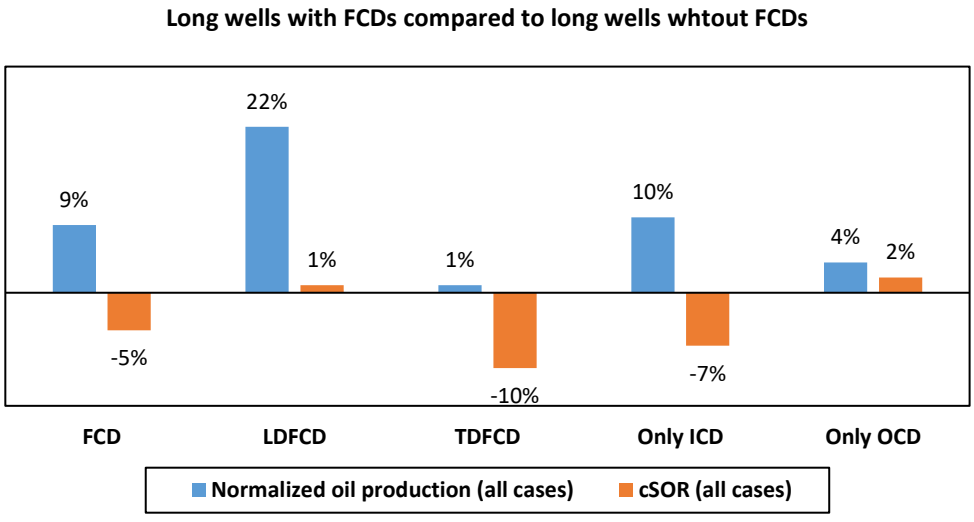

Fig. 4-19. Increase in normalized oil production and decrease in cSOR in all cases using FCD.

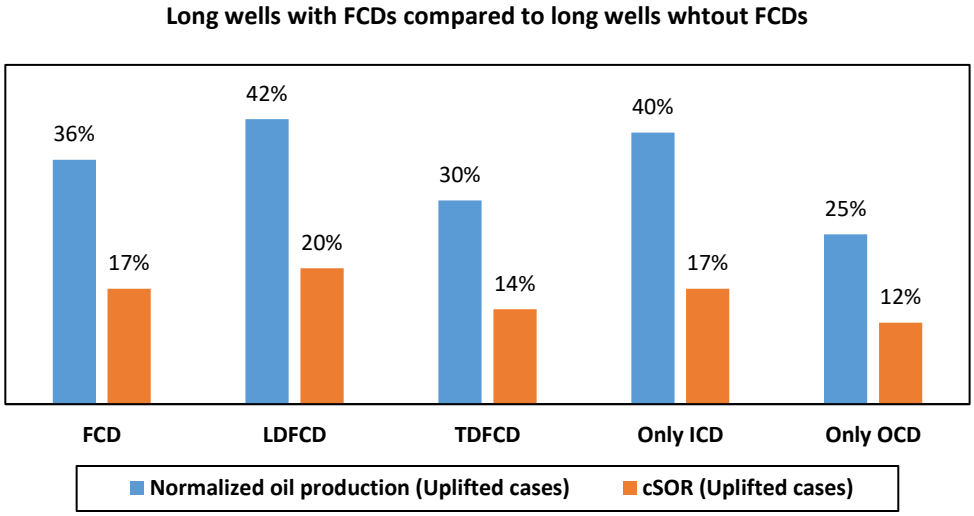

Fig. 4-20. Increase in normalized oil production and decrease in cSOR in uplifted cases using FCD. Uplifted cases introduce the wells with FCDs that improved normalized oil or cSOR compared to wells without FCDs.

The details of the evaluation of the contribution of FCDs, LDFCDs, and TDFCDs in long wells compared to short wells without FCDs in the same pad for seven projects are presented in Fig. 4-21 and Fig. 4-22. Based on Fig. 4-21 and Fig. 4-22:

- FCD deployment generally raised normalized oil production by 50% while decreasing cSOR by 8%. Uplifted cases, which is 64% of the wells completed by FCDs, increased normalized oil production by 96% while decreasing cSOR by 26%.
- LDFCDs boosted normalized oil production by 74% while decreasing cSOR by 3%. Uplifted cases, which is 71% of the wells completed by LDFCDs, increased normalized oil production by 117% while decreasing cSOR by 31%.
- Compared to normal wells in the same well pad, TDFCD-retrofitted wells boosted normalized oil production by 41% while decreasing cSOR by 12%, and uplifted cases, which is 62% of the wells completed by TDFCDs, increased normalized oil production by 88% while decreasing cSOR by 25%.
- ICDs enhanced normalized oil production by 51% while increasing cSOR by 7%. Uplifted cases, which is 56% of the wells completed by ICDs, increased normalized oil production by 118% while reducing cSOR by 30%.
- OCDs improved normalized oil production by 64% while reducing cSOR by 15%. Uplifted cases, which is 80% of the wells completed by OCDs, increased normalized oil production by 69% while reducing cSOR by 20%.

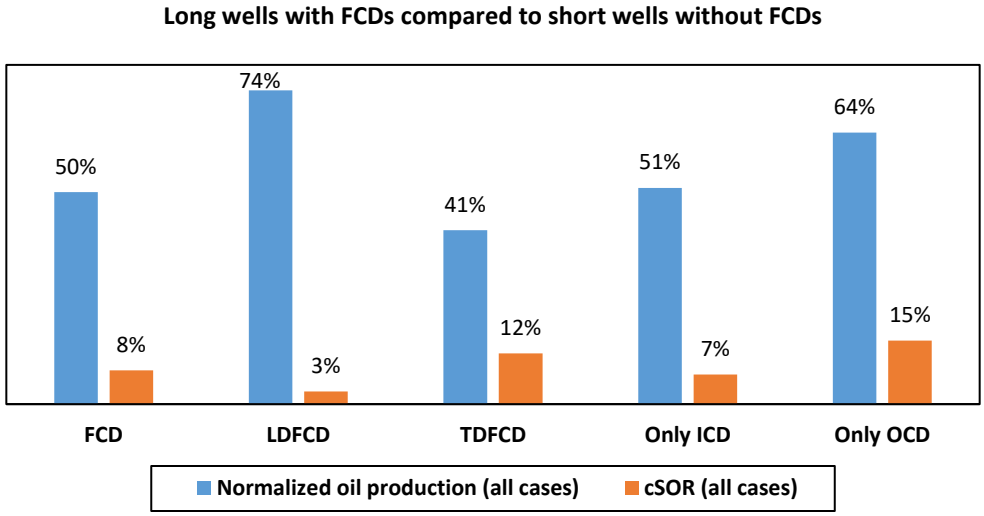

Fig. 4-21. Increase in normalized oil production and decrease in cSOR in all cases using FCD.

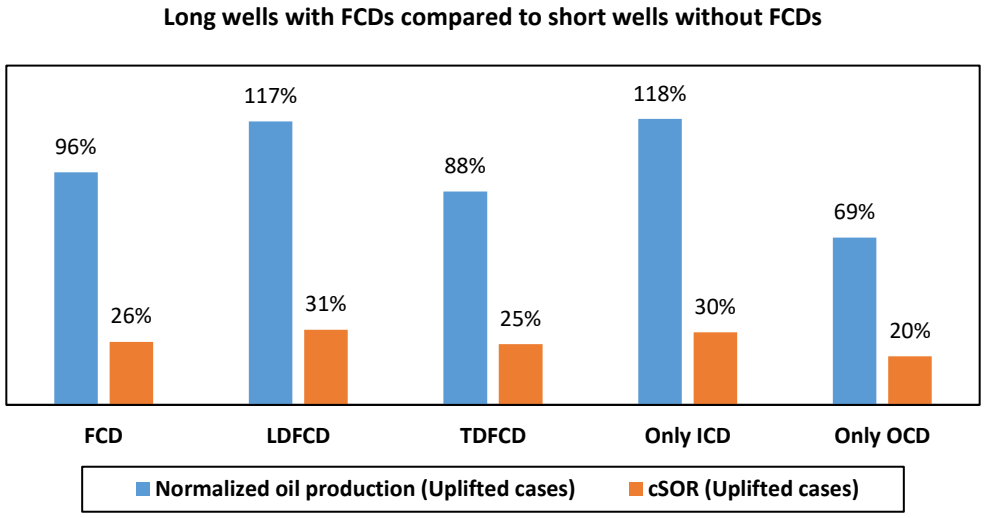

Fig. 4-22. Increase in normalized oil production and decrease in cSOR in uplifted cases using FCD. Uplifted cases introduce the wells with FCDs that improved normalized oil or cSOR compared to wells without FCDs.

Switching from short wells to long wells has become demanding in the industry, and FCDs, as a game changer in SAGD well performance and management, could contribute to this transition. Long wells with FCDs improved normalized oil production, as high as 50%, compared to short wells in the same pads, while it is 74% and 41%, for the wells with LD and TD FCDs, respectively. Accordingly, drilling long wells with FCDs is a synergic approach to increase oil production in SAGD projects.

4.6. Discussions

The production period selected for analysis varies among different wells. When comparing the production of well #1 to nearby wells, the analysis considers the minimum number of months for which production data is available for all wells involved. Consequently, the maximum possible period is used to calculate the average production value, which varies across different cases, as shown in Fig. 4-23 for 16 randomly selected wells in our database. It becomes apparent that in cases where FCDs have enhanced production in a well with FCDs, this improvement remains consistent over time, compared to its nearby well without FCDs.

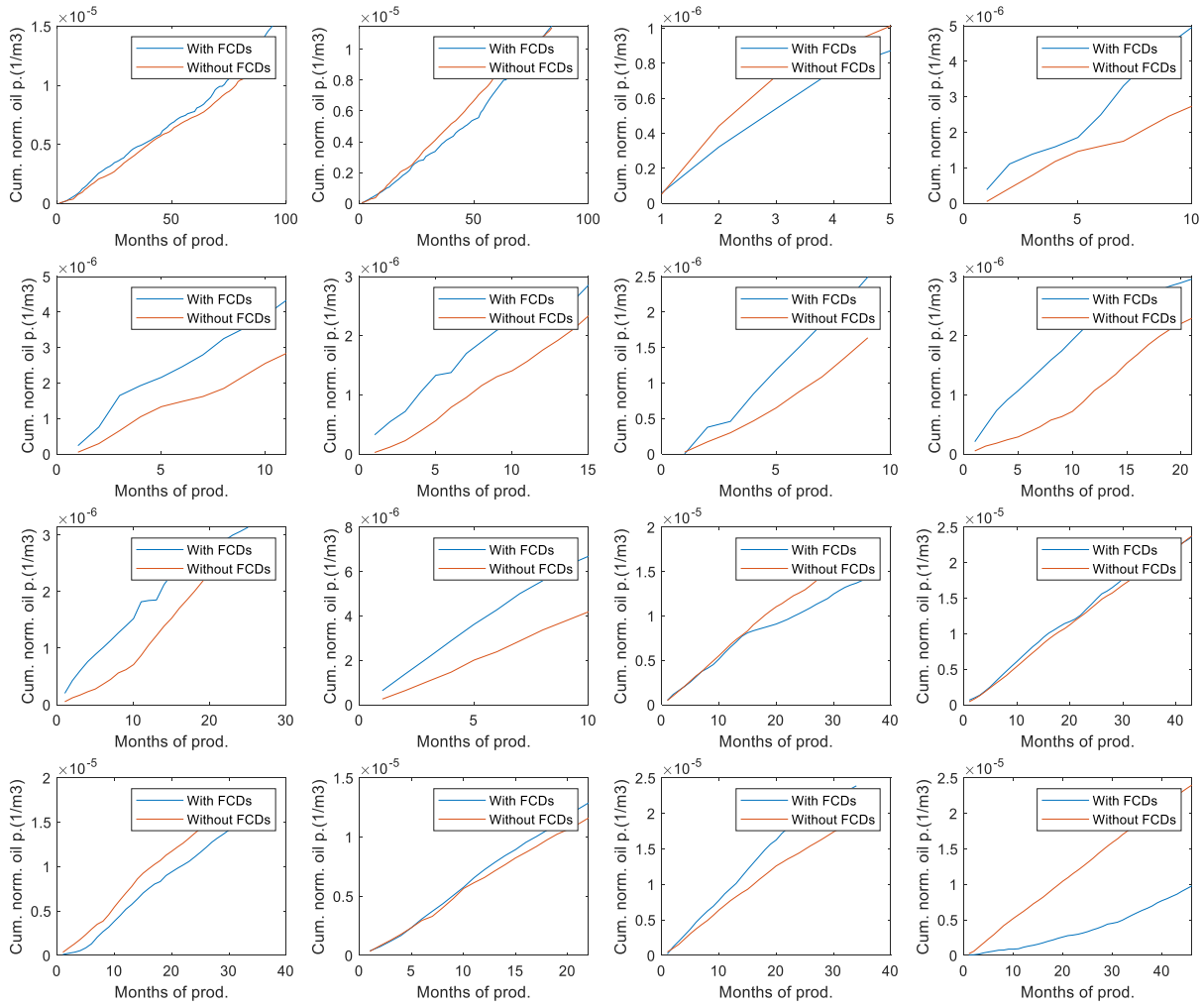

Fig. 4-23. In cases where FCDs have enhanced production in a well with FCDs, this improvement remains consistent over time compared to its nearby well without FCDs.

There has been an ongoing discussion in the industry regarding the tubing versus liner-deployed economic best practices. Well completions equipped with TDFCDs are sometimes more prone to

failure than LDFCDs due to operational considerations such as erosion [115]. Furthermore, increasing the injection pressure and rate for TDFCD-equipped wells to boost oil production is very challenging [3, 4, 115]. Our analysis suggests that TDFCDs are generally less efficient than LDFCDs. Furthermore, if ICDs are not properly designed, they will often limit productivity. The FCDs should be designed based on the reservoir quality along the producer wells to ensure that the FCDs do not significantly choke the flow and reduce the draw-down pressure by causing a large pressure drop across the FCDs [3, 4, 115].

In some cases, the application of TDFCDs could be a more economical alternative by delaying deployment until the challenges present themselves. Unfortunately, this is more challenging and often costs more than deploying LDFCDs. It should be noted that there are several critical differences between these approaches, with some of the most common challenges of TDFCDs described below:

- Limited deployment options due to well deformation and challenging isolation due to limited packer choices are common concerns in thermal wells, as many wells may have experienced well deformation and bypassing flow. Setting up the packers improperly can get the FCD string stuck in the middle of the well during installation.
- Due to condensation effects, increased spacing between devices may affect their ability to choke the steam flow.
- Significant existing drawdowns due to screen plugging may not be managed with FCDs without adding further drawdowns.
- Variable initial and remedial screen performance results in steam jetting onto the remedial tubing [124].
- Deformation and/or damage in the liner can make installing TDFCD very challenging.
- Leftover sediment inside the liner (e.g., bitumen or sand) can cause significant issues.

The results in this section show improved performance of liners exceeding that of remedial applications, and it is becoming best industry practice to deploy liner-based flow control for new projects where variable inflow has proved challenging. In many cases sidetracking the original producer proves more economically viable than remediating the existing well.

A large portion of the wells in the data set involve FCD designs that were not optimally designed for SAGD applications. As industry knowledge increases in the appropriate design and deployment

of SAGD flow control, results may show an increasing success rate. In addition, FCDs likely offer other benefits, such as improved screening, which may have contributed to performance enhancement; however, it is generally accepted that later wells are drilled in more challenging parts of reservoirs. It is remarkable how much of an impact FCDs have on oil production and cSOR in such challenging reservoirs. Fig. 4-24 illustrates the normalized oil production of 16 recently drilled nearby wells in Western Canada, comparing those with and without FCDs. In 13 out of the cases, the wells equipped with FCDs exhibited higher normalized oil production, highlighting the significant contribution of FCDs in enhancing oil production for a well with FCDs in challenging parts of reservoirs compared to its nearby well without FCDs.

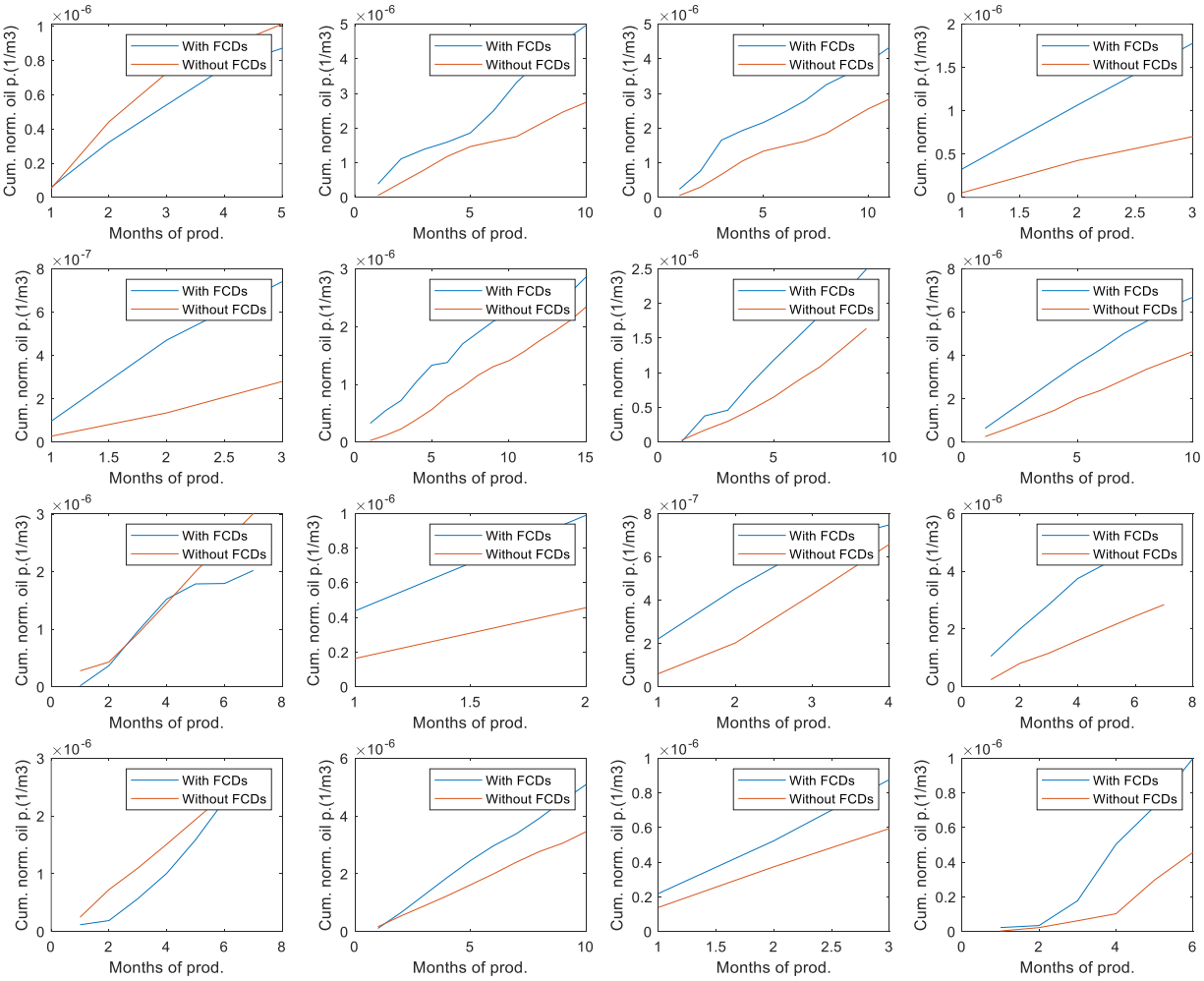

Fig. 4-24. Normalized oil production for 16 nearby wells with and without FCDs that have recently been drilled and operated in Western Canada.

The findings and analysis presented in this study rely on the utilization of the normalization relationship described in Eq. 14. Due to limited access to certain databases such as core analysis and porosity logs, the authors were unable to incorporate them into Eq. 14. Although this limitation is not significant for SAGD reservoirs in Western Canada, as porosity values are generally similar at shallow depths, including these data would have been advantageous. Additionally, the authors did not have access to seismic data to incorporate chamber growth into Eq. 14. Instead, the drainage box based on well spacing, lateral well length, and reservoir thickness were considered. Unfortunately, the primary well completion design information, such as wire-wrap, mesh-screen, or slotted-liner, was not provided in the database due to limited access to that specific data. Another limitation encountered by the authors is the restricted access to information regarding wells completed with different types of FCDs. By expanding the dataset to include a greater number of wells completed with FCD, the study could yield more generalizable results.

4.7. Conclusions and Future Works

For this study, a database was compiled using open-source resources such as the AccuMap^{TM} database and AER reports. To compare the productivity and cSOR of long wells to short wells, 5,246 wells from 1997 to mid-2022 in 13 major SAGD projects in Western Canada are extracted. To study the FCD's contribution to production and cSOR, another database from 2002 to mid-2022 containing 1,492 wells in seven SAGD projects in Western Canada is extracted.

Normalization of the reservoir production rate was essential for meaningful comparisons between wells. One could compare the performance of different well completions by normalizing the reservoir production rate using net-to-gross ratio, injected steam, reservoir thickness, well spacing, and well length.

Several techno-economic challenges exist for drilling longer wells, like the pressure loss across the wellbore and steam chamber conformance. However, there are competitive advantages for increasing the lateral length of the wells since CapEx with long wells is reduced, and oil production is increased by FCDs. It is worth mentioning that wells with FCDs tend to be longer than conventional ones, and it is even more intriguing and noteworthy that, despite this bias, the wells with FCDs perform better per meter. The effective per-meter production of a well should typically decrease as its length increases.

Based on this study, the following conclusions are made:

1. With regards to FCDs assessments, on average:
    a. **In general, FCDs enhance oil production while decreasing cSOR:** FCD deployment raised normalized oil production up to 52% while decreasing cSOR up to 18%.
    b. **Liner-deployed FCDs increase productivity and reduce cSOR**: boosted normalized oil production up to 59% while decreasing cSOR up to 20%.
    c. **Despite being remedial tools, tubing applied FCDs improve productivity and cSOR**: TDFCD-retrofitted wells boosted normalized oil production up to 47% while decreasing cSOR up to 16%. When comparing performance before and after the TDFCDs deployment date, all wells retrofitted with TDFCDs enhanced normalized oil production by 231% while lowering cSOR by 27%.
    d. **Inflow control devices alone improve productivity and cSOR**: ICDs enhanced normalized oil production up to 48% while reducing cSOR by 18%.
    e. **Outflow control devices alone boost productivity and cSOR**: OCDs improved normalized oil production up to 37% while reducing cSOR by 17%.
2. With regards to long wells assessments, on average:
    a. **Frequency and length of the long lateral wells:** During 26 years of the pad development for the studied projects, 2,764 long wells were drilled. The lateral length of long wells drilled till 2010 was 27% longer than short wells, while it reached to 41% after 2010. Furthermore, during the years of production, on average, the length of long wells was greater than short wells in the range of 12% to 54%, while it was on average equal to 38% for all wells.
    b. **Normalized oil production and cSOR of long wells versus short wells:** Comparing normalized oil production and cSOR for long wells to short wells for the 13 projects showed that on average, long wells produced more normalized oil compared to short wells as high as 18% while cSOR increased as 4% during all production years for all projects.
    c. **Lower environmental footprint by long wells:** The normalized oil production by a long well is more than a short well. It indicates that for a given amount of oil, fewer long wells need to be drilled compared to short wells. Accordingly, the

CapEx and drilling footprints would be decreased.

3. With regards to FCDs assessments for long wells to short wells, on average:
    a. **Contribution of FCDs for long wells:** Installing FCDs in long wells resulted in more normalized oil production, up to 96% while decreasing cSOR by 26% compared to nearby short wells without FCDs in the same pads.
    b. **Contribution of LDFCDs:** Long wells completed with LDFCDs boosted normalized oil production up to 117% while decreasing cSOR up to 31%.
    c. **Contribution of TDFCDs:** TDFCD-retrofitted wells produced up to 88% more normalized oil production while decreasing cSOR up to 25%.
    d. **Inflow control devices alone improve productivity and cSOR**: ICDs enhanced normalized oil production by up to 118% while decreasing cSOR up to 30%.
    e. **Outflow control devices alone boost productivity and cSOR**: OCDs improved normalized oil production by up to 69% while reducing cSOR up to 20%.
    f. **Combining long wells with FCD:** This study verifies the current drilling and completion trend of combining longer wells with FCDs to improve the normalized oil production (up to 96%) and cSOR (up to 26%) and production length (38%) in comparison to the traditional short wells.

Generally, FCDs contribute significantly to oil production in wells longer than 850 meters. Drilling long wells with FCDs is a win-win strategy that results in more oil production compared to short wells without FCDs; since CapEx with long wells is reduced and oil production is increased by FCDs. Even though LDFCDs provided higher normalized oil production compared to the TDFCDs, it should be considered that the problematic wells were retrofitted by TDFCDs, so the wells were already challenging. Accordingly, improving the normalized oil production even to the same level as "normal" wells, which refers to the non-problematic wells without FCDs, is very promising.

The authors suggest involving seismic monitoring and temperature data to infer steam chamber growth, in addition to reservoir thickness and well spacing parameters. Involving other reservoir parameters such as porosity and increasing the number of the wells with FCDs in the database could help develop a more generalizable assessment.

Chapter 5: Forecasting the Impact of Flow Rates Control on Well Performance

This chapter has been derived from the following paper:

Izadi, H., Leung, J.Y., Roostaei, M., Mahmoudi, Stevenson, J., Tuttle, A., Sutton, C., Mirzavand, R., and Fattahpour, V., **Submitted to the Journal of Engineering Application of Artificial Intelligence**. Performance Prediction of Different Flow Rates Control Strategies Using LSTM Networks.

Izadi, H., Roostaei, M., Mahmoudi, M., Rosi, G., Stevenson, J., Tuttle, A., Sutton, C., Mirzavand, R., Leung, J.Y. and Fattahpour, V., **2022**, November. Data-Driven Decision-Making Strategy for Thermal Well Completion. **In SPE Thermal Well Integrity and Production Symposium**. OnePetro.

5.1. Preface

Improving oil production and cSOR predictions in SAGD wells can enhance profitability, while minimizing freshwater and natural gas consumption for steam generation. However, forecasting future oil production and cSOR relies on various operational and reservoir factors, including steam injection volume, historical oil production, reservoir quality and saturation, and flow control strategies through different FCDs. This study addresses these challenges by utilizing a comprehensive real database of 642 wells, incorporating reservoir, production, injection, and well data from 70 operating well pads in Western Canada.

In this chapter, we employed an incremental clustering algorithm to group well-pads based on reservoir and operational parameters. Separate Long Short-Term Memory (LSTM) networks are trained within each cluster for wells with inflow and outflow rate control strategies using FCDs and wells without such strategies. The LSTM networks utilize actual operational practices and historical data to forecast future oil production and cSOR within each cluster.

Ten clusters have been created using the clustering algorithm, followed by different numbers of wells with and without FCDs within each cluster. It is observed that implementing flow control strategies by the completion of a new well with the use of FCDs has the potential to result in an oil production increase spanning from 12% to 130%. Additionally, the cSOR can be reduced within a range of 9% to 79%. The findings align with the current industry trend and results reported based on real databases, suggesting that managing the inflow and outflow rates in SAGD wells can contribute to enhanced oil production and cSOR.

This chapter advances existing literature by utilizing real operational data and considering the influence of various flow control strategies on oil production and cSOR forecasting. The findings contribute to optimizing SAGD operations and serve as a valuable guide for future well-pad planning and decision-making processes.

5.2. Introduction

The accurate prediction of oil production and cSOR in SAGD wells holds significant importance from economical, operational, and management perspectives. Improved oil production forecasts can lead to increased profitability, while reducing cSOR can help minimize freshwater and natural gas consumption for steam generation, thereby reducing GHG emissions. SAGD well performance

is influenced by many operational factors, including but not limited to well completion design, steam injection volume, subcool, steam injection temperature and pressure, as well as many geological properties [125,3 ,126]. Among these factors, the well completion design and its impact on steam distribution and equalizing the inflow rate to the production well are considered the most crucial elements [127]. If the injection volume is insufficient, it can result in suboptimal oil recovery. Conversely, excessive steam injection is an expensive process with notable GHG emissions. Moreover, the injection of steam and extraction of oil can exert stress and deformation on well casings and the surface, potentially leading to environmental concerns [128]. Furthermore, the overall steam volume generated per day is constrained by the capacity limitations of the steam generation facilities. Improving oil inflow rates from a reservoir into a producing wellbore, and optimizing steam outflow rates from an injector well to the reservoir, is crucial for enhancing steam conformance and oil production. This process relies heavily on the implementation of efficient flow control strategies customized for each well. Both reliable oil production forecast and cSOR prediction is needed to compare and assess different operating options.

As discussed in Chapter 4, several data-driven studies have been carried out to study the contribution of FCDs in SAGD projects. Although these studies and others have made strides in strengthening operating practices, a comprehensive study of SAGD well performance based on a big database of field data has not been considered yet. In addition, the literature did not involve more than two wells to compare the wells without and with FCDs concerning the differences between geological and operational parameters within different well-pads. Moreover, their comparative analysis of wells with and without FCDs largely overlooked the essential operational and reservoir factors. Additionally, they did not provide a monthly forecasting of the improvement percentage for newly drilled wells with FCDs based on the historical production data. Hence, initially clustering a substantial database according to operational and geological parameters becomes imperative for comparing wells within the same clusters, as these conditions play a crucial role in evaluating the effectiveness of FCDs [3, 101]. Subsequently, offering a predictive forecast for the enhancement of oil production and cSOR in new wells using a machine learning approach can provide a monthly progress rate derived from historical data. This, in turn, offers valuable insights for operators in their decision-making for future well-pad development.

Various time series prediction methods, such as Autoregressive Integrated Moving Average (ARIMA) [129], Artificial Neural Networks (ANNs) [130], Extreme Learning Machine (ELM) [131], and Elman Neural Network (ENN) [132], show promise in addressing oil production prediction challenges. However, long short-term memory (LSTM) networks offer several advantages over other neural network architectures, especially when dealing with sequential or time series data. LSTM networks are designed to overcome the vanishing gradient problem, which allows them to capture and retain information over longer sequences. They can effectively learn dependencies between distant time steps, making them suitable for modeling complex temporal patterns [133]. Other than that, LSTMs incorporate a memory cell, which can store and retrieve information over long periods. This memory cell allows LSTMs to selectively forget or remember information based on the input and current context, facilitating the modeling of long-term dependencies. LSTM networks exhibit robustness to noisy or missing data. The memory cell helps mitigate the impact of noisy inputs and can continue to learn and make predictions even with incomplete or corrupted data [134]. LSTMs have a more stable gradient flow during training compared to other recurrent neural networks. Memory cells and gating mechanisms helps mitigate the issues of exploding or vanishing gradients, enabling more effective and efficient training [135]. Furthermore, the gating mechanisms in LSTMs, such as the forget gate, input gate, and output gate, enable precise control over the flow of information within the network. This facilitates learning relevant patterns while filtering out irrelevant or noisy information. Overall, LSTM networks have proven to be powerful tools for modeling and predicting complex temporal patterns, making them advantageous in various applications involving sequential or time series data [136].

Several studies have addressed the contribution of machine learning algorithms to forecast future oil production. Yusof et al. (2010) utilized the ARIMA method to analyze monthly oil production data of Malaysia spanning from January 2005 to May 2010 and a substantial improvement in the predictability of oil production for the three subsequent months through the forecast generated using the ARIMA method has been observed [137]. Berneti and Shahbazian (2011) proposed a technique for forecasting oil flow rates in wells located in the Persian Gulf oil fields. Their approach involves combining ANN with the imperialist competitive algorithm (ICA) [138]. Liu et al. (2020) proposed an Ensemble Empirical Model Decomposition based Long Short-Term Memory neural network model called EEMD-LSTM for oil production prediction problem and demonstrated the effectiveness of the proposed model in oil production prediction [139]. Yang and

Wang (2021) presented a method to optimize the steam injection and predicted the future oil production using LSTM [140]. Wang et al. (2021) presented a method to predict the SAGD performance using recurrent neural networks based on database gathered from numerical simulations [141]. Reinforcement learning with function approximation has been successfully applied to the optimization of steam injection in a SAGD process [142]. Zhou and Wang (2022) applied an integrated framework based on deep learning algorithm for optimizing thermochemical production in heavy oil reservoirs [143]. Their model could predict the best conversion timing for different production stages. Huang and Chen (2023) employed different machine learning algorithms to dynamically predict the oil production for SAGD wells [144]. Existing literature predominantly relies on numerical simulations to train machine learning methods in the context of oil production, while cSOR has not been widely considered. While operational parameters have been optimized to enhance future production in some cases, there is a lack of extensive utilization of real data collected from past oil production practices. Moreover, inflow and outflow rates control strategies have not been extensively studied as a parameter to understand its potential impact on future oil production and cSOR. In addition, a forecast for a well that will be drilled in the future in a particular geology characterization may not be concluded by the methods introduced in the literature.

This paper focuses on the utilization of a comprehensive database consisting of geological, production, injection, and well data from 642 wells located within 70 operating well well-pads in Western Canada. Among these wells, 258 have been completed/ retrofitted by FCDs, while 384 wells operate without FCDs. The objective of the study is to forecast oil production and cSOR for a future well based on the data from existing wells within the database. To achieve this, an incremental clustering algorithm is initially employed to cluster the well-pads in the database using reservoir and operational parameters such as reservoir thickness, porosity, permeability, well spacing, initial oil saturation, average injection pressure, and initial reservoir temperature. Well-pad refers to a group of wells that are horizontally drilled next to each other and geological parameters are fairly the same for all wells within the well-pad. Within each cluster, various LSTM networks are trained: one for wells without FCDs and some others for wells equipped with various FCDs. The LSTM networks are trained to predict future oil production and cSOR within each cluster. The predictions demonstrate that wells with FCDs outperform wells without FCDs in terms of higher oil production and lower cSOR. By utilizing the trained LSTM networks and the

clustered database, the paper provides valuable insights into the benefits of FCD implementation in terms of enhanced oil production and reduced cSOR.

5.3. Database

The database used in this study was constructed by gathering data from various open-source resources, including the AccuMap^{TM} database and AER reports. The aim was to create a comprehensive dataset comprising geological, production, injection, and well data for 642 wells situated within 70 operating well pads in Western Canada. Among these wells, 258 were completed using FCDs, while 384 were operated without FCDs. Fig. 5-1-a represents the visualization of wells in the Accumap^{TM} database, and Fig. 5-1-b represents the corresponding well pad name and number. A summary of the extracted data is also shown in Table 15. The FCD types are shown in Fig. 5-2.

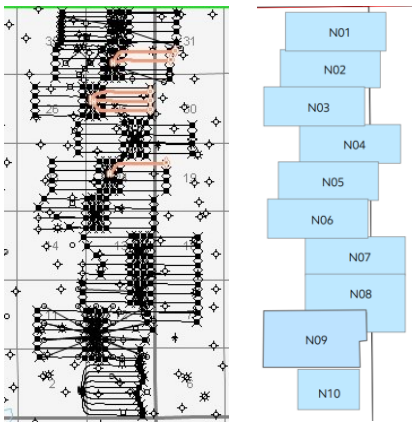

a b

Fig. 5-1. a) A visualization of wells in the Accumap^{TM} database and b) represents the corresponding well-pad name and number. Horizontal lines show the horizontal SAGD wells; circles are vertical (mostly observation) wells.

Table 15. Extracted database in this study.

Data category	Existing data
Well data	FCD placement: liner deployed - LDFCD, tubing deployed TDFCD Type: ICD and OCD
	Well length (m)
	Well spacing (m)
Production data (m^3/month)	Oil production and steam injection
Geological data	Reservoir thickness (m)
	Net to gross (NTG) ratio

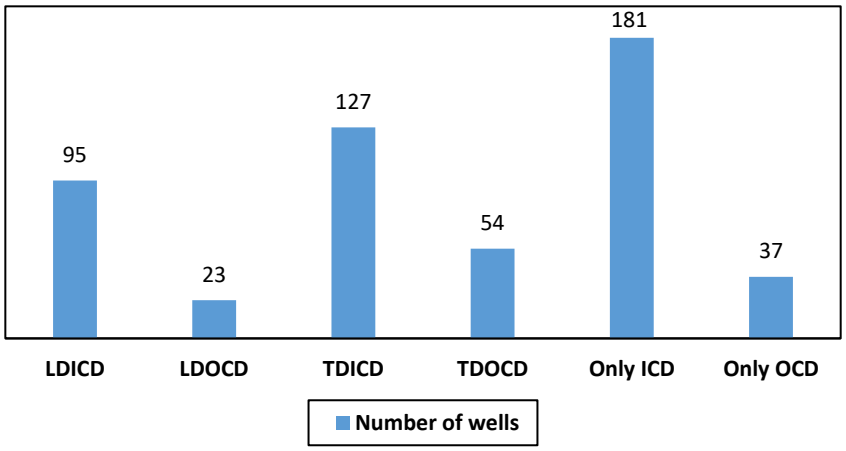

Fig. 5-2. Number of wells with different types of FCDs in the database (LD – liner deployed, TD – tubing deployed, ICD – inflow control device, OCD – outflow control device).

It should be considered that the wells retrofitted with TDFCDs were already classified as problematic, indicating inherent challenges [99]. Additionally, certain wells completed with slotted liners (SL) as the sand control design cannot be equipped with LDFCDs and can only be retrofitted with TDFCDs due to technical limitations. Consequently, two categories of TD-equipped wells exist: nonproblematic wells completed with SL (used in this study) and problematic wells that can be retrofitted with TDFCDs. However, nonproblematic wells equipped with TDFCDs may be more susceptible to failure than those equipped with LDFCDs due to operational factors such as erosion [115]. Furthermore, enhancing oil production by increasing injection pressure and production rate in nonproblematic wells equipped with TDFCD presents considerable challenges [34, 14]. As a result, the production rate of wells completed or retrofitted with TDFCDs may not surpass that of wells without FCDs.

5.4. Methodology

Normalizing the oil production data against geological, well, and operational parameters helps to account for variations in these factors and provides a fair basis for comparison among wells without and with FCDs [99, 115]. The normalized oil used in this study is calculated based on Eq. 14 presented in Chapter 4. Additionally, an initial step involves applying a clustering algorithm to group well-pads into multiple clusters such that a comparison can be made for wells with similar geological and operational parameters. Subsequently, LSTM networks are trained to forecast oil production and cSOR for a forthcoming well, both in the absence and presence of FCDs. The performance of these predictions is then compared to evaluate their effectiveness.

5.4.1. Clustering

Due to the difficulty in accurately estimating the exact number of clusters in the database, conventional clustering algorithms such as k-means or ANNs may not be suitable for the clustering of well-pads [145, 146, 147, 148]. These algorithms typically require a predetermined number of clusters as input, which is challenging to determine in cases where the optimal number of clusters is unknown. In the context of well-pad clustering, an alternative approach called an incremental clustering algorithm can be employed. This algorithm incrementally builds clusters by iteratively assigning data points to existing clusters or creating new clusters based on the minimum similarity threshold (δ). It allows the number of clusters to be determined dynamically based on the properties and distribution of the data [147, 148]. Therefore, in this study, the incremental clustering algorithm is employed to cluster the well-pads in the database based on reservoir thickness, porosity, permeability, well spacing, initial oil saturation, average injection pressure, and initial reservoir temperature, providing a flexible and adaptive method for grouping wells based on the parameters.

The similarity threshold for each well-pad and the centers of the created clusters is measured as Eq. 15.

$$Sim = \frac{1}{1 + (Euclidean\_distanse)^2} \quad , \quad 0 \leq Sim \leq 1 \quad , \quad 0 \leq Euclidean\_distanse < \infty \tag{15}$$

where $Euclidean\_distance = \sqrt{\sum_{i=1}^{n}(x_i - y_i)^2}$, n is the number of reservoir and operational parameters, $X=[\, x_1, x_2, \ldots, x_n]$ is the assigning well-pad parameters to the clustering algorithm and $Y=[\, y_1, y_2, \ldots, y_n]$ is a particular well-pad that already clustered and considered as the center of a particular cluster. The $Euclidean\_distance$ is measured between the assigned well-pad and all well-pads that considered as the centers of the clusters.

A merging process is incorporated to merge clusters that share a common well-pad. This merging step aims to improve the overall clustering results by considering the physical proximity and operational similarity of wells within the same well-pad [145- 148]. As shown in Fig. 5-3, x_i is i^{th} well-pad which assigned to the algorithm to join one or several previously created clusters with respect to δ, which is the similarity threshold, or to create a new cluster. The law of joining the input well-pad to the previously created clusters or creating a new cluster is described in Eq. 16.

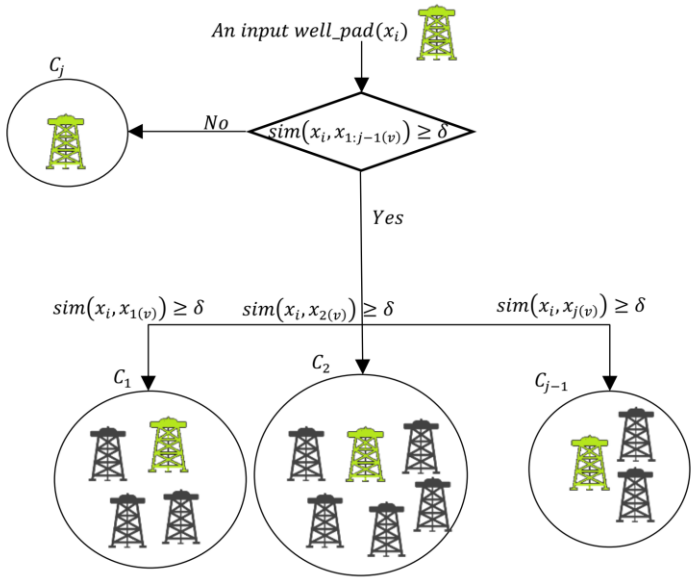

Fig. 5-3. An illustration of combining or creating a new cluster as a result of inputting a new well-pad. The assigned well-pad can be joined to more than one cluster based on δ.

$$\forall\, x_i \,\&\, C_{j,}\quad i = 1{:}N \,\&\, j = 1{:}P \begin{cases} Similarity\,(x_i, x_{j-1(v)}) \geq \delta \rightarrow x_i \in C_{j-1} \\ Similarity\,(x_i, x_{vj}) < \delta \rightarrow create\ C_j \,\&\, x_i = x_{j,(v)} \end{cases} \tag{16}$$

where j is the index of P created clusters, i is the index of N assigned well-pads, C_j is j^{th} cluster, x_{ji} are i^{th} well-pads that joined to j^{th} cluster, and $x_{j(v)}$ is the center of j^{th} cluster [148]. By incorporating the merging of clusters with a common well-pad, the clustering algorithm can achieve a more comprehensive and accurate representation of the underlying data, enabling better insights and analysis of the wells within each well-pad [145- 148].

5.4.2. LSTM Network

Thirty-two LSTMs have been trained for different FCD deployments and clusters: 16 for normalized oil production prediction and 16 for cSOR prediction. Twenty LSTM networks have also been trained for wells without FCDs in the 10 created clusters: 10 for normalized oil production prediction and 10 for cSOR prediction.

To assess the performance of the LSTM model under varying batch sizes and input sequence lengths, ten random wells within Cluster #2, which were completed with LDICDs-LDOCDs, have

been chosen. The relative error for production time and normalized oil production is computed, and Fig. 5-4 through Fig. 5-9 display the LSTM's performance results for each of these cases.

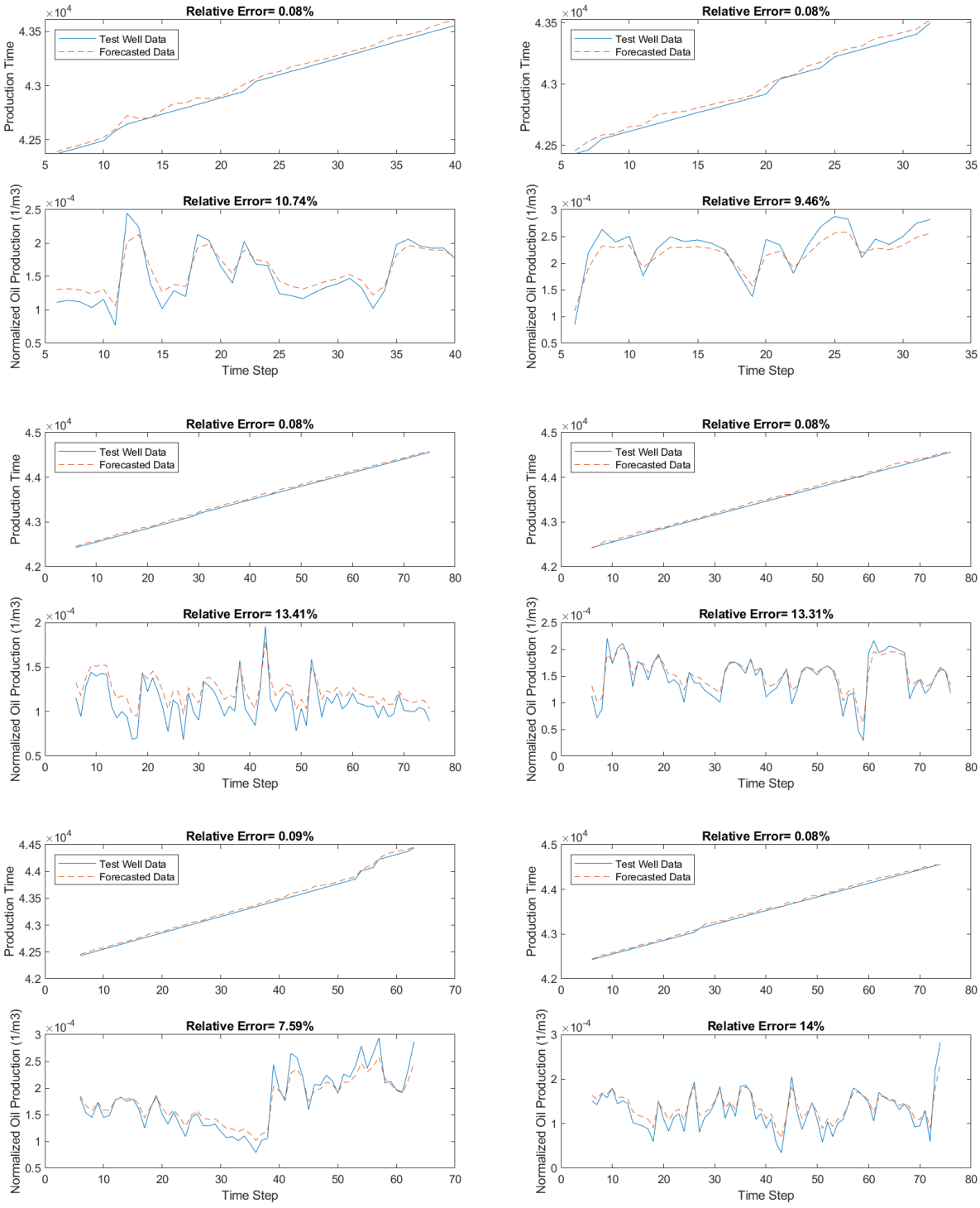

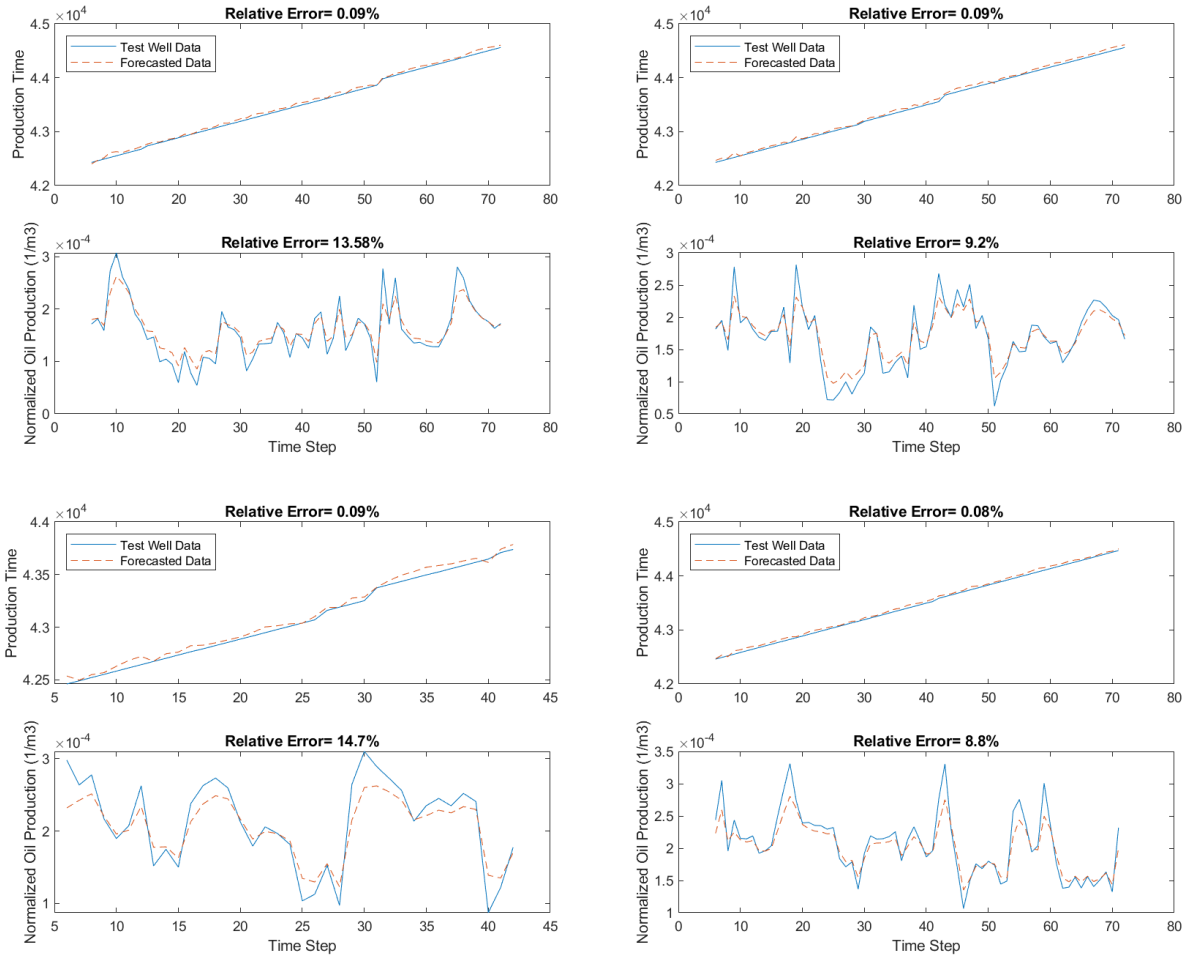

Fig. 5-4. LSTM trained based on a batch size of 16 input sequence length by 5 for ten random wells within Cluster #2. The average relative error for production time and normalized oil prediction are 0.08% and 11.47%, respectively.

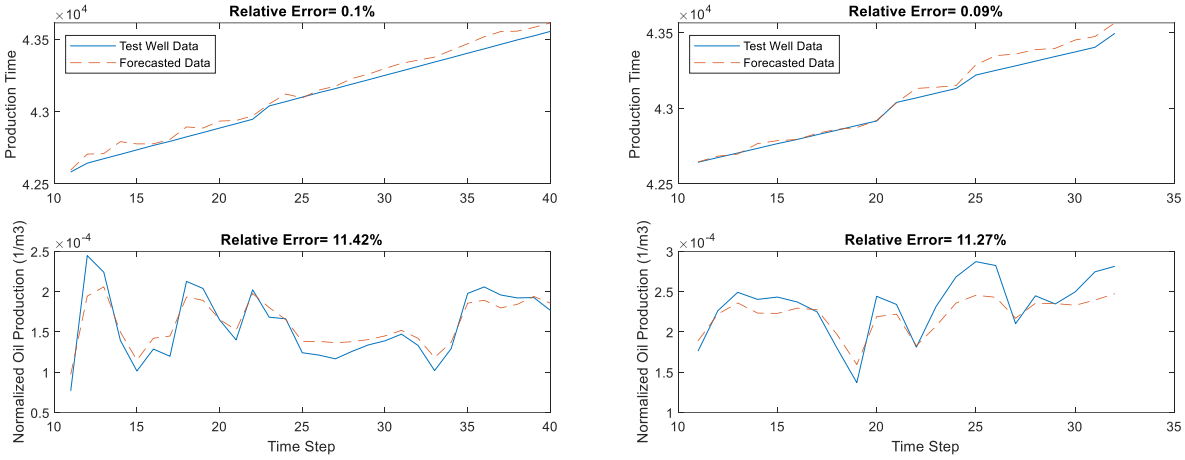

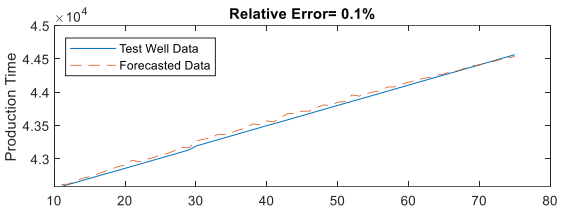
Relative Error= 0.1%
Test Well Data
Forecasted Data
Production Time

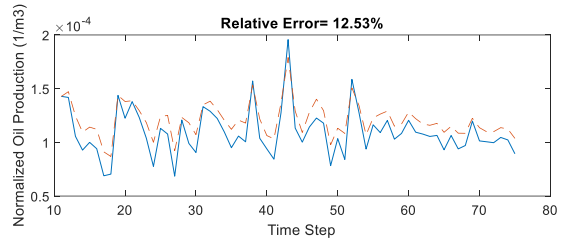
Relative Error= 12.53%
Normalized Oil Production (1/m3)
Time Step

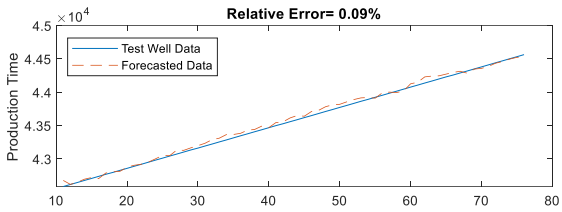
Relative Error= 0.09%
Test Well Data
Forecasted Data
Production Time

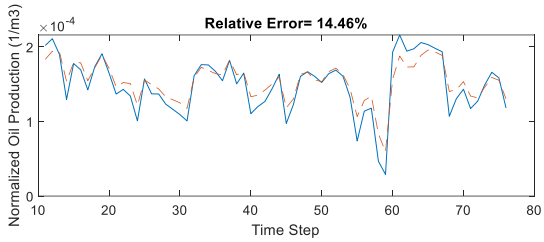
Relative Error= 14.46%
Normalized Oil Production (1/m3)
Time Step


Relative Error= 0.1%
Test Well Data
Forecasted Data
Production Time

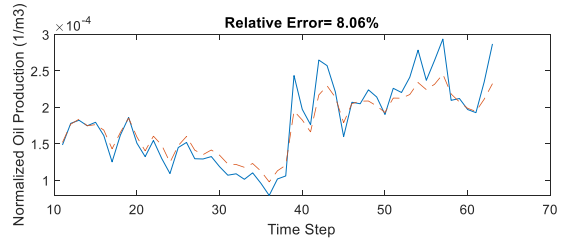
Relative Error= 8.06%
Normalized Oil Production (1/m3)
Time Step

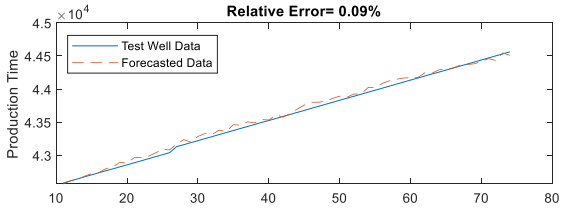
Relative Error= 0.09%
Test Well Data
Forecasted Data
Production Time

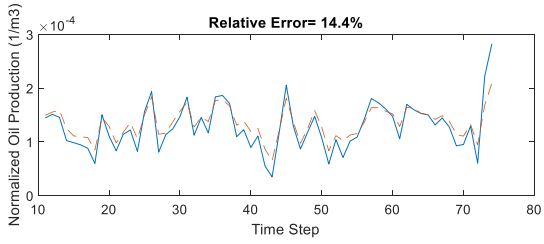
Relative Error= 14.4%
Normalized Oil Production (1/m3)
Time Step

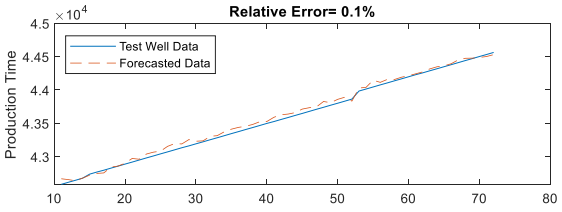
Relative Error= 0.1%
Test Well Data
Forecasted Data
Production Time

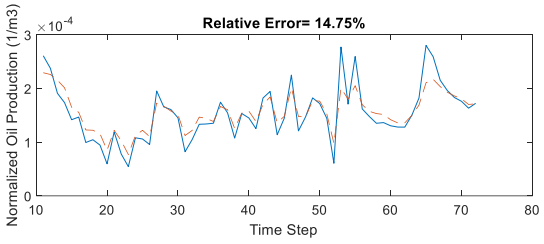
Relative Error= 14.75%
Normalized Oil Production (1/m3)
Time Step

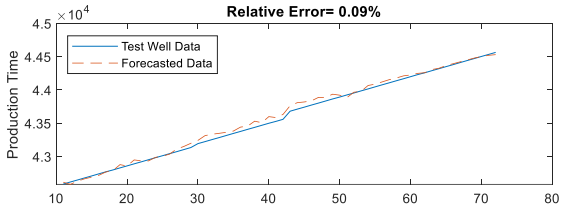
Relative Error= 0.09%
Test Well Data
Forecasted Data
Production Time

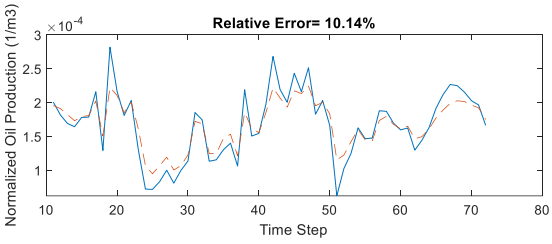
Relative Error= 10.14%
Normalized Oil Production (1/m3)
Time Step

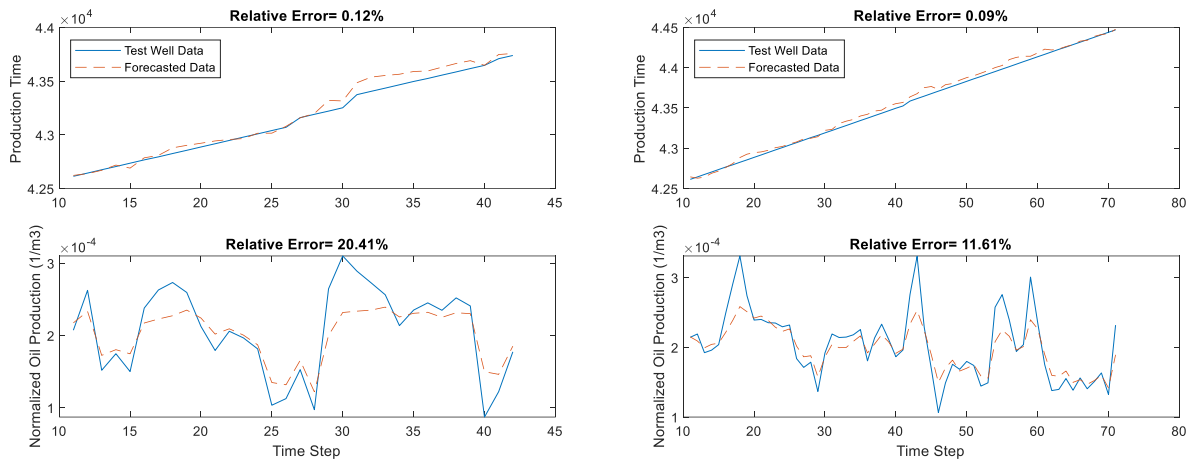

Fig. 5-5. LSTM trained based on a batch size of 16 input sequence length by 10 for ten random wells within Cluster #2. The average relative error for production time and normalized oil prediction are 0.12% and 11.82%, respectively.

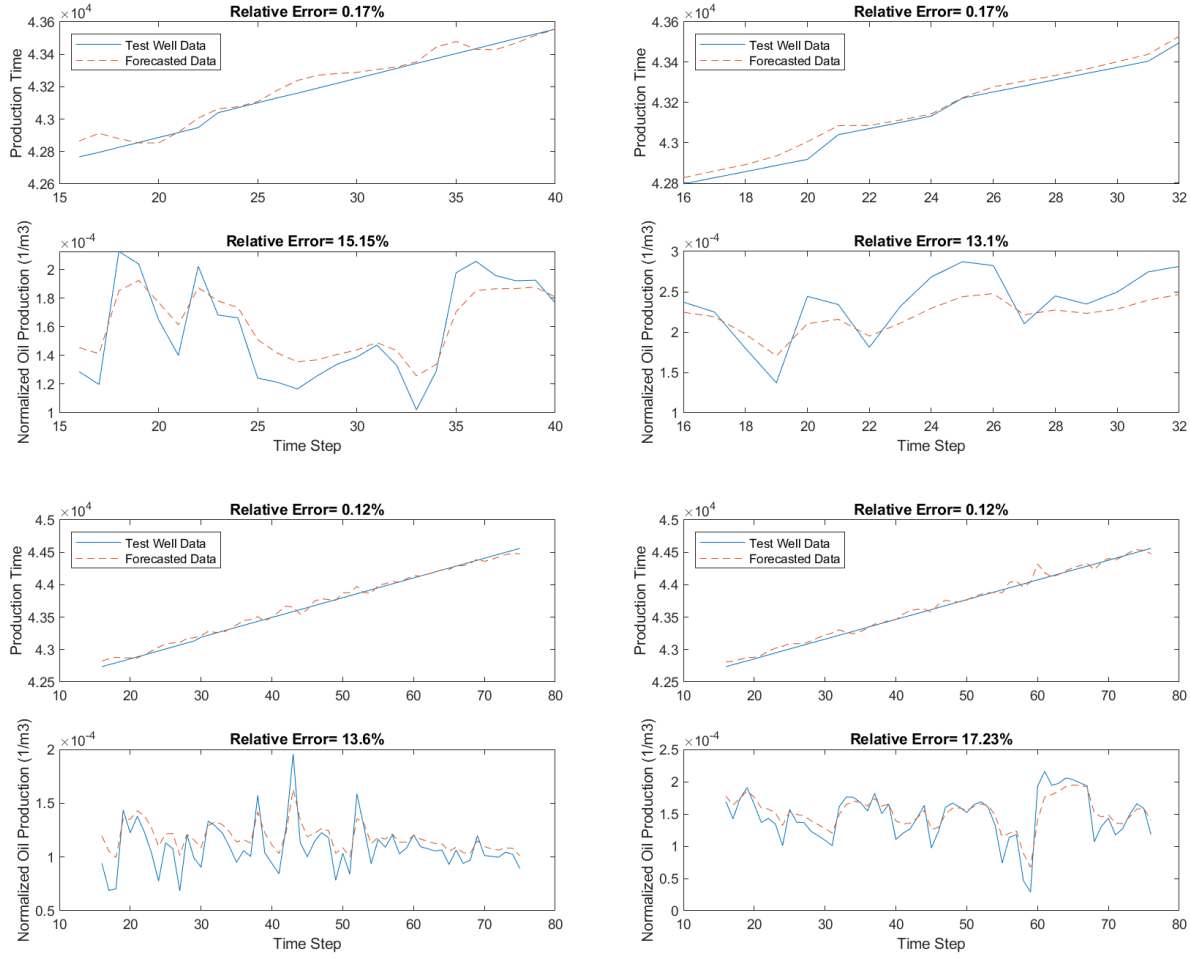

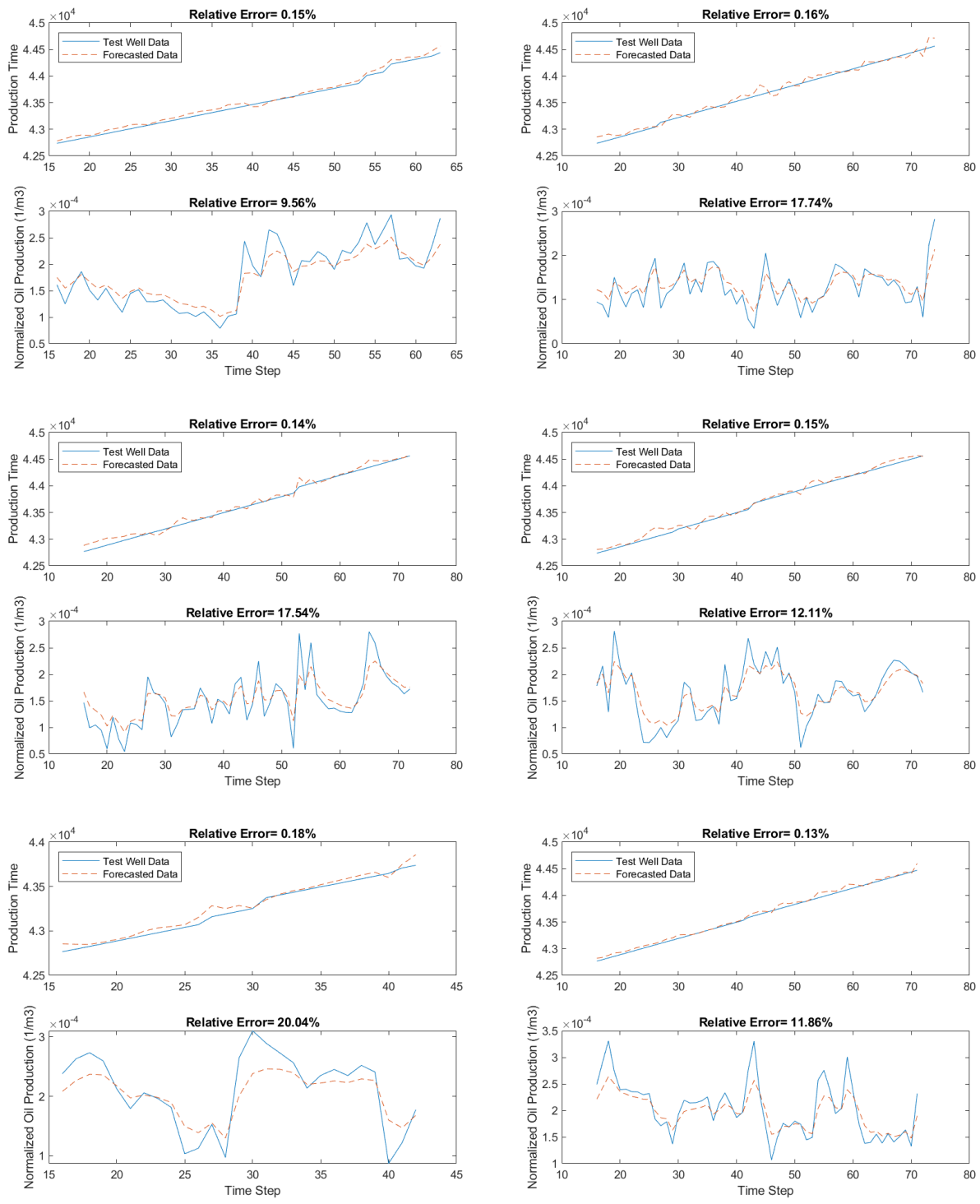

Fig. 5-6. LSTM trained based on a batch size of 16 input sequence length by 15 for ten random wells within Cluster #2. The average relative error for production time and normalized oil prediction are 0.09% and 12.41%, respectively.


Relative Error= 0.06%
Test Well Data
Forecasted Data
Production Time

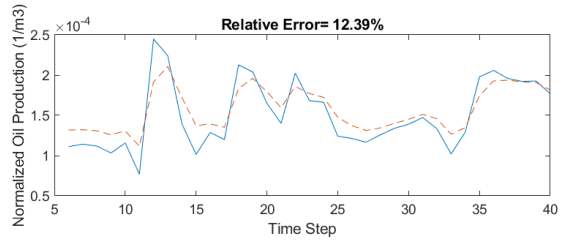
Relative Error= 12.39%
Normalized Oil Production (1/m3)
Time Step

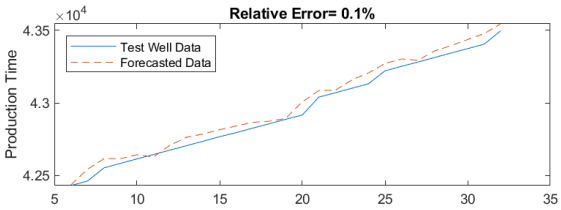
Relative Error= 0.1%
Test Well Data
Forecasted Data
Production Time

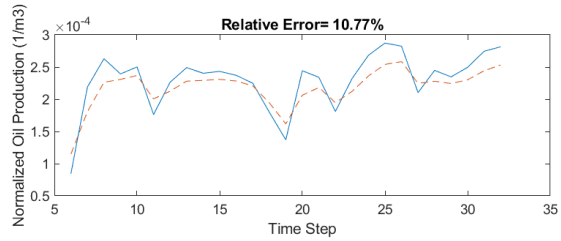
Relative Error= 10.77%
Normalized Oil Production (1/m3)
Time Step

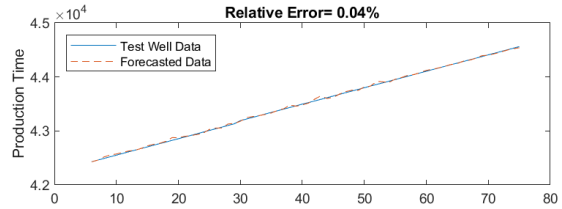
Relative Error= 0.04%
Test Well Data
Forecasted Data
Production Time

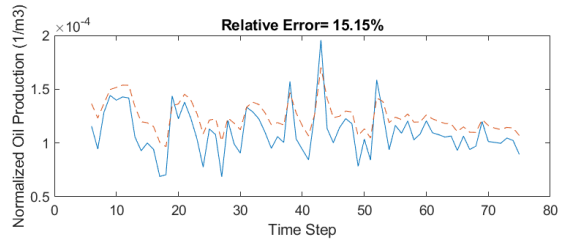
Relative Error= 15.15%
Normalized Oil Production (1/m3)
Time Step

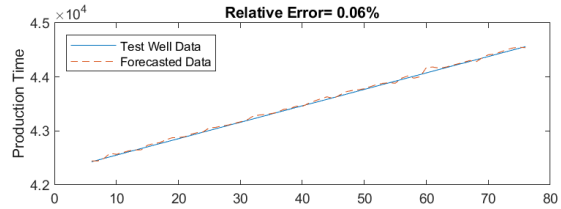
Relative Error= 0.06%
Test Well Data
Forecasted Data
Production Time

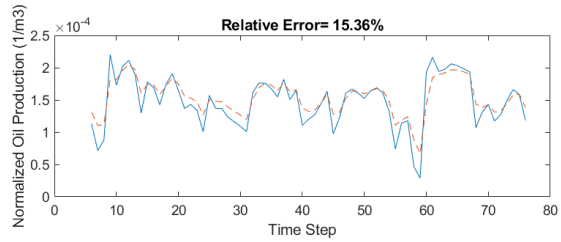
Relative Error= 15.36%
Normalized Oil Production (1/m3)
Time Step

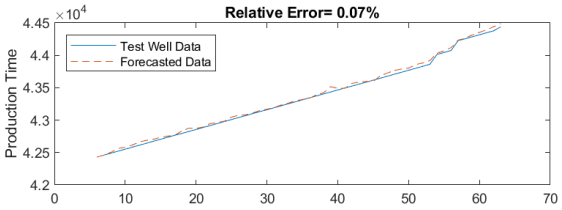
Relative Error= 0.07%
Test Well Data
Forecasted Data
Production Time

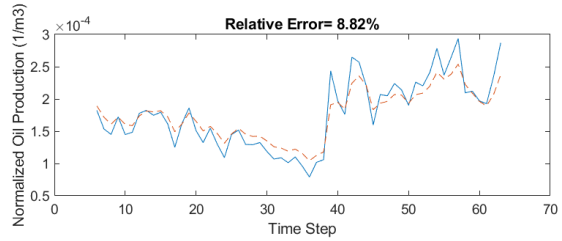
Relative Error= 8.82%
Normalized Oil Production (1/m3)
Time Step

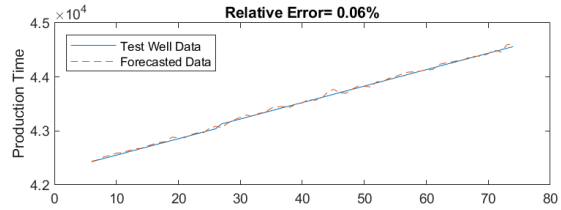
Relative Error= 0.06%
Test Well Data
Forecasted Data
Production Time

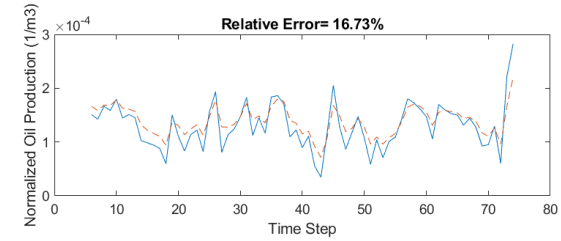
Relative Error= 16.73%
Normalized Oil Production (1/m3)
Time Step

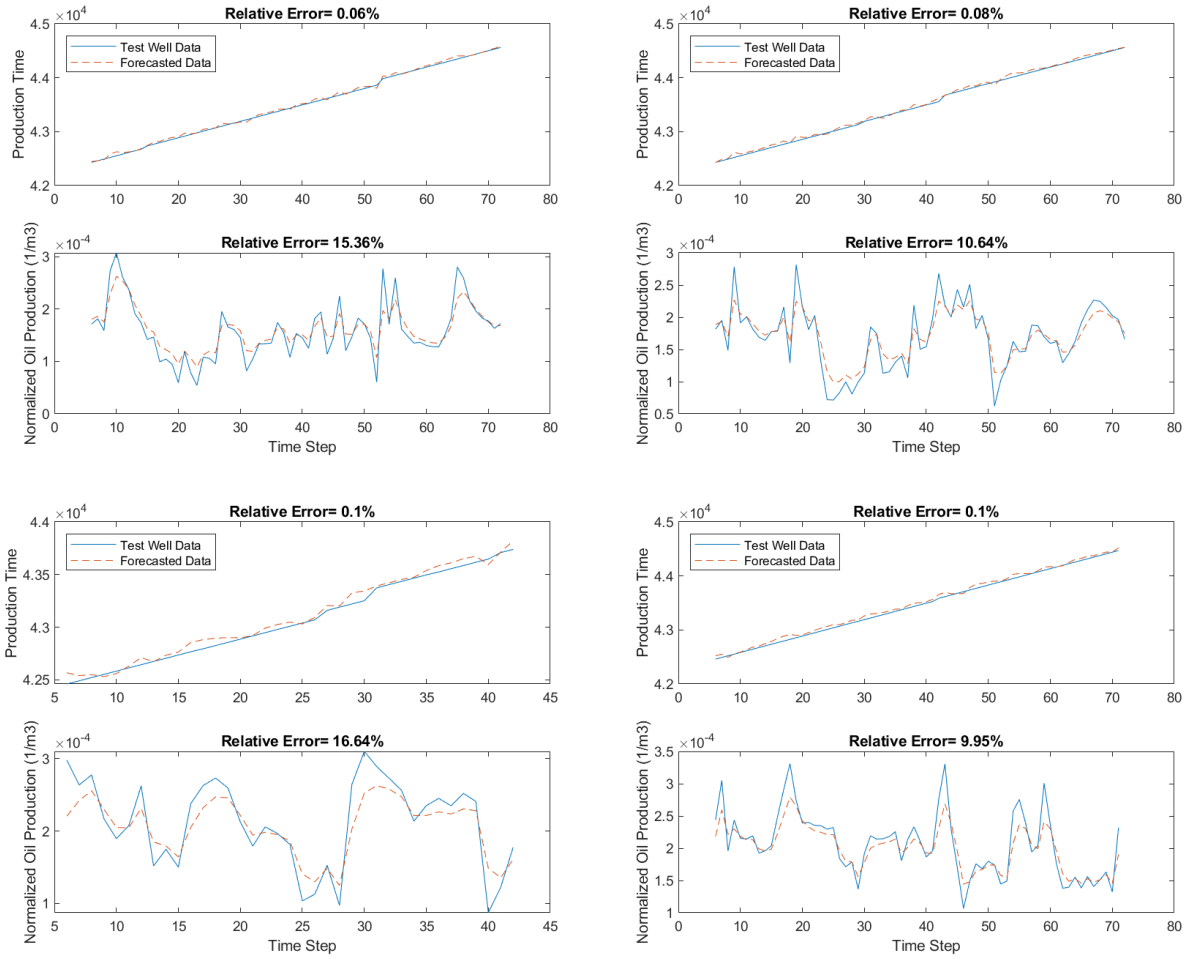

Fig. 5-7. LSTM trained based on a batch size of 32 input sequence length by 5 for ten random wells within Cluster #2. The average relative error for production time and normalized oil prediction are 0.08% and 11.40%, respectively.

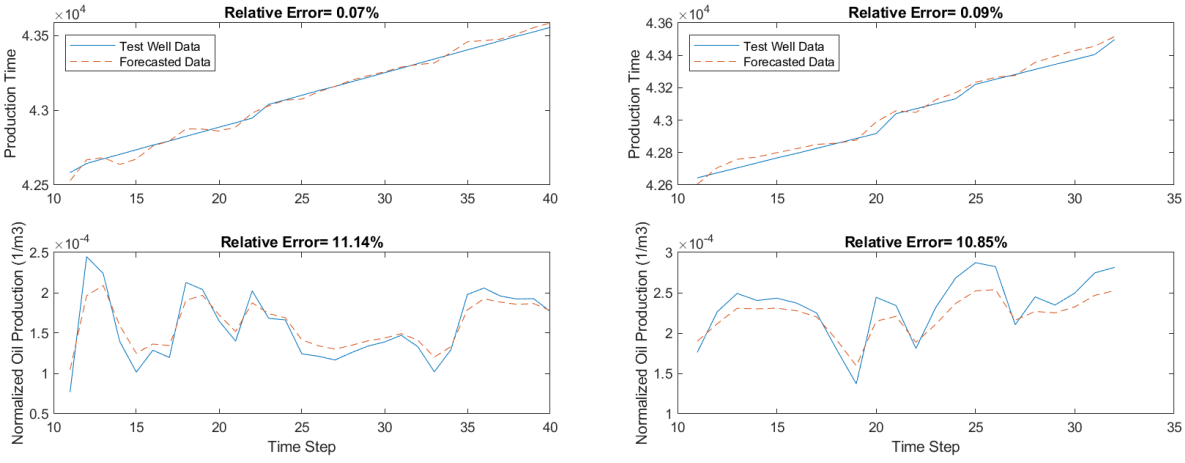

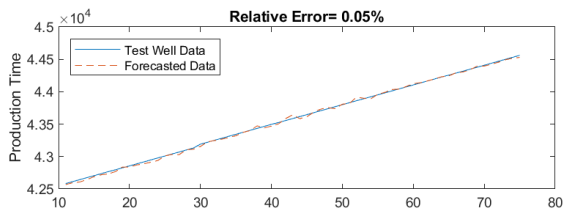
Relative Error= 0.05%
Test Well Data
Forecasted Data
Production Time

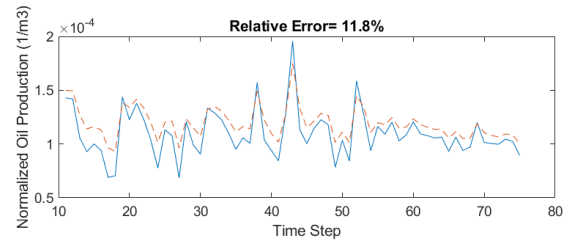
Relative Error= 11.8%
Normalized Oil Production (1/m3)
Time Step

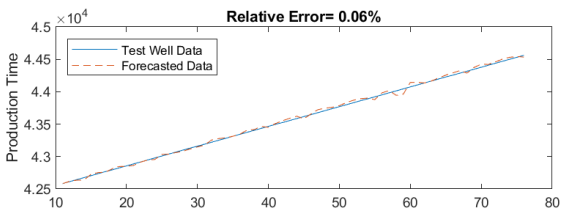
Relative Error= 0.06%
Test Well Data
Forecasted Data
Production Time

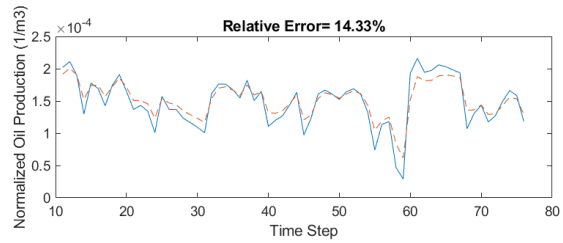
Relative Error= 14.33%
Normalized Oil Production (1/m3)
Time Step

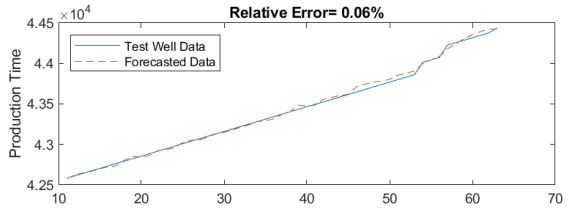
Relative Error= 0.06%
Test Well Data
Forecasted Data
Production Time

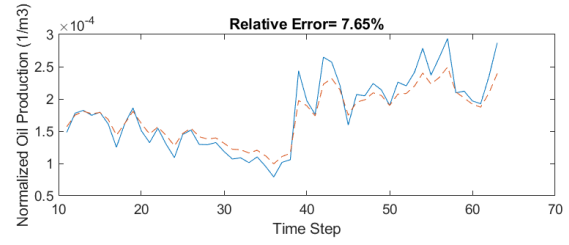
Relative Error= 7.65%
Normalized Oil Production (1/m3)
Time Step

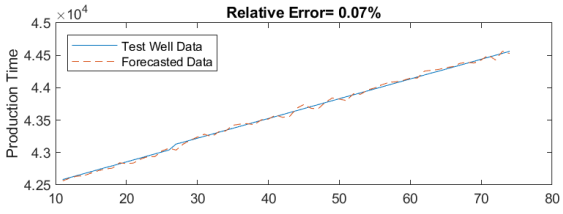
Relative Error= 0.07%
Test Well Data
Forecasted Data
Production Time

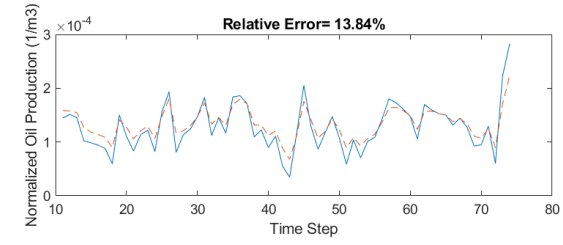
Relative Error= 13.84%
Normalized Oil Production (1/m3)
Time Step

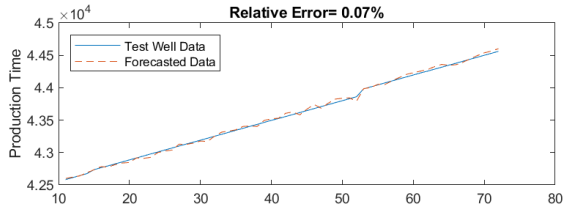
Relative Error= 0.07%
Test Well Data
Forecasted Data
Production Time

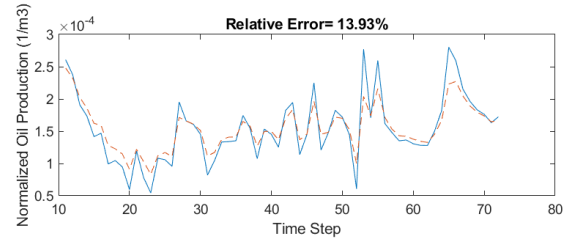
Relative Error= 13.93%
Normalized Oil Production (1/m3)
Time Step

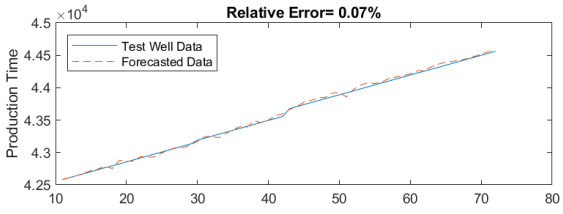
Relative Error= 0.07%
Test Well Data
Forecasted Data
Production Time

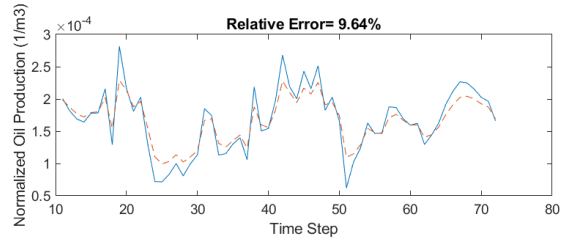
Relative Error= 9.64%
Normalized Oil Production (1/m3)
Time Step

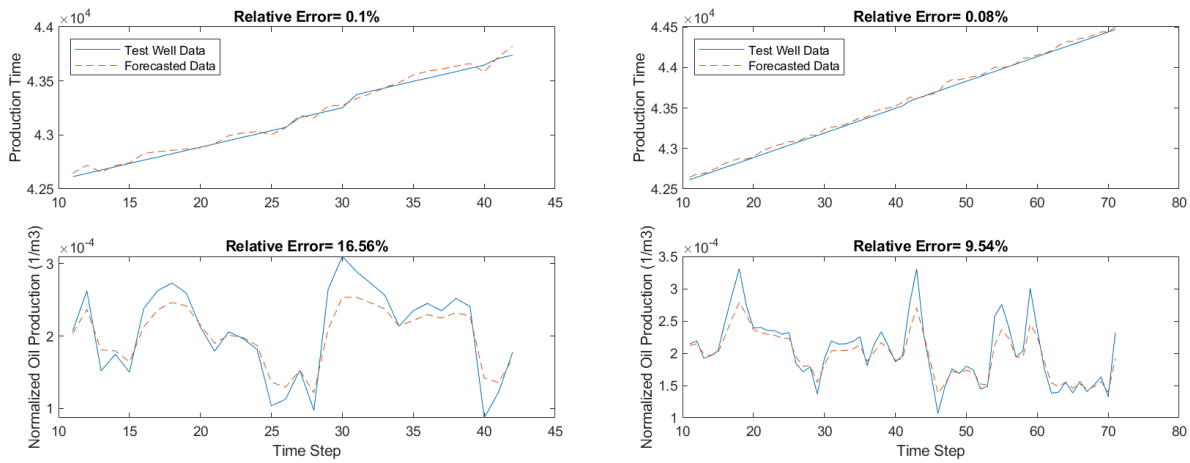

Fig. 5-8. LSTM trained based on a batch size of 32 input sequence length by 10 for ten random wells within Cluster #2. The average relative error for production time and normalized oil prediction are 0.11% and 12.12%, respectively.

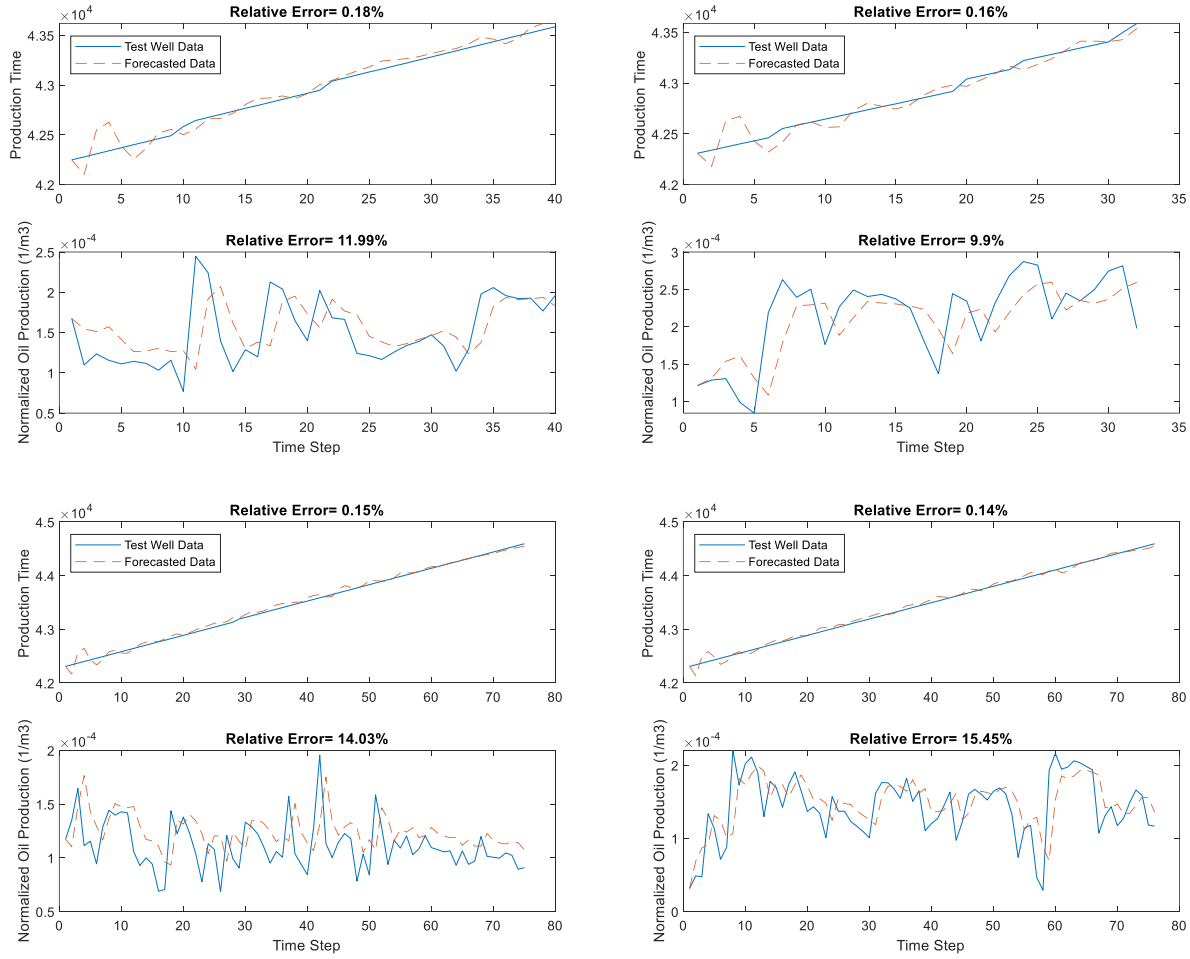

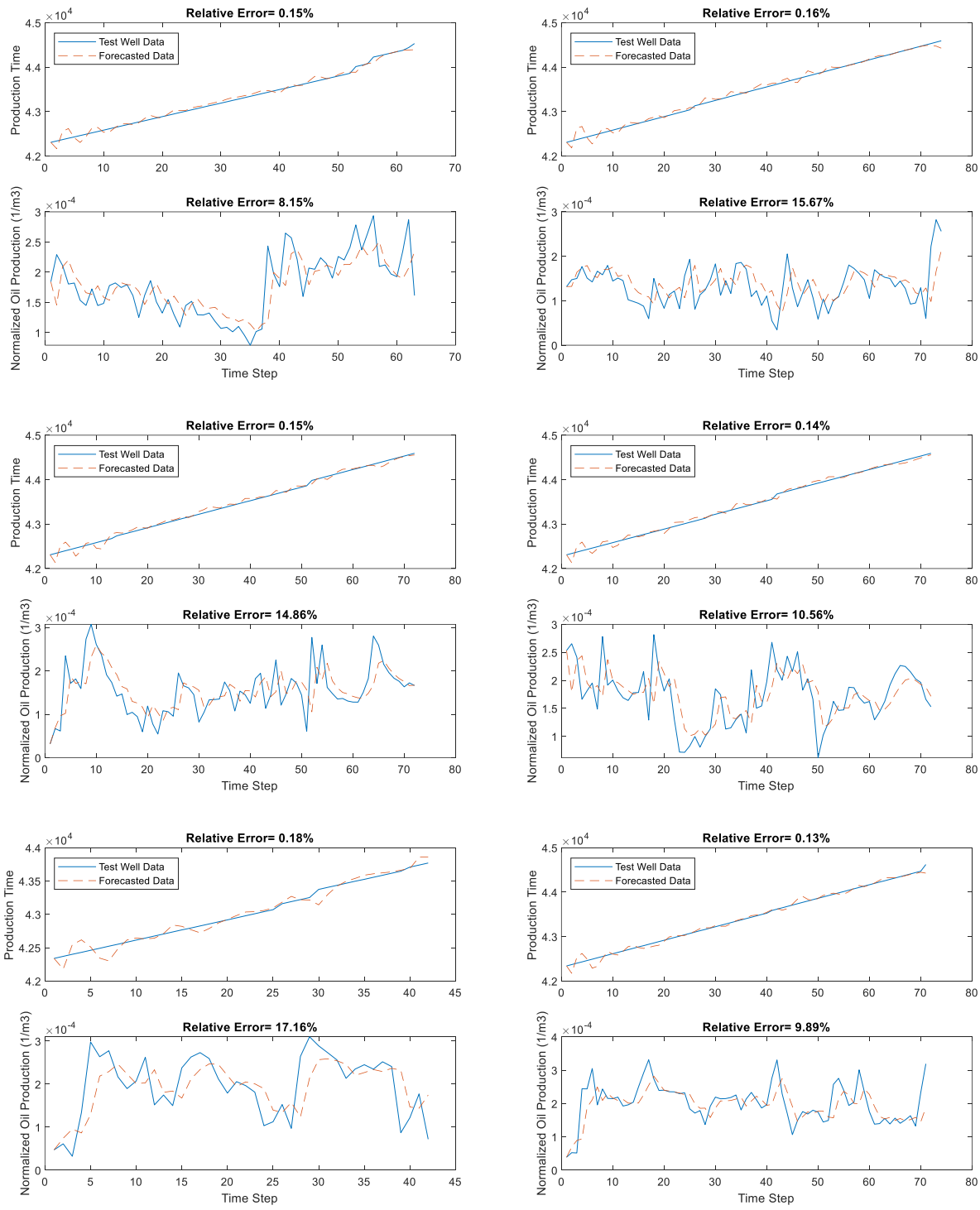

Fig. 5-9. LSTM trained based on a batch size of 32 input sequence length by 15. The average relative error for production time and normalized oil prediction are 0.15% and 12.61%, respectively.

Various batch sizes and input sequence lengths were experimented with to determine the optimal configuration for the LSTM model. Fig. 5-10 illustrates the relative error for production time

prediction, while Fig. 5-11 depicts the relative error for normalized oil production prediction. Upon analysis of these figures, it was observed that the configuration with a sequence length of 5 and a mini-batch size of 8 yielded the best results. Consequently, this configuration was selected for further predictive modeling.

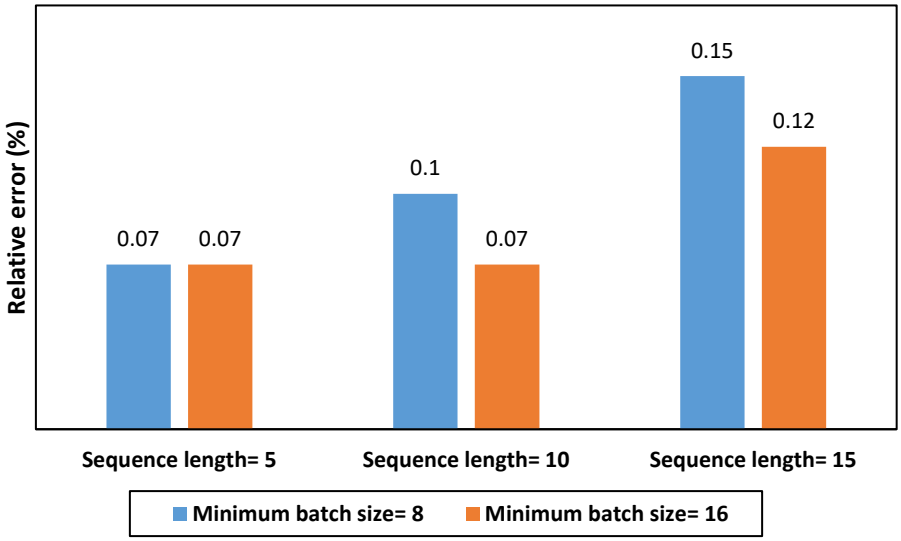

Fig. 5-10. Relative error for production time prediction.

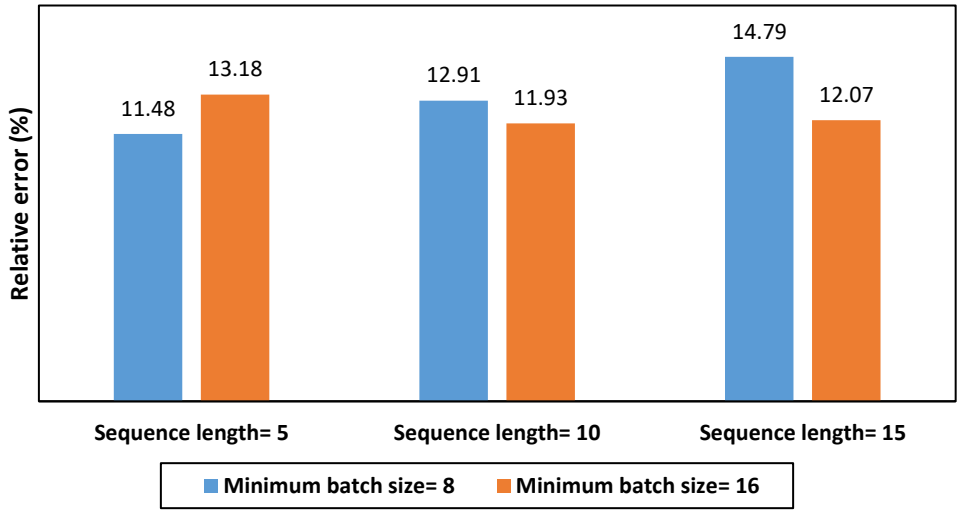

Fig. 5-11. Relative error for normalized oil production prediction.

The data split for the training and testing processes is depicted in Fig. 5-12. According to Fig. 5-12, a cluster consisting of n wells is assumed. In the training phase, sequence data of m wells (80% of the total in each cluster) is used to train the network, and well# $m+1$ to well# n are used in the testing phase. The production (q) and cSOR time series, associated with t, are assigned to separate

networks. As an autoregression method, for the optimal input sequence length of 5, the LSTMs employ data q_{t-5} to q_{t-1} as input sequences to predict q_t. A padding is also performed to make sure all input sequences reach the minimum batch sizes. To check different network architecture, different batch sizes and length of the input sequence to the network have been examined.

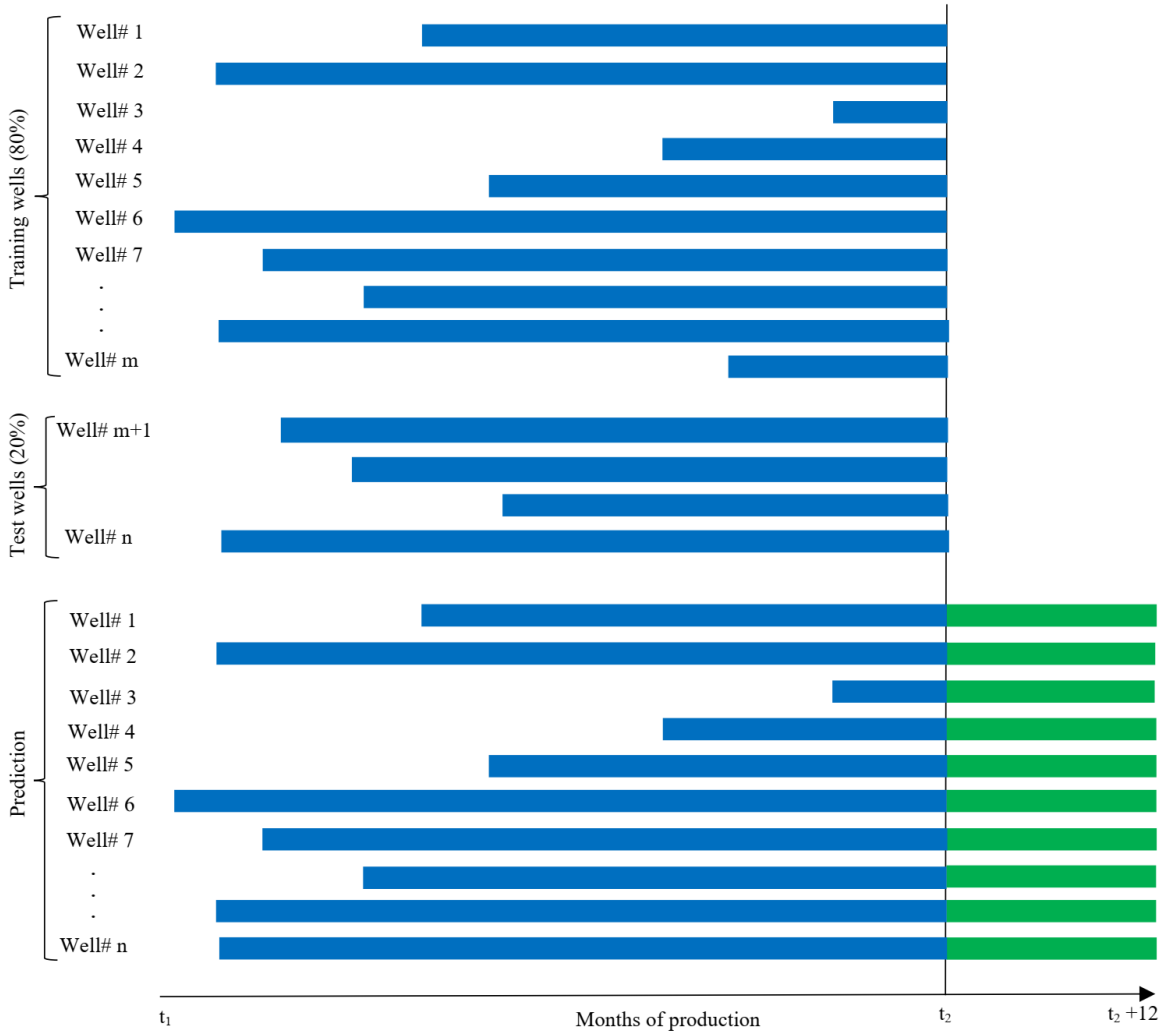

Fig. 5-12. The workflow of LSTM for each cluster and case.

Each well in each cluster has a number of months of production and cSOR data. As shown in Fig. 5-12, t_1 and t_2 represent the first and last production date among all n wells in the cluster. Although the length of the sequences has not been the same, all production data of the training wells is provided in the LSTM for training using cell arrays in MATLAB [149]. The trained LSTM network is then used to forecast 12 months of production and cSOR beyond t_2 for all wells in the database. As shown in Fig. 5-12, the wells within each cluster may belong to different well-pads

in different locations with different starting times for production. Time is included as an input attribute so the LSTMs can learn reservoir depletion and advancements in well completion and workover technologies. Within each cluster, the workflow in Fig. 5-12 is repeated numerous times, one LSTM model is built for wells without FCDs and a different model for each type of FCD deployment (e.g., LDICDs or retrofitted TDICDs). The LSTM networks employed in this study were trained within the MATLAB environment [149]. The training process encompassed 8000 iterations, referred to as network epochs, during which the learnable parameters were updated. This was achieved through a custom training loop that utilized the stochastic gradient descent with momentum (SGDM) algorithm. Notably, each LSTM layer within the networks consisted of 1200 hidden neurons.

Historical production data from existing wells is utilized to train the LSTMs. This approach is supported by the understanding that the behavior of the new wells is expected to resemble the production patterns observed in the last months of the wells present in our database. This is due to factors such as reservoir depletion and advancements in well completion and workover technologies, which have evolved significantly since the initial production dates of the training wells. An example is presented in Fig. 5-13. The reservoir in these cases is not intact, and the production pattern for the new well pad drilled in 2022 would be closer to the most recent stages of the other well-pads.

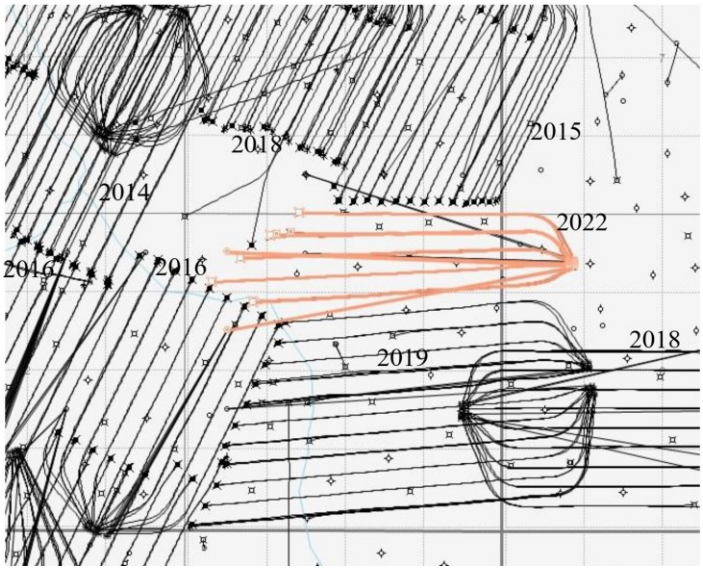

Fig. 5-13. Aan example of drilling a new well-pad nearby other pads that have been already drilled. The reservoir in these cases is not intact, and the production pattern would be closer to the most recent stages of the previous well-pads.

5.5. Results

5.5.1. Clustering

Three distinct values were chosen to establish the minimum similarity threshold (δ) for the clustering algorithm: 0.85, 0.90, and 0.95. The clustering algorithm was then executed on the database using each of these threshold values. Within each resulting cluster, a loop was initiated where one well-pad was designated and set aside, assuming a location for a new well to be drilled. An estimation was performed within this loop to assess the potential contribution of FCDs in enhancing oil production and the cSOR based on Eq. 17 [100].

$$\forall\, NW \in WP_i\,,\ i = 1{:}N \quad \begin{cases} Oil\_Prod_{NW} = \dfrac{\sum_{i=1}^{N-1} Oil\_Prod_{WP_i}}{N-1} \\ cSOR_{NW} = \dfrac{\sum_{i=1}^{N-1} cSOR_{WP_i}}{N-1} \end{cases} \tag{17}$$

where NW is the well-pad in which the new well will be drilled, WP_i is the i^{th} well-pad, N is the number of well-pads in the cluster, Oil_Prod_{NW} is the estimation of FCDs contribution to increase oil production, $Oil\_Prod_{WP_i}$ is the increased oil production by FCDs in the i^{th} well-pad, $cSOR_{NW}$ is the estimation of FCDs contribution to reduce cSOR, and $cSOR_{WP_i}$ is the reduced cSOR by FCDs in the i^{th} well-pad. After performing the estimation process described using Eq. 17 for all well pads within each cluster, the resulting values represent the percentage increase in production or decrease in cSOR. In each cluster, one well-pad is assumed as the well-pad where the new well will be drilled. Then, using the FCD performance for other well-pads in the cluster, the contribution of the FCDs for the assumed new well-pad would be estimated by Eq. 17. Then this estimation is divided by its real value. This process is repeated for all well-pads in all clusters. These values indicate the expected impact of implementing FCDs in each well-pad. By examining Fig. 5-14, one can observe that as the average estimation based on Eq. 17 approaches a value closer to 1 with lower standard deviation, it indicates that more similar well-pads have been assigned to the same cluster. This suggests that clustering has effectively grouped well-pads with comparable characteristics regarding their expected FCDs contribution to production improvement or cSOR reduction.

These statistical measures quantify the central tendency and variability of the estimations within each cluster. Fig. 5-15 illustrates the calculated average estimation values along with their corresponding standard deviations. Based on the analysis and evaluation of the clustering results

using different δ, a threshold value of 0.90 was selected for the clustering process, enabling meaningful comparisons and estimations of the impact of FCDs within each cluster.

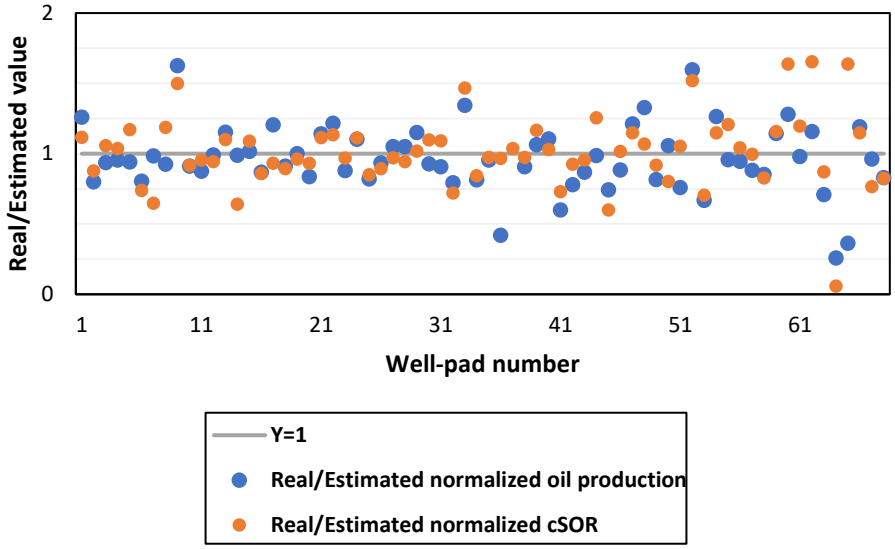

Fig. 5-14. The results of the contribution of FCDs in terms of increasing oil production and reducing the for well-pads in Western Canada.

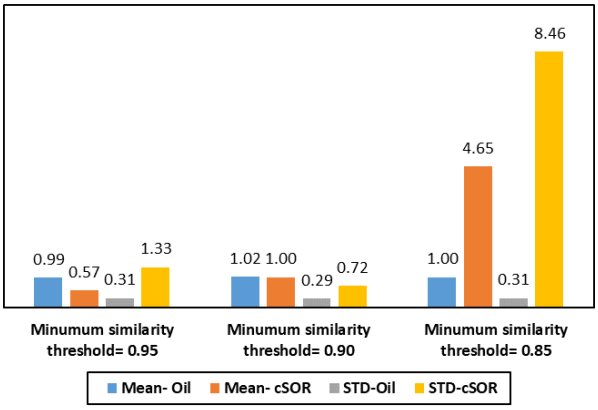

Fig. 5-15. Calculated average estimation values of the estimation of oil production using other wells in the same cluster along with their corresponding standard deviations for different δ.

By examining Fig. 5-16, it can be observed that as the clustering algorithm progresses, clusters with common well-pads are merged. This merging helps to consolidate similar well-pads within the same cluster, further refining the grouping and enhancing the overall clustering results. Number of wells without and with FCDs in each cluster is also shown in Fig. 5-17.

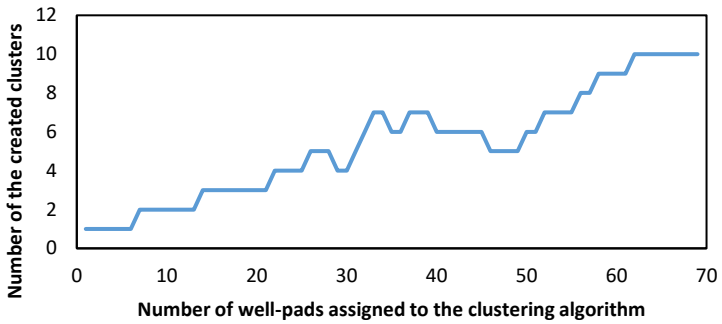

Fig. 5-16. Number of clusters during the clustering process. It shows how the clusters with a common well-pad merged.

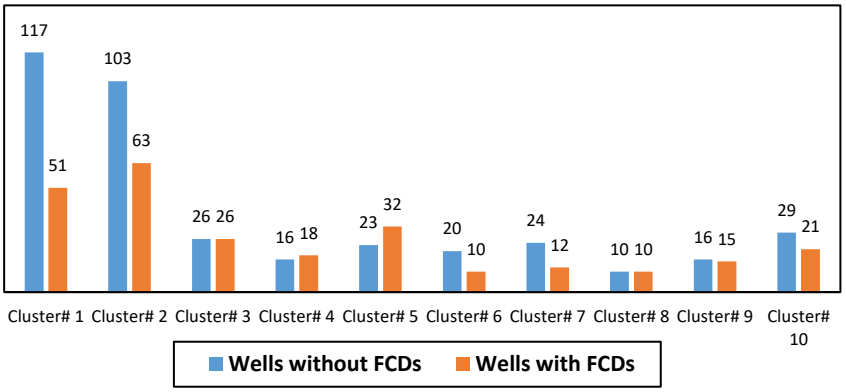

Fig. 5-17. The number of wells without and with FCDs in each cluster.

Fig. 5-18 illustrates the distribution of different parameters after the clustering within each cluster. Analyzing this figure allows for the observation of differences between clusters in terms of these parameters. By examining the parameter distribution within each cluster, one can observe a notable variation in these parameters among different clusters.

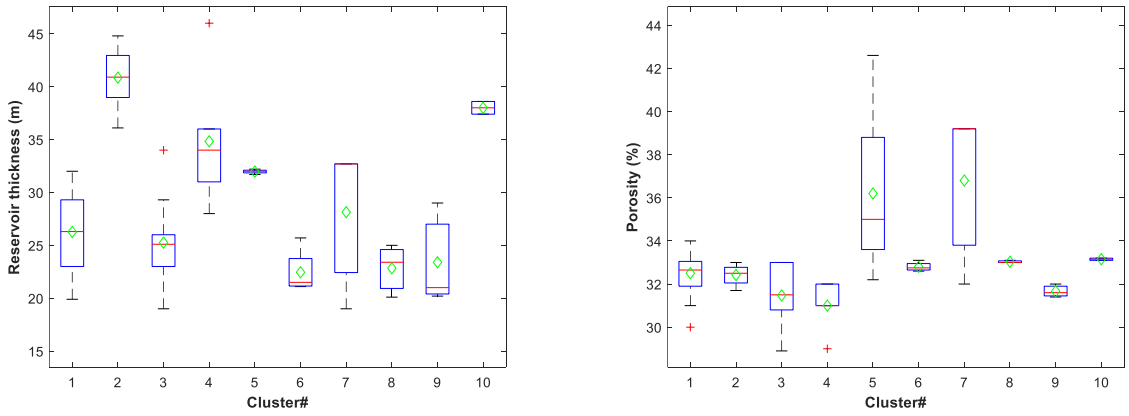

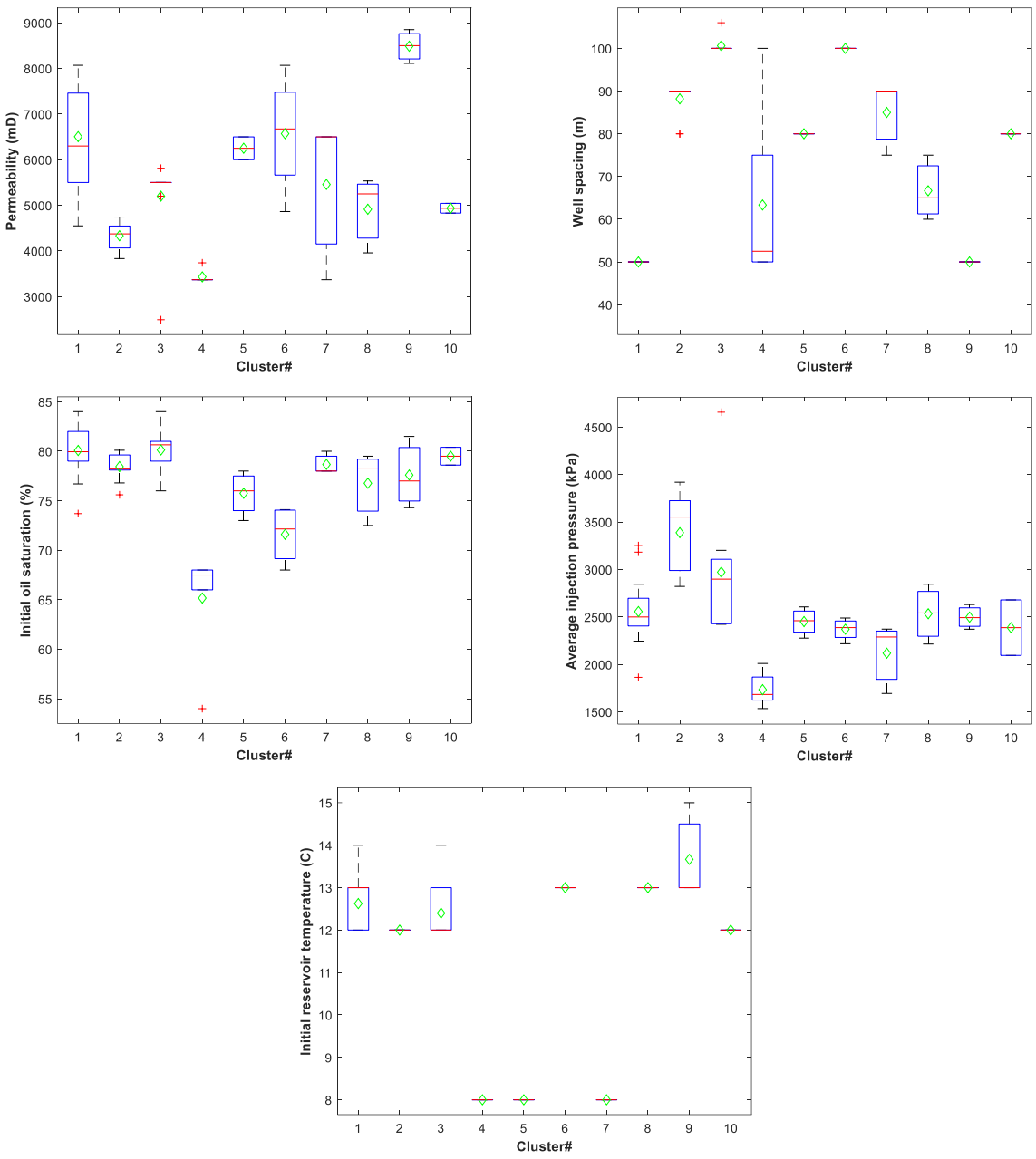

Fig. 5-18. The distribution of different parameters used in the clustering process within each cluster. Green diamond shows the average value while red line indicates the median value of each cluster.

Based on a study conducted by [101], reservoir heterogeneity is a critical parameter that needs to be considered in designing and evaluating FCDs. Fig. 5-19 illustrates the NTG ratio distributions, which is a sign of reservoir heterogeneity, for wells with and without FCDs. Green diamond shows the average value while red line indicates the median value of each cluster. Fig. 5-19 provides insights into the same variation and spread of the NTG ratios within each cluster, allowing for an unbiased comparison of the wells without and with FCDs in term of reservoir quality. In addition,

the NTG ratio in each cluster for wells without and with FCDs are proximately close together, showing a good clustering of the well-pads based on the reservoir quality.

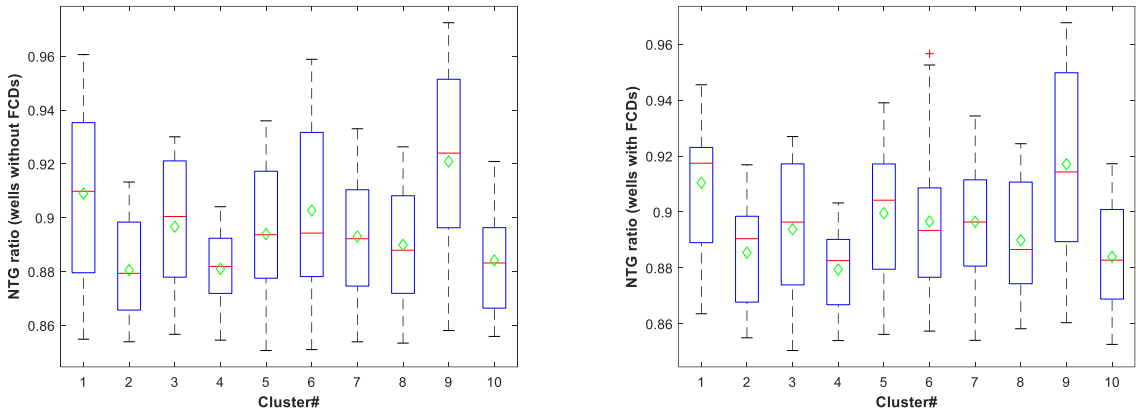

Fig. 5-19. NTG ratio distribution within each cluster for the wells without and with FCDs. Green diamond shows the average value while red line indicates the median value of each cluster.

5.5.2. Training Network

The training took around 10 hours on average with a conventional computer with core i7 9700 CPU and 32 GB RAM. An example of the real normalized oil production data for a test well and the estimated data by a trained LSTM for wells with LDICDs-LDOCDs is shown in Fig. 5-20. In accordance with the information presented in Fig. 5-12, the blue and orange data depicted in Fig. 5-20 corresponds to the ground truth (known, blue bars) and LSTM predictions, respectively, for one of the test wells *#m+1* to *#n*. A relative error for the estimated data shown in Fig. 5-20 is 16%.

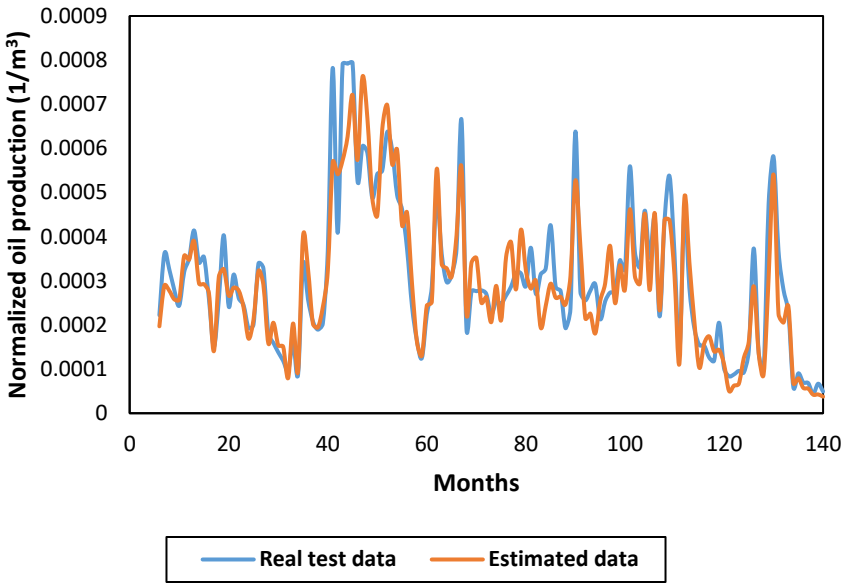

Fig. 5-20. Real test data and estimated data by trained LSTM for a well completed by LDICDs-LDOCDs.

5.5.3 Oil Production and cSOR Prediction

This section presents the anticipated future oil production and cSOR values across different flow control strategies, considering a range of FCD deployments within each cluster. Some clusters consist of a single completion strategy, while others encompass multiple strategies. Note that the curves presented in this Section stand for green parts shown in Fig. 5-12.

The future oil production and cSOR data are displayed through two distinct formats. In the initial format, the objective is to offer an overall perspective on how the production and cSOR trends might evolve over the subsequent 12 months. To achieve this, average forecasted values for all wells, both with and without FCDs, are determined within each cluster. This facilitates a comparison between scenarios involving and excluding FCDs. The second format focuses on providing insights into the potential magnitude of change that FCDs could bring about in oil production and cSOR over the next 12 months. This is achieved by presenting the average contribution of FCDs for each month within each FCD deployment scenario.

By analyzing the parameter distribution for each cluster shown in Fig. 5-19, one can assess the potential impact of deploying different FCDs strategies on altering production and cSOR for the forthcoming 12 months in the context of drilling a new well.

5.5.3.1. LDICDs

Except cluster# 7, in other clusters, LDICDs mostly increased normalized oil production and lowered cSOR compared to wells without FCDs (Fig. 5-21). Regarding cSOR, cluster #7 demonstrates a notably elevated cSOR value for both wells with and without FCDs. As indicated by AER reports from 2022, this well has been temporarily halted due to technical issues [121].

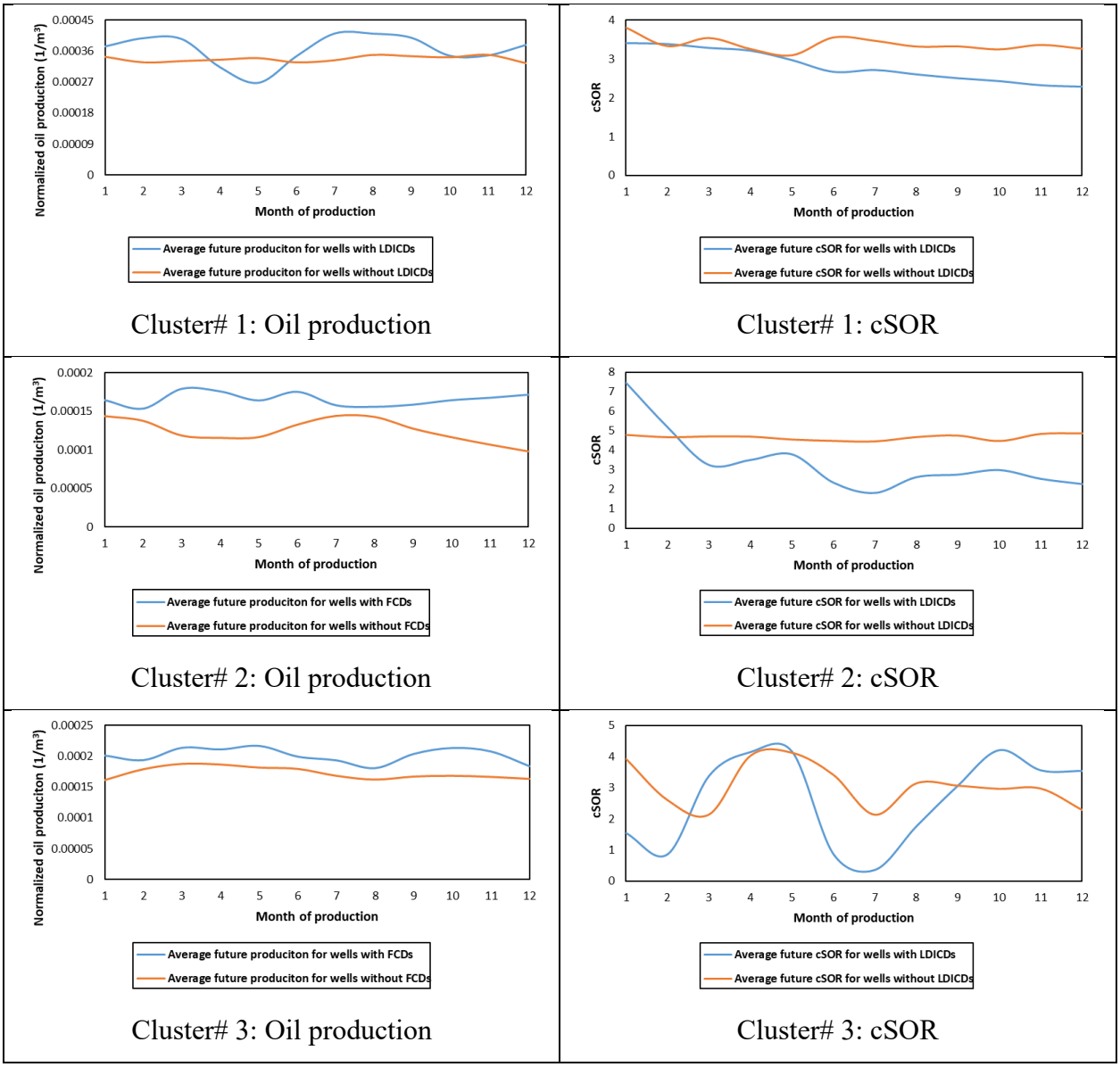

Cluster# 1: Oil production

Cluster# 1: cSOR

Cluster# 2: Oil production

Cluster# 2: cSOR

Cluster# 3: Oil production

Cluster# 3: cSOR

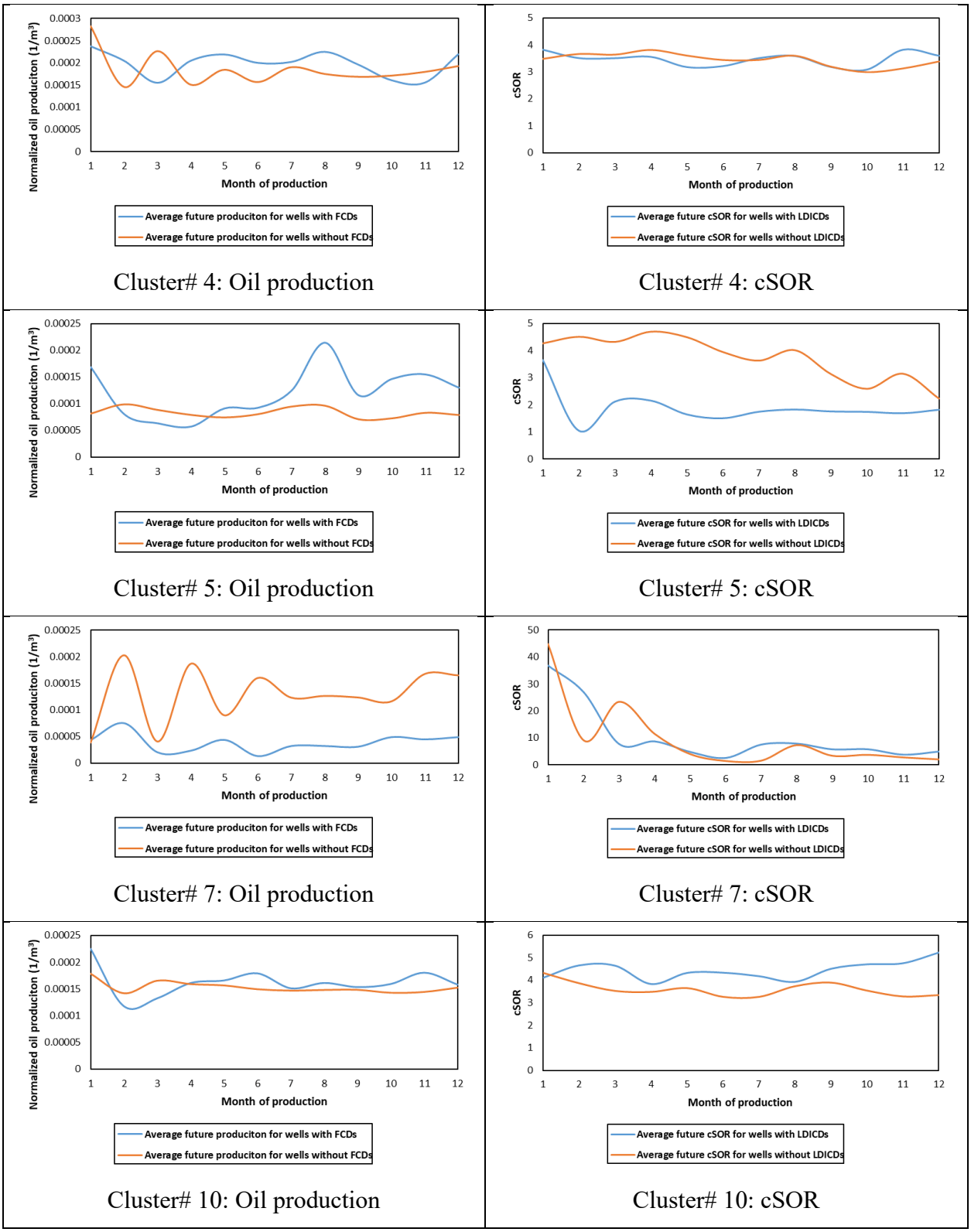

Fig. 5-21. The first presentation format of future oil production and cSOR prediction for a well to be drilled and completed by LDICDs compared to a well without FCDs.

Based on Fig. 5-22, the contribution of LDICDs to increase oil production is higher than decreasing cSOR. This is because LDICDs are primarily employed to mitigate the formation of hot-spot regions with higher inflow rates than other areas. This approach assists in redirecting the steam towards different reservoir sections, thereby raising their temperatures and enhancing the production rate along the entire producer well [101].

As shown in Fig. 5-22, wells completed by LDICDs are anticipated to increase oil production by up to 122%, while on average, it is 20%. In terms of reducing cSOR, it is expected that wells with LDICDs will lead to a decrease in cSOR of up to 77%; on average, it will be 9%. The average relative error of the trained LSTM to predict test date for oil production and cSOR is 24% and 28%, respectively.

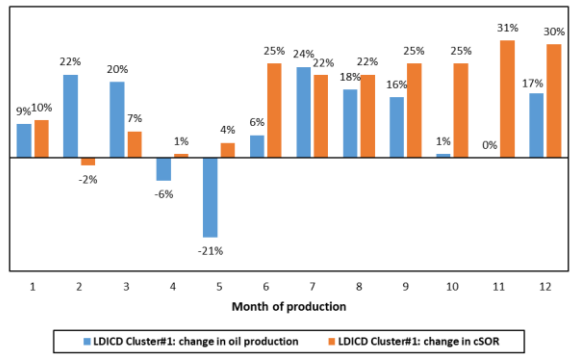

Cluster# 1: Future change in oil production and cSOR

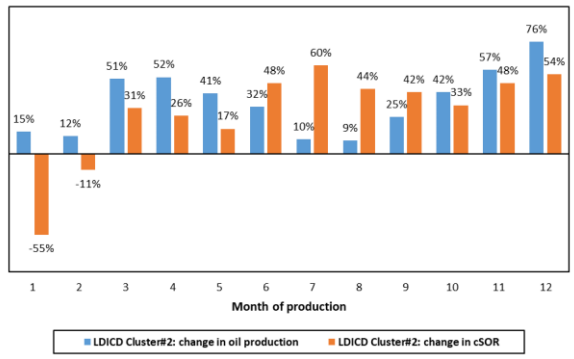

Cluster# 2: Future change in oil production and cSOR

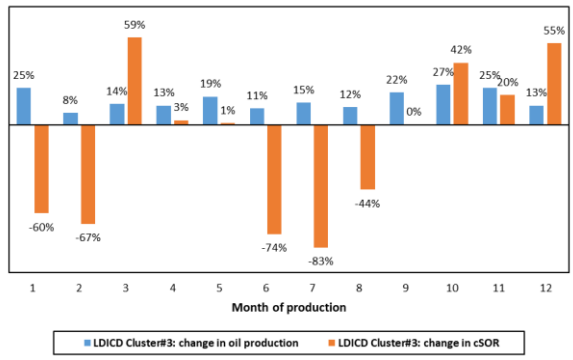

Cluster# 3: Future change in oil production and cSOR

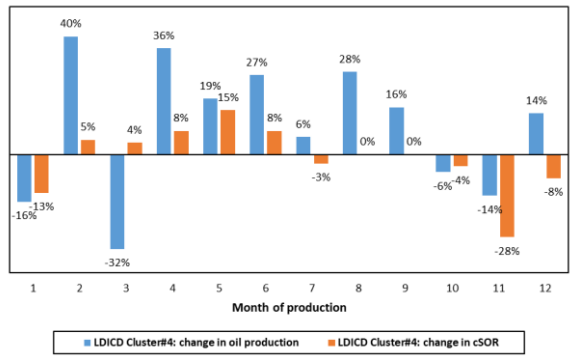

Cluster# 4: Future change in oil production and cSOR

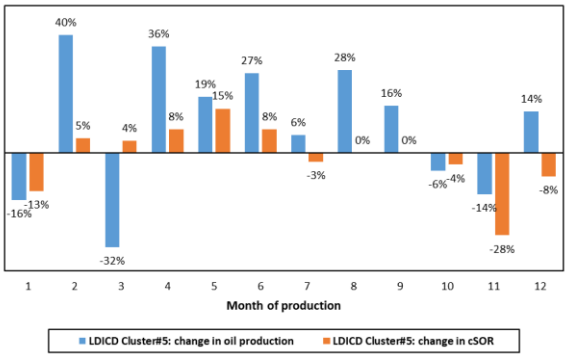

Cluster# 5: Future change in oil production and cSOR

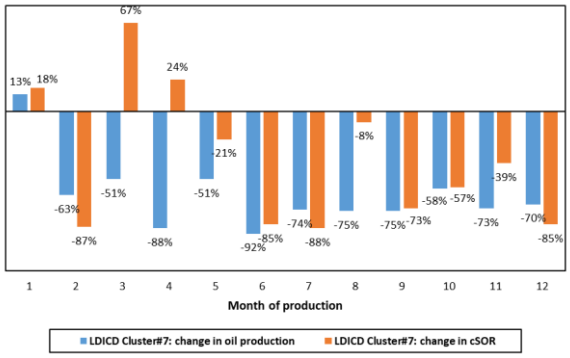

Cluster# 7: Future change in oil production and cSOR

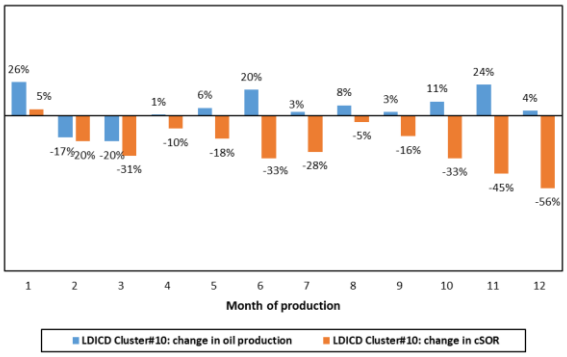

Cluster# 10: Future change in oil production and cSOR

Fig. 5-22. The second presentation format for predicting the impact of LDICDs on altering future oil production and cSOR for each cluster.

5.5.3.2. TDICDs

Based on Fig. 5-23, each cluster demonstrates a rise in oil production stemming from wells that have undergone retrofitting with TDICDs. However, those wells that were retrofitted with TDICDs exhibited greater steam consumption than their non-TDICD counterparts. According to AER reports, wells that retrofitted with TDICD in this paper didn't experience workovers or any problems in their historical records and were initially completed using slotted liners as their primary approach [121].

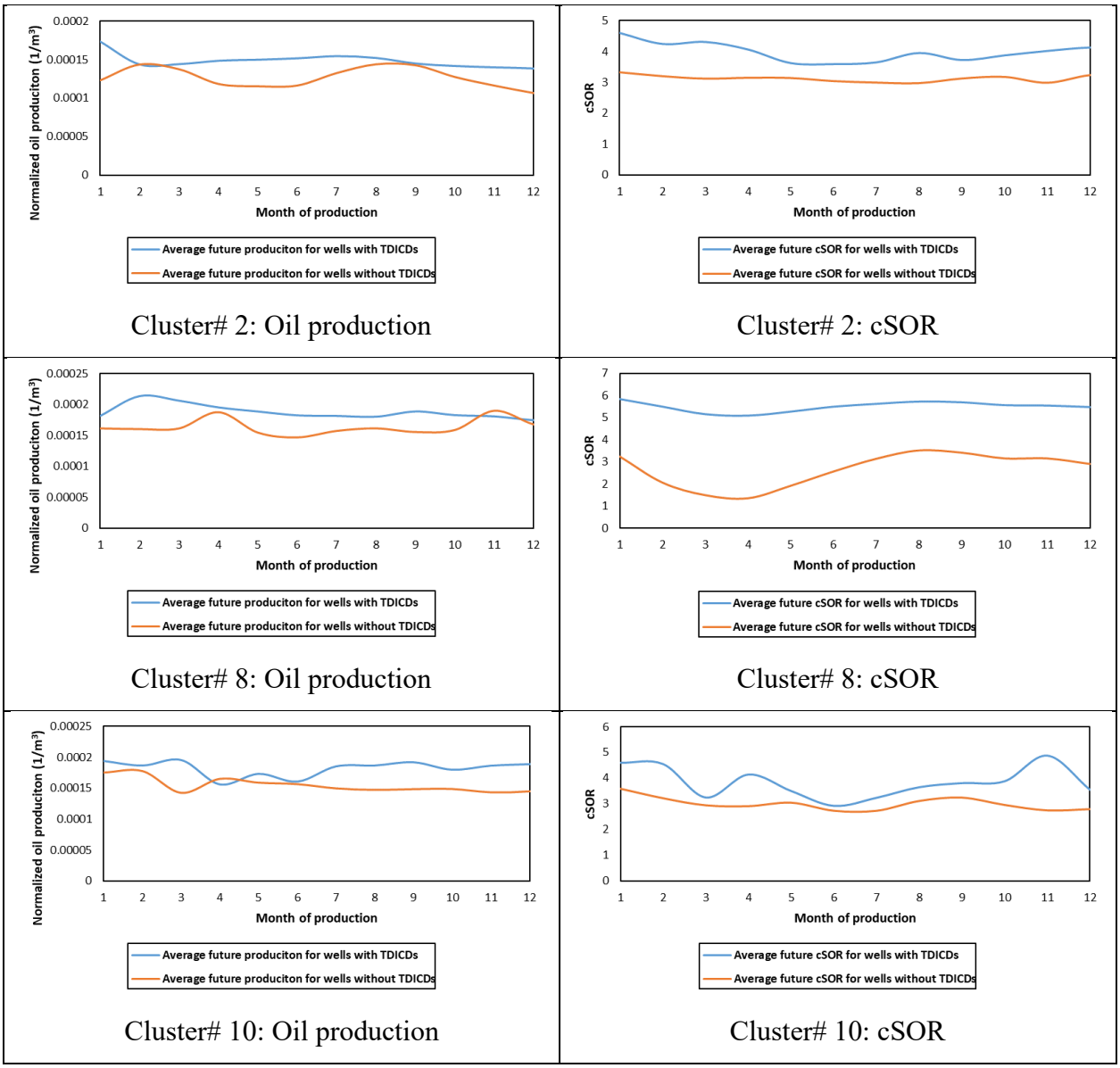

Fig. 5-23. The first presentation format of future oil production and cSOR prediction for a well to be retrofitted by TDICDs.

Based on Fig. 5-24, it is projected that wells which retrofitted using TDICDs will likely experience a maximum oil production enhancement of 38%, with an average increase of 18%. Nevertheless, with regards to reducing cSOR, it is anticipated that wells equipped with TDICDs will consume more steam compared to those without FCDs. Furthermore, the average relative error of the trained LSTM in predicting oil production for test data stands at 25%.

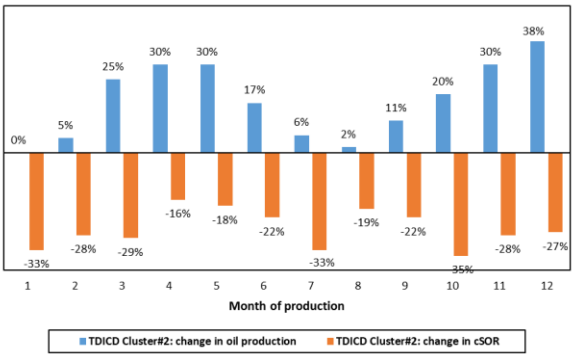

Cluster# 1: Future change in oil production and cSOR

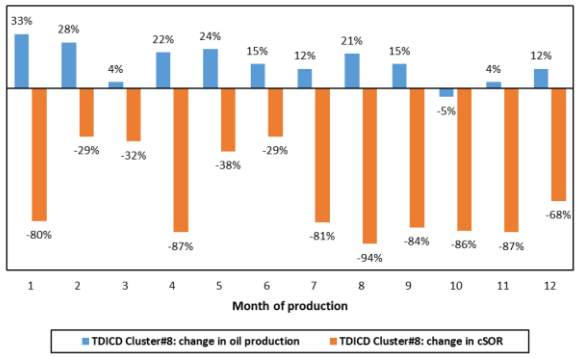

Cluster# 8: Future change in oil production and cSOR

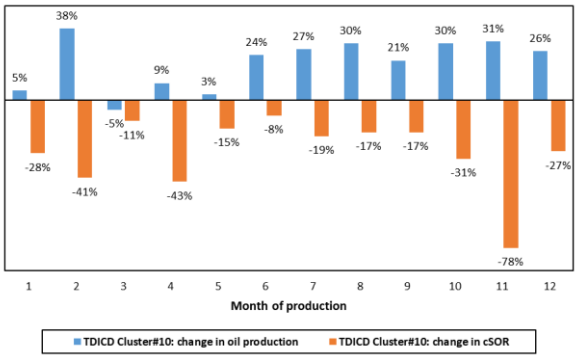

Cluster# 10: Future change in oil production and cSOR

Fig. 5-24. The second presentation format for predicting the impact of TDICDs on altering future oil production and cSOR for each cluster.

5.5.3.3. TDOCDs

Based on Fig. 5-25, cluster #6 exclusively contains a well that was retrofitted using TDOCDs. This particular well showcases an increase in oil production following its retrofitting with TDOCDs. Similarly, this well demonstrated reduced steam consumption compared to other wells in the same cluster without TDOCDs. As per AER reports, the well that underwent TDOCD retrofitting didn't encounter any problems or workovers in its historical records and was initially completed using slotted liners as the primary method [121].

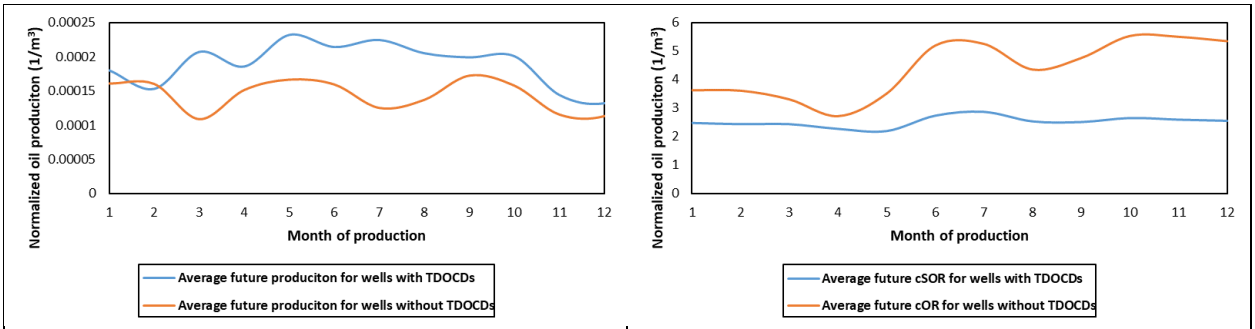

Cluster# 6: Oil production | Cluster# 6: cSOR

Fig. 5-25. The first presentation format of future oil production and cSOR prediction for a well to be retrofitted by TDOCDs.

Based on Fig. 5-26, wells completed by TDOCDs are anticipated to yield an increase in oil production of up to 90%, while on average, it is 34%. In terms of reducing cSOR, it is expected that wells with TDOCDs will lead to a decrease in cSOR of up to 79% and on average it will be 60%. The average relative error of the trained LSTM to predict test date for oil production and cSOR is 20% and 22%, respectively.

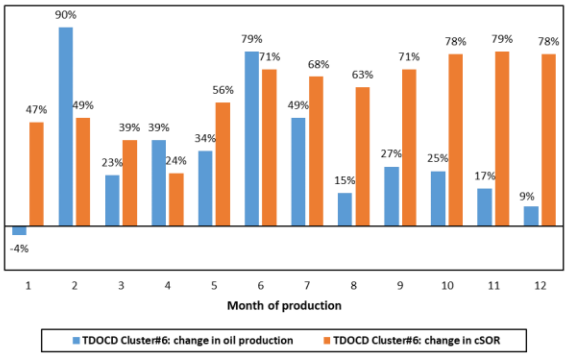

Fig. 5-26. The second presentation format for predicting the impact of TDOCDs on altering future oil production and cSOR for cluster#6.

5.5.3.4. LDICDs-LDOCDs

Every cluster indicates an increase in oil production originating from wells that were completed using LDICDs-LDOCDs (Fig. 5-27). On a general basis, wells in clusters#2 and #10, which were completed using LDICDs-LDOCDs, used less steam compared to wells that didn't utilize LDICDs-LDOCDs. Nonetheless, wells incorporating LDICDs-LDOCDs in cluster #1 showed higher steam consumption when contrasted with other wells in the same cluster that lacked these FCDs components.

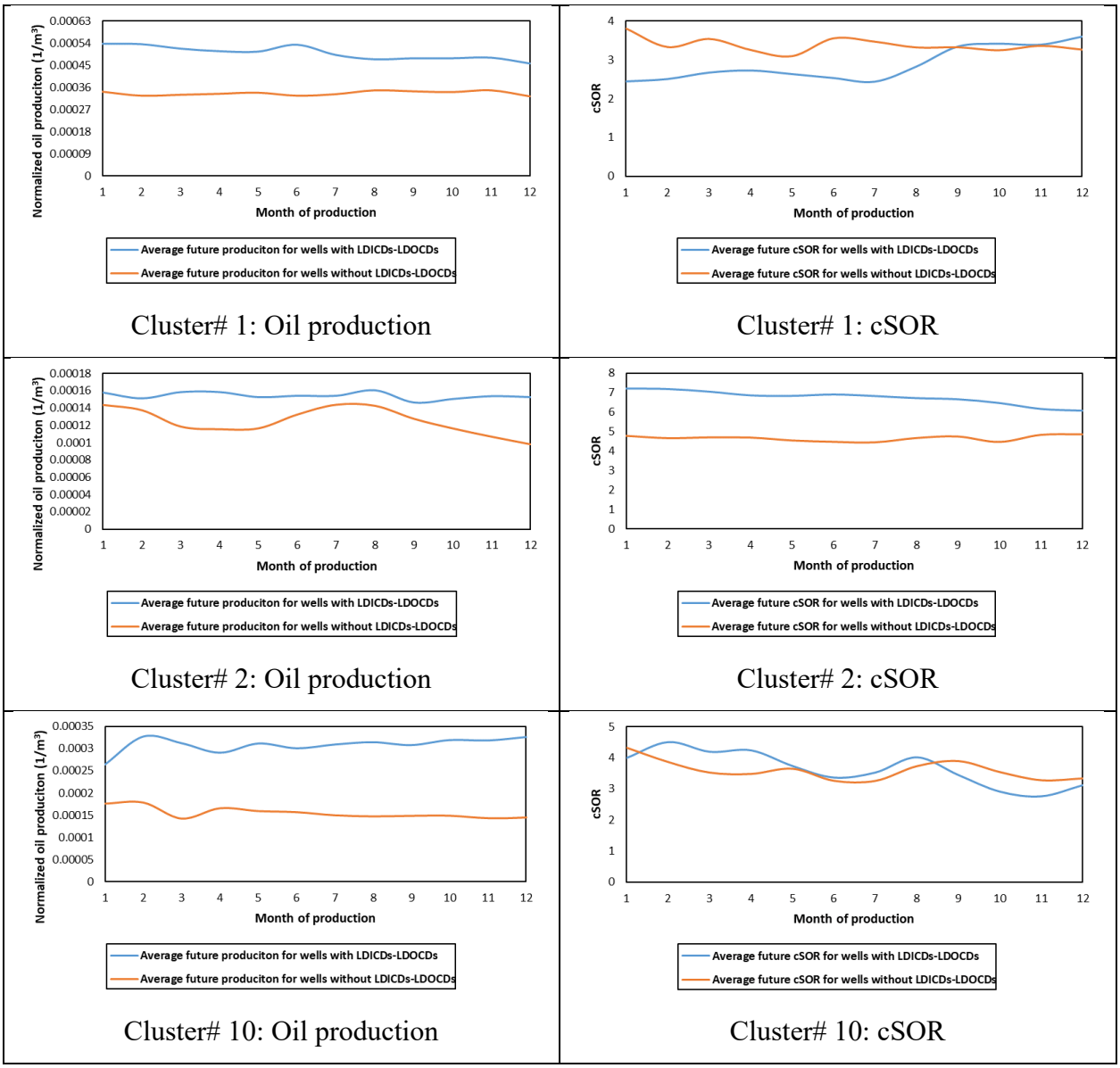

Fig. 5-27. The first presentation format of future oil production and cSOR prediction for a well to be completed by LDICDs-LDOCDs.

Referring to Fig. 5-28, it is anticipated that wells that have been completed with LDICDs-LDOCDs are likely to witness a maximum increase in oil production of 130%, accompanied by an average rise of 59%. In terms of mitigating cSOR, the implementation of LDICDs-LDOCDs in wells is predicted to result in a reduction of cSOR by a maximum of 36%. Nevertheless, when considering the average reduction in cSOR, it is projected that wells that have been completed using LDICDs-LDOCDs will utilize slightly more steam compared to those without FCDs. The average relative error of the trained LSTM in predicting test data for oil production and cSOR stands at 16% and 23%, respectively.

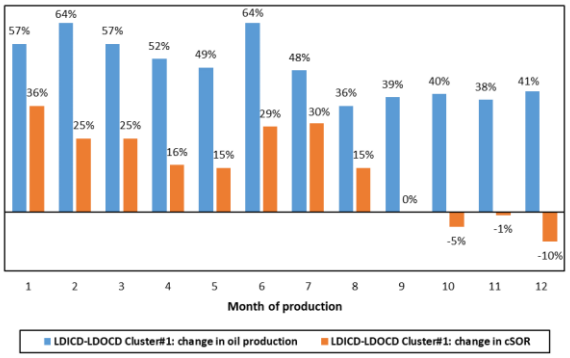

Cluster# 1: Future change in oil production and cSOR

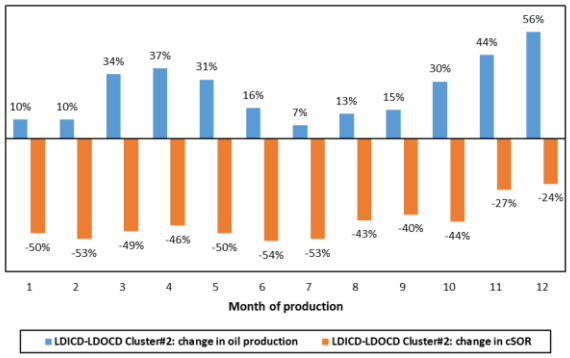

Cluster# 2: Future change in oil production and cSOR

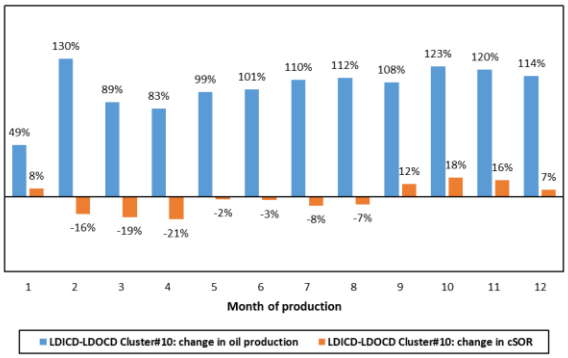

Cluster# 10: Future change in oil production and cSOR

Fig. 5-28. The second presentation format for predicting the impact of LDICDs-LDOCDs on altering future oil production and cSOR for each cluster.

5.5.3.5. TDICDs-TDOCDs

Every cluster illustrates a fluctuation in oil production curve from wells that have undergone retrofitting with TDICDs-TDOCDs and those without these FCDs components (Fig. 5-29). On average, wells that were retrofitted using TDICDs-TDOCDs consumed less steam in contrast to wells lacking these components.

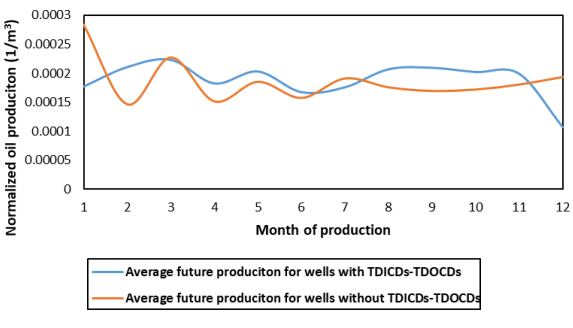

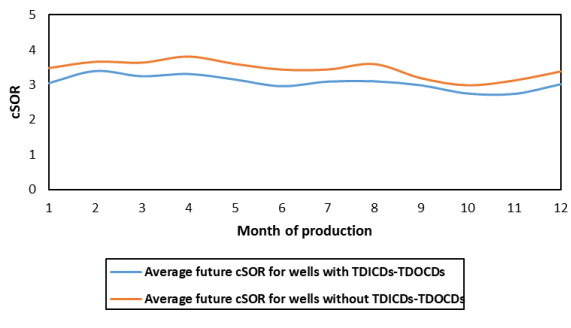

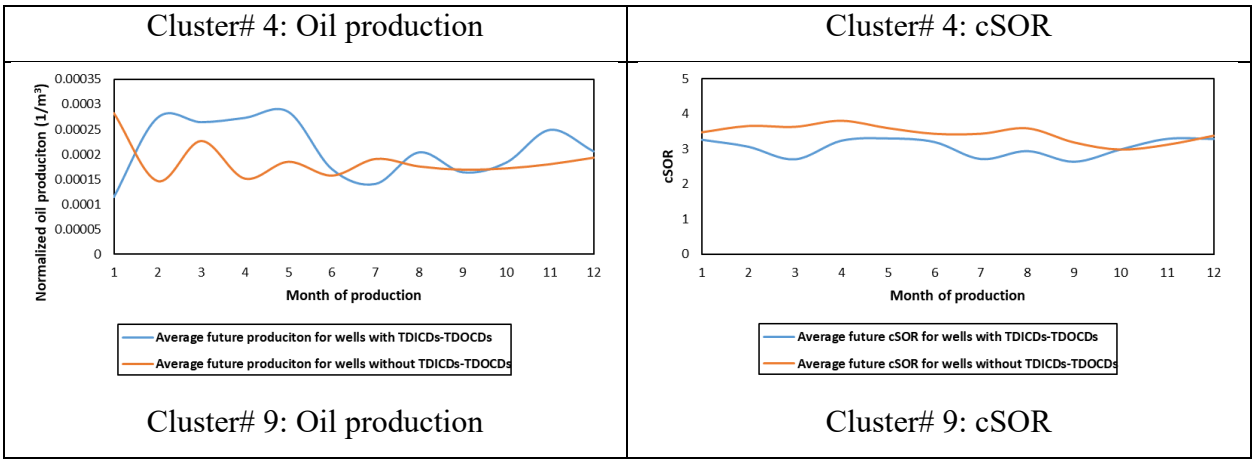

Fig. 5-29. The first presentation format of future oil production and cSOR prediction for a well to be completed by TDICDs-TDOCDs.

Referring to Fig. 5-30, it is anticipated that wells undergoing retrofitting with TDICDs-TDOCDs are likely to observe a maximum improvement in oil production by 87%, along with an average rise of 12%. Concerning the reduction of cSOR, it is anticipated that wells incorporating TDICDs-TDOCDs will result in a decrease of up to 25% in cSOR, with an average decrease of 11%. The trained LSTM's average relative error in predicting test data for oil production and cSOR is measured at 29% and 33%, respectively.

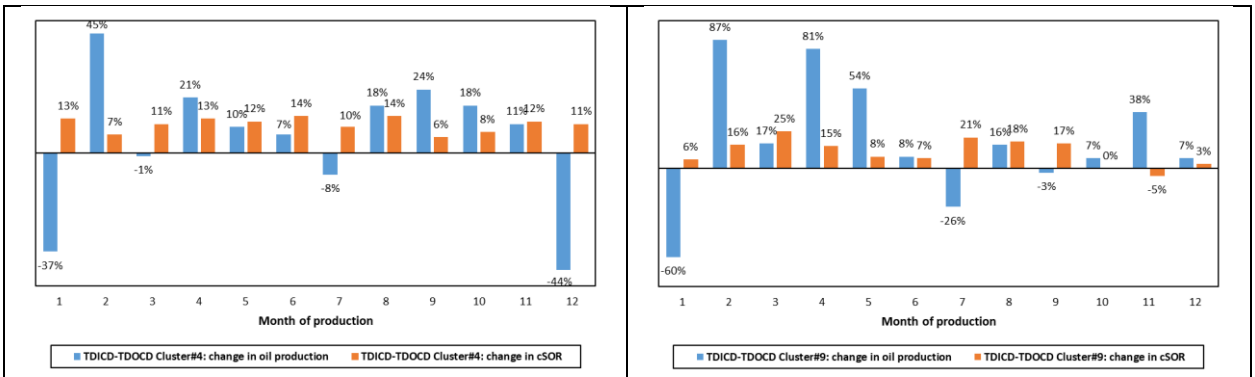

Cluster# 4: Future change in oil production and cSOR

Cluster# 9: Future change in oil production and cSOR

Fig. 5-30. The second presentation format for predicting the impact of TDICDs-TDOCDs on altering future oil production and cSOR for each cluster.

5.6. Discussions, Advantageous, Limitations, and Comparison

Based on the provided predictions for oil production and cSOR over the next 12 months, a general expectation is that wells equipped with FCDs will exhibit higher oil production and reduced steam consumption. In the results section, the oil production rate has been normalized against various

reservoir and well characteristics to facilitate an impartial comparison, to the extent possible. Nonetheless, certain influential factors have not been considered due to insufficient data. Among these factors, the drilling date of the wells holds significant importance. This date is influenced by the technological capabilities of the drilling operators at that time. The utilization of advanced methods and modern technology in well completion strategies is a crucial factor. As depicted in Fig. 5-31, it is evident that wells equipped with FCDs are comparatively more recently drilled than those without FCDs. This suggests that the latest drilling and completion technologies have been employed, excluding FCDs. Conversely, earlier wells were drilled in less challenging sections of the reservoir, while the challenging or depleted areas have been preserved for more recent drilling operations. Unfortunately, this paper does not delve into these two aspects due to the unavailability of information concerning the technology utilized in well completions. Additionally, details regarding the challenging sections of the reservoirs have not been publicly disclosed.

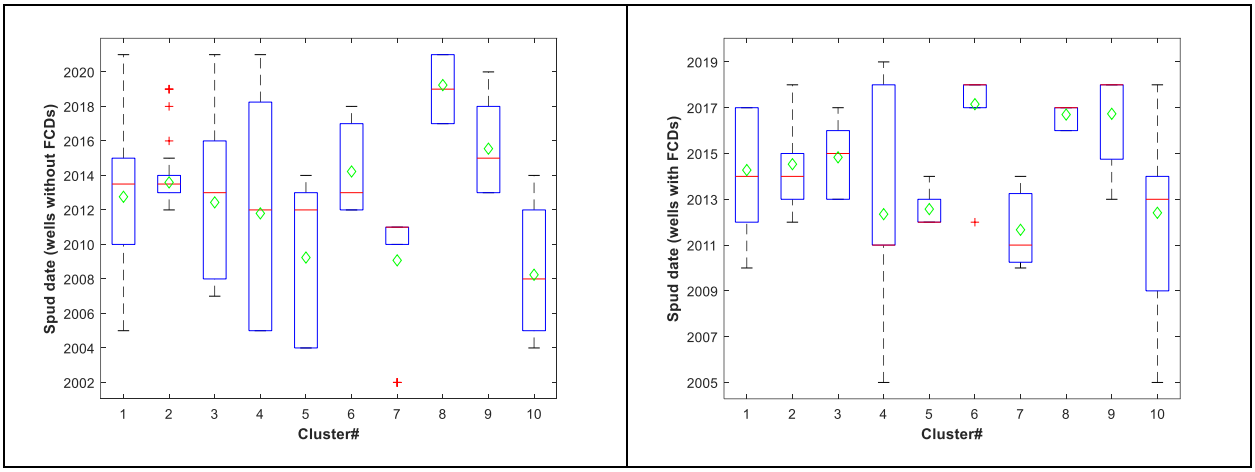

Fig. 5-31. The distribution of spud date of the wells with and without FCDs were used in this study.

A SAGD well can experience temporary shutdowns due to several factors, including maintenance, routine inspections, and safety precautions. These interruptions introduce gaps in the well's production history, leading to breaks in the continuous production rate record. This disruption in data flow can have a direct impact on the accuracy of the trained LSTM model. For example, in the case of wells retrofitted with TDICDs-TDOCDs, there were numerous of these interruptions. Consequently, the relative error in predicting test data increases to 29% for oil production and 33% for cSOR. While it is lower than 25% for other completion strategies. It's worth noting that, as part of the LSTM training process, these production dates were factored in. However, due to the nature of these gaps, they were overlooked, and as a result, zero production values were not incorporated

into the training procedure. This oversight contributes to the model's challenges in accurately predicting outcomes in cases where such interruptions are frequent or significant.

Izadi et al. (2023) conducted a data-driven analysis to elaborate on the contribution of FCDs on oil production and cSOR [99]. In their research, an average measurement was provided to quantify the effectiveness of FCDs in enhancing oil production and reducing cSOR. In their analysis, they did not forecast the monthly contributions of FCDs, nor did they use clustering. Instead, they conducted a comparative analysis of nearby wells to evaluate the impact of FCDs. However, utilizing the same methodology to estimate oil production and cSOR for the test data in our study using average values could yield inaccurate results, as depicted in Fig. 5-32. The inadequacy stems not only from the superior capabilities of LSTM over simple averaging but also from the fact that wells within each cluster might not necessarily be neighboring. Consequently, there exists a significant disparity in operational and reservoir characteristics among different wells, making the averaging approach unsuitable.

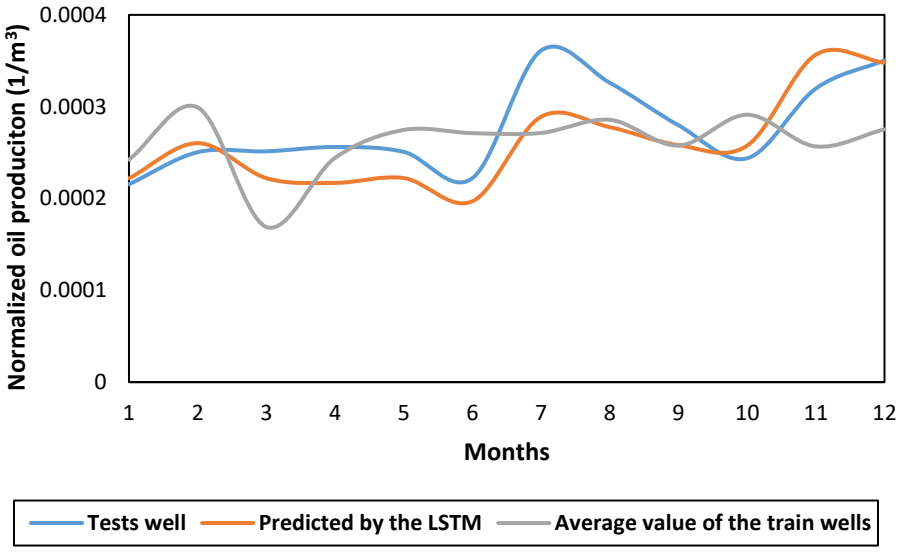

Fig. 5-32. Comparing the estimation made for a 12 month of a test well completed by LDICDs-LDOCDs.

A significant rationale behind integrating time into the LSTM training process is to account for reservoir depletion. As elucidated by [101], the reservoir holds a finite amount of oil, and the implementation of FCDs can amplify the production rate. Consequently, wells equipped with FCDs are poised to yield oil at an accelerated pace compared to those without FCDs. This phenomenon is demonstrated in Fig. 5-33 by [101], where it becomes evident that after

approximately 3200 days, the well lacking FCDs eventually surpasses the oil production of its FCD-equipped counterpart. Omitting the temporal aspect from consideration could lead to erroneous estimations for individual wells.

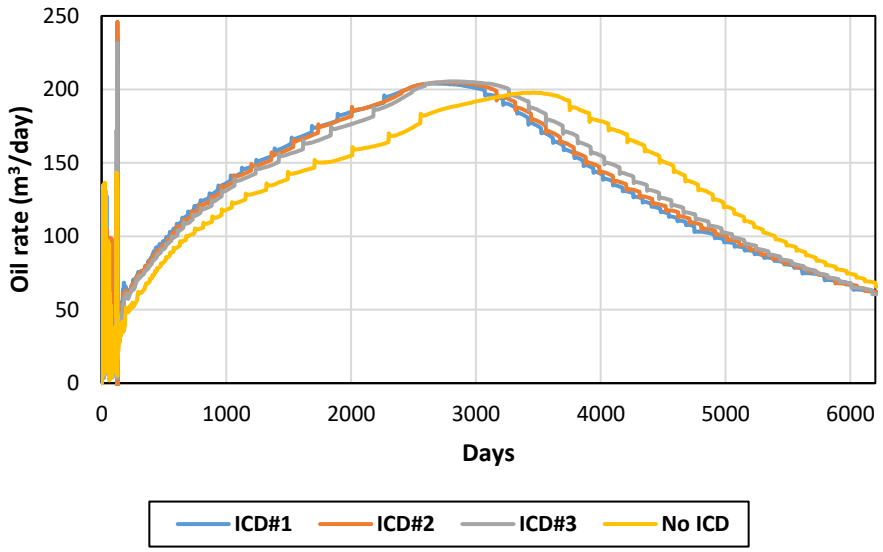

Fig. 5-33. Oil production rate obtained from a numerical simulation for cases with LDICDs and a case without LDICDs [101].

In their study [99], an analysis was conducted on the utilization of FCDs and their impact on increasing normalized oil production and reducing cSOR. They employed a methodology that involved comparing wells located in the same pad. Given the similar operating conditions of wells within a single pad and the assumption of uniform reservoir conditions, no clustering analysis was conducted in their research. Furthermore, their study exclusively compared historical well operations without providing any forecasting. In this section, we compare the outcomes reported by [99] for historical well production with the results presented in this paper for a 12-month forecasting period. The average influence of FCDs on enhancing oil production and lowering cSOR, as reported in both studies, is depicted in Fig. 5-34 and Fig. 5-35, respectively. Overall, the comparison demonstrates that the future forecasting of contribution of FCDs surpasses historical production, a trend that can be justified by referring to Fig. 5-33 and Fig. 5-31. Fig. 5-31 illustrates that the majority of wells equipped with FCDs were drilled after 2012, while Fig. 5-33 indicates that, up to a certain point, approximately more than 8 years into the simulation, oil production for FCD-equipped wells consistently increases over time. This same trend is observed in Fig. 5-34

and Fig. 5-35, suggesting that the forecasting presented in this paper aligns with the physical-based simulations previously published.

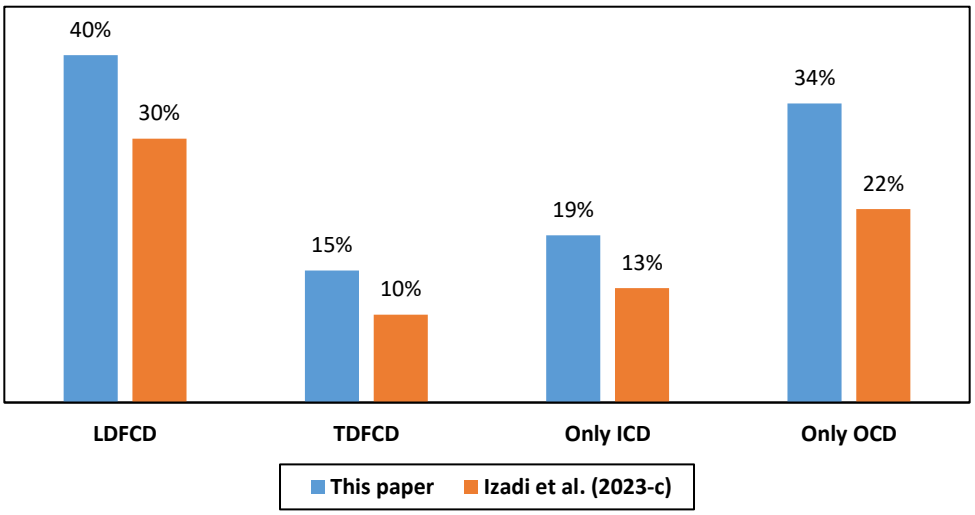

Fig. 5-34. Comparing the contribution of FCDs in increasing oil production for a 12-month forecasting (this chapter) and a historical production [99].

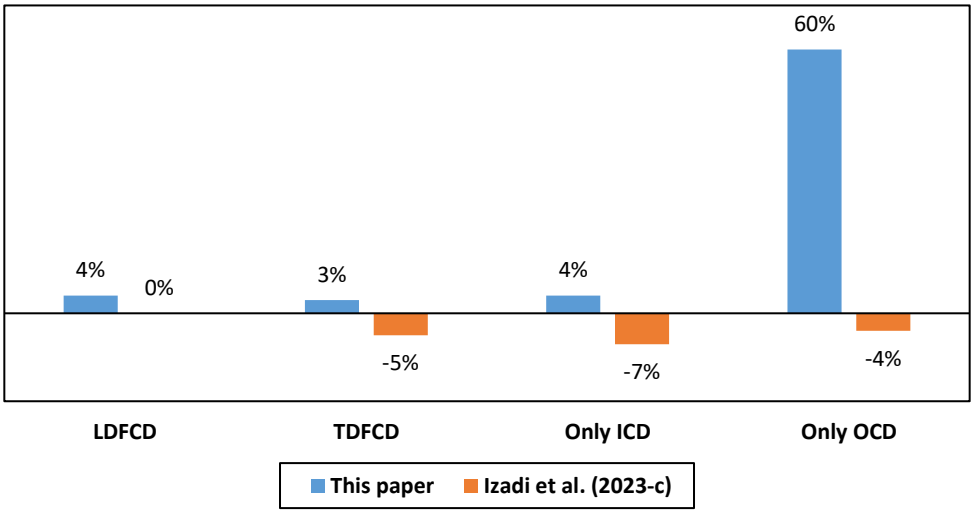

Fig. 5-35. Comparing the contribution of FCDs in decreasing cSOR for a 12-month forecasting (this chapter) and a historical production [99].

5.7. Conclusions

This paper focuses on predicting the impacts of inflow and outflow control strategies using FCDs on Canadian SAGD well performance in terms of oil production and cSOR. A key assumption is that near-term oil production and cSOR forecasts can be made reliably based on recent production data of existing wells. Our approach could be useful for new wells to be drilled in Western Canada.

A comprehensive dataset comprising geological, production, injection, and well data for 70 SAGD well pads has been created. Among these wells, 258 were completed using FCDs, while 384 wells were operated without FCDs. This dataset is then clustered using an incremental-dynamic clustering algorithm, and several LSTM networks have been trained for each FCD strategy within each cluster.

Our analyses supported the conclusion that FCD deployment boosted oil production and lowered cSOR, especially at the beginning of a SAGD operation. Wells completed by LDICDs are anticipated to yield an increase in oil production of up to 122%, while on average, it is 20%. In terms of reducing cSOR, it is expected that wells with LDICDs will lead to a decrease in cSOR of up to 77% and on average it will be 9%. It is projected that wells which retrofitted using TDICDs will likely experience a maximum oil production enhancement of 38%, with an average increase of 18%. Nevertheless, with regards to reducing cSOR, it is anticipated that wells equipped with TDICDs will consume more steam compared to those without FCDs. Wells completed by TDOCDs are anticipated to yield an increase in oil production of up to 90%, while on average, it is 34%. In terms of reducing cSOR, it is expected that wells with TDOCDs will lead to a decrease in cSOR of up to 79% and on average it will be 60%. Wells completed with LDICDs-LDOCDs will likely witness a maximum increase in oil production of 130%, accompanied by an average rise of 59%. In terms of mitigating cSOR, implementing LDICDs-LDOCDs in wells is predicted to reduce cSOR by a maximum of 36%. Nevertheless, when considering the average reduction in cSOR, it is projected that wells completed using LDICDs-LDOCDs will utilize slightly more steam than those without FCDs. It is anticipated that wells undergoing retrofitting with TDICDs-TDOCDs will likely observe a maximum improvement in oil production by 87%, along with an average rise of 12%. Concerning the reduction of cSOR, it is anticipated that wells incorporating TDICDs-TDOCDs will decrease up to 25% in cSOR, with an average decrease of 11%.

The outcomes of this study hold the potential to quantify the impacts of FCDs in well designs. The adoption of more efficient operational setup has a direct ripple effect on aspects like freshwater consumption and GHG emissions, as energy-intensive processes such as fluid injection, production, and treatment are optimized. Consequently, the implications of this research may lead to heightened efficacy in SAGD operations, fostering reduced environmental footprints, cost savings, and heightened oil production rates.

Chapter 6: Conclusions, Discussions, and Suggestions for Future Works

In conclusion, this comprehensive study has provided valuable insights into the optimization of SAGD wells in Western Canada, with a primary focus on inflow and outflow control strategies using FCDs. The findings underscore the critical role of well-designed inflow and outflow control strategies in influencing various factors, such as liquid pool thickness, subcool temperature, reservoir heterogeneity, well operational conditions, and the prevention of steam breakthrough, ultimately increasing oil production and lowering the cSOR and environmental sustainability.

The deployment of FCDs, representing cutting-edge technology, emerged as a pivotal solution to achieve efficient inflow and outflow control. The study showcased the effectiveness of FCDs in enhancing oil production rates while simultaneously addressing environmental concerns by reducing water usage. The evaluation involved simulations in different reservoir heterogeneity and subcooling scenarios, highlighting the versatility of FCD strategies.

To compare production rates of wells with varying technologies, it is essential to ensure an unbiased comparison. In this thesis, efforts were made to standardize oil production rates for wells with and without FCDs against reservoir and operational parameters, including steam injection rate, reservoir quality, well length, reservoir thickness, and well spacing. It was demonstrated that this normalization method is dependable for such comparisons. It's important to emphasize that the drilling dates of wells play a crucial role. This includes older wells completed using outdated technologies, as well as newer wells completed with more advanced technologies. Over time, the industry gained additional insights, leading to the completion of new wells with enhanced knowledge. In this thesis, our aim was to compare wells drilled within similar time frames. On the other side of the spectrum, newer wells will be drilled in more challenging parts of the reservoirs, as well as in the depleted reservoirs (brown fields). This needs to be considered as well when it comes to a comparison.

The study also delved into the impact of FCDs on long wells compared to short wells, emphasizing the competitive advantages of longer wells with FCDs in terms of reduced CapEx and increased oil production. It was noteworthy that despite the bias towards longer wells with FCDs, these wells outperformed conventional ones on a per-meter basis, emphasizing the overall efficiency gains with FCDs.

The thesis demonstrated that PSDs, as a readily available and easily collected database, could serve as a valuable tool in designing ICDs. According to the findings in this thesis, PSDs exhibit a

correlation with permeability, a crucial factor in ICD design. We aimed to assess the sensitivity of the entire range of D values in PSDs analysis concerning permeability. Additionally, we conducted a comprehensive literature review to establish fundamental correlations between PSDs and permeability data for SAGD reservoirs, both with and without porosity considerations. Following the identification of this research gap, we designed an intelligent algorithm to optimize the coefficients of the base correlation based on our database. We showed that a well-designed ICD has the potential to enhance oil production, reduce cSOR, and improve conformance. Additionally, it allows operators to delay steam breakthrough, thereby extending the well's lifespan, increasing oil production, and minimizing environmental footprint.

We thoroughly examined the influence of varying subcool temperature scenarios on the operation of SAGD wells, assessing their impact on production and injection rates. Managing the inflow and outflow rates under challenging and conservative subcool temperatures was investigated as a strategy for enhanced reservoir management, aiming to optimize oil production and reduce cSOR. The key technological insight derived from this thesis for Canadian SAGD operations involves adjusting the thickness of the liquid pool and implementing different subcool temperatures, achieved by introducing a designed additional pressure drop in the producer wells.

The analysis in this thesis revealed that a combination of different FCD types, such as LDICDs and LDOCDs, proved to be the best practice in homogenous reservoirs, leading to a substantial improvement in average oil production and a reduction in cSOR. Furthermore, in challenging scenarios with shale barriers and heterogeneous reservoirs, joint implementation of LDICDs and LDOCDs demonstrated significant enhancements in oil production and reductions in cSOR. Wells equipped with FCDs have the potential to yield a more substantial liquid pool. This allows operators to operate the well at a lower subcooling temperature, facilitating higher oil production rates without encountering steam breakthrough.

Various types of historical data have been gathered and put them together to be used as a comparison tool in Canadian SAGD operations. The historical data on normalized oil production and cSOR gathered in this thesis could provide the trend of the impact of inflow and outflow rates control for future decision-making and guide strategies in well-pad development in Canadian SAGD projects, and the exact values are limited to our database. The monthly improvement forecasts presented in this thesis have the potential to quantify the effects of flow rates control by

FCDs in well designs. The results support the prevailing industry practice of incorporating FCDs into new well designs and pad developments. The adoption of more efficient operational setups and FCDs design, as an assistive technology among others, has a direct impact on factors such as freshwater consumption and GHG emissions, optimizing energy-intensive processes like fluid injection, production, and treatment. This aligns with climate change objectives for achieving Net-Zero Emission by 2050. As a result, the implications of this research may enhance the efficiency of SAGD operations, leading to reduced environmental impact, cost savings, and increased oil production rates.

Suggestions for Future Works:

1. Incorporate Additional Reservoir Parameters: Expand the assessment by including more reservoir parameters such as porosity, seismic monitoring, and temperature data to provide a more comprehensive understanding of steam chamber growth and its impact on well performance.
2. Enhance Database Generalizability: Increase the number of wells with FCDs in the database to enhance generalizability and consider incorporating diverse reservoir conditions to ensure a more representative dataset.
3. Long-Term Performance Monitoring: Implement a long-term monitoring plan to track the performance of wells with FCDs over an extended period, providing insights into their sustainability and longevity.
4. Environmental Impact Assessment: Conduct a comprehensive environmental impact assessment to quantify the overall reduction in greenhouse gas emissions and freshwater consumption resulting from optimized SAGD operations with FCDs.
5. Collaborative Industry Research: Foster collaboration with industry partners to validate findings and ensure real-world applicability, facilitating the adoption of optimized well designs across the SAGD industry.
6. Studying the impact of tilted wellbores (not horizontals) on FCDs performance would be another interesting topic for future works.
7. Developing a dimensionless variable instead of normalized oil (Eq. 14) and comparing the results.

By addressing these aspects in future research endeavors, the industry can further refine operational strategies, reduce environmental footprints, and achieve more sustainable and efficient SAGD operations.

Nomenclature

a	Coefficient of the permeability correlation
A_1	Inlet area at a cross-section of the flow
A_2	Outlet area at a cross-section of the flow
ART	Adaptive resonant theory
b	Coefficient of the permeability correlation
B	Formation volume factor
BHP	Bottom-hole pressure
c	Coefficient of the permeability correlation
C_d	Discharge coefficient
C_v	Flow coefficient
CERI	Canadian Energy Research Institute
CFD	Computational fluid dynamic
CHOPS	Cold heavy oil production with sand
cSOR	Cumulative steam oil ratio
CSS	Cyclic steam stimulation
CWE	Cold water equivalent
D	Diameter of the pipe
d	Coefficient of the permeability correlation
D_{40}	40% of the cumulative retained PSD curve
D_{90}	90% of the cumulative retained PSD curve
D_{95}	95% of the cumulative retained PSD curve
D_n	n % cumulative passing PSD curve
e	Coefficient of the permeability correlation
ERD	Extended reach drilling
ESPs	Electric Submersible Pumps
F	Friction factor
f	Coefficient of the permeability correlation
$F(\phi)$	Porosity function
FCD	Flow control device
G	Acceleration of gravity
g	Coefficient of the permeability correlation
GA	Genetic algorithm
GBPSO	Genetic-binary particle swarm optimization
GHG	Greenhouse gas
h_i	Enthalpy of phase i
H_s	Enthalpy of steam
H_w	enthalpy of boiler feed water
i	Number of particle size distribution curves
j	Number of created clusters
k	Permeability
k_{th}	Thermal conductivity tensor
L	Length of the pipe
LD	Liner-deployed
LDFCD	Liner-deployed flow control device
LDICD	Liner-deployed inflow control device
LHV	Lower heating value of natural gas
$\dot{m}$	Mass flow rate
M_r	Volumetric heat capacity of the reservoir's rocks
MAE	Mean absolute error
MOP	Maximum operation pressure
MSE	Mean square error
n	Number of mesh sizes
OCD	Outflow control device
PSD	Particle size distribution
PSO	Particle swarm optimization
Q	Energy input per unit volume
q	Heat transfer flux
Q_s	Steam quality
R	Solution-gas ratio
SAGD	Steam-assisted gravity drainage
SBT	Steam breakthrough
So	Sorting coefficient
T	Temperature
TD	Tubing deployed
TDFCD	Tubing deployed flow control device
TVD	Tru vertical depth
u	Specific internal energy
U	Phase velocity
Uc	Uniformity coefficient
v	Fluid velocity
x_i	i^th particle size distribution curve
x_{jc}	Center of the jth cluster
Z	Elevation above the datum location
δ	Minimum similarity threshold
μ	Viscosity
ρ	Fluid density

ICD	Inflow control device
ICDs	Inflow control devices
IPR	Inflow Performance Relationship
iSOR	Instantaneous steam oil ratio
ϕ	Porosity
$\nabla\Phi$	Potential gradient includes pressure and gravity
η_b	Steam boiler efficiency
ΔP	Pressure drop

References

[1] Irani, M. and Cokar, M., 2016. Discussion on the effects of temperature on thermal properties in the steam-assisted-gravity-drainage (SAGD) process. Part 1: thermal conductivity. SPE Journal, 21(02), pp.334-352.

[2] Kumar, A. and Hassanzadeh, H., 2021. Impact of shale barriers on performance of SAGD and ES-SAGD—A review. Fuel, 289, p.119850.

[3] Irani, M., 2019. On Subcool Control in SAGD Producers—Part II: Localized-Hot-Spots Effects and Optimization of Flow-Control Devices. SPE Journal, 24(04), pp.1613-1629.

[4] Irani, M. and Ghannadi, S., 2020. Modeling the conformance improvement using flow control devices in infill wells adjacent to SAGD well pairs: No flashing. SPE Journal, 25(02), pp.800-819.

[5] Ahmed Elfeel, M., Goh, G. and Biniwale, S., 2021, March. Advanced Completion Optimization ACO: A Comprehensive Workflow for Flow Control Devices. In International Petroleum Technology Conference. OnePetro.

[6] Zhang, Y., Li, P., Sun, X., Chen, H. and Liu, Y., 2021. Steam conformance investigation of flow control devices deployed in SAGD injection and production horizontal wells. Journal of Petroleum Science and Engineering, 205, p.108907.

[7] Al-Bahlani, A.M. and Babadagli, T., 2009. SAGD laboratory experimental and numerical simulation studies: A review of current status and future issues. Journal of Petroleum Science and Engineering, 68(3-4), pp.135-150.

[8] Irani, M. and Ghannadi, S., 2013. Understanding the heat-transfer mechanism in the steam-assisted gravity-drainage (SAGD) process and comparing the conduction and convection flux in bitumen reservoirs. SPE Journal, 18(01), pp.134-145.

[9] Giacchetta, G., Leporini, M. and Marchetti, B., 2015. Economic and environmental analysis of a Steam Assisted Gravity Drainage (SAGD) facility for oil recovery from Canadian oil sands. Applied Energy, 142, pp.1-9.

[10] Butler, R.M., 1994. Steam-assisted gravity drainage: concept, development, performance and future. Journal of Canadian Petroleum Technology, 33(02), pp.44-50.

[11] Lazzaroni, E.F., Elsholkami, M., Arbiv, I., Martelli, E., Elkamel, A. and Fowler, M., 2016. Energy infrastructure modeling for the oil sands industry: Current situation. Applied energy, 181, pp.435-445.

[12] Baldwin, C., 2018. Fiber optic sensors in the oil and gas industry: current and future applications. In Opto-mechanical fiber optic sensors (pp. 211-236). Butterworth-Heinemann.

[13] Irani, M., Ghannadi, S., Nick Daprocida, N.D., Lacoste-Bouchet, P. and DiStefano, V., 2022, March. On Numerical Modelling of the Hydraulic-Fractured Closed Loop Systems: Single Producer. In SPE Canadian Energy Technology Conference (p. D021S018R001). SPE.

[14] Irani, M., 2018. On subcool control in steam-assisted-gravity-drainage producers—part I: Stability envelopes. SPE Journal, 23(03), pp.841-867.

[15] Yuan, J.Y. and Nugent, D., 2013. Subcool, fluid productivity, and liquid level above a SAGD producer. Journal of Canadian Petroleum Technology, 52(05), pp.360-367.

[16] Al-Khelaiwi, F.T., Birchenko, V.M., Konopczynski, M.R. and Davies, D.R., 2010. Advanced wells: a comprehensive approach to the selection between passive and active inflow-control completions. SPE Production & Operations, 25(03), pp.305-326.

[17] Baker, R.O., Fong, C., Li, T., Bowes, C. and Toews, M., 2008, October. Practical considerations of reservoir heterogeneities on SAGD projects. In International Thermal Operations and Heavy Oil Symposium. OnePetro.

[18] Nasr, T.N., Law, D.H.S., Golbeck, H. and Korpany, G., 2000. Counter-current aspect of the SAGD process. Journal of Canadian Petroleum Technology, 39(01).

[19] Yang, G. and Butler, R.M., 1992. Effects of reservoir heterogeneities on heavy oil recovery by steam-assisted gravity drainage. Journal of Canadian Petroleum Technology, 31(08).

[20] Llaguno, P.E., Moreno, F., Garcia, R., Mendez, Z. and Escobar, E., 2002, June. A reservoir screening methodology for SAGD applications. In PETSOC Canadian International Petroleum Conference (pp. PETSOC-2002). PETSOC.

[21] Edmunds, N. and Chhina, H., 2001. Economic optimum operating pressure for SAGD projects in Alberta. Journal of Canadian Petroleum Technology, 40(12).

[22] Tabatabaei, M. and Ghalambor, A., 2011. A new method to predict performance of horizontal and multilateral wells. SPE Production & operations, 26(01), pp.75-87.

[23] Wang, M. and Leung, J.Y., 2015. Numerical investigation of fluid-loss mechanisms during hydraulic fracturing flow-back operations in tight reservoirs. Journal of Petroleum Science and Engineering, 133, pp.85-102.

[24] Kenji, F., Zhu, D. and Hill, A.D., 2005. A Comprehensive Skin-Factor Model of Horizontal-well Completion performance. SPE production and facilities.

[25] Tam, E.S., Modien, R.M. and Best, D.A., 1988. The effect of production well open interval on steamflood performance. Journal of Canadian Petroleum Technology, 27(03).

[26] Ipek, G., Frauenfeld, T. and Yuan, J.Y., 2008, June. Numerical study of shale issues in SAGD. In PETSOC Canadian International Petroleum Conference (pp. PETSOC-2008). PETSOC.

[27] Le Ravalec, M., Morlot, C., Marmier, R. and Foulon, D., 2009. Impact des hétérogénéités sur la production d'huiles lourdes mobiles par SAGD. Oil Gas Sci. Technol, 64, pp.469-476.

[28] Pooladi-Darvish, M. and Mattar, L., 2002. SAGD operations in the presence of overlying gas cap and water layer-effect of shale layers. Journal of Canadian Petroleum Technology, 41(06).

[29] Bois, A.P. and Mainguy, M., 2011, December. Importance of thermal consolidation of shale during SAGD process. In SPE Heavy Oil Conference and Exhibition. OnePetro.

[30] Gates, I.D., Adams, J. and Larter, S., 2008. The impact of oil viscosity heterogeneity on the production characteristics of tar sand and heavy oil reservoirs. Part II: Intelligent, geotailored recovery processes in compositionally graded reservoirs. Journal of Canadian Petroleum Technology, 47(09).

[31] Larter, S., Adams, J., Gates, I.D., Bennett, B. and Huang, H., 2008. The origin, prediction and impact of oil viscosity heterogeneity on the production characteristics of tar sand and heavy oil reservoirs. Journal of Canadian Petroleum Technology, 47(01).

[32] Nimana, B., Canter, C. and Kumar, A., 2015. Energy consumption and greenhouse gas emissions in the recovery and extraction of crude bitumen from Canada's oil sands. Applied energy, 143, pp.189-199.

[33] Li, L., Ma, Y., Mahmoudi, M., Fattahpour, V. and Lange, C.F., 2018, March. Steps Toward Designing the Optimum Outflow Control Device for SAGD using Computational Fluid Dynamics Simulation. In SPE Canada Heavy Oil Technical Conference. OnePetro.

[34] Yusuf, Y., Roostaei, M., Soroush, M., Rosi, G., Berner, K., Tegegne, N., Mohammadtabar, F., Izadi, H., Zhu, D., Mahmoudi, M. and Fattahpour, V., 2021, January. Single and Multi-Phase Flow Loop Testing for Characterization and Optimization of Flow Control Devices Used in SAGD: The Effect of Viscosity and Gas-to-Liquid Ratio on Tool Performance. In SPE Thermal Integrity and Design Symposium. OnePetro.

[35] Gohari, K., Becerra Moreno, O., Romanova, U., O'Hagan, D., Mende Anjaneyalu, A. and Gaviria, F., 2019, September. Technical Review of Tubing-deployed Flow Control Devices at MacKay River. In SPE Annual Technical Conference and Exhibition. OnePetro.

[36] Gohari, K. and Becerra, O., 2019. Understanding Tubing-deployed Flow Control Devices in SAGD. The Journal of the Canadian Heavy Oil Association, (July 2019), pp.22-25.

[37] De Paulo Ferreira, L., Surmas, R., Tonietto, S.N., da Silva, M.A.P. and Peçanha, R.P., 2020. Modeling reactive flow on carbonates with realistic porosity and permeability fields. Advances in Water Resources, 139, p.103564.

[38] Rao, P. and Schaefer, L., 2020. Permeability Estimation on Tomographic Images using Curved Boundary Schemes in the Lattice Boltzmann Method. Advances in Water Resources, p.103685.

[39] Esmaeilpour, M., Ghanbarian, B., Liang, F. and Liu, H.H., 2021. Scale-dependent permeability and formation factor in porous media: Applications of percolation theory. Fuel, 301, p.121090.

[40] Ghanbarian, B., Esmaeilpour, M., Ziff, R.M. and Sahimi, M., 2021. Effect of Pore-Scale Heterogeneity on Scale-Dependent Permeability: Pore-Network Simulation and Finite-Size Scaling Analysis. Water Resources Research, 57(12), p.e2021WR030664.

[41] Borgman, O., Darwent, T., Segre, E., Goehring, L. and Holtzman, R., 2019. Immiscible fluid displacement in porous media with spatially correlated particle sizes. Advances in Water Resources, 128, pp.158-167.

[42] Arshad, M., Nazir, M.S. and O'Kelly, B.C., 2020. Evolution of hydraulic conductivity models for sandy soils. Proceedings of the Institution of Civil Engineers-Geotechnical Engineering, 173(2), pp.97-114.

[43] Elhakim, A.F., 2016. Estimation of soil permeability. Alexandria Engineering Journal, 55(3), pp.2631-2638.

[44] Hazen, A., 1892. Some physical properties of sand and gravel with special reference to their use in filtration. 24th Ann, Rep., Mass. State Board of Health, Boston.

[45] Slichter, C.S., 1899. Theoretical investigation of the motion of ground waters. The 19th Ann. Rep. US Geophys Survey., pp.304-319.

[46] Kruger, E,. 1918. Die grundwasserbewegung (in German). Internationale Mitteilungen fur Bodenkunde, 8, 105.

[47] Terzaghi, K., 1925. Principles of soil mechanics. Engineering News-Record, 95(19-27), pp.19-32.

[48] Zamarin, EA., 1928. The Calculus of the Groundwater Flow. Izd-vo IVCH, Tashkent. (In Russian)

[49] Sauerbrey, I.I., 1932. On the problem and determination of the permeability coefficient. Proceedings VNIIG, (3-5), pp.115-145.

[50] Zunker, F., 1932. Fertilization and soil science. Journal of Plant Nutrition A25. (In German)

[51] Kozeny, J., 1953. Das wasser im boden. Grundwasserbewegung. In Hydraulik (pp. 380-445). Springer, Vienna.

[52] Beyer W, 1964. Zur Bestimmung der Wasserdurchlässigkeit von Sanden und Kiesen, aus der Kornverteilungskurve. Z Wasserwirt-Wassertech 14:165–168 (in German)

[53] Terzaghi, K., and Peck, R.B. 1964. Soil mechanics in engineering practice. John Wiley & Sons, New York USBR. Drainage Manual: A Water Resources Technical Publication. 1978. URL http://www.usbr.gov/pmts/wquality_land/DrainMan.pdf.

[54] Amer, A.M. and Awad, A.A., 1974. Permeability of cohesionless soils. Journal of Geotechnical and Geoenvironmental Engineering, 100(Proc. Paper 10981 Tech. Note).

[55] USBR United States Bureau of Reclamation, earth manual, third edition, 1978.

[56] Kenney, T.C., Lau, D. and Ofoegbu, G.I., 1984. Permeability of compacted granular materials. Canadian Geotechnical Journal, 21(4), pp.726-729.

[57] Shahabi, A.A., Das, B.M. and Tarquin, A.J., 1984. An empirical relation for coefficient of permeability of sand. Geomechanics — Interaction: Proceedings of the Fourth Australia–New Zealand Conference on Geomechanics, Perth, Western Australia.

[58] Chapuis, R.P., Gill, D.E. and Baass, K., 1989. Laboratory permeability tests on sand: influence of the compaction method on anisotropy. Canadian Geotechnical Journal, 26(4), pp.614-622.

[59] Koenders, M.A. and Williams, A.F., 1992. Flow equations of particle fluid mixtures. Acta Mechanica, 92(1-4), pp.91-116.

[60] Alyamani, M.S. and Şen, Z., 1993. Determination of hydraulic conductivity from complete grain-size distribution curves. Groundwater, 31(4), pp.551-555.

[61] Kasenow, M., 2002. Determination of hydraulic conductivity from grain size analysis. Water Resources Publication.

[62] Mbonimpa, M., Aubertin, M., Chapuis, R.P. and Bussière, B., 2002. Practical pedotransfer functions for estimating the saturated hydraulic conductivity. Geotechnical & Geological Engineering, 20(3), pp.235-259.

[63] Carrier III, W.D., 2003. Goodbye, hazen; hello, kozeny-carman. Journal of geotechnical and geoenvironmental engineering, 129(11), pp.1054-1056.

[64] Kisman, K.E. and Yeung, K.C., 1995, June. Numerical study of the SAGD process in the Burnt Lake oil sands lease. In SPE international heavy oil symposium. OnePetro.

[65] Chen, Q., Gerritsen, M.G. and Kovscek, A.R., 2008. Effects of reservoir heterogeneities on the steam-assisted gravity-drainage process. SPE Reservoir Evaluation & Engineering, 11(05), pp.921-932.

[66] Shin, H. and Choe, J., 2009, October. Shale barrier effects on the SAGD performance. In SPE/EAGE reservoir characterization & simulation conference (pp. cp-170). European Association of Geoscientists & Engineers.

[67] Fatemi, S.M., 2012. The effect of geometrical properties of reservoir shale barriers on the performance of steam-assisted gravity drainage (SAGD). Energy Sources, Part A: Recovery, Utilization, and Environmental Effects, 34(23), pp.2178-2191.

[68] Dang, T.Q.C., Chen, Z., Nguyen, T.B.N., Bae, W. and Mai, C.L., 2013. Numerical simulation of SAGD recovery process in presence of shale barriers, thief zones, and fracture system. Petroleum Science and Technology, 31(14), pp.1454-1470.

[69] Wang, C. and Leung, J.Y., 2015. Characterizing the effects of lean zones and shale distribution in steam-assisted-gravity-drainage recovery performance. SPE Reservoir Evaluation & Engineering, 18(03), pp.329-345.

[70] Xia, Y., Huang, S., Chen, X., Cao, M. and Yang, L., 2018, December. Study on the characteristics of production performance and steam chamber of SAGD considering interlayer. In SPE International Heavy Oil Conference and Exhibition. OnePetro.

[71] Gallardo, E. and Deutsch, C.V., 2019. Approximate physics-discrete simulation of the steam-chamber evolution in steam-assisted gravity drainage. SPE Journal, 24(02), pp.477-491.

[72] Huang, S., Yang, L., Xia, Y., Du, M. and Yang, Y., 2019. An experimental and numerical study of a steam chamber and production characteristics of SAGD considering multiple barrier layers. Journal of Petroleum Science and Engineering, 180, pp.716-726.

[73] Zhang, L., Li, J., Sun, L. and Yang, F., 2021. An influence mechanism of shale barrier on heavy oil recovery using SAGD based on theoretical and numerical analysis. Energy, 216, p.119099., C.V., 2019. Approximate physics-discrete simulation of the steam-chamber evolution in steam-assisted gravity drainage. SPE Journal, 24(02), pp.477-491.

[74] Kyanpour, M. and Chen, Z., 2013, June. A new approach for designing steam splitters and inflow control devices in steam assisted gravity drainage. In SPE Heavy Oil Conference-Canada. OnePetro.

[75] Kyanpour, M. and Chen, Z., 2014, September. Design and optimization of orifice based flow control devices in steam assisted gravity drainage: a case study. In SPE Heavy and Extra Heavy Oil Conference: Latin America. OnePetro.

[76] Ghesmat, K. and Zhao, L., 2015. SAGD well-pair completion optimization using scab liner and steam splitters. Journal of Canadian Petroleum Technology, 54(06), pp.387-393.

[77] Su, Y. and Gates, I., 2015, June. Impact of Flow Control Devices on SAGD Performance from Less Heterogeneous to Strongly Heterogeneous Reservoirs. In SPE Canada Heavy Oil Technical Conference. OnePetro.

[78] Becerra, O., Kearl, B.J., Zaini, F., Melo, M. and Woiceshyn, G., 2018, March. Liner-deployed inflow control devices ICD production results in MacKay river SAGD wells. In SPE Canada Heavy Oil Technical Conference. OnePetro.

[79] Nejadi, S., Hubbard, S.M., Shor, R.J., Gates, I.D. and Wang, J., 2018, November. Optimization of placement of flow control devices under geological uncertainty in steam assisted gravity drainage. In SPE Thermal Well Integrity and Design Symposium. OnePetro.

[80] Ertekin, T., Sun, Q. and Zhang, J., 2019. Reservoir simulation: problems and solutions. Richardson, Texas, USA: Society of Petroleum Engineers.

[81] Wang, J. and Gates, I.D., 2021. Time scales for steam injection and bitumen production in steam-assisted gravity drainage. Energy, 227, p.120430.

[82] CMG STARS, 2021, Users' Guide, Advanced Processes & Thermal Reservoir Simulator (Version 2021), Computer Modeling Group, Calgary, AB, Canada.

[83] Sadri, J. and Suen, C.Y., 2006, July. A genetic binary particle swarm optimization model. In 2006 IEEE International Conference on Evolutionary Computation (pp. 656-663). IEEE.

[84] Izadi, H., Roostaei, M., Hosseini, S.A., Soroush, M., Mahmoudi, M., Devere-Bennett, N., Leung, J.Y. and Fattahpour, V., 2022. A hybrid GBPSO algorithm for permeability estimation using particle size distribution and porosity. Journal of Petroleum Science and Engineering, 217, p.110944.

[85] Tabe-Bordbar, S., Emad, A., Zhao, S.D. and Sinha, S., 2018. A closer look at cross-validation for assessing the accuracy of gene regulatory networks and models. Scientific reports, 8(1), pp.1-11.

[86] Fushiki, T., 2011. Estimation of prediction error by using K-fold cross-validation. Statistics and Computing, 21(2), pp.137-146.

[87] Abram, M. and Cain, G., 2014. Particle-size analysis for the pike 1 project, McMurray formation. Journal of Canadian Petroleum Technology, 53(06), pp.339-354.

[88] Izadi, H., Fattahpour, V., Roostaei, M., Mahmoudi, M., Leung, J., Devere-Bennett, N., 2020. Hybrid Intelligent Algorithm for Permeability Estimation Based on Particle Size Distribution and Porosity Data. Geoconvention.

[89] Carrigy, M. 1966. Lithology of the Athabasca Oil Sands. Bulletin. 18, Edmonton: Research Council of Alberta.

[90] Luo, F., Latifur, K., Bastani, F. et al. 2004. A Dynamically Growing Self-Organizing Tree (DGSOT) for Hierarchical Clustering Gene Expression Profiles. Bioinformatics. 20(16): 2605–2617.

[91] Mahmoudi, M., Fattahpour, V., Nouri, A. et al. 2015. Oil Sand Characterization for Standalone Screen Design and Large-Scale Laboratory Testing for Thermal Operations. Presented at SPE Thermal Well Integrity and Design Symposium, Banff, Alberta, 23-25 November.

[92] Fattahpour, V., Maciel, V., Mahmoudi, M., Chen, K., Nouri, A., and Leitch, M. 2017. Classification of Alberta Oil Sands Based on Particle Size Distribution for Sand Control Design and Experimental Applications, SPE Canada Heavy Oil Technical Conference, Calgary, Alberta, Canada, 15-16 February.

[93] ASTM D. Standard test method for particle-size analysis of soils; 2007.

[94] Izadi, H., Sadri, J., Hormozzade, F. and Fattahpour, V., 2020. Altered mineral segmentation in thin sections using an incremental-dynamic clustering algorithm. Engineering Applications of Artificial Intelligence, 90, p.103466.

[95] Miller, R.W., 1983. Flow measurement engineering handbook.

[96] Zheng, J., Leung, J.Y., Sawatzky, R.P. and Alvarez, J.M., 2019. An AI-based workflow for estimating shale barrier configurations from SAGD production histories. Neural Computing and Applications, 31(9), pp.5273-5297.

[97] Bai, T. and Tahmasebi, P., 2022. Sequential Gaussian simulation for geosystems modeling: a machine learning approach. Geoscience Frontiers, 13(1), p.101258.

[98] Vinsome, P.K.W. and Westerveld, J., 1980. A simple method for predicting cap and base rock heat losses in'thermal reservoir simulators. Journal of Canadian Petroleum Technology, 19(03).

[99] Izadi, H., Leung, J.Y., Roostaei, M., Mahmoudi, M., Stevenson, J., Tuttle, A., Sutton, C., Mirzavand, R. and Fattahpour, V., 2023. Data-driven analysis of using flow control devices and extended reach wells on SAGD well performance. Geoenergy Science and Engineering, 231, p.212336.

[100] Izadi, H., Roostaei, M., Mahmoudi, M., Rosi, G., Stevenson, J., Tuttle, A., Sutton, C., Mirzavand, R., Leung, J.Y. and Fattahpour, V., 2022-a, November. Data-Driven Decision-Making Strategy for Thermal Well Completion. In SPE Thermal Well Integrity and Production Symposium. OnePetro.

[101] Izadi, H., Leung, J.Y., Roostaei, M., Mahmoudi, M., Stevenson, J., Tuttle, A., Sutton, C., Mirzavand, R. and Fattahpour, V., 2024. A practical workflow to design inflow control devices in SAGD projects to increase production and lower freshwater usage. *Fuel*, *356*, p.129454

[102] Izadi, H., Roostaei, M., Mahmoudi, M., Rosi, G., Stevenson, J., Tuttle, A., Sutton, C., Mirzavand, R., Leung, J. and Fattahpour, V., 2023, March. Unsupervised PSD Clustering to Assess Reservoir Quality Along the Horizontal Wells: An Efficient Inflow Control Devices Design. In SPE Canadian Energy Technology Conference. OnePetro.

[103] Agbaji, A.L., 2011, May. Optimizing the planning, design and drilling of extended reach and complex wells. In SPE/DGS Saudi Arabia Section Technical Symposium and Exhibition. OnePetro.

[104] Izadi, H., Roostaei, M., Mahmoudi, M., Hosseini, S.A., Soroush, M., Rosi, G., Stevenson, J., Tuttle, A., Sutton, C., Leung, J. and Fattahpour, V., 2022, March. The Impact of Increase in Lateral Length on Production Performance of Horizontal Thermal Wells. In SPE Canadian Energy Technology Conference. OnePetro.

[105] Economic Spotlight Oil Sands Industry Adjusts to Lower Oil Prices, 2019, available online at: https://open.alberta.ca/dataset/13ab3f73-6e4e-4aac-b56b-bff38800aa65/resource/e5c850e9-d479-494c-9343-284320d10ac7/download/2019-06-economic-spotlight.pdf.

[106] Verney, M. J. 2015, Evaluating SAGD Performance due to Changes in Well Spacing and Length. Presented at the SPE Canada Heavy Oil Technical Conference, Calgary, Alberta, Canada, June 9–11. SPE-174481-MS. https://doi.org/10.2118/174481-MS.

[107] Lauritzen, J. E. and Martiniussen, I. B. 2011, Single and Multi-Phase Flow Loop Testing Results for Industry Standard Inflow Control Devices. Presented at the SPE Offshore Europe Oil and Gas Conference and Exhibition, Aberdeen, UK, 6-8 September. SPE-146347-MS. https://doi.org /10.2118/146347-MS.

[108] Lee, B. O., Rabeh, M. N., Vicario, R. et al. 2013, Multi-Phase (Oil–Water) Loop Flow Test for Helical and Hybrid Passive Inflow Control Devices. Presented at the International Petroleum Technology Conference, Beijing, China, 26-28 March. IPTC-17125-MS. https://doi.org/10.2523/IPTC-17125-MS.

[109] Stone, T., Damas, C.E., Woiceshyn, G., Law, D.H.S., Brown, G., Olapade, P. and Bailey, W.J., 2013, February. Advanced wellbore simulation of flow control devices with feedback control for thermal operations. In SPE Reservoir Simulation Symposium. OnePetro.

[110] Noroozi, M., Melo, M., Montoya, J. and Neil, B., 2015, November. Optimizing flow control devices in SAGD operations: How different methodologies are functional. In SPE Thermal Well Integrity and Design Symposium. OnePetro.

[111] Banerjee, S. and Hascakir, B., 2018. Flow control devices in SAGD completion design: Enhanced heavy oil/bitumen recovery through improved thermal efficiency. Journal of Petroleum Science and Engineering, 169, pp.297-308

[112] Lastiwka, M., Burke, L.H., Booy, D., Chineme, E.C., Gaviria, F. and Ortiz, J.D., 2019, September. Laboratory and Field Testing of a Steam-Limiting Flow Control Device Developed for Thermal Applications. In SPE Annual Technical Conference and Exhibition. OnePetro.

[113] Gorham, T., Sims, J., Buell, R.S., Miller, R., Fermaniuk, B. and Heukelman, H., 2019, November. Horizontal steam injection liner-deployed flow control device design development and testing. In SPE Thermal Well Integrity and Design Symposium. OnePetro.

[114] Zhu, D. and Uzcategui, A., 2021, April. Flow Control Devices in Steam Assisted Thermal Applications: A Way to Optimize Both Steam Injection and Fluids Production. In SPE Western Regional Meeting. OnePetro

[115] Gohari, K., Ortiz, J., Nespor, K., Sanchez, J., Betancur, A., Irani, M., Bashtani, F., Sabet, N., Ghannadi, S., Abraham, A. and Bilic, J., 2021, January. Analysis of the Performance of Various Well Liner Completion Strategies in Surmont. In SPE Thermal Integrity and Design Symposium. OnePetro

[116] Martinez Santiago, M., Ortiz, J., Bethapudi, B., Noordin, F., Trisnadi, D., Mohammed, T., Al Obeidi, M., Permana, K. and Soufi, A., 2022, September. Unlocking Solutions in Oil Field Production: Innovative & Advanced Autonomous Flow Control Device application. In SPE Annual Technical Conference and Exhibition. OnePetro.

[117] Zhu, D., 2022. A Dual-Directional Flow Control Device for Cyclic Steam Stimulation Applications. SPE Production & Operations, 37(01), pp.151-158.

[118] Liang, G., Xie, Q., Liu, Y., Liu, S., Zhou, J. and Bao, Y., 2022, June. Design and Application Evaluation of Revolutionary Inflow Control Devices Enhanced Bitumen Recovery and Thermal Efficiency in SAGD Process. In SPE EuropEC-Europe Energy Conference featured at the 83rd EAGE Annual Conference & Exhibition. OnePetro.

[119] Dosunmu, I. and Osisanya, S., 2015, November. An Economic Approach to Horizontal Well Length Optimization. Presented at the In Abu Dhabi International Petroleum Exhibition and Conference, Abu Dhabi, UAE, 9-12 November. SPE-177866-MS. https://doi.org/10.2118/177866-MS.

[120] Virk, M. M., Al Hammadi, K. E., Recham, R. et al. 2020, Screening Study for an Optimal Horizontal Section Length of a Maximized Reservoir Contact Well. Presented at the Abu Dhabi International Petroleum Exhibition & Conference, Abu Dhabi, UAE, November 9–12. SPE-202664-MS. https://doi.org/10.2118/202664-MS.

[121] AER reports, 2022., Online Available: https://www.aer.ca/providing-information/data-and-reports/activity-and-data/in-situ-performance-presentations.

[122] Gonzalez, R.C., 2009. Digital image processing. Pearson education india.

[123] Hauke, J. and Kossowski, T., 2011. Comparison of values of Pearson's and Spearman's correlation coefficients on the same sets of data. Quaestiones geographicae, 30(2), pp.87-93.

[124] Nespor, K., Chacin, J., Ortiz, J. et al. 2019, An Overview of the Field Performance of Tubing-deployed Flow Control Devices in the Surmont SAGD Project. Presented at the SPE Thermal Well Integrity and Design Symposium, Banff, Alberta, Canada, 19-21 November. SPE-198704-MS. https://doi.org/10.2118/198704-MS.

[125] Dong, X., Liu, H., Hou, J., Chen, Z. and Zhang, T., 2015, October. An empirical correlation to predict the SAGD recovery performance. In SPE/IATMI Asia Pacific Oil & Gas Conference and Exhibition. OnePetro.

[126] Liu, H., Cheng, L., Huang, S., Jia, P. and Chen, M., 2018. Evolution characteristics of SAGD steam chamber and its impacts on heavy oil production and heat consumption. International Journal of Heat and Mass Transfer, 121, pp.579-596.

[127] Gates, I.D. and Larter, S.R., 2014. Energy efficiency and emissions intensity of SAGD. Fuel, 115, pp.706-713.

[128] Yuan, Z., Liu, P., Zhang, S., Li, X., Shi, L. and Jin, R., 2018. Experimental study and numerical simulation of nitrogen-assisted SAGD in developing heavy oil reservoirs. Journal of Petroleum Science and Engineering, 162, pp.325-332.

[129] Ho, S.L. and Xie, M., 1998. The use of ARIMA models for reliability forecasting and analysis. Computers & industrial engineering, 35(1-2), pp.213-216.

[130] Ahmadi, M.A., Ebadi, M., Shokrollahi, A. and Majidi, S.M.J., 2013. Evolving artificial neural network and imperialist competitive algorithm for prediction oil flow rate of the reservoir. Applied Soft Computing, 13(2), pp.1085-1098.

[131] Zhang, C., Zhou, J., Li, C., Fu, W. and Peng, T., 2017. A compound structure of ELM based on feature selection and parameter optimization using hybrid backtracking search algorithm for wind speed forecasting. Energy Conversion and Management, 143, pp.360-376.

[132] Liu, H., Tian, H.Q., Liang, X.F. and Li, Y.F., 2015. Wind speed forecasting approach using secondary decomposition algorithm and Elman neural networks. Applied Energy, 157, pp.183-194.

[133] Yu, Y., Si, X., Hu, C. and Zhang, J., 2019. A review of recurrent neural networks: LSTM cells and network architectures. Neural computation, 31(7), pp.1235-1270.

[134] Sherstinsky, A., 2020. Fundamentals of recurrent neural network (RNN) and long short-term memory (LSTM) network. Physica D: Nonlinear Phenomena, 404, p.132306.

[135] Sengupta, S., Basak, S., Saikia, P., Paul, S., Tsalavoutis, V., Atiah, F., Ravi, V. and Peters, A., 2020. A review of deep learning with special emphasis on architectures, applications and recent trends. Knowledge-Based Systems, 194, p.105596.

[136] Jain, P.K., Pamula, R. and Srivastava, G., 2021. A systematic literature review on machine learning applications for consumer sentiment analysis using online reviews. Computer science review, 41, p.100413.

[137] Yusof, N.M., Rashid, R.S.A. and Mohamed, Z., 2010, December. Malaysia crude oil production estimation: an application of ARIMA model. In 2010 International Conference on Science and Social Research (CSSR 2010) (pp. 1255-1259). IEEE.

[138] Berneti, S.M. and Shahbazian, M., 2011. An imperialist competitive algorithm artificial neural network method to predict oil flow rate of the wells. International journal of computer applications, 26(10), pp.47-50.

[139] Liu, W., Liu, W.D. and Gu, J., 2020. Forecasting oil production using ensemble empirical model decomposition based Long Short-Term Memory neural network. Journal of Petroleum Science and Engineering, 189, p.107013.

[140] Yang, C. and Wang, X., 2021. A steam injection distribution optimization method for SAGD oil field using LSTM and dynamic programming. ISA transactions, 110, pp.198-212.

[141] Wang, Y., Liu, H. and Zhou, Y., 2021. Development of a deep learning-based model for the entire production process of steam-assisted gravity drainage (SAGD). Fuel, 287, p.119565.

[142] Guevara, J.L. and Patel, R., 2021. Optimization of steam injection in SAGD using reinforcement learning. Journal of Petroleum Science and Engineering, 206, p.108735.

[143] Zhou, Y. and Wang, Y., 2022. An integrated framework based on deep learning algorithm for optimizing thermochemical production in heavy oil reservoirs. Energy, 253, p.124140.

[144] Huang, Z., Li, R. and Chen, Z., 2023. Integration of data-driven models for dynamic prediction of the SAGD production performance with field data. Fuel, 332, p.126171.

[145] Sadri, J., Ching, Y.S., Bui, T.D. 2006. A New Clustering Method for Improving Plasticity and Stability in Handwritten Character Recognition Systems, 18th International Conference on Pattern Recognition.

[146] Izadi, H., Sadri, J. and Bayati, M., 2017. An intelligent system for mineral identification in thin sections based on a cascade approach. Computers & Geosciences, 99, pp.37-49.

[147] Izadi, H., Sadri, J. and Mehran, N.A., 2015. A new intelligent method for minerals segmentation in thin sections based on a novel incremental color clustering. Computers & geosciences, 81, pp.38-52.

[148] Izadi, H., Sadri, J., Hormozzade, F. and Fattahpour, V., 2020. Altered mineral segmentation in thin sections using an incremental-dynamic clustering algorithm. Engineering Applications of Artificial Intelligence, 90, p.103466.

[149] The MathWorks Inc. (2022-b). Deep Learning HDL Toolbox™ (R2022a), Natick, Massachusetts: The MathWorks Inc. https://www.mathworks.com.